2000

The laser in biophysical and analytical chemistry: Investigating biophysical processes and dynamics, as well as analytical techniques, as applied to systems of biological and chemical relevance

Kyle Donald Ashby
Iowa State University

INFORMATION TO USERS

This manuscript has been reproduced from the microfilm master. UMI films the text directly from the original or copy submitted. Thus, some thesis and dissertation copies are in typewriter face, while others may be from any type of computer printer.

The quality of this reproduction is dependent upon the quality of the copy submitted. Broken or indistinct print, colored or poor quality illustrations and photographs, print bleedthrough, substandard margins, and improper alignment can adversely affect reproduction.

In the unlikely event that the author did not send UMI a complete manuscript and there are missing pages, these will be noted. Also, if unauthorized copyright material had to be removed, a note will indicate the deletion.

Oversize materials (e.g., maps, drawings, charts) are reproduced by sectioning the original, beginning at the upper left-hand corner and continuing from left to right in equal sections with small overlaps.

Photographs included in the original manuscript have been reproduced xerographically in this copy. Higher quality 6" x 9" black and white photographic prints are available for any photographs or illustrations appearing in this copy for an additional charge. Contact UMI directly to order.

Bell & Howell Information and Learning
300 North Zeeb Road, Ann Arbor, MI 48106-1346 USA
800-521-0600

The laser in biophysical and analytical chemistry: Investigating biophysical processes and dynamics, as well as analytical techniques, as applied to systems of biological and chemical relevance

by

Kyle Donald Ashby

A dissertation submitted to the graduate faculty

in partial fulfillment of the requirements for the degree of

DOCTOR OF PHILOSOPHY

Major: Analytical Chemistry

Major Professor: Jacob W. Petrich

Iowa State University

Ames, Iowa

2000

UMI Number: 9977311

UMI Microform 9977311

Bell & Howell Information and Learning Company
300 North Zeeb Road
P.O. Box 1346
Ann Arbor, MI 48106-1346

Graduate College

Iowa State University

This is to certify that the Doctoral dissertation of

Kyle Donald Ashby

has met the dissertation requirements of Iowa State University

Signature was redacted for privacy.

Major Professor

Signature was redacted for privacy.

For the Major Program

Signature was redacted for privacy.

For the Graduate College

To my mom and dad,

"...having been born of goodly parents..."

TABLE OF CONTENTS

ACKNOWLEDGMENTS

Foremost, I would like to thank my major professor, Jacob W. Petrich, for the knowledge he imparted and the many research opportunities he provided. I also thank him for his patience especially during my time as a temporary instructor.

I would like to thank my mom and dad for the investments they made in me from early in my life. They gave so much of themselves, time, and energy to allow me to see beyond myself toward the opportunities that were ahead of me.

I thank my wife Kim, for all she has had to put up with during my graduate studies at Iowa State University and for sending in my graduate school application in the first place. I would not have been able to make it through without you. I also appreciated the love and support of my kids, Spencer, Shea and Nathan, and for Spencer's constant reminders of how long it was taking me to complete the introduction of this dissertation.

So much of what I know about our laser systems and time-resolved spectroscopy in general, I owe to Kaustuv Das. Thanks for your patience and time you took to explain things in a way I could understand. I also thank Anindya Dutta for his help and ideas, his many anecdotes and sense of humor. Thanks for the late night billiards, bowling, and Bengali: "Bhat bokishna!"

I especially want to thank Mark Rasmussen and Tom Casey from the National Animal Disease Center, Ames, for allowing me the opportunity to work with them in bringing their F-Detector ideas into reality. I also thank them for not forcing me to collect my own samples!

I wish to acknowledge other Petrich Group members: Doug English, Alexandre Smirnov, Jin Wen, Jaehun Park, and Pramit Chowdhury. Thanks for your friendship and help during my graduate studies.

ABSTRACT

The unique properties of the laser have permitted the investigation of important biological molecules and systems, and aided in the development of the F-Detector, important in the area of food safety. The laser offers narrow pulses of high peak power to probe chromophore interactions with micelles, protein structure and dynamics, excited-state photophysics, and selective fluorescence detection.

Using the laser based time-correlated single photon counting technique, the effect of a surfactant (Brij-35) on the fluorescence properties of indole, 1-methylindole, and 3-methylindole in aqueous solutions were investigated. 3-methylindole is a component in animal waste and can be trapped within micelles or other surfactants to reduce its vapor pressure. Indole chromophores partition very well into the Brij-35 micelle as indicated by blue shifts in the steady-state spectra as well as the triple exponential necessary to describe the fluorescence decays. The interaction of 3-methylindole with the micelle was quantified and the equilibrium constant was determined to be $2.6 \times 10^4\ M^{-1}$.

Using the same time-resolved technique, tropomyosin mutants containing either tryptophan, 5-hydroxytryptophan, or 7-azatryptophan were expressed in *Escherichia coli* and their fluorescence properties studied. The fluorescent amino acids were located at position 122 of the tropomyosin primary sequence, corresponding to a solvent-exposed position c of the coiled-coil heptapeptide repeat. The emission spectrum of the probe in each mutant is blue-shifted slightly with respect to that of the probe in water. Incorporation into tropomyosin induces triple-exponential fluorescence decay in 5-hydroxytryptophan and double-exponential

fluorescence decay in 7-azatryptophan. The 5-hydroxytryptophan chromophore exists in several solvent environments in both its protonated and unprotonated forms.

Utilizing fluorescence upconversion, measurements of hypericin and its methylated analog, *O*-hexamethoxyhypericin, which possesses no labile protons, confirm excited-state hydrogen atom transfer as the primary photophysical event in hypericin and that the ground state of hypericin is heterogeneous. A rising component in the time-resolved fluorescence of hypericin and its absence for the hexamethoxy analog are consistent with this physical assignment and is in good agreement with previous transient absorbance measurements.

Laser based pump-probe transient absorption spectroscopy was utilized to determine that the activation energies for excited-state hydrogen atom transfer of hypericin and hypocrellin are respectively, 0.044 ± 0.008 and 2.12 ± 0.070 kcal/mol. The excited-state intramolecular hydrogen atom transfer reactions were measured as a function of temperature in an ethanol/methanol mixture. The low activation energies are consistent with the hydrogen atom transfer reactions being adiabatic. The larger value for hypocrellin suggests that a much larger amplitude displacement, than for hypericin, in at least one other coordinate comprises the overall reaction coordinate. The viscosity independent part of the hypocrellin activation barrier is 0.41 ± 0.088 kcal/mol.

The laser based F-Detector was designed and built for selective detection of fecal and ingesta contamination on meat carcasses as they are processed. Initially, F420, a methanogenic electron carrier, was utilized as the fluorescent marker. Later investigations revealed that the chlorophyll metabolite, pheophorbide, was better suited as a fluorescent marker for fecal contamination. A 100 ms detector time constant offers "instantaneous" detection.

Pheophorbide detection limits (in solution) are as low as 10^{-10} M. A 25 mV signal correlates a pheophorbide concentration of 1.0×10^{-6} M to an equivalent fecal concentration of 1.8 mg/mL. The F-Detector will make it possible for meat producers to provide cleaner and safer meat products and more importantly, to decrease the number of *E. coli.* related illnesses.

These investigations illustrate the utility and importance of the laser in biophysical and analytical chemistry. The experimental information obtained would otherwise be almost impossible to obtain using more conventional light sources.

GENERAL INTRODUCTION

Plinius in the first century A.D. wrote that the "the laser is numbered among the most miraculous gifts of nature and lends itself to a variety of applications"[1][1,2]. The impossibility of a "laser" as we know it today to have existed during the first century A.D. may make one question the reality of such a statement. To those of the Mediterranean in 1st century A.D. the Laser was an herb valued for its seemingly miraculous properties and diverse applications, ranging from the garnishing of feasts to curing diseases to ridding the body of poisons. No less miraculous is the laser of today with its seemingly endless applications within a wide variety of fields; medicine, biology, chemistry, physics, manufacturing, audio/video systems, and computers, to name just a few.

The laser, with its unique properties and characteristics, is set apart from other, more conventional light sources. In biophysical and analytical chemistry, laser sources make it possible to obtain information about biological and chemical systems that are difficult, if not impossible, to obtain with conventional light sources, especially in the time-domain. Reactions on the picosecond and femtosecond time scales are routinely investigated with the use of pulsed lasers.

My work in the areas of biophysical and analytical chemistry utilized the laser's unique characteristics to study the dynamics and properties of indole and its derivatives in organized media as well as tryptophan, 7-azatryptophan, and 5-hydroxytryptophan incorporated into

---

[1] English translation from Plinius', Naturalis Historia, XXII: "Laser...inter eximia naturae dona numeratum plurimis compositionibus inseritur." Obtained from Orazio Svelto, *Principles of Lasers, 2nd Edition*; Plenum Press: New York, NY, 1982; page v.

protein. This work utilized time-correlated single photon counting with a synchronously pumped dye laser as the excitation source. Another part of my work, although just a portion of the many years of continuing research in the Petrich lab, was the study of the antiviral agents hypericin and hypocrellin *a*. The purpose of the work was to further understand their physical properties as well as the photophysics behind their biological activity. This work utilized two different laser systems, a 30 Hz transient absorption pump-probe system and a fluorescence upconversion system. And finally, in the area of food safety with regard to the detection of fecal and ingesta contamination of meat during its initial processing, we developed a laser based detector to excite a specific fluorescent marker within the fecal material and collect the emission signaling its presence on the carcass.

These areas of my work make up the bulk of this dissertation. It includes papers that have been published or have been submitted for publication. More detail will be given concerning the different chapters, comprised of the specific manuscripts, later in this General Introduction. I will also discuss some basics of the laser as well as a few details concerning the specific laser systems mentioned previously. I will conclude this dissertation with brief concluding remarks and a few added details in the Appendix section.

The Basics of the Laser

In order to describe the properties of lasers that have made them so valuable in biophysical and analytical chemistry, I feel it beneficial to discuss briefly the basic optical transitions of molecules or atoms between two hypothetical states, i and j, upon interaction with electromagnetic radiation. These events are dipicted in figure 1 [2,3]. Absorption (figure 1a) occurs when a photon with a frequency, ν_{ij}, equal in energy to the difference between the two

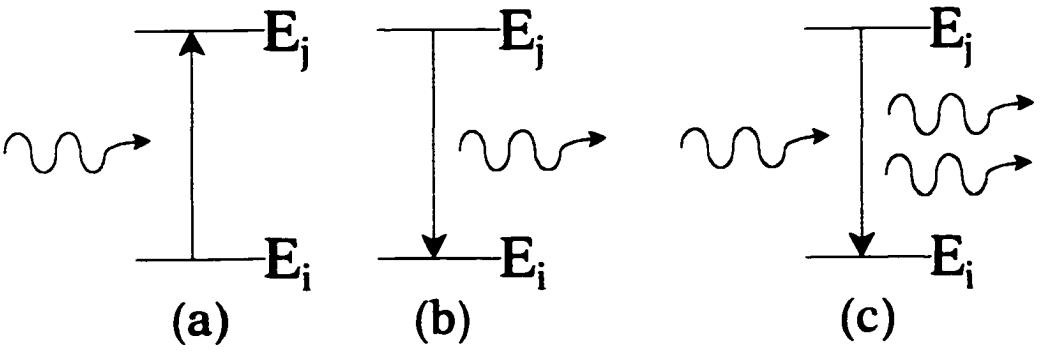

Figure 1. Hypothetical two-state systems illustrating (a) absorption, (b) spontaneous emission and (c) stimulated emission.

energy levels, $E_j - E_i = h\nu_{ij}$, interacts with the lower energy state, E_i. This lower energy state absorbs the energy promoting the molecule or atom into a higher energy state, E_j: $M_i + h\nu_{ij} \rightarrow M_j$, where M_i is the population of state i with a population density, η_i (particles/cm^3). The rate of the transition, or the rate of change of the population density, $-(d\eta_i/dt)$, is proportional to η_i, the initial number of absorbers in state i, as well as U_ν, the energy density of the electromagnetic radiation, ν_{ij}, incident upon the molecule or atom. Therefore,

$$-\frac{d\eta_i}{dt} \propto \eta_i U_\nu = B_{ij}\eta_i U_\nu$$

where B_{ij} is the Einstein coefficient for absorption which is characteristic of the particular molecule or atom and the two energy levels i and j. A large value of B_{ij} means a rapid transition rate and is therefore quantum mechanically allowed. For absorption, E_j and E_i could be any two energy levels within a given material.

Once in the excited-state, E_j, the molecule or atom may spontaneously emit a photon and return to the lower energy-state, E_i: $M_j + h\nu_{ij} \rightarrow M_i$, where M_j is the population of the excited-state, j, with a population density, η_j (particles/cm^3). Thus, the rate of depopulation of the excited state is given by:

$$-\frac{d\eta_j}{dt} = A_{ji}\eta_j$$

where A_{ji} is the transition probability or the rate constant for spontaneous emission which is characteristic of the particular atom or molecule and the levels involved in the transition. The frequency of the photon, ν_{ij}, is equal to the energy difference between the two states, E_j and E_i (figure 1b). Usually for spontaneous emission E_j is the first excited electronic singlet-state and E_i is the electronic ground-state. The spontaneous emission lifetime, τ, is given by $1/A_{ji}$.

Stimulated emission (figure 1c) occurs when a photon, of the same frequency as the initially absorbed photon, interacts with a molecule or atom in the excited-state and causes a deactivation of the excited-state, E_j, with a subsequent emission of a photon: $M_j + h\nu_{ij} \rightarrow M_i + 2h\nu_{ij}$, where the second photon has the same frequecy, phase, and direction as the first photon incident on the molecule or atom. The rate of stimulated emission or the rate of depopulation of the excited-state by stimulated emission is given by:

$$-\frac{d\eta_j}{dt} = B_{ji}\eta_j U_\nu$$

where B_{ji} is the stimulated transition probability which depends upon the particular molecule or atom, the particular levels i and j, and the intensity (energy density) of the incident light, U_ν.

The Jablonski Diagram in figure 2 illustrates these and other processes, radiative and non-radiative, that may occur following the interaction of a ground-state molecule or atom with

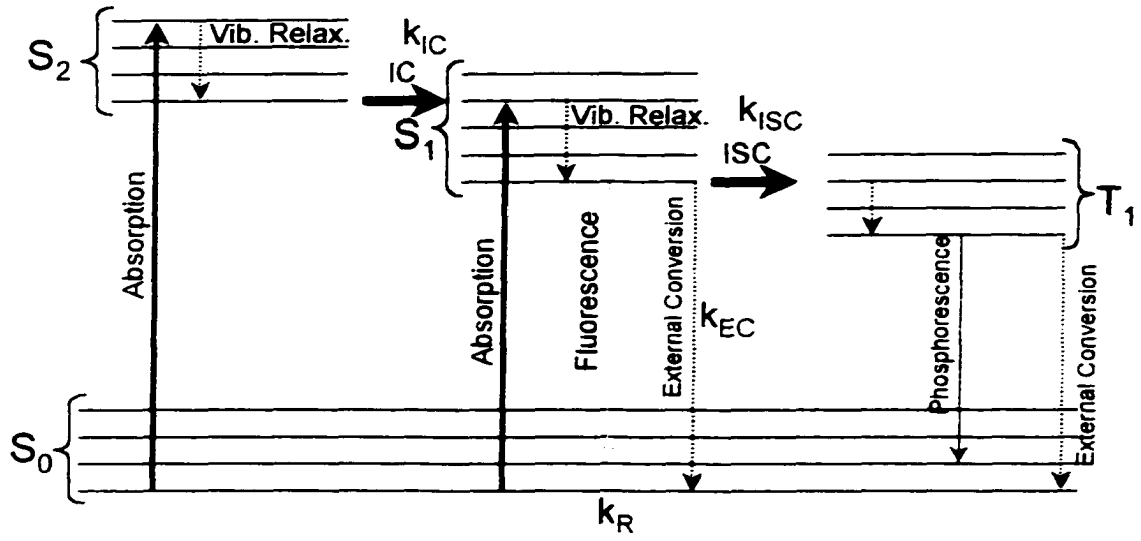

Figure 2. Jablonski diagram illustrating absorption events to singlet states, S_1 or S_2, from the ground state S_0, and the many different fates of the excited state. If absorption occurs to S_2 and sufficient coupling exists between S_2 and the lowest excited singlet state S_1, internal conversion (IC) occurs between corresponding vibrational states. This process occurs with a rate constant k_{IC}. From state S_1 the excited state may become depopulated by both radiative (fluorescence) and nonradiative pathways with respective rate constants, k_R and k_{EC}. Nonradiative pathways are external conversion (EC) processes such as energy transfer, collisional quenching, etc. If sufficient coupling exists between S1 and the lowest triplet state, T_1, intersystem crossing (ISC) may occur between the corresponding vibrational levels with a rate constant of k_{ISC}. The triplet state may also become depopulated by radiative (phosphorescence) and nonradiative pathways.

electromagnetic radiation. The rate constants for the processes are also depicted.

The properties and characteristics of the laser can now be described based upon the optical transitions previously discussed. The laser is an optical oscillator. The laser cavity consists of an "active medium" of molecules or atoms between two mirrors and a "pump" source to provide the population inversion necessary for light to oscillate with high gain. One

mirror is the high reflector (with high reflectivity) and the other is the output coupler that allows a certain small percentage of the laser light to escape the cavity. Consider an active medium, M, in which incident light with intensity, Φ, travels through the medium a distance dM. Two processes can occur if the incident light is of the proper transition frequency, namely absorption and stimulated emission. The change in intensity of the incident light due to absorption by the medium is given by:

$$-d\Phi_{ABS} = \Phi\eta_i\sigma\, dM$$

where the negative sign describes a situation where the intensity decreases after passing through the active medium, σ is the transition cross section and η_i is the population density of the lower electronic state, i, of the medium. For the process of stimulated emission for those molecules or atoms in the excited state, the change in intensity of the light after passing through the active medium is given by:

$$d\Phi_{STIM} = \Phi\eta_j\sigma\, dM$$

where the positive value describes an increase in intensity of the incident light after passing through the active medium, σ is the transition cross section and η_j is the population density of the excited-state j. Both changes in intensity due to absorption and stimulated emission depend upon the energy density of the incident light.

The overall change in intensity of the incident light, $d\Phi$, is the combination of the two intensities from the two processes,

$$d\Phi = d\Phi_{ABS} + d\Phi_{STIM}$$
$$d\Phi = \Phi\left(\eta_j - \eta_i\right)\sigma\, dM$$

The overall change in intensity of the light, $d\Phi$, passing through the active medium is dependent

upon the relative population densities of the upper state, η_j, and the lower state, η_i. If $\eta_i > \eta_j$ as is the case in a conventional thermal system, $d\Phi$ would be negative and represent a loss in intensity with more absorption events than stimulated emission events. But if $\eta_j > \eta_i$, $d\Phi$ would represent a net increase in intensity due to more stimulated emission events than absorption events. This can only be accomplished with an additional energy source acting as a "pump". The molecules or atoms in the active medium absorb energy from this energy source causing a population inversion where $\eta_j > \eta_i$. This additional source can be a conventional light source, another laser, photodiodes or an electrical discharge into which the active medium is placed. Oscillation of the amplified laser light will occur when the gain of active medium is greater than the losses within the laser cavity.

As previously discussed, the light from stimulated emission events is of the same frequency, phase and direction as the incident light. Since a LASER is *L*ight *A*mplification ***by*** *S*timulated *E*mission of *R*adiation, these properties of monochromaticity (output light is all the same frequency or at least has a very narrow frequency distribution), coherence in time (constant phase difference between electric fields at any time, t) and space (difference in the phase of the electric field at time, t = 0, is zero), and directionality (very little divergence in the light's propagation) have made lasers indispensable in many fields, especially within the fields of biophysical and analytical chemistry. Other highly valuable properties of lasers include the high photon flux or energy flux ($J/cm^2/s$) due to the high amplification and directionality of the laser beam and the ability to produce pulsed lasers of very narrow time and spectral bandwidth (narrow full width at half maximum: FWHM) on the order of picoseconds and smaller.

The narrow spectral bandwidth (monochromaticity) allows the selective excitation of

chromophores which is made especially effortless with the relatively wide range of wavelengths available with dye lasers. This is especially evident when investigating protein dynamics and structure. Tryptophan can be selectively excited from the other two fluorescent natural amino acids, tyrosine and phenylalanine. Although conventional continuum or line sources may be used with the use of a monochromator, the dispersion of the incident light and the use of small slit widths can drastically reduce the throughtput of the incident light. The laser source provides narrow spectral bandwidths with much higher photon flux. This high photon flux is beneficial when exciting low quantum yield or low concentration chromophores as well as placing the greatest number of molecules in the excited state as desired in pump-probe experiments.

Probably the most important is the ability to obtain very narrow laser pulses with high repetition rates. The most direct way of producing modulated laser light is to have an eternal modulation device, such as a mechanical chopper, which periodically transmits the light at a certain frequency. This simplistic method has some obvious drawbacks. First, the modulation is very inefficient because the device blocks part of the energy during the "off-time". Second, the power of the output pulses cannot exceed the power of the CW laser source. The more common means of producing laser pulses utilize internal devices (intracavity) that provide output pulses that have highly efficient duty cycles as well as high peak powers. These methods include, gain switching, Q-switching, cavity dumping, and mode-locking [3-6].

Gain switching. This is the more direct method for producing pulsed laser output. This method consists of simply turning the laser pump on and off at specified repetition rates. A common example of this is in semiconductor lasers where the electric pumping current can easily be modulated on and off.

Q-switching. The quality factor (Q) of the cavity is spoiled (large cavity loss) in a periodic fashion. Oscillation of the light within the cavity is prevented during spoiling. The pumping power remains constant so that during the "off" times when oscillation within the cavity is prevented the active medium continues to store the pump energy and a large population inversion is accumulated. When the cavity spoiling is turned off the energy stored within the active medium is allowed to oscillate and a high-energy, narrow pulse is produced. Electro-optic devices such as a Pockels cell positioned between cross polarizers allows the oscillation of the laser light by periodically rotating the polarization of the light so it can be transmitted through the cross polarizers. Another method for Q-switching utilizes a saturable absorber in the cavity. This is usually an organic dye in solution. The dye absorbs the light in the cavity creating high losses and preventing oscillation. When the radiance within the cavity reaches a critical level, the dye becomes bleached (transparent to the light) and oscillation is allowed.

Cavity dumping. Light within a cavity dumped laser is not allowed to exit or leak out of the cavity (both end mirrors of cavity are high reflectors). Thus, photons are stored within the cavity and the energy within the cavity becomes large. At a specified frequency, a voltage is applied to a piezoelectric transducer generating an acoustic wave in a transparent crystal within the cavity. The acoustic wave pattern acts like a diffraction grating and the light is then diffracted (dumped) out of the cavity with narrow, high energy pulses.

Mode-locking. An extremely large number of longitudinal cavity modes are allowed to oscillate for a given cavity length, L, which are separated in frequency by c/2L, where c is the speed of light. The phases of the cavity modes can be locked in order to produce a pulse train in the cavity. The loss (or gain) of the cavity is modulated at a frequency of the round-trip time

of a photon, 2L/c. Only those photons from any one of the modes which returns to the gain medium, when the gain is at it maximum and in phase together, will be amplified. Those photons that are out of phase will not be amplified. Therefore, the modes that oscillate within the cavity become locked together in phase and constructively interfere at the exact time and space when the gain is maximum to produce narrow, high energy pulses [4,5].

There are two modelocking regimes; *active* and *passive* modelocking. In general, modelocking is accomplished by an external element inserted into the laser cavity. If the element is driven by an energy source external to the laser itself, the regime is considered *active* modelocking. In this case an acousto-optic modulator is inserted into the laser cavity to modulate the cavity loss.

The other modelocking regime, *passive* modelocking, occurs where the only energy available is in the laser cavity itself. In this case, a nonlinear saturable absorber is inserted into the laser cavity. Lasers may also become "self modelocked" due to nonlinear interactions within the lasing medium itself [5].

Many lasers and laser systems utilize important nonlinear processes within anisotropic crystals such as, LBO (lithium triborate), BBO (β-barium borate), etc., or other transparent media such as H_2O or sapphire. These important processes depend upon high-energy, narrow laser pulses produced by the methods previously described. Second harmonic generation (SHG) and sum frequency generation (SFG) are just two of these important nonlinear processes stemming from narrow, high peak power laser pulses within the anisotropic crystals. SHG provides a way to extend the available wavelengths of dye laser output needed for excitation of indole or tryptophan, for example, down into the UV portion of the electromagnetic spectrum.

SFG is the result of optical mixing of two pulses of different frequencies and generating the frequency sum as an output. This process is fundamental to the light gate in a fluorescence upconversion spectrometer. Also, the necessary high power pulses that pulsed lasers provide allow white light to be generated and used as probe sources in pump-probe experiments when the pulses are focused into transparent media such as sapphire or water. Time-resolved experiments requiring pulsed lasers provide a wide variety of information both directly and indirectly, such as, fluorescence lifetimes, distances between molecules or even specific sites on the same molecule, molecular dynamics such as, rotations and vibrations, and the type of interactions and environments that exist within the binding sites of proteins as well as the kinetics and mechanisms of binding. Temperature dependence of exited-state reactions, such as proton or hydrogen atom transfer, to determine the energy barrier associated with the reaction can also be investigated using time-resolved techniques as well as solvent relaxation dynamics and the determination of micelle composition. The determination of excited-state lifetimes are necessary in understanding the nature of emitting states. Time-resolved emission spectra can be obtained to observe changes in the emission properties of chemical systems on time-scales on the order of nanoseconds and smaller. Illustrations of some of these techniques using pulsed lasers will be seen in the chapters following.

Lasers are also becoming less and less bulky and are being built on very small scales allowing them to be extremely portable and easily handled for use in miniature and remote instrumental systems. Many of these lasers no longer need bulky power supplies with special voltage requirements. An illustration of this is found in the later chapters of this dissertation with the production of the laser based F-Detector for the detection of fecal and ingesta

contamination of meat products.

These distinctions between lasers and conventional light sources make lasers well suited for application to biophysical and chemical systems whose properties and dynamics otherwise could not be investigated.

A Brief Description of the Laser Systems

Three main laser systems were utilized for this work and will be described in greater detail.

The Time-Correlated Single Photon Counting System

The workhorse of the Petrich laboratory is the time-correlated single photon counting apparatus. In spite of its many applications, the overall purpose of single photon counting is to obtain excited-state fluorescence lifetimes. The excited state, following the absorption of a photon, may experience many possible fates. In general, the excited state may undergo radiative and non-radiative processes (internal conversion, intersystem crossing, and external conversion, see figure 2) back to the ground state. Generally, the rate of excited-state depopulation by radiative processes is expressed as a unimolecular first order process. With reference to figure 1 in which the excited-state is state j and the lower state is state i:

$$\text{rate of depopulation of state } M_j = \frac{d[M_j]}{dt} = -k[M_j]$$

where k is the first order rate constant for the depopulation of the excited-state, j. Thus, the time dependence of M_j is described by:

$$[M_j] = [M_j]_0 e^{(-kt)}$$

where $[M_j]_0$ is the population or concentration of excited-state species at time, t = 0,and called

the preexponential factor. Thus, the fluorescence intensity decays exponentially with time. The lifetime of the excited state, τ, is defined as the time it takes for the initial excited-state population to be reduced by a factor of $1/e$. For the exponential decay, $\tau = 1/k$, where k is the rate constant for the depopulation of the excited-state. Since there are many routes for depopulating the excited-state the rate constant, $k = k_R + k_{IC} + k_{ISC} + k_{EC}$ (figure 2). The, lifetime that is measured in time-correlated single photon counting is the fluorescence lifetime, τ_F, and

$$\tau_F = \frac{1}{k_R + k_{IC} + k_{ISC} + k_{EC}}$$

So, one can see that by measuring the fluorescence lifetime, τ_F, one could measure purely radiative processes, if the other routes for excited-state depopulation were negligible, or obtain a measure of external conversion processes, such as quenching or energy transfer. The quantum yield of fluorescence, ϕ_F, is essentially the ratio of the number of photons emitted to the number of photons absorbed, and is given by:

$$\phi_F = \frac{k_R}{k_R + k_{IC} + k_{ISC} + k_{EC}}$$

Thus, $\phi_F = k_R \tau_F$.

The time-correlated single photon counting apparatus is shown in figure 3. A Coherent Antares 76-s Nd:YAG CW mode-locked laser with a ~2W frequency doubled output of 532 nm synchronously pumps a Coherent 701 Rhodamine 6G dye laser with output wavelengths in the range of 560 - 610 nm. Synchronous pumping of the dye lasers refers to the situation where the cavity length of the dye laser is set equal to the cavity of the Nd:YAG pumping laser. Thus the gain of the dye laser is driven synchronously with the cavity round-trip repetition rate of the pumping laser producing short dye laser pulses [10]. The dye laser is cavity dumped to provide

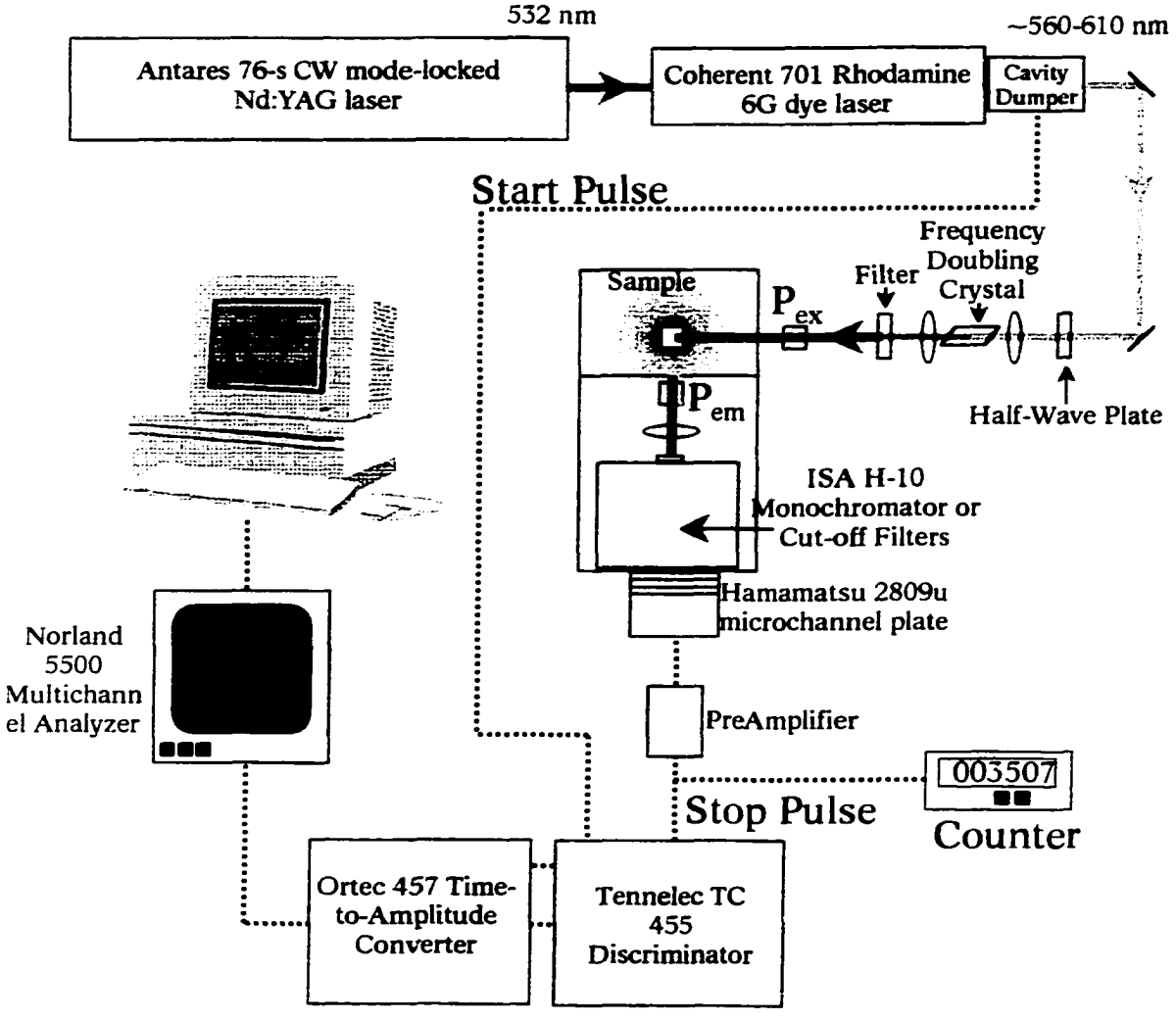

Figure 3. Time-correlated single photon counting apparatus.

a ~7 ps pulse with a repetition rate of 3.8 MHz, a slower repetition rate than the pump laser, but necessary to provide higher peak powers and more time between pulses to avoid pulse pile up. The time scale for the experiment is set on the Ortec 457 time-amplitude-converter (TAC). Two signals pass from the discriminator to the TAC. One is a "start" signal, usually the output from

the microchannel plate which detects a fluorescence photon event (Hamamatsu 2809u). This "start" pulse, in essence, begins the linear ramping of voltage across a capacitor within the TAC. The other signal is the "stop" signal, usually the output from the cavity dumper driver (provides the RF for the Bragg cell in the cavity dumper), which stops the voltage ramping. The voltage amplitude is subsequently converted to time in accordance with the overall TAC settings. The "time" signal is transferred to a multichannel analyzer and placed into the channel corresponding to the time measured for that particular photon event or count. Essentially the time between the initial excitation event and the random emission event is measured and a histogram of the fluorescence decay curve is built up in the multichannel analyzer.

Much consideration has gone into the subsequent analysis of the collected fluorescence decay curve in order to obtain the lifetime, τ_F, and the preexponential factor $[M_j]_0$ (the preexponential factor also commonly given the designation, A). One must fit the decay collected to extract the desired information. In some cases, it may be necessary to describe the fluorescence decay by a sum of exponentials:

$$I(t) = \sum_{i=1} A_i e^{(-t/\tau_i)}$$

Once the data is obtained, there remains the question as to what physical significance can be placed on the data relative to the system under investigation. Caution is usually warranted in the placing of any physical significance on the measured lifetimes and preexponential factors, especially where nonexponential fluorescence decays are concerned. Some knowledge about the chemical system in question is required to place physical significance on the parameters obtained from fitting the fluorescence decay. But, perhaps more important than the question of physical significance, is how reliable and accurate is the data (the

fluorescence decay) and the extracted parameters from fitting the data. To answer these questions one must first look at some experimental factors. For instance, it is necessary to have very pure solvents so as not to introduce solvent or other effects due only to the impurities as well as components in the decay data form fluorescence of the impurities themselves. It is desirable to make up new samples on a daily basis as samples might degrade or form aggregates over time that would give seemingly bizarre results from day to day. The concentration of the sample must be low enough that undesired quenching or energy transfer effects do not become significant and dominate the fluorescence decay. Both lasers, the dye laser as well as the pumping laser, need to be optimized so as to produce pulses of maximum power and stability. An autocorrelator is necessary to measure the laser pulses; it utilizes an interferometric noncollinear experimental setup, designed to provide background-free correlation using second harmonic generation in a nonlinear crystal. One must also insure that the number of excitation events, N_E, is significantly higher than the number of fluorescence photo events detected, N_D. This will avoid "pulse pile up" distortions in the fluorescence decay which will show up at short times in the decay and induce nonexponentiality. The ratio, N_D/N_E, must be kept on the order of 0.001 or lower as a good rule of thumb [7]. For 3.8 MHz cavity dumped laser pulses it is necessary to adjust the intensity of the excitation light with neutral density filters and/or dilution of the sample concentration in order that the counts (detected anode pulses at the microchannel plate) are kept to less than 4000 counts per second as indicated on the frequency counter. Another source of distortion in the fluorescence decay curve is the excitation pulse itself. The excitation pulse has a finite width (it is not a δ function). As the excitation pulse enters the sample one can visualize the leading edge of the pulse causing emission events while at later

times the middle portion and tail of the same pulse also causing emission events. This range of emission events for the same pulse distorts the fluorescence decay, especially if the lifetime of the sample is short. This effect can be taken care of by collecting an instrument response function (IRF) by placing a scattering sample in the cell holder and collecting a decay. The IRF is then convoluted with the trial decay function during the fitting process so that the extracted fitting parameters will not be influenced by the effects of the excitation pulse. A final source of error in the collected fluorescence decay is scattered light, either from room light or by scatter off of the sample cell or from the contents of the sample itself. The problem of room light can easily be attended to by placing the sample in a light tight box and dimming the room lights. Scattering problems with the sample itself are harder to overcome. Cutoff filters placed after the emission polarizer (figure 3) allow the sample fluorescence to reach the detector while blocking the scattered excitation light. At times even this is insufficient to totally eliminate the scattered light. One must also attempt to eliminate reflections off of the sample cell or other surfaces such as lenses and polarizers with a pin hole aperture before the sample cell. Care must be taken when placing the cell into the sample holder to assure that the excitation beam is passing properly through the cell. When these many items have been attended to one can feel reasonably confident that the fluorescence decay collected is reliable and truly represents the system under investigation.

A least-squares iterative convolution routine is employed to extract the fluorescence lifetime and preexponential factor. The collected fluorescence decay, $I(t) = A \exp(-t/\tau)$ (if $I(t)$ is nonexponential then $I(t) = \Sigma A_i \exp(-t/\tau_i)$), is fit by convoluting a trial decay function $F(t)$

with the IRF, P(t) [7]:[2]

$$I_0(t) = \int_0^t P(t')F(t-t')dt'$$

After convolution, the calculated decay, $I_0(t)$, is compared to the experimental fluorescence decay, I(t), and the statistical parameter, χ^2, is determined [7-9]:

$$\chi^2 = \sum_{i=1}^{n} \frac{[I(t_i) - I_0(t_i)]^2}{\sigma_i^2},$$

where n is the number of MCA channels and σ_i is the statistical standard deviation of the counts in each channel. In essence the χ^2 parameter is a comparison of how well the difference between the calculated and experimental decays agrees with the statistical deviation of counts in each channel. The power of the χ^2 parameter can be fully realized for time-correlated single photon counting because the statistics of this type of experiment are entirely known. The statistical distribution of counts within each channel is described by the Poisson distribution [7,8,10] in which the standard deviation, σ_i, is given by:

$$\sigma_i = \sqrt{I(t_i)}.$$

The numerical value of χ^2 should therefore approach n if the calculated decay well describes the actual experimental fluorescence decay[3]. Since the experimental statistics are known one can be highly confident on whether the extracted fluorescence parameters, the lifetime and

---

[2] I(t) and P(t) contain spurious counts in each channel of the MCA due to detector dark counts and room light leakage. These uncorrelated background counts are subtracted before the data fitting routine is employed.

[3] The actual expectation value of χ^2 is, n - p, where p equals the number of calculated parameters: n - p = v, the number of degrees of freedom [7-9].

preexponential factor, are those that best describe the experimental fluorescence decay based upon the value of the χ^2 parameter. The actual statistical parameter that is determined in our least-squares fitting routine is the reduced χ^2, χ^2_ν which is given by:

$$\chi^2_\nu = \frac{\chi^2}{\nu},$$

where ν is the number of degrees of freedom: n - p [7-10]. Therefore, for a calculated fit to optimally describe an experimental fluorescence decay, χ^2_ν should equal 1.0. Generally, a fit is determined to be good when a χ^2_ν value between 0.8 and 1.2 is obtained. Continuous iterations are performed by reconvoluting trial decay functions with the IRF until the χ^2_ν parameter is minimized.

Another means of determining the "goodness" of a fitted fluorescence decay is by observing the distribution of the weighted residuals. The analysis of residuals is to be utilized along with the χ^2_ν parameter. Residuals are basically the differences between the counts per channel of the observed experimental decay data and the fit to the decay, where the residuals, r_i, are given by [7,9]:

$$r_i = \frac{I(t_i) - I_0(t_i)}{\sigma_i}.$$

Residuals from successful fits when plotted against channel number (or time) should be randomly distributed about zero. Deviations from a random distribution can then be visually determined.

Thus, if a χ^2_ν close to 1.0 is obtained with completely random residuals about zero, one can confidently affirm that the assumed exponential or non-exponential model *and* the determined lifetimes and pre-exponential factors correctly describe the system under

investigation. Care is necessary in assigning physical significance to the determined model, for one can always obtain a better fit to a fluorescence decay by assuming a higher order exponential trial decay function as the model of the system. Therefore, just because a good fit is obtained for a particular model does not mean that it correctly describes the experimental system unless prior knowledge about the system is available that will aid in assigning physical significance to the determined parameters.

In some cases, multiple data sets or fluorescence decays are collected under different conditions in which unknown parameters are linked between them. The different conditions under which each decay is obtained within the family of fluorescence decay experiments include temperature, concentration, and excitation or emission wavelengths. To extract the desired parameters that link these fluorescence decays together the simultaneous analysis of each decay is performed and is referred to as *global analysis* [9]. This is done to more accurately recover complex decay phenomena over single-curve analysis.

Global analysis was performed using Spectra Solve™ in which an iterative convolution procedure was employed to fit sets of data and their corresponding instrument response functions. Global parameters (preexponential factors) are defined for the entire collection of decays while local parameters (time constants) are defined for each curve. During the fitting routine, local parameters are varied for each curve while the global parameters are held constant and the decays are fit individually. Subsequently, a global χ^2 is determined and then the global parameters are varied. The fitting routine attempts to minimize the global χ^2 which is defined as

$$\chi^2 = \frac{\sum_{i=1}^{n} \frac{\chi^2_{local,\,i}}{\chi^2_{best,\,i}}}{n}$$

where χ^2_{best} is the best fit found by letting all parameters vary and n is the number of curves [11].

Simultaneous global type analysis is also performed to recover rotational time constants and intrinsic anisotropy parameters as well as the overall anisotropy decay curve from time-resolved polarization experiments. In figure 3 there are two polarizers shown, one before the sample, the excitation polarizer (P_{ex}), and one after the sample, the emission polarizer (P_{em}). P_{ex} maintains the vertical polarization of the laser light. This vertically polarized light selectively excites only those molecules that have an absorption transition dipole that is oriented parallel to the excitation light. Due to this selective excitation the emission is no longer isotropic and is biased or polarized in the direction of the emission transition dipole. Obtaining time-correlated fluorescence decays at perpendicular ($\perp$) and parallel ($\parallel$) orientations by changing the orientation of the emission polarizer, P_{em}, one can track the depolarization/anisotropy of the emission.[4] The anisotropy decay, r(t), is determined by the relationship

$$r(t) = \frac{I_{\parallel}(t) - I_{\perp}(t)}{I_{\parallel}(t) + 2I_{\perp}(t)}$$

where $I_{\parallel}(t)$ and $I_{\perp}(t)$ are the time-dependent fluorescence decay components measured parallel and perpendicular to the vertically polarized excitation light, respectively [7,12]. The total fluorescence, F(t), for isotropic emission is given by [7,9,12]:

---

[4] In normal fluorescence decay experiments this bias of emission polarization still exists. But, orienting the emission polarizer, P_{em}, at an angle of 54.7° (the magic angle) the collected emission mimics the total *isotropic* fluorescence and therefore, polarization effects in the fluorescence decay are avoided.

$$F(t) = I_{\parallel}(t) + 2I_{\perp}(t).$$

Therefore the individual polarized components are expressed as:

$$I_{\parallel}(t) = \frac{F(t)}{3}\left(1 + 2r(t)\right)$$

$$I_{\perp}(t) = \frac{F(t)}{3}\left(1 - r(t)\right)$$

which show that I (t) and $I_{\perp}(t)$ are determined by the same set of fitting functions and thus, the same fitting parameters. The anisotropy decay (of a spherical chromophore) can be expressed as:

$$r(t) = r_0 e^{-t/\phi}$$

where r_0 is the anisotropy at time, t = 0, and is considered the intrinsic anisotropy in absence of any free rotation of the chromophore and ϕ is the rotational correlation time. Simultaneous global type fitting of the parallel and perpendicular fluorescence components will allow for a more accurate recovery of the anisotropy decay parameters.

Our time-correlated single photon apparatus utilizes a computer controlled, motorized polarizer (P_{cm}) that rotates to the parallel and perpendicular orientations at a desired interval, usually 1 to 2 minutes, until the desired precision is obtained, about 16,000 counts in the channel of maximum counts for I (t). Each polarized decay component is thus collected for the same amount of time and at short enough intervals so that laser instability will not affect the decay measurement. This eliminates the so called "G-factor" which corrects for instrumental instability as well as differences in transmission and detection of the two polarization components.

Time-correlated single photon counting allows reactions and molecular dynamics on a

nanosecond and subnanosecond time scale to be investigated. Although these time scales are very satisfactory for many applications, investigation of picosecond and femtosecond reactions and dynamics becomes rather limited. The main reason for this is that the time resolution for time-correlated single photon counting is determined by the jitter of the electronics and not the width of the laser pulse. The dye laser pulses have a FWHM of ~7 ps but due to electronic noise and jitter the IRF is actually much larger (FWHM 80-150 ps). Theoretically, fluorescence decay components can be recovered that are on the same order of the FWHM of the IRF or even slightly smaller but the confidence in such recovered parameters decreases also.

The 30 Hz Pump-Probe Transient Absorption Spectrometer

Many molecular reactions and dynamics occur on subpicosecond time scales. Therefore, to study such reactions, a pump-probe laser system that generates very short laser pulses is necessary. The 30 Hz pump-probe transient absorption spectrometer shown in figure 4 [13] utilizes a modelocked Antares 76-s Nd:YAG laser with 532-nm output to synchronously pump a Coherent 701 Rhomamine 6G dye laser which provides a continuous modelocked pulse train tunable over approximately 50 nm. Unlike the time-correlated single photon counting system, the time resolution of the pump-probe system *only depends upon* the width of the pulse exiting the dye laser. Thus, it is necessary to obtain the shortest pulse width possible. To aid in this, a DODCI/ethylene glycol saturable absorber is placed within the dye laser cavity. The ~7 ps dye laser pulses are further shortened to ~1 ps pulses due to the absorption of the leading edge of the pulse by the saturable absorber.

This tunable 1 ps pulse does not have the sufficient energy to provide the large population changes needed in the sample to observe the desired signal changes nor the energy

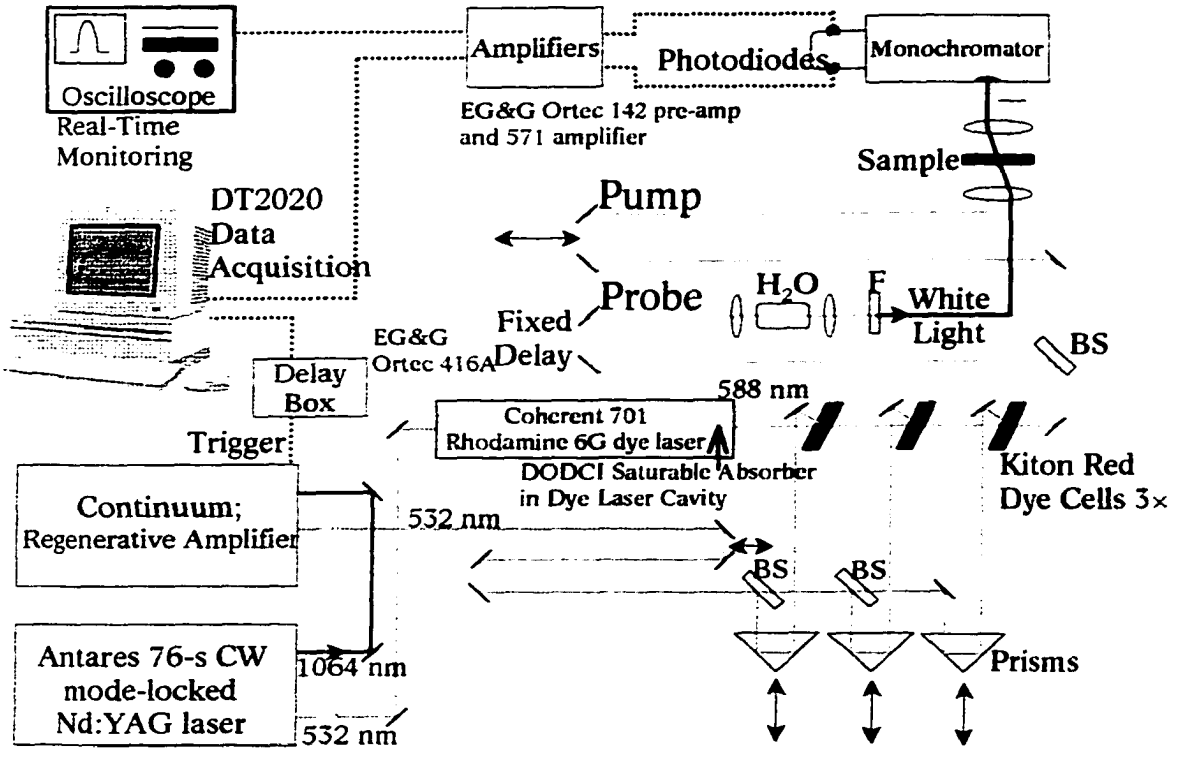

Figure 4. 30 Hz pump-probe transient absorption spectrometer.

(large electric fields) to take advantage of nonlinear effects in H_2O or sapphire to produce the white-light continuum necessary for two-color pump-probe experiments. Two-color experiments are preferable to one-color because they avoid coherent coupling artifacts (spikes) in the collected data when the two pulses are overlapped coherently at time zero ($t = 0$), as well as increase the probing range.

To produce the high energy electric fields the dye laser output pulses need to be amplified. This is accomplished through the combination of a Continuum 30 Hz regenerative amplifier and the Kiton Red dye amplifier system that it pumps. The regenerative amplifier accepts a 1064 nm seed pulse from the Antares Nd:YAG pumping laser and amplifies the ~100

ps 200 nJ pulses to ~200 mJ which are then frequency doubled via a KDP crystal and sent out to the dye amplifier.

The dye amplifier is based upon design by Perry et. al. [14]. The short, ~100 ps regenerative amplifier pulses, enters the Kiton Red dye cells of the dye amplifier and produces a large gain. When the timing is correctly matched, the dye laser pulses will enter the dye cells just shortly after the maximum of the regenerative amplifier pulse and become amplified at each stage in the amplifier system. A gain on order of 10^6 is obtained.

Time resolution is achieved by splitting the amplified pulses and sending part to a fixed delay stage ("probe") and the other to a variable translation stage ("pump") (Compumotor Model LX-L20-P54-AC), which is computer controlled via an IEEE interface. The "probe" side contains an H_2O cell for producing the white light continuum. The white light results from the nonlinear response of the index of refraction in the H_2O medium. For pumping in the visible the percentage of light going to the pump and probe are 20% and 80%, respectively. Since the pump is on a variable delay stage it is possible to vary the time between the pump and the probe pulses as to when they reach the sample while keeping the spatial overlap of both beams in the sample (figure 5). Knowing the speed of light and the delay step size in mm, the time delay between the pump and probe is known.

"Zero time" occurs when the pump and probe beams traverse the same distance and the pulses enter the sample at the same time. If the probe pulse enters the sample before the pump pulse, there will only be an attenuation of the probe beam (if there is ground state absorption at that particular wavelength) and no reactions or dynamics will be observed. When the probe pulse enters the sample after the pump pulse the probe pulse interrogates the change induced in

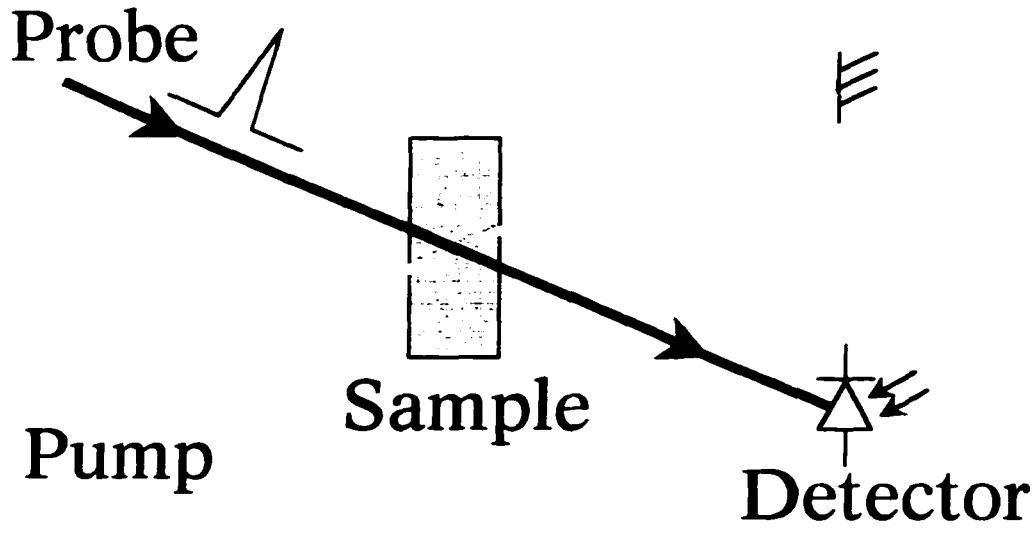

Figure 5. Depiction of the crossing or overlapping of the pump and probe pulses in the sample cell. The pump pulse induces a large population change in the sample. The white-light continuum probe pulse interrogates the sample when it arrives after the pump pulse. The pump beam is blocked while a photodiode detector monitors the transmission intensity of the probe beam versus delay time of the pump.

the sample by the pump pulse. The probe interrogation may reveal changes in the form of the following:

A *bleaching* of the sample may occur when probing in a region where there is ground state absorption of the sample. *Bleaching* is the result of there being *fewer* molecules in the ground state because of being promoted to the excited state by the pump beam. Therefore, there are *fewer* molecules to absorb the probe beam which results in an increase in transmission (decrease in absorbance) of the probe beam in comparison to before zero time.

Excited-state absorption may occur as the result of the probe beam being absorbed by the excited state of the sample (after the initial absorption of the pump beam). Thus, it is possible to interrogate S_1 to S_n transitions. This result would be observed as a decrease in the transmission of the probe beam through the sample or an increase in absorbance in comparison to before zero time.

Stimulated emission may occur as the result of probing in a region where the probe beam will interact with the excited state of the sample and cause the depopulation of the excited state by radiative means (given that the sample possesses a relatively large radiative lifetime). This *stimulated emission* causes an observed increase in transmission of the probe beam (decrease in absorbance) in comparison to before zero time. This makes *stimulated emission* difficult to distinguish from *bleaching* of the ground state unless the increase in transmission is observed in a spectral region where there is no ground-state absorption.

And finally, if excited-state reactions occur then changes in absorbance of the photoproducts will be observed and these processes will compete with the previously mentioned signals.

Each one of these signals can be present to some extent in a particular sample and would depend upon the wavelengths used to pump and probe. This makes interpretation of the data collected challenging.

Pump-probe kinetic traces are collected as a change in probe intensity versus stage delay converted into units of time. Prior to the sample the probe beam is split into the probe and a reference. Both the probe and reference beams are passed into a monochromator and detected

by two photodiodes. The reference is used for shot-to-shot normalization. The signals are amplified and sent to a DT2020 computer data acquisition board which also receives a trigger pulse from the regenerative amplifier. Real-time monitoring of both the pump and probe beams as well as the trigger pulse is accomplished via an oscilloscope. This is necessary to ensure that the trigger pulse is delayed properly to occur at the maximum of the detected probe pulse as well as monitoring the relative intensities of the probe and reference to determine if both beams are properly aligned in the monochromator. The blocking of one beam and then the other should result in their respective intensities going completely to zero. The jitter (noise) of each pulse (probe and reference) should occur in unison.

Customarily, the collected data is converted from probe intensity to absorbance, A, by the relation

$$A = \log\left(\frac{I_0}{I_t}\right)$$

where I_0 is the intensity at time, $t = 0$, and I_t is the intensity at any time, $t > 0$. This is done in order to directly relate the change in absorbance to a change in population of the sample.

The kinetic traces of absorbance change (ΔA) versus time are fit by iterative convolution of the trace with the laser pulse using Spectra Solve™. The laser pulse or instrument function is not directly measured as it is for time-correlated single photon counting. The laser pulse is assumed to approximately model a two-sided exponential, which is true for laser pulses shortened by a saturable absorber. In order to determine the appropriate temporal FWHM laser pulse to use for fitting the kinetic traces, a trace of a Nile Blue/methanol standard is collected and the rise time of the *bleach* is fit with computer generated laser pulses of various widths. The pulse that provides the best fit of the rising edge is the correct laser pulse to fit the subsequent

traces as long as the experimental conditions are held constant. Any changes or optimization of the pump-probe system would require a new standard trace to be collected.

By observing the rising edge of the standard as it is collected and displayed on the computer screen one can determine if the laser pulse is satisfactorily narrow. Typically, the rise of the Nile blue bleach should occur within 6-10 ps for a 4-5 ps pulse. An additional standard, Hypericin in sulfuric acid, is used to determine whether the translation stage is "flat" and if changes (steps) are observed in the trace due to a second laser pulse entering the sample within the time scale of the experiment. On a relatively long time scale, ~200 ps, hypericin in sulfuric acid should not show any transient behavior except a bleach when pumping and probing in areas of ground-state absorbance (lifetime of hypericin in sulfuric acid is 5.5 ns). Thus, the trace of Hypericin in sulfuric acid should appear flat after the instantaneous rise time of the bleach. If the translation stage is not "flat" the spatial overlap of the pump and probe beams (figure 5) will change and the trace may appear as a rise or a decay. Steps necessary to "flatten" the translation stage would need to be carried out before any further traces should be collected. This includes making sure that the pump beam is level as it enters the retroreflector on the translation stage and traverses the exact same level path after the retroreflector.

Kinetic traces are customarily fit to a sum of exponentials in order to extract the time constants for the processes of interest. In order to fit rising components in a trace, a negative pre exponential factor is utilized.

The 30 Hz pump-probe transient absorption spectrometer provides the necessary short pulses and high power to investigate fast molecular reactions and dynamics. The dye laser provides a tunable pump beam (~50 nm range) and after amplification, a white light continuum

probe beam is produced in which most of the visible spectrum can be utilized. This system thus lends itself to a variety of applications. Even in cases where the molecule may not be fluorescent, transient absorption traces may still be collected.

The Fluorescence Upconversion Spectrometer.

The backbone of the fluorescence upconversion system (figure 6 [15]) is the Ti:sapphire oscillator [16] which operates in a self mode-locked regime (passive mode-locking) to produce ~50 fs pulses with a broad gain bandwidth of 670 to 1100 nm, offering a large tuning range. The Ti:sapphire oscillator is within the large boxed region in figure 6. Optimized operation of the oscillator will provide stable output at ~500 mW and whose spectral bandwidth is centered around 800 nm. Self mode-locking is the result of nonlinear interactions induced by large electric fields within the 4.75 mm, 0.015% doped Ti:sapphire active medium. The Ti:sapphire oscillator is pumped by a intracavity doubled diode-pumped CW Millenia V from Spectra Physics. The active medium for this pump laser is a Nd:YVO_4 crystal with 5 W maximum, 532-nm output.

The prisms inside the cavity (P1,P2: figure 6) and just outside the cavity (P3,P4) are important to compensate for group velocity dispersion (GVD) due to differences in the group velocities of the modes oscillating within the cavity. This dispersion broadens the temporal shape of the laser pulse. As with the 30 Hz pump-probe system the ultimate time-resolution of the fluorescence upconversion system *depends only* upon the temporal width of the pulse. The prisms therefore, help to keep the pulse as short as possible and preserve the time-resolution of the experiment which is on the order of picoseconds to subpicoseconds. P1 and P2 are fused silica and cut at Brewster's angle while P2 and P3 are made of SF10 glass (higher refractive index glass) also cut at Brewster's angle. A small portion of the 800 nm oscillator output is

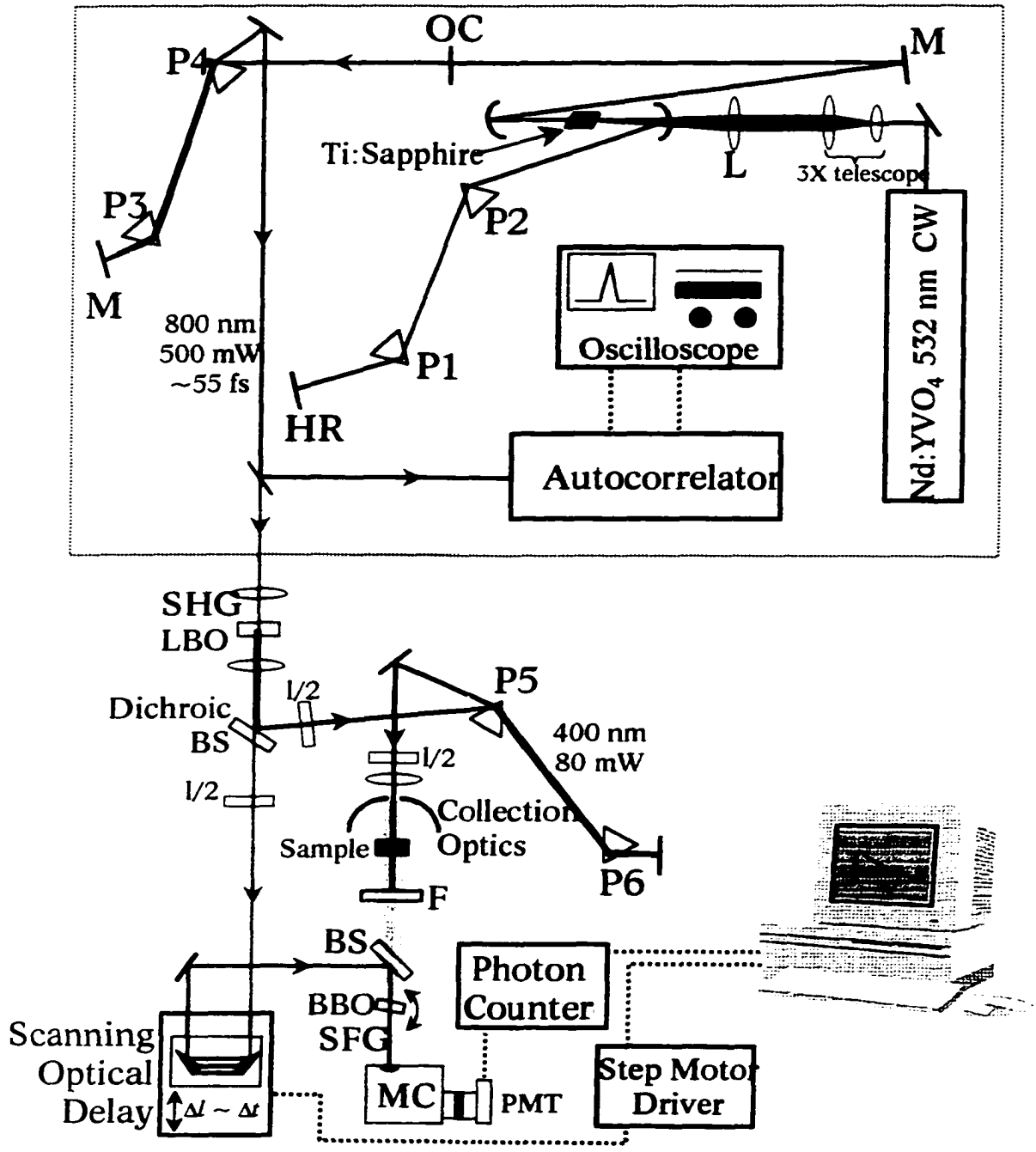

Figure 6. The fluorescence upconversion spectrometer. The Ti:sapphire oscillator is located within the boxed region.

deflected via a glass microscope slide into an autocorrelator of similar design as used in the single photon counting system. A measure of the temporal profile of the oscillator pulses can therefore be obtained and continuously monitored throughout the experiment.

Optimization of the oscillator's power and stability is critical in order to obtain the maximum possible power from second harmonic generation of the 800 nm fundamental in an oven protected LBO (or BBO) nonlinear crystal. The crystal is 1 mm thick and specially cut for use with the 800 nm fundamental oscillator output. Fine adjustments of the SHG crystal in both the angle and distance from the first focusing lens are necessary to maximize the 400 nm second harmonic power. Typically, 60-120 mW of vertically polarized SHG is obtained (15-20% conversion efficiency). Prisms, P5 and P6, are placed in the 400 nm beam path to compensate for the blue light GVD in order to maintain the shortest possible pulse.

A dichroic mirror splits the SHG from the residual fundamental after the LBO (or BBO) crystal. The residual 800 nm light is transmitted to a scanning optical delay stage and then focused into a BBO nonlinear crystal, phase-matched for sum frequency generation (SFG). The SHG 400 nm light is focused into the sample cell. The sample cell is a quartz flow cell where the sample is allowed to circulate. The sample fluorescence is collected by a parabolic reflector (a microscope objective has also been successfully used) and focused into the phase-matched SFG BBO crystal where it is mixed with the delayed residual 800 nm fundamental.

This nonlinear optical mixing technique creates a light *gate* [17]. The light gate is "open" only when the higher power fundamental (800 nm) gate pulse is temporally overlapped with the fluorescence signal (figure 7). The resultant sum frequency or upconverted signal is proportional to the instantaneous fluorescence intensity. Thus, the whole temporal shape of the

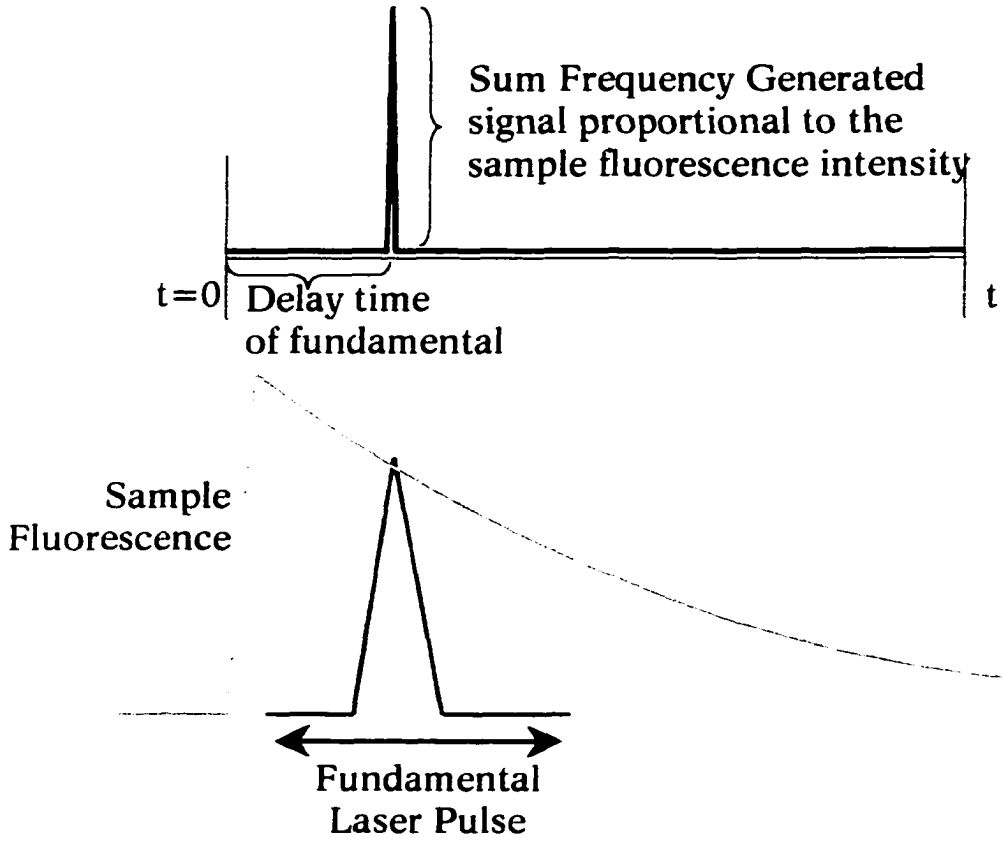

Figure 7. Depiction of the fluorescence upconversion light gate. The gate is open and a SFG signal is detected only when the fundamental laser pulse is overlapped with the sample fluorescence. The SFG signal at time, t, is directly proportional to the fluorescence intensity of the sample at the corresponding time. The amount of time the light gate is open and the overall time resolution of the experiment is determined by the fundamental laser pulse.

fluorescence decay can be mapped out or reconstructed by delaying the fundamental pulse with respect to the sample fluorescence (or more properly, with respect to the SHG sample excitation laser pulse). The collected data essentially consists of the measured upconverted signal as a function of delay time.

More rigorously, the observed signal S(t) at the sum frequency, $\nu_f + \nu_g$, as a function of delay time, t, is given by:

$$S(t) = \int_{-\infty}^{t} F_{\nu}(t')P_{\nu}(t-t')dt'$$

where $P_{\nu}(t)$ is the pulse shape of the gate pulse at the frequency ν_g and $F_{\nu}(t)$ is the sample's temporal fluorescence profile at time t and frequency, ν_f.

$F_{\nu}(t)$, as explained in the single photon counting section, is the convolution of the true fluorescence decay, $F'_{\nu}(t)$,with the 400 nm second harmonic sample excitation pulse, $P_{2\nu}(t)$, and is given by:

$$F_{\nu}(t) = \int_{-\infty}^{t} F'_{\nu}(t')P_{2\nu}(t-t')dt'$$

Combining $S(t)$ and $F_{\nu}(t)$ gives:

$$S(t) = \int_{-\infty}^{t} F'_{\nu}(t')C_{3\nu}(t-t')dt'$$

where $C_{3\nu}(t)$ is the measured cross-correlation function for the fundamental gate pulse and SHG sample excitation pulse which is given by:

$$C_{3\nu}(t) = \int_{-\infty}^{t} P_{2\nu}(t')P_{\nu}(t-t')dt'$$

This cross-correlation function is the appropriate instrument response function to be used in fitting (nonlinear least-squares iterative convolution) the collected gated fluorescence data to extract the parameters, amplitude and lifetime, that best describes the true fluorescence decay, $F'_{\nu}(t)$, of the sample. The cross-correlation is measured by the generation of the third harmonic of the fundamental gate pulse through the same optics used for the upconversion of the sample fluorescence.

Because of the low efficiency of SFG process the upconverted signal is detected by means of single photon counting. A monochromator spectrally isolates the upconverted signal and is detected using a Hamamatsu R760 photomultiplier tube (PMT). The PMT utilizes a UG11 UV-pass filter and is operated at maximum sensitivity. The PMT output is amplified by an SRS SR-445 DC-300 MHz preamplifier. A SR400 gated photon counter operated in CW mode registers the arrival of photon events at the respective delay time of the gate pulse and is subsequently recorded via personal computer.

Fluorescence anisotropy decays are also determined by collecting sum frequency correlation functions for emission polarized parallel, $S_{\parallel}(t)$, and perpendicular, $S_{\perp}(t)$, to the excitation polarization. Cross-correlation functions for the gate and excitation pulses are measured also. The excited-state decay law, F(t), as well as the anisotropy decay, r(t), are related to the "deconvoluted" fluorescence decays, as shown similarly for time-correlated single photon counting data, by:

$$F(t) = F_{\parallel}'(t) + 2F_{\perp}'(t)$$

$$r(t) = \frac{F_{\parallel}'(t) - F_{\perp}'(t)}{F_{\parallel}'(t) + 2F_{\perp}'(t)}$$

The obvious advantage then of utilizing the Ti:sapphire oscillator with the narrow femtosecond pulses is that the open time and resolution of the light gate are determined by the fundamental gate pulse width. The detected upconverted signal has an additional advantage of being spectrally isolated from both the sample fluorescence and the fundamental laser pulse. This aids in detection. One disadvantage is the extremely careful alignment of the sample fluorescence, laser fundamental, and the phase-matching angle (controlled within ±0.1 degrees)

of the crystal in order to upconvert the desired fluorescence wavelengths. Another disadvantage is the generally low efficiency of nonlinear processes. Above all else, the main advantage in utilizing this technique, especially for our group's work, is the fact that *fluorescence upconversion measures only excited-state fluorescence*. The collected data does not have any contributions from ground-state bleaching, excited-state absorbance or stimulated emission processes as does regular pump-probe techniques. Used along with pump-probe techniques, fluorescence upconversion can help to interpret more clearly the kinetics displayed in pump-probe traces.

Background and Dissertation Organization

Chapters I-V in this dissertation consist mainly of individually published papers or papers submitted for publication. Chapter VI, which discusses the real-time detection of fecal and ingesta contamination, has not been submitted for publication as it appears in this thesis, but a revised version of this chapter has been submitted to *The Proceedings of the National Academy of Sciences* for publication. Each chapter includes its own general conclusion section. Following the numbered chapters, the remainder of the dissertation is comprised of a brief overall General Conclusion and Summary section followed by two Appendix sections. Appendix A briefly illustrates, in a mathematical fashion, the concept of phase-sensitive detection of the lock-in amplifier. It also illustrates the reason for a dual lock-in amplifier design used in the development of the F-Detector prototypes discussed in chapter VI. Appendix B is also related to chapter VI and shows general schematic diagrams of two op amp circuits used in the second generation prototype F-Detector. Finally, as part of this section, I will briefly explain some background to the work in the chapters that follow.

The photophysics and properties of the indole chromophore (figure 8a) have been intensively investigated for many years. One of the major reasons for this is that indole is the chromophore of the amino acid tryptophan (figure 8b). Tryptophan is one of three fluorescent amino acids that are constituents of peptides and proteins in biological systems (phenylalanine and tyrosine being the others). Tryptophan has received much of the attention due to the unusually large Stokes shift when the indole chromophore experiences polar environments [18,19]. This sensitivity of tryptophan to its environment has been exploited to elucidate protein structure and dynamics as well as indole's (and its derivatives) equilibrium partitioning within organized media, such as micelles.

The sensitivity of the indole chromophore to the polarity of its environment is due to the presence of two low-lying excited singlet states which have been designated as ^1L_a and ^1L_b [18,20,21]. Normally in nonpolar media the ^1L_b state is the lower lying of the two states and is therefore the emitting state. ^1L_b is rather insensitive to the polarity of the environment. In contrast, the ^1L_a state is very sensitive to the polarity of the environment as a result of its large transition dipole moment and greater charge transfer character. In polar media the ^1L_a relaxes to lower energies and in some cases may lower itself below the ^1L_b state and become the emitting state. This relaxation is the reason for the large Stokes shift in the steady-state emission of the indole moiety in polar solvents. Rehms and Callis, using polarized two-photon fluorescence techniques, have resolved these two states and verified the established scheme regarding their response to solvent perturbations [20].

Laser based time-resolved experimental techniques also exploit the properties of these two low-lying states of the indole moiety. In general, it is found that the radiative rate of the ^1L_a

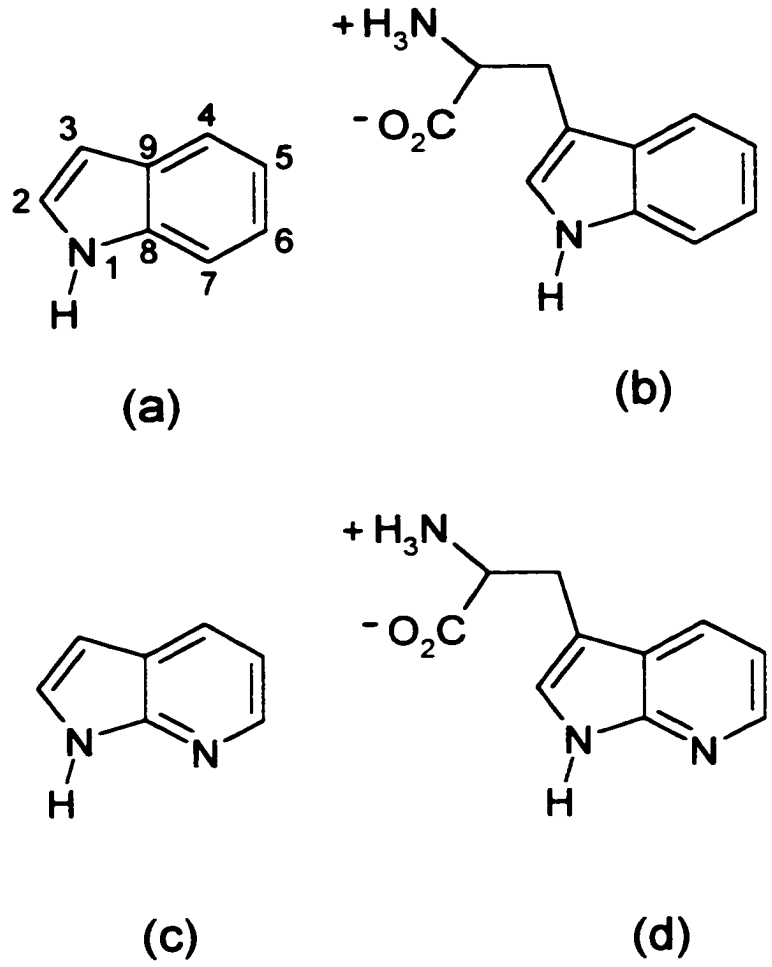

Figure 8. Structures of (a) indole, (b) tryptophan, (c) 7-azaindole, and (d) 7-azatryptophan.

state is longer than that of the ^1L_b [18]. Therefore it is possible (in theory) to determine the environment of the indole moiety based upon the magnitude of the Stokes shift and the lifetime of the fluorescence decay. A nonexponential decay would then reveal more than one type of environment experienced by the chromophore.

In chapter I we exploit these properties as a means to determine the partitioning of 3-methylindole into Brij-35 micelles. Because 3-methylindole is hydrophobic one can conclude that it will have an affinity for the nonpolar micelle phase. 3-methylindole is a rather foul smelling, volatile component of animal waste, especially sensed near hog farms. Organized media, such as micelles, present a means of trapping 3-methylindole and subsequently lowering its vapor pressure. We quantified 3-methylindole's interaction with the nonpolar phase of the micelle by obtaining time-correlated fluorescence decays of the 3-methylindole/micelle system. The parameters of the fluorescence decays allowed us to determine the equilibrium concentrations of 3-methylindole in three generalized phases of the system. The fluorescence decays were well described by three exponentials which seemed to model our system quite well. But, fitting a heterogeneous system such as this to a finite number of discrete exponentials actually may not accurately represent the system. In heterogeneous systems where a chromophore may experience a distribution of environments it is more proper to fit the fluorescence decays with distributions of lifetimes, each environment contributing to the overall observed decay [22,23]. Each distribution mode would have a certain FWHM centered around the fitted discrete lifetime. The FWHM would be a measure of the distribution of environments the chromophore experiences. Unfortunately, sufficient lifetime distribution fitting software was not available at the time this work was completed. But, for our purposes, our discrete lifetime fitting was sufficient to quantify the 3-methylindole/micelle interaction.

Although it might seem that the detectable differences in the radiative rates of the two low-lying excited singlet states, ^1L_a and ^1L_b, might be extended to the study of protein structure and dynamics using tryptophan as a probe, as in the case of the "simple" 3-methylindole/micelle

system, there are some important complications. The foremost complication is the intrinsic nonexponential fluorescence decay of tryptophan. Indole and 3-methylindole have single exponential fluorescence decays. Also, in natural proteins there may very well be multiple occurrences of the tryptophan residue. Consequently, any attempt to assign any specific physical significance to the fluorescence decay of any one or all tryptophans within the protein is rendered completely ambiguous.

As a result, the Petrich group has devoted considerable effort in developing and characterizing nonnatural amino acids, such as 7-azatryptophan (figure 8d), and their incorporation into peptides and proteins [24]. 7-azatryptophan has a single exponential fluorescence lifetime decay in water and its absorption and emission spectra are red shifted 46 nm and 10 nm respectively from that of tryptophan. Thus, 7-azatryptophan can be selectively excited and detected efficiently when incorporated into proteins, even in the presence of other tryptophan residues, and has great potential as an alternative probe of protein structure and dynamics.

Chapter II is an example of such an investigation in which 7-azatryptophan and 5-hydroxytryptophan (another promising nonnatural amino acid) were incorporated into the protein tropomyosin. Movement is fundamental to all living creatures. Of great importance to the further understanding of the human body is the investigation of what regulates the movement or contraction of muscle tissue. The protein tropomyosin works in combination with troponin and actin in the regulation of muscle contraction (figure 9) [25,26]. Incorporation of the aforementioned nonnatural amino acids into one or all of these proteins followed by laser-based time-resolved investigation will shed further light in the structure and function of these proteins.

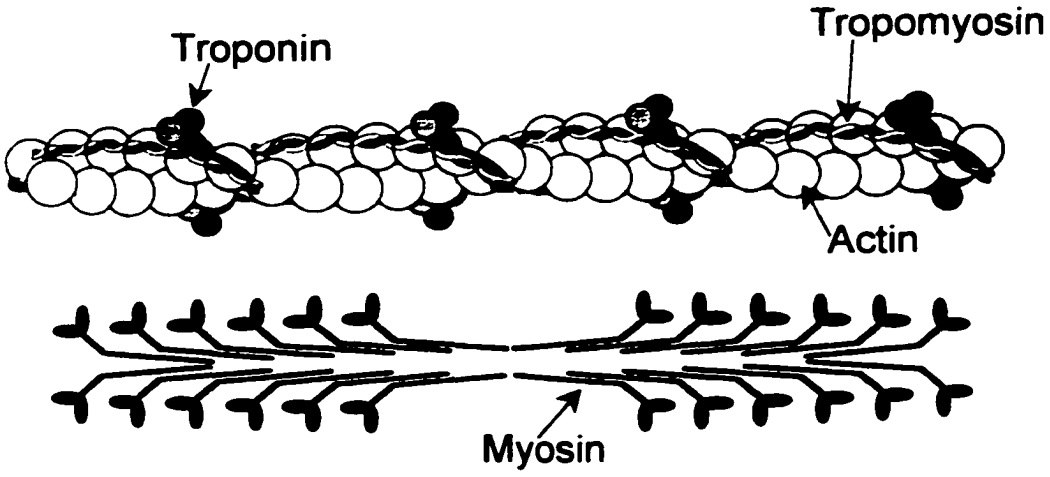

Figure 9 The top picture is the muscle thin filament made up of troponin, tropomyosin, and actin proteins. Myosin (bottom picture), makes up the muscle thick filaments. For muscle contraction to occur the myosin headgroups must interact with the actin monomers on the thin filament. Ca^{2+} induced changes in troponin cause movement of the tropomyosin dimers away from the myosin/actin interaction sites allowing myosin and actin to interact and contract the muscle. Figures from ref. 25 with kind permission from Kluwer Academic Publishers.

Prior to this, one must elucidate the properties of these nonnatural amino acids within the protein itself. Dr. Chuck Farah at the University of São Paulo in Brazil, incorporated 7-azatryptophan and 5-hydroxytryptophan into tropomyosin and allowed us the opportunity to spectroscopically investigate their properties.

Tropomyosin possesses a heptad repeat and forms an α-helical coiled-coil dimer. Each tropomyosin dimer extends across seven actin protein monomers that make up muscle thin filaments. Troponin is actually made up of three subunits one of which is a Ca^{2+} binding protein [25]. The myosin proteins (figure 9) make up the thick muscle filaments. Muscle contraction

occurs when the projecting heads of myosin reach out and make contact with the actin molecules on the thin filaments. The release of Ca^{2+} initiates the "signal" for muscle contraction. Ca^{2+} ions bind to troponin which subsequently modifies the position of the tropomyosin dimer so that myosin can interact with the actin protein monomers [26]. Therefore, to elucidate the mechanisms and dynamics of this complex process the structures of the proteins must be known as well as the types of interactions that exists between the proteins themselves. Chapter II provides a rich summary of the properties of tropomyosin incorporated with 7-azatryptophan and 5-hydroxytryptophan that will further enhance the progress toward understanding muscle contraction.

Along with the study of protein structure and dynamics and elucidating the photophysical properties indole and 7-azaindole based chromophores, additional effort has been expended in investigating the naturally occurring antiviral/antitumor compounds, hypericin and hypocrellin a (figure 10). Laser-based pump-probe and fluorescence upconversion spectroscopies were utilized to determine the photophysical properties and biological action of these two molecules.

Hypericin is extracted naturally from the yellow flowering tops of St. John's Wort (*Hypericum perforatum*) (figure 11). St. John's Wort is found growing in many parts of the world and has been used as a folk medicine to treat a wide variety of illnesses for many centuries. The recent upsurge in scientific and clinical study of hypericin is due to its high toxicity toward tumors and viruses, including HIV. Extracts of St. John's Wort are also under investigation because of antidepressant properties, although there is some debate as to whether hypericin is the actual compound responsible for the antidepressant properties. The interesting feature of hypericin's viral toxicity is the requirement that light must first be absorbed by the

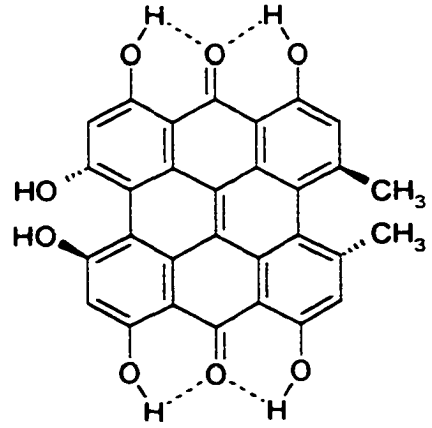

Hypericin

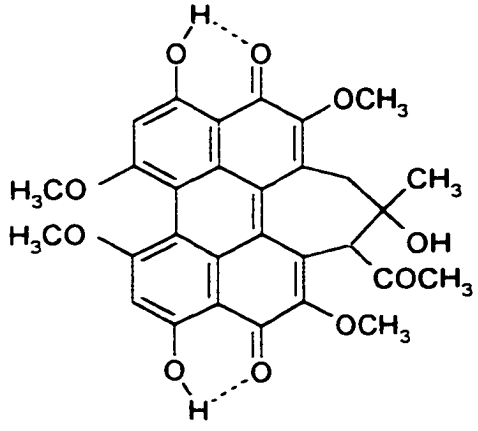

Hypocrellin

Figure 10. 2D structures of the naturally occurring antiviral/antitumor agents hypericin and hypocrellin a.

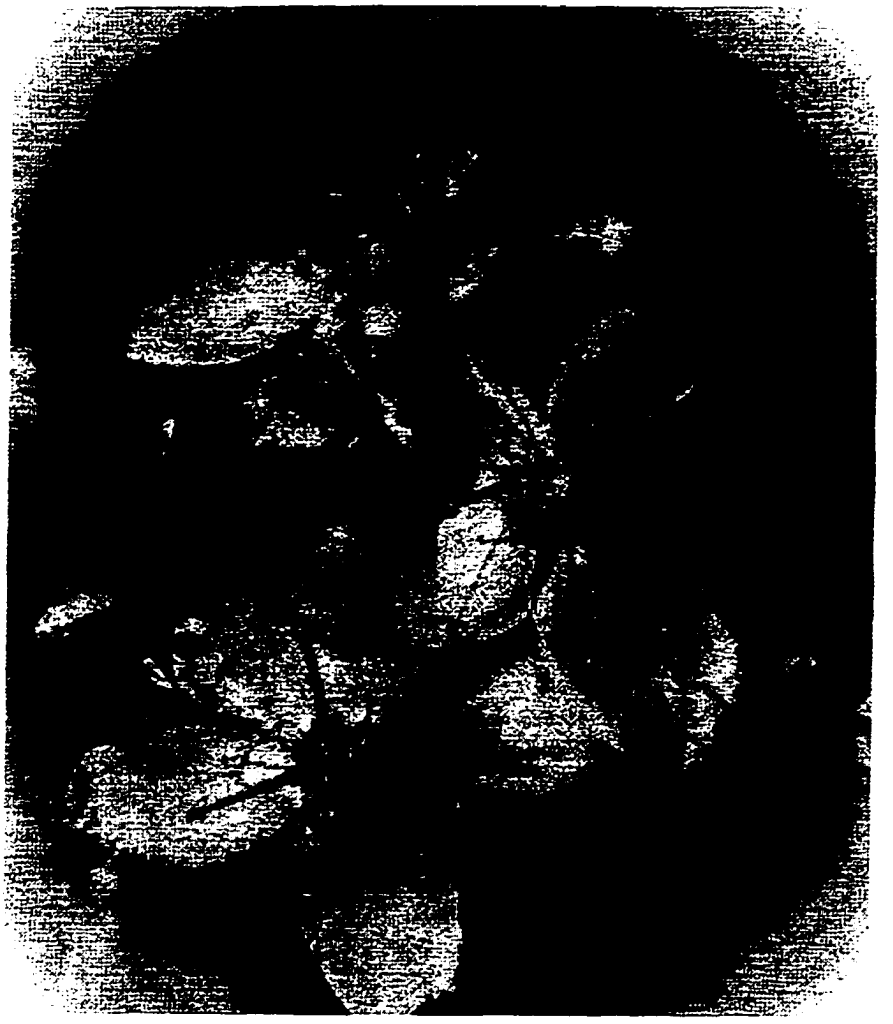

Figure 11. The yellow flowers of St. John's Wort (*Hypericum perforatum*). Light-activated antiviral agent hypericin can be extracted from the yellow petals and leaves.

molecule [27]. Therefore, the elucidation of its photophysical properties is of fundamental biological importance. Synthetic hypericin analogs including *O*-hexamethoxy hypericin and mesonaphthobianthrone, and a related compound, hypocrellin *a*, have been instrumental in elucidating hypericin's photophysics.

In previous work [13,15,16], the Petrich group utilized pump-probe techniques to study hypericin and other related compounds. Many workers have thought that hypericin's photodynamic and pharmacological properties where due to the production of singlet oxygen. But Fehr et al. [28], revealed that hypericin retains its photodynamic antiviral properties even under hypoxic conditions. Hypericin does generate triplet species [29] and subsequently generates singlet oxygen but, it was revealed that there were other photodynamic processes that involved the excited-state of hypericin. Hypericin undergoes intramolecular hydrogen atom transfer and is able to photoacidify its surroundings [30]. This light-induced pH decrease in hypericin's surroundings is implicated in its pharmacological function even when under hypoxic conditions. Excited-state hydrogen atom transfer is evident in the time-resolved absorption (stimulated emission) spectra and kinetic traces that indicate that the excited-state of hypericin grows in on a time scale of ~10 ps. Because synthetic model compounds, which do not have labile protons that can undergo hydrogen-atom transfer (or if hypericin's carbonyl groups are protonated in the ground state by the addition of sulfuric acid), do not exhibit this growing in of the excited state, this ~10 ps process is attributed to excited-state hydrogen-atom transfer [31]. It is also shown that for mesonaphthobianthrone to exhibit emission spectra similar to hypericin its carbonyl groups *must* be protonated.

As discussed previously, pump-probe kinetic traces can be difficult to interpret and

assign physical significance to extracted rate constants due to the many competing processes that may contribute to the observed transient behavior, namely, stimulated emission, ground-state absorbance, ground-state bleach, and transient kinetics. Therefore, chapter III describes the use of fluorescence upconversion spectrometry, which *only detects excited-state emission*, to confirm that the 10 ps second transient in the pump-probe data is due to excited-state hydrogen atom transfer and is the primary photophysical event in hypericin. There are no ambiguities in time-resolved fluorescence as there are in pump-probe transient absorption. Fluorescence upconversion is utilized to complement the pump-probe technique.

To further characterize this excited-state hydrogen-atom transfer process in hypericin and hypocrellin a, in developing a unified picture describing the overall photophysics, the excited-state intramolecular hydrogen-atom transfer reactions were measured as a function of temperature. Chapter IV describes these experiments and confirms that the negligible activation energy for hypericin is consistent with an adiabatic hydrogen-atom transfer process [32]. For the low temperature studies a MMR Technologies Joule-Thompson refrigerator was utilized. The temperature drop of the sample arises from the adiabatic expansion of nitrogen or argon gas from high pressure to low (atmospheric) pressure. Relatively stable temperatures can be obtained as low as 80 K.

Chapters V and VI describe a laser-based detection system, the F-Detector, to detect fecal and ingesta contamination on meat carcasses utilizing intrinsic fluorescent markers. F420, a methanogenic electron carrier, was the first consideration for the intrinsic marker. It has an absorption maximum at 420 nm and an emission maximum at 470 nm. Investigation of actual fecal and ingesta samples revealed an additional marker with much broader absorption

throughout the visible spectrum and a relatively large narrow emission maximum at around 670 nm. This marker was identified as pheophorbide *a*, a chlorophyll metabolite of herbivorous animals. Therefore, the F-Detector was designed and built to detect pheophorbide *a* within the fecal material.

By detecting the fecal material on the carcass we in essence detect bacterial contamination, namely *E. coli*. contamination. This system will provide a much faster and more sensitive means of inspecting meat carcasses as they are processed.

References

1. Plinius, Naturalis Historia, XXII; 49.

2. Svelto, O. *Principles of Lasers*, 2nd Edition; Plenum Press: New York, 1982. Reprinted from Principles of Lasers, page *v*: "An elaboration of the quotation from Pliny the Elder: The Laser during the Graeco-Roman civilization - During the Graeco-Roman civilization (roughly from the 6th century B.C. to the 2nd century A.D.) the Laser was well known and much celebrated. It was in fact a plant (perhaps belonging to the *Umbelliferae*) which grew wild over a large area around Cyrene (in present-day Libya). Sometimes also called *Laserpitium*, it was considered to be a gift of God due to its almost miraculous properties. It was used to cure a variety of diseases, from pleurisy to various epidemic infections. It was an effective antidote against the poison of snakes, scorpions, and enemy arrows. Its delicate flavor led to its use as an exquisite dressing in the best cuisine. It was so valuable as to be the main source of Cyrenaean prosperity and it was exported to both Greeks and Romans. During the period of Roman domination, it was the only tribute paid by the Cyrenaeans to the Romans, who kept the Laser in their coffers together with their golden ingots. What is perhaps the best testimony to the Laser of those days is to be found on the celebrated Arcesilao cup (now in the Cyrene Museum), where porters can be seen loading the Laser onto a ship under the supervision of King Arcesilao. Both Greeks and Romans tried hard, but without success, to grow the Laser in various parts of *Apulia* and *Ionia* (in the south of Italy). Consequently the Laser became more and more rare and seems to have disappeared around the 2nd century A.D. Ever since then, despite several efforts, no one has been able to find the Laser in the deserts south of Cyrene, and so it remains the lost treasure of the Graeco-Roman civilization.

3 Ingle, J.D.; Crouch, S.R. *Spectrochemical Analysis*; Prentice Hall: New Jersey, 1988; chapters 1 and 4.

4. Wright, J.C.; Wirth, M.J. *Anal. Chem.* **1980**, *52*, 1087A-1095A.

5. Couillaud, B.; Fossati-Bellani, V. *Lasers & Applications* 1985, *January*, 79-94.

6. Saleh, B.E.A.; Teich, M.C. *Fundamentals of Photonics*; John Wiley & Sons, Inc.: New York, 1991; Chapter 14.

7. O'Connor, D.V.; Phillips, D. *Time-correlated Single Photon Counting*; Academic Press: New York, 1984.

8. Bevington, P.R.; Robinson, D.K. *Data Reduction and Error Analysis for the Physical Sciences*; McGraw-Hill, Inc.: New York, 1992.

9. Lakowicz, J.R., Ed. *Topics in Fluorescence Spectroscopy, Volume 2; Principles*; Plenum Press: New York, 1991; Chapters 4 & 5.

10. Lakowicz, J.R., Ed. *Topics in Fluorescence Spectroscopy, Volume 1; Techniques*; Plenum Press: New York, 1991; Chapter 1.

11. Das, K.; Ashby, K.D.; Smirnov, A.V.; Fernando, C.R.; Petrich, J.W.; Farah, C.S. *Photochem. Photobiol.* **1999**, *70*(5), 719-730.

12. Lakowicz, J.R. *Principles of Fluorescence Spectroscopy*; Plenum Press: New York, 1983; Chapter 5.

13. Fehr, M.J. *Photophysics and mechanism of photoinduced antiviral action of the natural products, hypericin and hypocrellin a*; Iowa State University: Ames, IA, 1995.

14. Perry, M.D.; Landon, O.L.; Weston, J.; Ettlebrick, R., *Opt. Lett.* **1989**, *14*, 42.

15. Smirnov, A.V. *Primary photoprocesses of light-activated antiviral and antitumor agents, hypericin and hypocrellin*; Iowa State University: Ames, IA, 1999, chapter 2.

16. English, D.S. *Elucidation of the primary photophysical processes in the light-activated agents, hypericin and hypocrellin*; Iowa State University: Ames, IA, 1998.

17. Mahr, H.; Hirsch, M.D. *Optics Communications* **1975**, *13*, 96-99.

18 Meech, S.R.; Phillips, D. *Chem Phys.* **1983**, *80*, 317-328.

19. Meech, S.R.; Phillips, D.; Lee A.G. *Chem. Phys. Letters* **1982**, *92*, 523-527.

20. Rehms, A.A.; Callis, P. R. *Chem. Phys. Letters* **1987**, *140*, 83-89.

21. Hansen, J.E.; Rosenthal, S.J.; Fleming, G.R. *J. Phys. Chem.* **1992**, *96* ,3034-3040.

22. Ramamurthy, V., Ed., *Photochemistry in organized & constrained media*; VCH Publishers, Inc.: New York, 1991; Chapter 13.

23. James, D.R.; Ware, W.R. *Chem. Phys. Letters* **1985**, *120*, 455-465.

24. Smirnov, A.V.; English, D.S.; Rich, R.L.; Lane, J.; Teyton, L.; Schwabacher, A.W.; Luo, S.; Thornburg, R.W.; Petrich, J.W. *J. Phys. Chem.* **1997**, *101B*, 2758-2769.

25. Bagshaw, C.R. *Muscle contraction*, 2nd edition; Chapman & Hall: London (now Kluwer Academic Publishers), 1993. Chapter 4, *Contractile proteins* and Figures 4.7 and 4.14.

26. Cohen, C. *Sci. Am.* **1975**, *233*(5), 36-45.

27. Carpenter, S.; Kraus, G.A.; *Photochem. Photobiol.* **1991**, *53*, 169-174.

28. Fehr, M.J.; Carpenter, S.; Petrich, J.W. *Bioorg. Med. Chem. Lett.* **1994**, *4*, 1339-1344.

29. Park, J.; English, D.S.; Wannemuehler, Y.; Carpenter, S.; Petrich, J.W. *Photochem. Photobiol.* **1998**, *68*, 593-597.

30. Fehr, M.J.; McCloskey, M.A.; Petrich, J.W. *J. Am. Chem. Soc.* **1995**, *117*, 1833-1836.

31. Gai, F.; Fehr, M.J.; Petrich, J.W. *J. Phys. Chem.* **1994**, *98*, 5784-5795.

32. Das, K.; English, D.S.; Petrich, J.W. *J. Phys. Chem.* **1997**, *101A*, 3241-3245.

CHAPTER I. THE EFFECT OF MICELLES ON THE STEADY-STATE AND TIME-RESOLVED FLUORESCENCE OF INDOLE, 1-METHYLINDOLE, AND 3-METHYLINDOLE IN AQUEOUS MEDIA

A paper published in *Analytical Chemistry*[1]

Kyle D. Ashby, Kastuv Das, and Jacob W. Petrich[2]

Abstract

3-Methylindole (skatole) is a component of animal waste and is, consequently, a primary component in odor problems arising in livestock management, notably swine production. The ability to probe and to exploit the interactions of 3-methylindole with micelles has important implications for monitoring and controlling odor problems. The effect of a surfactant (Brij-35) on the fluorescence properties of indole, 1-methylindole, and 3-methylindole in aqueous solutions is reported. Steady-state fluorescence spectra reveal a blue shift in the emission as the surfactant concentration is increased, while the absorption spectra are practically unaffected. Time-resolved fluorescence measurements reveal shorter average lifetimes for 3-methylindole (3-MI) as the Brij-35 concentration is increased. The fluorescence decay of 3-MI in water is described well by a single exponential, whereas, at the highest Brij-35 concentration, a triple exponential is necessary to describe the fluorescence decay. The contributions of each component in the fluorescence decay are used to determine the extent of 3-MI partitioning into the micelle phase. It is found that 93% of the 3-MI molecules partition into the micelle at the

---

[2] Author to whom correspondence should be addressed.

highest Brij-35 concentration used. The equilibrium constant for the association between the micelles and the 3-MI molecules is determined to be 2.6×10^4 M^{-1}. In addition, the reduction of 3-MI in the vapor phase by addition of a dry surfactant, lecithin, is also demonstrated.

Introduction

3-Methylindole (skatole) is an important component of animal waste. Because of its noxious odor, 3-methylindole is a primary problem in livestock management, especially in swine production [1-7]. In this article, we consider the effect of surfactants on the steady-state and time-resolved fluorescence of indoles in the aqueous and vapor phases. Micelles can be used as model, and perhaps practical, systems capable of trapping small molecules such as indoles. Understanding under what conditions 3-methylindole can be sequestered and developing means of detecting it are of great practical interest.

The fluorescence properties of indoles (Figure 1.1a-c) are extremely sensitive to the environment. This sensitivity arises from the presence of two closely spaced excited singlet states (Figure 1.2), which are traditionally denoted ^1L_a and ^1L_b [8-15]. The energy of the ^1L_b state is insensitive to the solvent, and it is the lower lying of the two excited singlet states in nonpolar solvents. In nonpolar solvents, ^1L_b is the emissive state [16]. On the other hand, the ^1L_a state interacts strongly with the solvent. In nonpolar media it lies above ^1L_b, but in polar media the ^1L_a state strongly interacts with the solvent and subsequently lowers its energy relative to that of ^1L_b, thus becoming the emissive or fluorescent state. Because of the interaction of these two excited states with their environment (and with each other), shifts of emission spectra to higher energies (blue shifts) are excellent signatures of the probe molecule moving to a nonpolar environment [17,18]. Also, as the indole moves to a nonpolar environment, the fluorescence

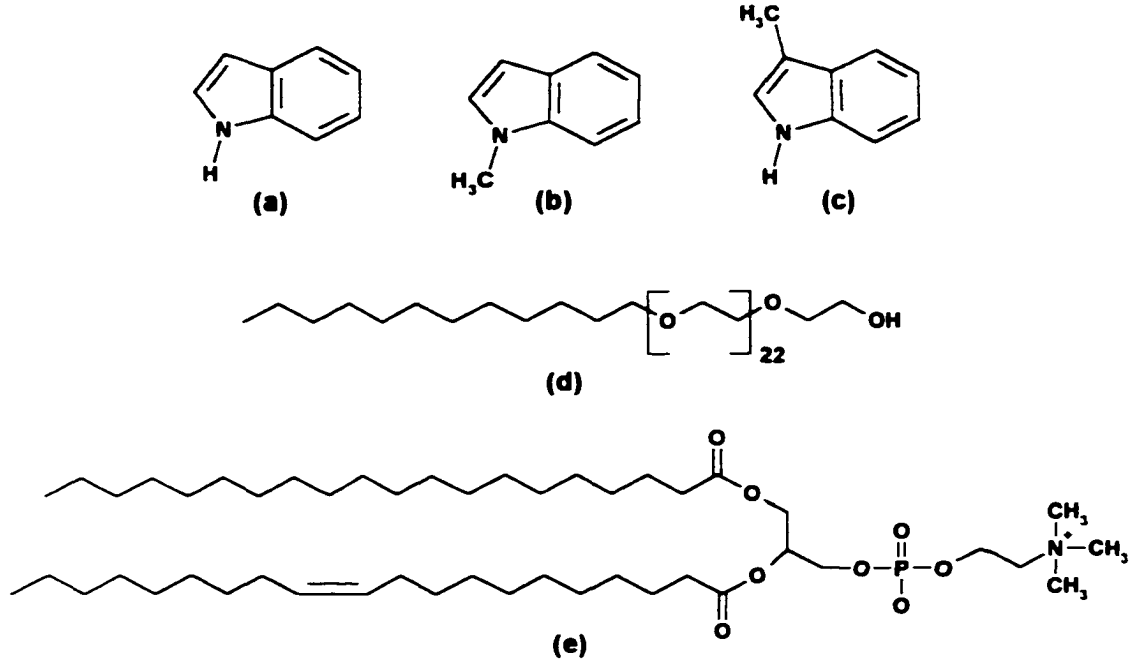

Figure 1.1. Structures of (a) indole, (b) 1-methylindole, (c) 3-methylindole, and (d) Brij-35 (poly(oxyethylene)23 lauryl ether). (e) A general chemical structure of lecithin (phosphatidylcholine). The long-chain fatty acid groups, by convention, occupy positions 1 and 2 of the glycerol bridge, while the phosphorylcholine headgroup occupies position 3. The hydrocarbon chains vary in length and saturation, with the more unsaturated chain in position 2, as represented by the double bond in the chain at this position.

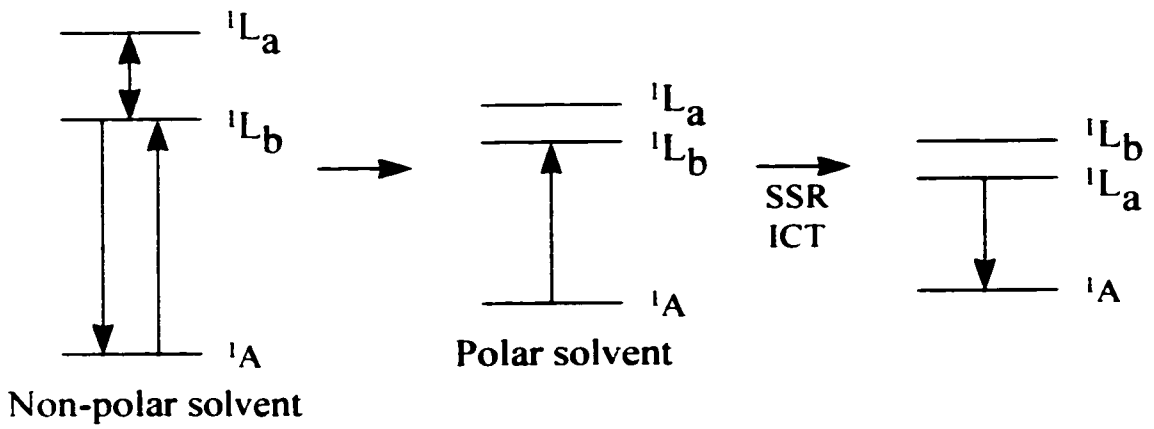

Figure 1.2. Representation of the two low-lying excited states of indole and its derivatives and the effect of solvent on the fluorescence. The figure is adapted from that in the article by Meech et al. [15]. In nonpolar solvents, the ^1L_b state is the lower lying of the two excited states. Consequently, it is the fluorescent state. The ^1L_a state is very sensitive to solvent polarity, whereas the ^1L_b state is not. As the polarity of the solvent increases, the energy of the ^1L_a state lowers, and it can become the fluorescent state. The specific behavior of the fluorescence lifetimes of the ^1L_b and the ^1L_a states is determined largely by their radiative rates. Meech et al. note that the increase of fluorescence lifetime of 3-MI with increasing polarity cannot be attributed to the lowering of the energy of the ^1L_a state but must take into account nonspecific interactions with the solvent that can arise because the dipole moment of the ^1L_a state is greater than that of the ^1L_b state. The ability of the ^1L_a state to lower its energy in polar solvents is referred to as "solute-solvent interaction" (SSR). The ability of the ^1L_a state to interact with the solvent in such a way as to modify its radiative properties is referred to as "internal charge transfer" (ICT). These processes are denoted in the figure.

lifetime shortens, due largely to the different radiative properties of the ^1L_b state with respect to those of the ^1L_a state [15](Figure 1.2).

Organic molecules are generally hydrophobic in nature. The interior of micelles consists of a nonpolar region, which offers an ideal environment into which organic molecules may partition from the aqueous phase. Consequently, the micelle phase can induce substantial changes in the fluorescence properties of indoles. In the nonpolar micelle phase, the indole emits from the ^1L_b state, whose fluorescence will be blue shifted and shorter lived with respect to those molecules in the polar aqueous phase having no interaction with the micelle and which emit from the ^1L_a state. The chromophore may also be located between the inner core of the micelle and the aqueous phase (water/micelle boundary) [20,21], which would be expected to afford different fluorescence behavior which is intermediate to those of the two just mentioned (Figure 1.3). The distinct fluorescence properties of the indoles in these different environments permit their association with the micelle to be quantified.

Given the biological importance of indoles, that indole is the chromophoric moiety of the amino acid tryptophan, and the considerable effort that has been devoted to understanding their fluorescence properties and exploiting these properties as probes of environment (e.g., see refs 22-25), it is remarkable that, with only a few exceptions of which we are aware (e.g., see refs 17-19 and 22), quantitative investigations of the interactions of indoles with micelles have been ignored.

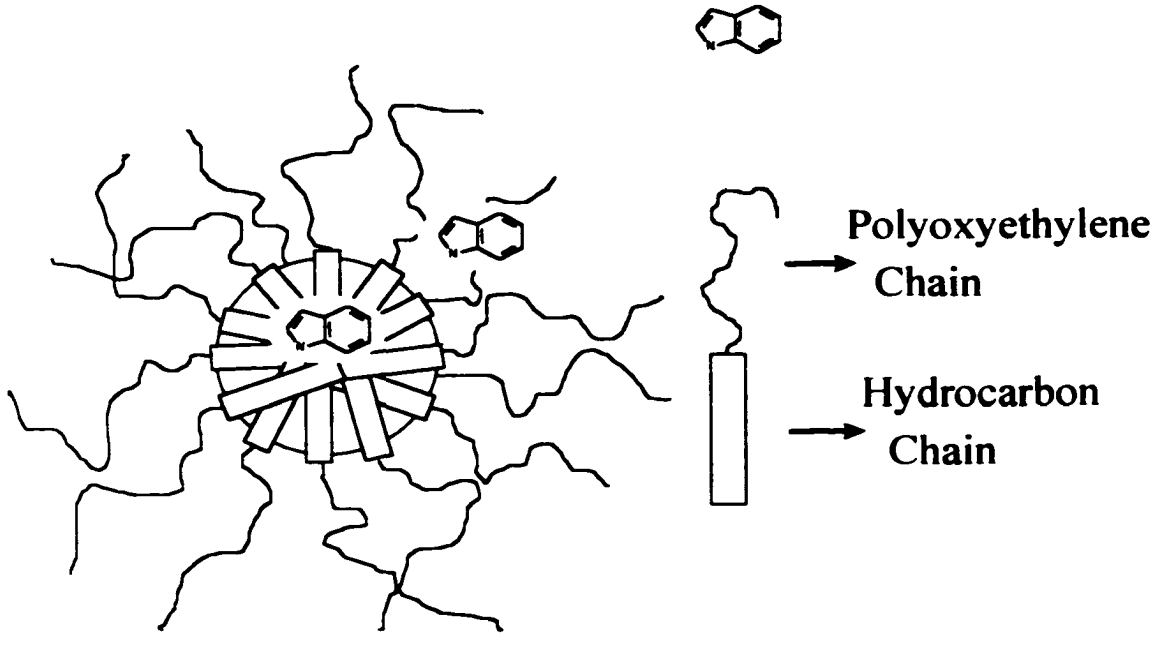

Figure 1.3. Schematic drawing of a Brij-35 micelle and possible depictions of the indole-micelle complex. The indole chromophore could be located within the nonpolar core of the micelle, solubilized between the inner core and the water phase in the hydrated oxyethylene phase or in the aqueous phase with no interaction with the micelle.

Experimental Section

Materials

Indole, 1-methylindole (1-MI), and 3-methylindole (3-MI) were obtained from Sigma Chemical Co. and were used without further purification. The neutral surfactant, poly(oxyethylene)23 lauryl ether (Brij-35, Figure 1.1d [20]), was also used as received. For Brij-35, micelles begin to form at a concentration of about 7×10^{-5} M [26,27] (the critical micelle concentration). The number of Brij-35 monomers that become incorporated into a single micelle is about 40 (the aggregation number)[27]. Solutions were prepared using Nanopure water.

Lecithin, a phosphoglyceride, also referred to as phosphatidylcholine, was obtained from Sigma and was used as received. The particular lecithin used in our experiments was derived from soybeans. Lecithin consists of two long-chain fatty acid ester groups and a phosphorylcholine dipolar headgroup attached to a glycerol backbone (Figure 1.1e)[28]. A lecithin solution was prepared by diluting 50 mg of solid lecithin with 2.0 mL of a 2:1 chloroform/methanol mixture [28](25 mg/mL) and then diluting an aliquot of the 25 mg/mL solution to a final concentration of 0.025 mg/mL.

Sample Preparation

A 100 mL aqueous stock solution of each chromophore was prepared to have an optical density of 0.126 ± 0.009 at 280 nm. The concentration of the 3-MI in solution was $\sim 1.48 \times 10^{-5}$ M. Sonication was necessary to ensure that the chromophore was dissolved. One hundred milligrams of Brij-35 was dissolved in 4.0 mL of the chromophore stock solution to obtain a surfactant concentration of 2.1×10^{-2} M, followed by sonication for approximately 20 min. A 2.0 mL aliquot form the 2.1×10^{-2} M solution was diluted to 4.0 mL with the 3-MI aqueous stock

solution to a concentration of 1.0×10^{-2} M Brij-35. This process of diluting each successive solution in half was repeated until the final dilutions for the indole and 1-MI solutions had a Brij-35 concentration of 8.1×10^{-5} M. For the 3-MI solutions, the final Brij-35 concentration was 1.6×10^{-4} M. In all cases, the chromophore concentration was kept constant.

Sample preparations for the study of the effect of lecithin on the vapor of 3-MI were performed in the following manner. A 0.5 mL aliquot of the 9.8×10^{-5} M 3-MI/ethanol stock solution (6.4 μg of 3-MI) was placed into a sealed quartz cuvette with a syringe. Aliquots of the 0.025 mg/mL lecithin stock solution were added to 3-MI sample in amounts of 0, 12.5, 25.0, and 37.5 μg. The solvent was then evaporated by passing argon over the sample.

Steady-State Measurements

Steady-state fluorescence measurements were performed using a Spex Fluoromax. All solutions were excited at 280 nm, and emission was monitored over a range of 300-500 nm. Absorption spectra from 250 to 350 nm were obtained for each of the 3-MI/Brij-35 solutions with a Perkin-Elmer Lambda 18 UV-visible spectrometer. For both fluorescence and absorption measurements, a 1 cm path length quartz cuvette was used.

The fluorescence measurements of the 3-MI vapor from the dry 3-MI/lecithin samples were performed on the same instrument as mentioned above. The 3-MI vapor was excited at 280 nm, and the emission was observed over a wavelength range from 290 to 330 nm. The integration time for each point on the spectrum was 3 s. The band-pass for both the excitation and emission monochromators was 4 nm. All measurements were performed at room temperature, approximately 23 °C. The emission of 3-MI vapor without the addition of lecithin was measured initially with subsequent measurements of the vapor from the three 3-MI/lecithin samples.

Time-Resolved Measurements

Time-correlated single-photon counting was performed on the 3-MI aqueous solution and at the various Brij-35 concentrations. The apparatus is described elsewhere [29]. Fluorescence decays were obtained by collecting emission wavelengths >320 nm and using an excitation wavelength of 288 nm. The time window was 17 ns full-scale. All lifetime measurements were performed at 20.5 °C. The fluorescence lifetime obtained for 3-MI in water (8.5 ns) was comparable to that found in the literature [15]. Fluorescence decays were fit to a sum of not more than three exponentially decaying components:

$$F(t) = \sum A_i \exp(-t / \tau_i) \qquad (1)$$

where A_i is the preexponential factor representing the contribution to the decay curve of the component with lifetime τ_i. The preexponential factors, lifetimes, and χ^2 values were obtained from nonlinear least-squares fitting and global analysis using the program Spectra Solve [30]. An Instruments SA Inc. monochromator (8 nm band-pass) was used to obtain fluorescence decays at the blue (320 nm) and red (410 nm) edges of the 3-MI/Brij-35 fluorescence spectrum at the highest Brij-35 concentration.

Results and Discussion

Steady-State Spectra

The absorbance maxima for the 3-MI solutions were practically unaffected by the presence of Brij-35 (Figure 1.4). The fluorescence spectrum of each chromophore studied was strongly dependent on the amount of Brij-35, and hence the amount of micelle, in solution. With the addition of micelle, the fluorescence spectra showed a blue shift in the emission

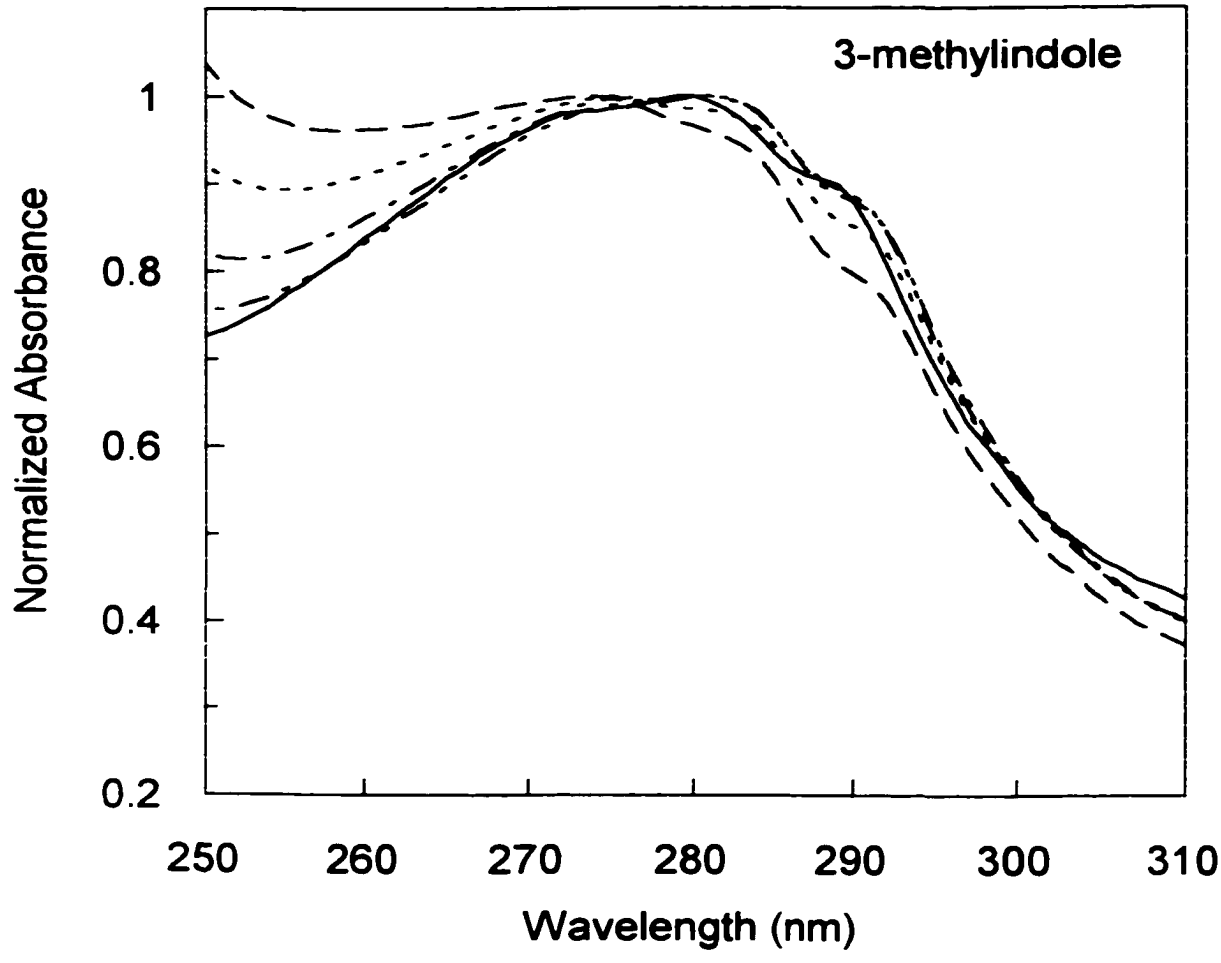

Figure 1.4. Absorbance spectra of 3-methylindole in Brij-35 micelles. The solid line is the absorbance in water without micelles. Concentration of Brij-35 in each broken line spectrum (from top to bottom): 2.1×10^{-2} M, 1.0×10^{-2} M, 5.2×10^{-3} M, and 2.6×10^{-3} M. Below 2.6×10^{-3} M, the spectra were identical to that of water with no micelle.

maxima. The emission maxima of the indole and 1-MI showed less of a blue shift at the lower concentrations of Brij-35: no blue shift was apparent below concentrations of 6.5×10^{-4} M. On the other hand, 3-MI exhibited larger blue shifts in the emission maxima with the lower concentrations of Brij-35 (Table 1.1). Thus, 3-MI tends to have a greater affinity towards the nonpolar micelle than indole and 1-MI.

Time-Resolved Fluorescence

Time-resolved fluorescence was performed on the 3-MI solutions at the various Brij-35 concentrations. The 3-MI in water had a fluorescence lifetime of about 8.5 ns and fit very well to a single-exponential decay curve, $\chi^2 = 1.10$. As Brij-35 was added to the aqueous 3-MI solutions, the decay curves exhibited contributions from more than one component. Each component revealed the different environment from which fluorescence of the 3-MI is emitted. To verify which of the decay components was the result of emission from partitioning of 3-MI into the micelle phase, the red and blue edges of the emission band of a 3-MI/H_2O/Brij-35 mixture were studied with the use of a monochromator. The red edge decay resembled the decay of the 3-MI in water and included the long component characteristic of emission in polar environments. The blue-edge decay exhibited the shorter components typical 3-MI emission in nonpolar environments, and global analysis revealed the lack of any long component (Figure 1.5). We conclude that the long component of the fluorescence decay is due to the 3-MI in water and the shorter components are due to the 3-MI associated with micelle. Thus, 3-MI leaves the aqueous phase and partitions into the nonpolar micelle phase.

To obtain a more quantitative view of how much 3-MI remains in the aqueous phase, a global fit was performed using all decay curves, and fixing the long component from water at 8100 ps, and fitting each to a triple exponential. A triple exponential fit was chosen to take into

Table 1.1. Steady-state fluorescence emission maxima for indole, 1-MI, and 3-MI

	λ_{max} (nm)		
[Brij-35] (M)	Indole	1-MI	3-MI
0.0	346	355	367
$8.1 \cdot 10^{-5}$	346	353	-------
$1.6 \cdot 10^{-4}$	347	353	366
$3.3 \cdot 10^{-4}$	346	355	365
$6.5 \cdot 10^{-4}$	347	353	362
$1.3 \cdot 10^{-3}$	343	353	358
$2.6 \cdot 10^{-3}$	340	351	353
$5.2 \cdot 10^{-3}$	338	348	351
$1.0 \cdot 10^{-2}$	331	343	348
$2.1 \cdot 10^{-2}$	328	336	342

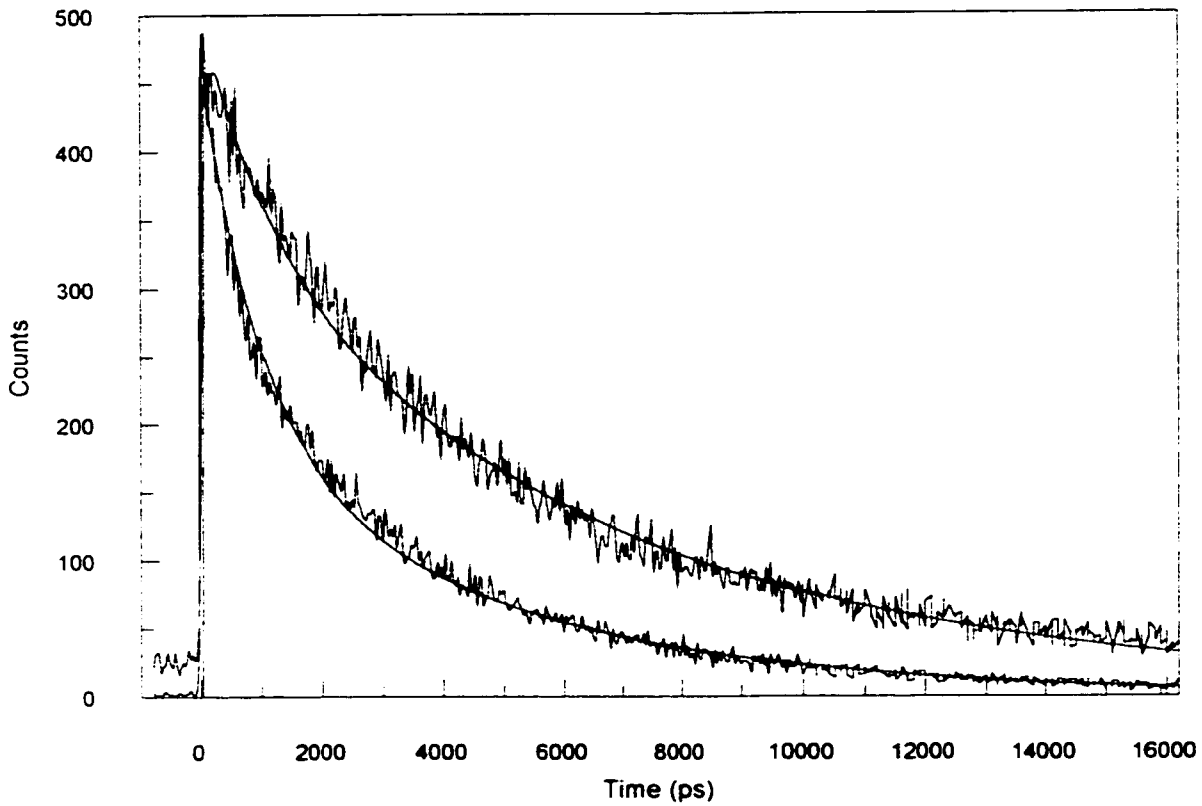

Figure 1.5. Time-resolved emission of the red (top decay) and the blue (lower decay) edges of the 3-MI/Brij-35 emission band ([Brij-35] = 2.1×10^{-2} M). Blue edge emission was collected at 320 nm, and red edge emission was collected at 410 nm. An 8 nm band-pass monochromator with a 1 mm slit was used. Global fitting parameters were used to fit each fluorescence decay. Lifetimes were fixed at 8100, 4671, and 955 ps, and the amplitudes were varied (eq 1). The blue edge can be fit to two components (the amplitude for the longest component is zero): $F(t) = 0.67 \exp(-t/955 \text{ ps}) + 0.33 \exp(-t/4671 \text{ ps})$, $\chi^2 = 1.3$. The red edge requires three components to be fit: $F(t) = 0.29 \exp(-t/955 \text{ ps}) + 0.34 \exp(-t/4671 \text{ ps}) + 0.37 \exp(-t/8100 \text{ ps})$, $\chi^2 = 1.3$. The fluorescence decay from the blue edge is contaminated by some scattered light, against which we could not discriminate.

account the three possible environments for the 3-MI: the aqueous phase, the nonpolar micelle phase, and the hydrated poly(oxyethylene) phase between the two (Figure 1.3). In the latter two cases, the indole can be considered to be partitioned into or associated with the micelle. The weight of the long component decreased dramatically with increasing micelle concentration (Table 1.2). At our highest surfactant concentration, the sum of the preexponential factors of the two short components of the fluorescence decay was ~0.93. Thus, 93% of the total fluorescence is composed of the two shorter components, which are attributed to the 3-MI associated with the micelle. The contribution of the 3-MI in the aqueous phase is 7%.

To obtain an initial estimate of the association (equilibrium) constant, K_{eq}, a Benesi-Hildebrand plot was made on the basis of a 1:1 3-MI/micelle association [26,31,32]. The equilibrium between 3-MI and a micelle is given by:

$$3MI + M \leftrightarrow 3MI \cdot M \tag{2}$$

where M represents the micelle, and 3MI•M represents the 3-MI/micelle complex. The corresponding association constant is

$$K_{eq} = \frac{[3MI \cdot M]}{[3MI][M]} \tag{3}$$

where the bracketed terms are the respective molar concentrations. The above expression can be rewritten in terms of initial known concentrations by substituting $[3MI]_0$-[3MI•M] for [3MI], and $[M]_0$-[3MI•M] for [M]: $[3MI]_0$ and $[M]_0$ are the initial concentrations of 3-MI and micelle respectively:

$$K_{eq} = \frac{[3MI \cdot M]}{([3MI]_0 - [3MI \cdot M])([M]_0 - [3MI \cdot M])} \tag{4}$$

We assume that the complex concentration is much less than the concentration of micelle.

Table 1.2. Global fitting parameters of 3-MI/Brij-35 solutions

[Brij-35] (M)	A_1	A_2	A_3
$6.5 \cdot 10^{-4}$	0.81	0.13	0.06
$1.3 \cdot 10^{-3}$	0.59	0.34	0.07
$2.6 \cdot 10^{-3}$	0.41	0.52	0.07
$5.2 \cdot 10^{-3}$	0.24	0.68	0.08
$1.0 \cdot 10^{-2}$	0.13	0.76	0.11
$2.1 \cdot 10^{-2}$	0.07	0.79	0.14
	τ_1 = 8100 ps	τ_2 = 4671 ps	τ_3 = 955 ps

Therefore $[M] \approx [M]_0$ and $[M]_0-[3MI\bullet M] \approx [M]_0$. Substituting and solving for $1/[3MI\bullet M]$ gives

$$\frac{1}{[3MI \cdot M]} = \frac{1}{[3MI]_0} + \frac{1}{K_{eq}[3MI]_0[M]_0} \tag{5}$$

The association between 3-MI and a micelle is responsible for the blue-shifted emission spectra of the steady-state fluorescence and also for the increasing contribution of the short components in the time-correlated fluorescence decays. The preexponential factors of the short components are a measure of the contribution to the fluorescence from the 3-MI/micelle complex. Thus, the fluorescence intensity of the complex, 3MI•M, is proportional to the preexponential factor multiplied by its respective lifetime for each component of interest. In our case, concerning the triple exponential global fits, the fluorescence intensity, F, of the complex is the sum of the two short-component fluorescence intensities:

$$F = A_2\tau_2 + A_3\tau_3 \propto [3MI \cdot M] \tag{6}$$

Using eq 6, eq 5 becomes

$$\frac{1}{F} = \frac{1}{[3MI]_0} + \frac{1}{K_{eq}[3MI]_0[M]_0} \tag{7}$$

A plot of $1/F$ vs. $1/[M]_0$ should reveal a straight line for a 1:1 association between the micelle and 3-methylindole. $[M]_0$ for each solution was determined from the molar concentration of the Brij-35 and its aggregation number. The plot in Figure 1.6a shows our data with a linear correlation of 0.997. This suggests that our data indicate a 1:1 association. The association constant, K_{eq}, is calculated by dividing the intercept by the slope of the best fit line through the data. K_{eq} in our case is $1.8\times10^{4}\ M^{-1}$. The same procedure using the magnitude of the blue shift from the steady-state fluorescence data as a measure of the complex concentration in eq 7 also provided a K_{eq} of the same order of magnitude as previously determined.

The K_{eq} calculated above was based on the assumption that $[M] \approx [M]_0$. To obtain a

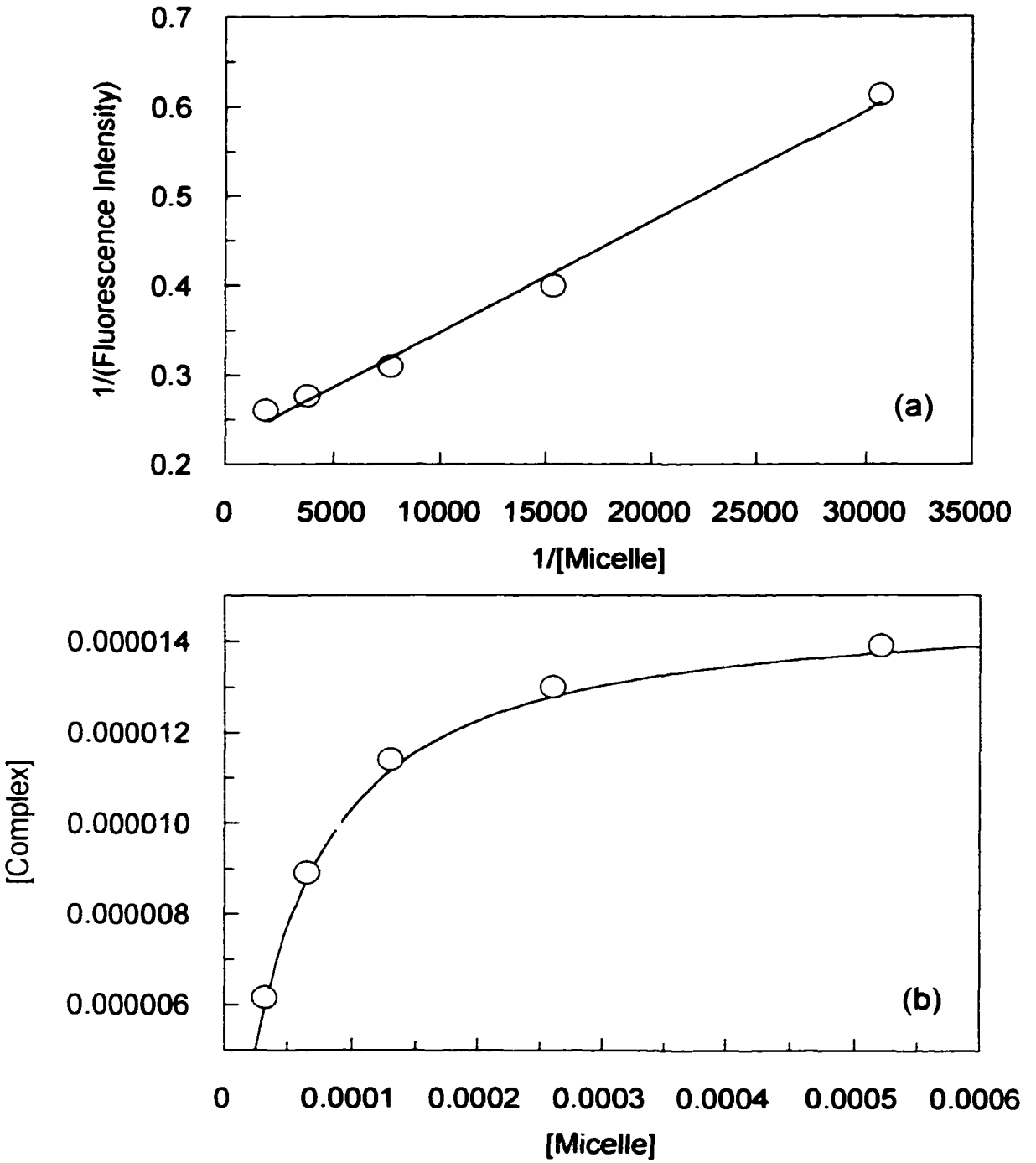

Figure 1.6. (a) Benesi-Hildebrand plot for the 3-MI/Brij-35 micelle complex with a linear correlation of 0.997. The value 1/F was determined using $F = A_2\tau_2 + A_3\tau_3$, where F is the fluorescence intensity of the chromophore that has partitioned into the micelle. A_2 and A_3 are the preexponential factors of the two shorter components in the triple-exponential global analysis; τ_2 and τ_3 are the respective lifetimes. The plot in (b) is the result of the nonlinear fit.

better determination of the association constant without any assumptions, eq 4 was solved for the complex concentration, [3MI•M], and a nonlinear fitting procedure was employed to obtain K_{eq}:

$$[3MI \cdot M] = \frac{1}{2K_{eq}} \left(\begin{array}{l} K_{eq}[3MI]_0 + K_{eq}[M]_0 + 1 - \\ \sqrt{K_{eq}^2[3MI]_0^2 - 2K_{eq}^2[3MI]_0[M]_0 + 2K_{eq}[3MI]_0 + K_{eq}^2[M]_0^2 + 2K_{eq}[M]_0 + 1} \end{array} \right) \quad (8)$$

In this case, because we previously showed that the association was 1:1, the complex concentration was calculated using the sum of the preexponential factors and the initial 3-MI concentration. A plot of [3MI•M] vs. $[M]_0$ was subject to a nonlinear fitting procedure, and K_{eq} was determined to be $2.6 \cdot 10^4\ M^{-1}$ (Figure 1.6b).

The partition coefficient, K_p, was determined to be 13.2 for our highest Brij-35 concentration as calculated by

$$K_p = \frac{[3MI \cdot M]}{[3MI]_{aq}} \quad (9)$$

where $[3MI]_{aq}$ is the free uncomplexed 3-MI in solution. The concentrations were again determined from the preexponential factors from the time-correlated fluorescence decays and the initial 3-MI concentration.

In this example, the amplitudes and lifetimes obtained from the fluorescence decay profiles are a direct measure of different probe environments and permit a straightforward evaluation of the association constant. Bound and unbound probes are immediatley distinguished by the form of the fluorescence decay. If steady-state spectra are employed to construct a Benesi-Hildebrand plot, care must be taken to deconvolute the contributions of the

bound and the unbound chromophores to the spectra (33).

Conclusions

Indole, 1-MI, and 3-MI are hydrophobic in nature. Thus, when micelles are formed in aqueous solutions of these chromophores, they will partition into the micelle. We have shown that time-correlated single photon counting is an effective technique for probing the chromophore/micelle interaction. The sensitivity of the indole fluorescence to the environment permits a quantitative measurement of the amount of chromophore that has associated with the micelle.

Of particular interest is the association of 3-methylindole (3-MI) with micelles. 3-MI is a volatile, noxious compound whose presence is particularly acute at swine production facilities [1-7]. 3-MI is produced in the intestine of pigs by microbial degradation of L-tryptophan and is thus one of the most common malodorous compounds found in swine manure. Along with other odorous compounds and gases formed from bacteria in the manure, 3-MI poses serious problems for the environment and the health of animals, workers, and surrounding communities.

Exploiting the interactions of 3-MI with micelles or other organized media may prove to be useful in addressing odor problems. Our results indicate an association constant to be on the order of 10^4 M^{-1} for 3-MI with Brij-35 micelles and thus demonstrate that 3-MI has a fairly high affinity for surfactant molecules. This affinity for surfactants suggests a means of reducing the amount of 3-MI that can escape into the vapor phase as an airborne contaminant. In closing, we note that 3-MI vapor is easily measured by fluorescence techniques (Figure 1.7) and that the experiments with model micelle systems discussed above led us to examine to what extent the

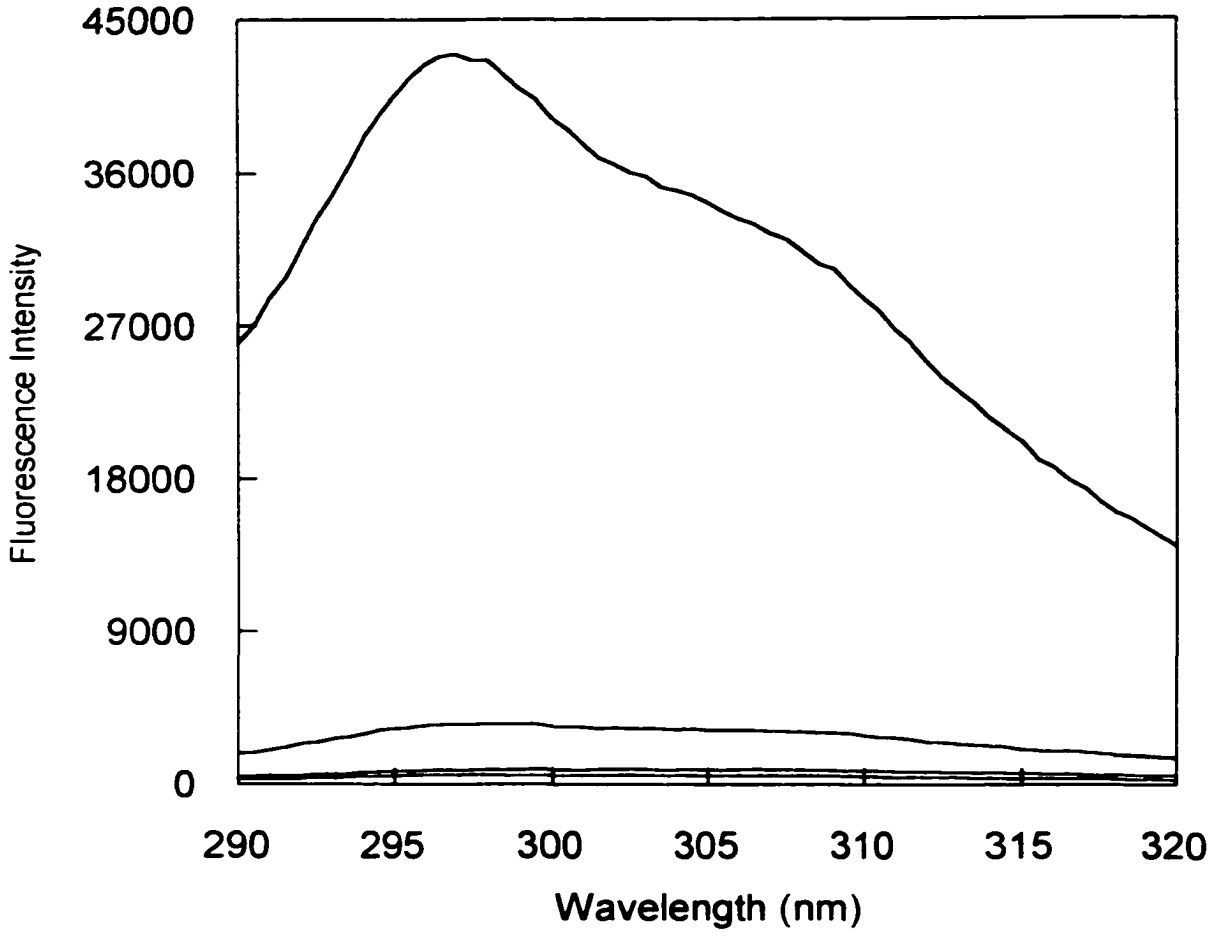

Figure 1.7. Fluorescence spectra of 3-methylindole vapor in equilibrium with its solid. The top spectrum is the emission of 3-MI vapor without lecithin added. The spectra of lower intensity are the emission of 3-MI vapor with the addition of dry lecithin. In each case, the 3-MI concentration was the same, 6.4 μg. For the spectra, from top to bottom, the amount of dry lecithin added was 0.0, 12.5, 25.0, and 37.5 μg, respectively. All fluorescence measurements were performed at room temperature, ~23 °C. Excitation wavelength, 280 nm; integration time, 3 s each point. The band-passes of the excitation and emission monochromators were 4 nm.

3-MI vapor is reduced by addition of a dry surfactant such as lecithin. Figure 1.7 demonstrates that the effect is dramatic. Notably, at the higher lecithin amounts used, the 3-MI *odor, as measured by nose,* was no longer detectable.

Acknowledgment

Support for this research was provided by the Iowa Soybean Promotion Board, the Iowa Pork Producers Association, and the Iowa Corn Promotion Board. We thank Emily Dertz for technical assistance.

References

1. Muehling, A. J. *Swine Housing and Waste Management*; Department of Agricultural Engineering, College of Agriculture, University of Illinois: Urbana-Champaign, 1969.

2. Smith, A. T.; Lawrence, T. L. *Pig Housing and the Environment*, BSAP Occasional Publication, Number 11; The British Society of Animal Production: Edinburgh, 1987.

3. Nielson, V. C.; Voorburg, J. H.; L'Hermite, P. *Volatile Emissions From Livestock Farming and Sewage Operations*; Elsevier Science Publishing Co., Inc.: New York, 1988.

4. Leffel, R. E.; Parthum, C. A. *Odor Control for Wastewater Facilities*, Manual of Practice No.22; Lancaster Press Inc.: Pennsylvania, 1979.

5. Jensen, M. T.; Cox, R. P.; Jensen, B. B. *Appl. Environ. Microbiol.* **1995**, *61*, 3180-3184.

6. Jensen, M. T.; Cox, R. P.; Jensen, B. B. *Animal Science* **1995**, *61*, 293-304.

7. Hansen, L. L.; Larsen, A. E.; Jensen, B. B.; Hansen-Møller, J.; Barton-Gade, P. *Anim. Prod.* **1994**, *59*, 99-110.

8. Platt, J. R. *J. Chem. Phys.* **1951**, *19*, 101-111.

9. Strickland, E. H.; Horwitz, J.; Billups, C. *Biochemistry* **1970**, *25*, 4914-4921.

10. Callis, P. R. *J. Chem. Phys.* **1991**, *95* 4230-4240.

11. Valeur, B.; Weber, G. *Photochem. Photobiol.* **1977**, *25*, 441-444.

12. Ruggiero, A. J.; Todd, D. C.; Fleming, G. R. *J. Am. Chem. Soc.* **1990**, *112*, 1003-1014.

13. Eftink, M. R.; Selvidge, L. A.; Callis, P. R.; Rehms, A. A. *J. Phys. Chem.* **1990**, *94*, 3469-3479.

14. Rich, R. L.; Chen, Y.; Neven, D.; Negrerie, M.; Gai, F.; Petrich, J. W. *J. Phys. Chem.* **1993**, *97*, 1781-1788.

15. Meech, S. R.; Phillips, D. *Chem. Phys.* **1983**, *80*, 317-328.

16. This statement must be qualified. The ^1L_a and ^1L_b levels are typically closely spaced, so the lower state can thermally populate the higher one. Furthermore, on a fast (subpicosecond) time scale, the emission from the higher lying state is detecable. These two phenomena contribute to the low limiting anisotropy values of most indoles (12).

17. Eftink, M. R.; Ghiron, C. A. *J. Phys. Chem.* **1976**, *80*, 486-493.

18. Hill, B. C.; Horowitz, P. M.; Robinson, N. C. *Biochemistry* **1986**, *25*, 2287-2292.

19. Lakowicz, J. R.; Keating, S. *J. Biol. Chem.* **1983**, *258*, 5519-5524. Wimley, W. C.; White, S. H. *Biochemistry* **1993**, *32*, 6307-6312.

20. Schick, M. J. *Nonionic Surfactants*, Surfanctant Science Series, Vol. 1; Marcel Dekker, Inc.: New York, 1966: Chapter 17.

21. Shinoda, K.; Nakagawa, T.; Tamamuchi, B.; Isemura, T. *Colloidal Surfactants*, 1963, p. 140.

22. Beecham, J. M.; Brand, L. *Annu. Rev. Biochem.* **1985**, *54*, 43-71.

23. Creed, D. *Photochem. Photobiol.* **1984**, *39*, 537-562.

24. Szabo, A. G.; Rayner, D. M. *J. Am. Chem. Soc.* **1980**, *102*, 554-563.

25. Petrich, J. W.; Chang, M. C.; McDonald, D. B.; Fleming, G. R. *J. Am. Chem. Soc.* **1983**, *105*, 3824-3832.

26. Roberts, E. L.; Chou, P. T.; Alexander, T. A.; Agbaria, R. A.; Warner, I. M. *J. Phys. Chem.* **1995**, *99*, 5431-5437.

27. McIntire, G. L. *Crit. Rev. Anal. Chem.* **1990**, *21*, 257-275.

28. New, R. R. C. *Liposomes, A Practical Approach*; Oxford University Press: New York, 1990; Chapters 1 and 2.

29. Chen, Y.; Rich, R. L.; Gai, F.; Petrich, J. W. *J. Phys. Chem.* **1993**, *97*, 1770-1780.

30. Das, K.; English, D. S.; Fehr, M. S.; Smirnov, A. V.; Petrich, J. W. *J. Phys. Chem.* **1996**, *100*, 18275-18281.

31. Benesi, H. A.; Hildebrand, J. H. *J. Am. Chem. Soc.* **1949**, *71*, 2703.

32. Chou, P. T.; Wei, C. V.; Chang, C. P.; Meng-Shen, K. *J. Phys. Chem* **1995**, *99*, 11994-12000.

33. Hoenigman, S. M.; Evans, C. E. *Anal. Chem.* **1996**, *68*, 3274-3276.

CHAPTER II. FLUORESCENCE PROPERTIES OF RECOMBINANT TROPOMYOSIN CONTAINING TRYPTOPHAN, 5-HYDROXYTRYPTOPHAN AND 7-AZATRYPTOPHAN

A paper published in *Photochemistry and Photobiology*[1]

Kaustuv Das[2], Kyle D. Ashby[2], Alex V. Smirnov[2], Fernando C. Reinach[3,4], Jacob W. Petrich[2,5] and Chuck S. Farah[3,5]

Abstract

Tropomyosin mutants containing either tryptophan (122W), 5-hydroxytryptophan (5OH122W), or 7-azatryptophan (7N122W) have been expressed in *Escherichia coli* and their fluorescence properties studied. The fluorescent amino acids were located at position 122 of the tropomyosin primary sequence, corresponding to a solvent-exposed position c of the coiled-coil heptapeptide repeat. The emission spectrum of the probe in each mutant is blue-shifted slightly with respect to that of the probe in water. The fluorescence anisotropy decays are single exponential, with a time constant of 2-3 ns while the fluorescence lifetimes of the probes incorporated into the proteins, in water, are nonexponential. Because tryptophan in water has an intrinsic nonexponential fluorescence decay, it is not surprising that the fluorescence decay

---

[1] Reproduced with permission from *Photochemistry and Photobiology*, (1999), **70**(5), 719-730.

[2] Iowa State University, Department of Chemistry, Ames, IA 50011-3111 USA. K.D. Ashby performed much of the work on the 5-hydroxyindole and 5-hydroxytryptophan chromophores, as well as the 5OH122W mutant protein, and the energy transfer studies.
[3] Departamento de Bioquimica, Instituto de Quimica, and
[4] Howard Hughes Medical Institute, Universidade de São Paulo, São Paulo, Brazil.
[5] Authors to whom correspondence should be addressed.

of 122W is well described by a triple exponential. The fluorescence decays in water of the nonnatural amino acids 5-hydroxytryptophan and 7-azatryptophan (when emission is collected from the entire band) are single exponential. Incorporation into tropomyosin induces triple-exponential fluorescence decay in 5-hydroxytryptophan and double-exponential fluorescence decay in 7-azatryptophan. The range of lifetimes observed for 5-hydroxyindole and 5-hydroxytryptophan at high pH and in the nonaqueous solvents were used as a base with which to interpret the lifetimes observed for the 5OH122W and indicate that the chromophore exists in several solvent environments in both its protonated and unprotonated forms in 5OH122W.

Introduction

Tryptophan (Fig. 2.1) is a common optical probe for studying protein structure and dynamics. Its intrinsic nonexponential fluorescence decay and its frequent multiple occurrence in proteins, however, often renders the interpretation of its photophysics ambiguous [1-10]. 5-Hydroxytryptophan (Fig. 2.1) has been proposed as an alternative probe [11]. It has a single exponential fluorescence decay under certain conditions. However, in water at neutral pH, its fluorescence lifetime is comparable to that of the long component of tryptophan, thus rendering its distinguishability with respect to tryptophan difficult [11,12]. The nonnatural amino acid, 7-azatryptophan (Fig. 2.1), has also been presented as an alternative to tryptophan as a photophysical probe [13-23].

Many biological systems of interest involve supermolecular aggregates of a large number of proteins, the detailed study of which by fluorescence techniques is often limited by the large number of different tryptophan residues and by the small number of sites in which to specifically

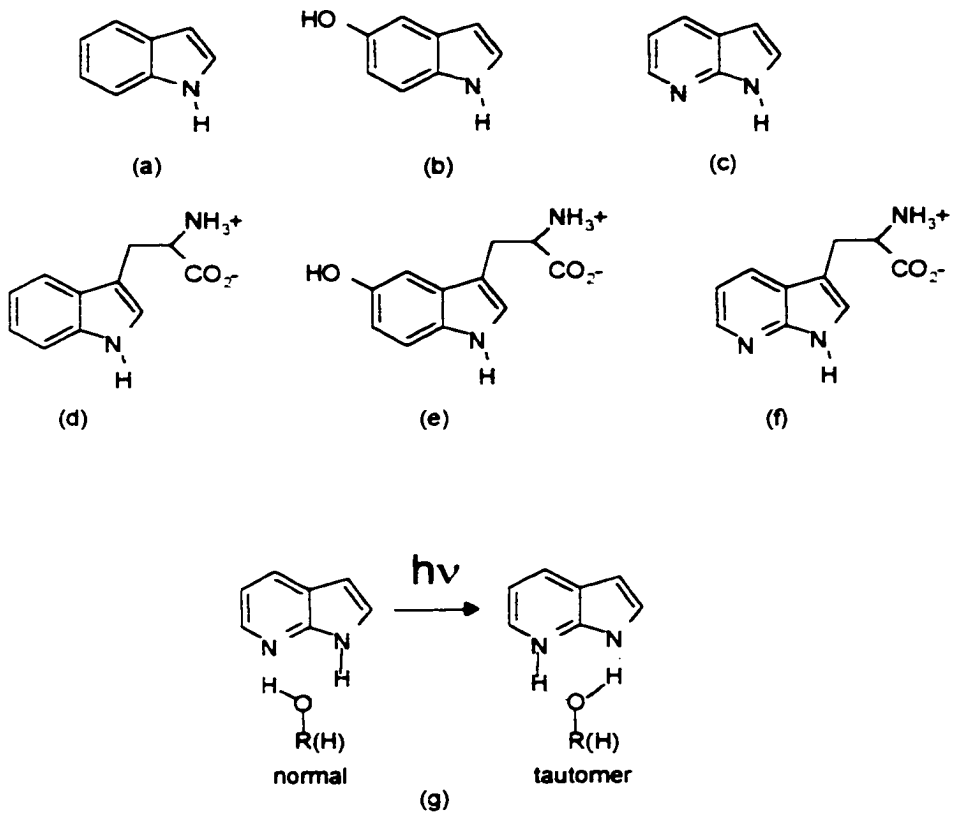

Figure 2.1. The optical probes (a) indole, (b) 5-hydroxyindole, (c) 7-azaindole, (d) tryptophan, (e) 5-hydroxytryptophan, (f) 7-azatryptophan, and (g) the scheme for excited-state solvent assisted proton transfer in 7-azaindole.

attach covalent probes. For example, the principal components of the muscle thin filament—actin, tropomyosin and troponin from adult chicken fast skeletal muscle—contain 4, 0 and 4 tryptophans each. Because these proteins are present in a molar ratio of 7:1:1, each repeating structural thin filament unit has, in principle, 32 (=[7×4]+4) unique tryptophan residues. The ability to introduce amino acid analogues with unique fluorescent characteristics into recombinant proteins promises to open up avenues by which to study protein interactions in these complex systems. Muscle tropomyosin is a filamentous coiled-coil protein made of a dimer of 284-amino-acid, parallel, in-register, α-helical chains [24]. The primary sequence of tropomyosin is characterized by a conserved heptapeptide repeat (abcdefg) in which hydrophobic residues at positions a and d form a hydrophobic dimerization interface [24,25]. In skeletal and cardiac muscle, it is thought that Ca^{2+}-induced changes in troponin control the topology of each tropomyosin's interaction with seven consecutive actin monomers along one strand of the actin filament, thereby influencing the accessibility to specific myosin binding sites on actin [26-32]. In this article, we report fluorescence studies on different forms of a recombinant tropomyosin containing either tryptophan, 5-hydroxytryptophan or 7-azatryptophan at position 122 of the tropomyosin primary sequence, corresponding to a solvent-exposed position c of the coiled-coil heptapeptide repeat [24,25]. Elsewhere (Farah and Reinach, submitted), it is shown that tropomyosin with 5-hydroxytryptophan at this position is sensitive to both actin binding and Ca^{2+} binding to troponin. The fluorescence of this residue therefore may be a useful probe in dynamical studies of conformational changes in the muscle thin filament associated with the regulation of muscle contraction. However, before the results of studies of such a complex system as reconstituted muscle filaments may be interpreted, we need

to have a firm understanding of the behavior of the probes on their own and in isolated tropomyosin. While there have been several previous studies of the time-resolved fluorescence properties of 5-hydroxytryptophan and 7-azatryptophan [23,33,34], there have been relatively few reports in which both probes have been studied at the same position within a protein. This study therefore provides a baseline for future work by furnishing comparisons of the fluorescence lifetimes and anisotropy decays of the chromophores in aqueous solution and incorporated in a protein as well as an analysis of the factors that influence the photophysics of these chromophores in their respective environments.

Materials and Methods

Preparation of Mutants

Recombinant chicken fast skeletal tropomyosin containing tryptophan or tryptophan analogues at position 122 was produced as described in the accompanying paper (Farah and Reinach, submitted). The three tropomyosins, 122W (tryptophan), [†] 5OH122W (5-hydroxytryptophan) and 7N122W (7-azatryptophan) had no more than 5% protein impurity as determined by sodium dodecyl sulfate-polyacrylamide gel electrophoresis. We estimated the incorporation of 7-azatryptophan into 7N122W to be >90% (*i.e.* <10% tryptophan) based first on the fluorescence excitation spectra (comparing emissions collected at 330 nm and 450 nm) and emission spectra (comparing excitations at 280 and 315 nm), second on the fact that if no

---

† *Abbreviations:* 122W, tropomyosin mutant containing tryptophan; 5OH122W, tropomyosin mutant containing 5-hydroxytryptophan; 7N122W, tropomyosin mutant containing 7-azatryptophan; DMSO, dimethylsulfoxide.

tryptophan or derivative is added to the media after cellular resuspension (15 min after addition of isopropyl β-D-thiogalactopyranoside, see above), no recombinant protein is expressed, and finally based on a small and wavelength-dependent contribution of a long-lived fluorescence lifetime component (see below, and Table 2.2). We assume that the long-lived emission in 7N122W arises from tryptophan contamination and from the intrinsic tyrosine (12 per coiled-coil dimer). As expression levels are higher with 5-hydroxytryptophan than with 7-azatryptophan, we expect the incorporation of 5-hydroxytryptophan to be at least as efficient as that of 7-azatryptophan. We also attempted to incorporate the tryptophan analog, N_1-methyl-7-azatryptophan [19] but were unsuccessful. Our failure is consistent with previous studies on the substrate specificity of tryptophanyl-$tRNA^{Trp}$ synthetase [35] in which N_1-methyltryptophan and ATP did not react to form a stable aminoacyl-adenylate complex with the enzyme.

Fluorescence Studies

The tropomyosins were dissolved in 25 mM 3-(N-morpholino)propanesulfonic acid (pH 7), 50 mM NaCl, 5 mM $MgCl_2$, 1 mM dithiothreitol. Under these conditions, the recombinant tropomyosins exist in their unpolymerized form (*i.e.* the coiled-coil dimer) [36]. The corrected steady-state spectra were recorded using a Spex Fluoromax with an emission and excitation bandpass of 2 nm. The time-resolved studies were carried out with an apparatus described elsewhere [18]. Among the naturally occurring amino acids, only phenylalanine, tyrosine and tryptophan are fluorescent. The fluorescence of wild-type tropomyosin is dominated by that of its 12 tyrosine residues per dimer. The absorption spectra, however, of tryptophan and especially the two tryptophan derivatives, are red shifted with respect to that of tyrosine so that excitation at longer wavelengths affords selective excitation of the probe at position 122. For

example, at 290 nm, the ratio of extinction coefficients for the total number of tyrosine residues to tryptophan, 5-hydroxytryptophan and 7-azatryptophan is 1:7, 1:7 and 1:10, respectively. The absorption spectrum of tyrosine extends up to 295 nm and its emission (λ_{max} ~300 nm) extends up to 370 nm. Tyrosine emission is evident for excitation wavelengths 270 nm and 280 nm (Fig. 2.2a). For the weakly fluorescent 7N122W, the excitation spectrum clearly shows the presence of tyrosine fluorescence (Fig. 2.2f). To filter out the tyrosine fluorescence and observe the signal from only 7-azatryptophan, it was therefore necessary to use excitation wavelengths greater than 280 nm and to collect the fluorescence at wavelengths greater than 370 nm.

Data were fit to one, two or three decaying exponentials by an iterative convolution procedure using a nonlinear least-squares algorithm. The quality of the fit was determined by visual inspection of the residuals and the χ^2 criterion [37].

In some cases, mentioned below in the Results section, it was desirable to use a global fitting routine (Spectra Solve™) to fit groups of decay curves simultaneously. Sets of data and corresponding instrument response functions are fit using an iterative convolution procedure. Global parameters (the preexponential factors) are defined for the entire collection of curves, and local parameters (time constants) are defined for each curve. Local parameters are varied for each curve while holding the global parameters constant and all curves are individually fit. After all curves are fit, a global χ^2 is found and then the global parameters are varied. The algorithm searches for a minimum in the global χ^2. The global χ^2 is defined as:

$$\chi^2 = \frac{\sum_{i=1}^{n} \frac{\chi^2_{local,\,i}}{\chi^2_{best,\,i}}}{n}$$

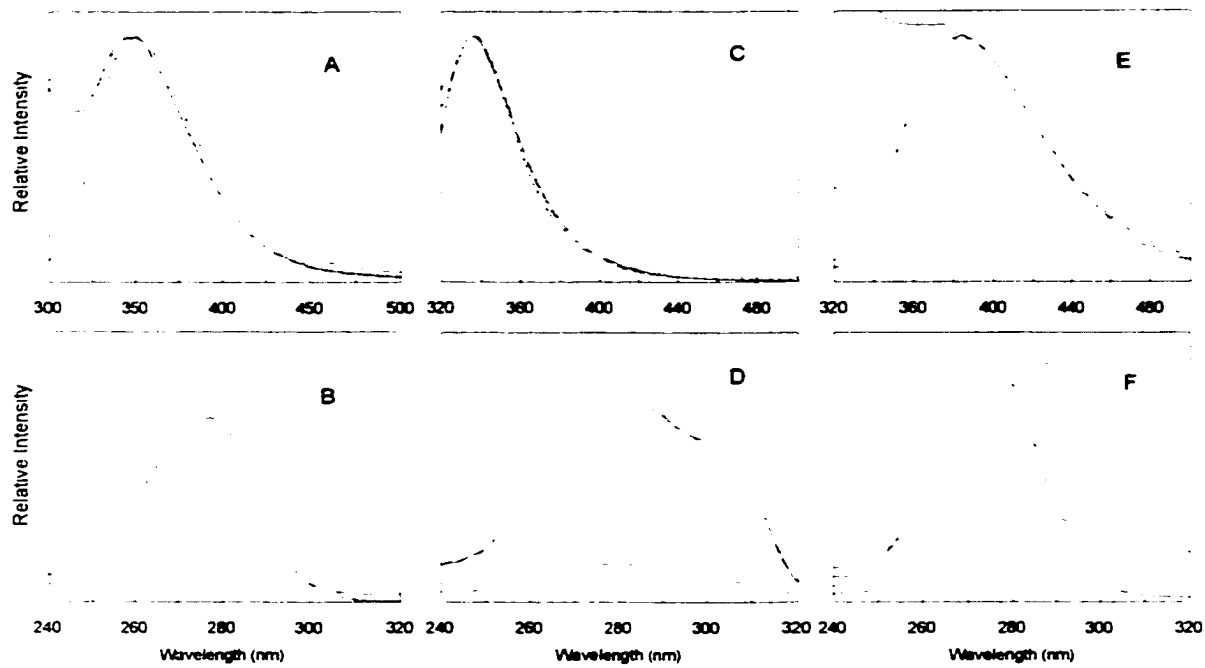

Figure 2.2. (a) Emission spectra of 122W (9 μM), the excitation wavelengths are: (———) 270 nm, (– – – –) 280 nm, (· · · · ·) 290 nm, and (– · – · – · –) 295 nm. (b) Excitation spectra of 122W, the emission wavelengths are: (———) 330 nm, (– – – –) 350 nm, (· · · · ·) 380 nm, and (– · – · – · –) 400 nm. (c) Emission spectra of 5OH122W (9 μM), the excitation wavelengths are: (———) 280 nm, (– – – –) 295 nm, (· · · · ·) 310 nm, and (– · – · – · –) 315 nm. (d) Excitation spectra of 5OH122W, the emission wavelengths are: (———) 330 nm, (– – – –) 350 nm, (· · · · ·) 380 nm, and (– · – · – · –) 400 nm. (e) Emission spectra of 7N122W (9 μM), the excitation wavelengths are: (———) 280 nm, (– – – –) 290 nm, (· · · · ·) 300 nm, and (– · – · – · –) 310 nm. (f) Excitation spectra of 7N122W, the emission wavelengths are: (———) 330 nm, (– – – –) 380 nm, (· · · · ·) 420 nm, and (– · – · – · –) 450 nm.

where χ^2_{best} is the best fit found by letting all parameters, global and local, vary and n is the number of curves.

Results and Discussion

Fluorescence Properties of Optical Probes in Tropomyosin Mutants

Figure 2.2 presents the emission and excitation spectra for the three tropomyosin mutants that bear an optical probe at position 122: 122W (tryptophan), 5OH122W (5-hydroxytryptophan) and 7N122W (7-azatryptophan). The red shifts in the excitation spectra of 5OH122W (Fig. 2.2D) and 7N122W (Fig. 2.2F) with respect to that of 122W (Fig. 2.2B) indicate clearly that the modified tryptophans were successfully incorporated into the recombinant protein.

Table 2.1 summarizes the fluorescence decay parameters of the indole and amino acid forms of the three optical probes in various solvents, and Table 2.2 presents the same parameters for the three tropomyosin mutants in aqueous solution. The fluorescence lifetimes for all three tropomyosins are nonexponential; and in all cases the data can be best fit to a sum of three exponentials (Table 2.2). For 122W, this is not unexpected because the fluorescence decay of tryptophan in water at neutral pH is well described by a sum of two exponentials. Because 5-hydroxytryptophan has a single exponential fluorescence decay in water at neutral pH [11,12] (Table 2.1) it is striking to find that the fluorescence decay of 5OH122W is also well described by a triple exponential whose components are each present with amplitudes of >20%. The 7N122W mutant also exhibits a triple-exponential fluorescence decay; but unlike the other two proteins, the third component has a much smaller amplitude (see below). In order to obtain

Table 2.1. Fluorescence decay properties of optical probes

Sample	Solvent*	λ_{ex} (nm)	λ_{em} (nm)	(a_1)†	τ_1 (ps)‡	τ_2 (ps)
Indole	H_2O,pH 7 (12)	288	>320	1.00	4550 ± 20	
	MeOH (12)	288	>320	1.00	3400 ± 100	
	DMSO (12)	288	>320	1.00	4800 ± 200	
Tryptophan	H_2O,pH 7 (6)	295	>320	0.22 ± 0.01	620 ± 50	3210 ± 120
	pH 11 (7)	295	>320	1.00	8180 ± 240	
	MeOH (12)	295	>320	0.05	200 ± 100	1900 ± 50
	DMSO (12)	295	>320	0.12 ± 0.02	1200 ± 200	7200 ± 400
5-OH-Indole	H_2O, pH 11.9	288	>305	0.15	2008	23††
	pH 11.5	288	>305	0.37	2676	29††
	pH 6.0	280/316‖	>335	1.00	3278 ± 35	
	pH 4.6	288	>305	1.00	3225	
	MeOH	288	>305	1.00	3979 ± 497	
		288	313	1.00	3653	
		288	390	0.44	3622	192
	CH_3CN	288	>305	1.00	4318#	
		288	350	1.00	4334#	
		288	>400	0.56 ± 0.09	4521 ± 59	600 ± 4
	DMSO	288	>305	1.00	3687 ± 52#	
		288	313-350¶	1.00	3783 ± 46#	
		288	370	0.85	3660	801
		288	390	0.84 ± 0.05	3726 ± 72	970 ± 149
5-OH-Tryptophan	H_2O, pH 11.8	288	>305	0.13	3087	24¶
	pH 11.5	288	>305	0.34	3704	32¶
	pH 11.2	288	>305	0.46	4031	31¶
	pH 10.5	288	>305	1.00	4278	
	pH 6.4	280/310‖	>335	1.00	3680 ± 53	
	pH 1	290	>335	0.45	1712	395
	MeOH	288	>305	1.00	4023	
	DMSO	288	>305	1.00	3895	
7-Azaindole	H_2O, pH 7 (16)	305	>320	1.00	886 ± 15	
	MeOH (16)	285	>320	0.90	147 ± 3**	730
	DMSO (12)	305	>320	1.00	9300 ± 200	
	CH_3CN (12)	305	>320	1.00	5700 ± 200	
7-Azatryptophan	H_2O, pH 7 (12)	305	>320	1.00	780 ± 10	
	MeOH (12)	305	>320	1.00	140 ± 3**	
	DMSO (23)	288	>320	0.10 ± 0.02	1080 ± 50	15400 ± 863
	CH_3CN (23)	288	>335	0.25	953	6978
NAc-P(7AT)N-NH_2§	H_2O, pH 7 (20)	310	>345	1.00	833 ± 20	
KACP(7AT)NCD-NH_2§	H_2O, pH 7 (23)	290	>335	0.20 ± 0.04	189 ± 31	845 ± 9

Table 2.1. (continued)

* The numbers in parentheses in this column are the references from which the data were taken.

† For double exponential decays $a_1 + a_2 = 1.00$.

‡ Uncertainties were obtained from replicate measurements.

§ Synthetic 7-azatryptophan-containing tripeptide and octapeptide that mimic the active site of the potato chymotrypsin inhibitor II in which leucine has been replaced by 7-azatryptophan [20,23].

‖ The fluorescence lifetime is insensitive to excitation wavelength.

¶ Collecting emission with 313 nm, 334 nm, and 350 nm interference filters of 10 nm bandpass produced little change in the lifetime.

\# A slight improvement in the χ^2 and residuals is observed when a second component is used to fit these data (see text).

** Emission collected over the normal band [10,18]: 320 nm < λ_{em} < 480 nm.

†† Given the time-scale used to collect these data (9 ns full scale) and the duration of our instrument response function (~50 ps), the uncertainty in this lifetime value is quite large.

Table 2.2. Fluorescence decay parameters of mutant proteins*

Mutant	λ_{ex} (nm)	λ_{em} (nm)	τ_1 (a_1)	τ_2 (a_2)	τ_3 (a_3)
122W	290	>335	207 (0.28)	1469 (0.33)	5272 (0.39)
5OH122W	290	>335	130 ± 20	1430 ± 50	4660 ± 200
			(0.29 ± 0.01)	(0.46 ± 0.02)	(0.25 ± 0.01)
	290	>400	130 ± 20	1430 ± 50	4660 ± 200
			(0.36 ± 0.02)	(0.39 ± 0.01)	(0.25 ± 0.01)
	300	>335	130 ± 20	1430 ± 50	4660 ± 200
			(0.25 ± 0.02)	(0.52 ± 0.01)	(0.23 ± 0.03)
	300	>400	130 ± 20	1430 ± 50	4660 ± 200
			(0.56 ± 0.01)	(0.28 ± 0.02)	(0.16 ± 0.02)
7N122W	290	>335	240 ± 10	800 ± 50	5100 ± 100
			(0.20 ± 0.01)	(0.70 ± 0.02)	(0.10 ± 0.01)
	290	>350	240 ± 10	800 ± 50	5100 ± 100
			(0.18 ± 0.01)	(0.75 ± 0.03)	(0.07 ± 0.01)
	290	>375	240 ± 10	800 ± 50	5100 ± 100
			(0.16 ± 0.01)	(0.78 ± 0.02)	(0.06 ± 0.01)
	300	>375	240 ± 10	800 ± 50	5100 ± 100
			(0.31 ± 0.01)	(0.64 ± 0.02)	(0.05 ± 0.01)
	300	>430	240 ± 10	800 ± 50	5100 ± 100
			(0.27 ± 0.01)	(0.69 ± 0.03)	(0.04 ± 0.02)
	300	>490	240 ± 10	800 ± 50	5100 ± 100
			(0.18 ± 0.02)	(0.77 ± 0.01)	(0.05 ± 0.01)

* Data are fit to a sum of three exponentials: $F(t) = a_1\exp(-t/\tau_1) + a_2\exp(-t/\tau_2) + a_3\exp(-t/\tau_3)$. Time constants are given in picoseconds. The results for the mutants containing 5-hydroxytryptophan and 7-azatryptophan were obtained using a global fitting procedure described in the text. Uncertainties were obtained from replicate measurements.

consistent values for the lifetimes of the mutant proteins containing 5-hydroxytryptophan and 7-azatryptophan, we have used the global fitting analysis described in the Materials and Methods.

The emission maximum of tryptophan in water is 351 nm and its lifetime at neutral pH at 20°C is best described by two decaying components of 620 and 3200 ps [1,12]. For 122W, the emission maximum is ~349 nm and the fluorescence lifetimes are 207, 1469 and 5272 ps (Table 2.2). This small blue shift is consistent with the position of the tryptophan residue on the outer solvent-exposed surface of the tropomyosin coiled-coil dimer (position c of the heptad repeat; see Fig. 2.7). The nonexponential decay, therefore, most likely reflects the different microenvironments sensed by each individual probe. For purposes of comparison, we note that Chang and Ludescher [38] have studied the photophysics of the myosin rod, a long coiled-coil domain of myosin having two pairs of tryptophan residues. These tryptophans are located in positions d of the heptad repeat and hence experience a more hydrophobic (though not completely buried) environment than the tryptophans in 122W consistent with their emission maximum of 340-342 nm. It is interesting that the global analysis of their lifetime data yielded three lifetimes of 250, 1490 and 5180 ps, very similar to those observed in 122W.

Little is known about the excited-state photophysics of 5-hydroxytryptophan and 5-hydroxyindole. The lifetime of the former is single exponential in water (3800 ps) with an emission maximum at 340 nm [11,12]. In 5OH122W, the emission maximum of 5-hydroxytryptophan is ~337 nm. The small blue shift is, once again, indicative of a mainly solvent-exposed environment. The fluorescence decay in the protein is nonexponential (Table 2.2). A global fitting of the data collected at different wavelengths yields three components

whose time constants are 130, 1430 and 4660 ps (Table 2.2).

For 7N122W, the 7-azatryptophan emission maximum is 384 nm, which is closer to the emission maximum of 7-azatryptophan in methanol (382 nm) than that in water (397 nm) [12]. In addition, the fluorescence decay is nonexponential with two dominant short-lived components (240 and 800 ps) and a small contribution from a long-lived 5 ns component. We estimated the efficiency of 7-azatryptophan incorporation in the protein to be at least 90% (see the Materials and Methods). As 7-azatryptophan does not exhibit such a long-lived component in water or methanol and because the contribution from this component in 7N122W decreases as both λ_{ex} and λ_{em} are increased, a reasonable hypothesis is that the long-lived component is due to intrinsic tyrosine and contaminating tryptophan residues. Therefore, we believe that the fluorescence decay of 7-azatryptophan in the protein is best described by a double exponential.

We note that there have been two reports of long-lived emission (>1 ns) in systems containing 7-azatryptophan. In the case of the complex of tryptophyl-tRNA synthetase and 7-azatryptophan-AMP [35], a 10 ns lifetime was observed. A 10 ns lifetime is typical of the 1-methyl-7-azatryptophan chromophore incorporated in a peptide environment [19,23]. The other case is that of Wong and Eftink (34) in which 7-azatryptophan was reported to have been incorporated into staphylococcal nuclease A. In this case the fluorescence lifetime of the 7-azatryptophan-containing protein can be fit to the function $F(t) = 0.68\exp(-t/1.83\ \text{ns}) + 0.32\exp(-t/4.35\ \text{ns})$, whereas the wild-type protein containing a tryptophan residue is fit to the function $F(t) = 0.81\exp(-t/1.81\ \text{ns}) + 0.19\exp(-t/5.62\ \text{ns})$. Given the different optical properties of tryptophan and 7-azatryptophan, the similarity of these results is very surprising.

As mentioned below, the main nonradiative process for 7-azaindole and 7-azatryptophan

is excited-state double-proton transfer that is made possible by a proper solvation environment [14-23]. In water, this proton transfer is significantly impeded; and it is required that fluorescence be detected on the blue or red edges of the emission band in order for this process to be monitored. In 7N122W, however, the double exponential fluorescence decay is very similar to that observed in a 7-azatryptophan-containing octapeptide [22,23] and can be detected even when fluorescence is collected from the entire emission band. We have interpreted the photophysics of the octapeptide in terms of the amino acid side chain inducing a solvation environment propitious for excited-state double-proton transfer for a certain population of the 7-azatryptophan chromophores. A similar process may be occurring in tropomyosin. The double-exponential decay thus reflects the population of chromophores that can and cannot execute an excited-state double-proton transfer. Unlike the study with the octapeptide, in the case of 7N122W we were unable to collect decays at wavelengths greater than 500 nm owing to the weak fluorescence intensity of the sample. Hence, we could not determine whether there is a rising component corresponding to medium-assisted excited-state proton transfer.

Using a computer model of the tropomyosin coiled-coil, we attempted to model possible hydrogen-bond interactions between the N_1 and N_7 atoms of 7-azatryptophan and neighboring tropomyosin residues. These attempts were unsuccessful, mainly because the edge of the indole ring that contains the N_1 and N_7 atoms preferentially points away from the coiled-coil surface and therefore away from any potential protein-derived hydrogen bond donors or acceptors (Fig. 2.7). (Note that in the case of 5-hydroxytryptophan, however, the 5-hydroxy group points back at the coiled-coil surface and could possibly interact with other amino acid side chains [see below and Fig. 2.7].) Assuming a stable coiled-coil structure, it is therefore unlikely that the

7-azatryptophan residue in 7N122W is forming intramolecular hydrogen bonds directly with neighboring side chains. We suggest that the unique environment defined by neighboring residues stabilizes a hydration shell around the 7-azatryptophan residue that favors excited-state double-proton transfer (see below).

Fluorescence Anisotropy Decay of Tropomyosin Mutants

Figure 2.3 presents the time-resolved polarized fluorescence traces for the three mutant proteins. For all three, the fluorescence anisotropy decay is well described by a single exponential, but the depolarization times and the limiting anisotropy values are somewhat different. The probe rotational diffusion times in 122W and 7N122W were the same within experimental error (2.1-2.5 ns, Fig. 2.3). The rotational diffusion time of the probe in 5OH122W was 3.2 ns (Fig. 2.3). In all three cases the rotational diffusion times are too large to be attributed to the rotational motion of tryptophan by itself (~45 ps) [39,40]. The absence of a more rapid component suggests that either there is no unrestricted motion of the probe at this position or that such unrestricted motion is not resolvable with our time resolution of ~50 ps. It is important to note, however, that there is a significant reduction of the limiting anisotropy of the probe in the protein matrix as opposed to free in solution. In glasses, for excitation at 290 nm, r(0) is approximately 0.15, 0.14, 0.11 for indole [15], 5-methoxyindole (41) and 7-azaindole [15], respectively. In the time-resolved experiment, for excitation at 290 nm, r(0) is 0.09, 0.10 and 0.05 for 122W, 5OH122W and 7N122W, respectively (Fig. 2.3). For discussions of the measurement and the interpretation of the limiting anisotropy in indoles, see the literature [15,39,41-44].

The anisotropy decay times that we report are compatible with those obtained by other

Figure 2.3. Decays of polarized fluorescence for tropomyosin mutants (9 μM). The residuals for the fluorescence collected parallel to the excitation beam are given just above the residuals for the perpendicular emission. Uncertainties are determined from replicate measurements.

(a) 122W (λ_{ex} = 290 nm, λ_{em} > 335 nm): r(t) = (0.09 ± 0.01) exp(-t/2478 ± 200 ps), χ^2 = 1.16.

(b) 5OH122W (λ_{ex} = 290 nm, λ_{em} > 335 nm): r(t) = (0.095 ± 0.025) exp(-t 3227 ± 271 ps), χ^2 = 1.20.

(c) 7N122W (λ_{ex} = 290 nm, λ_{em} > 375 nm): r(t) = (0.05 ± 0.01) exp(-t/2137 ± 179 ps), χ^2 = 1.15.

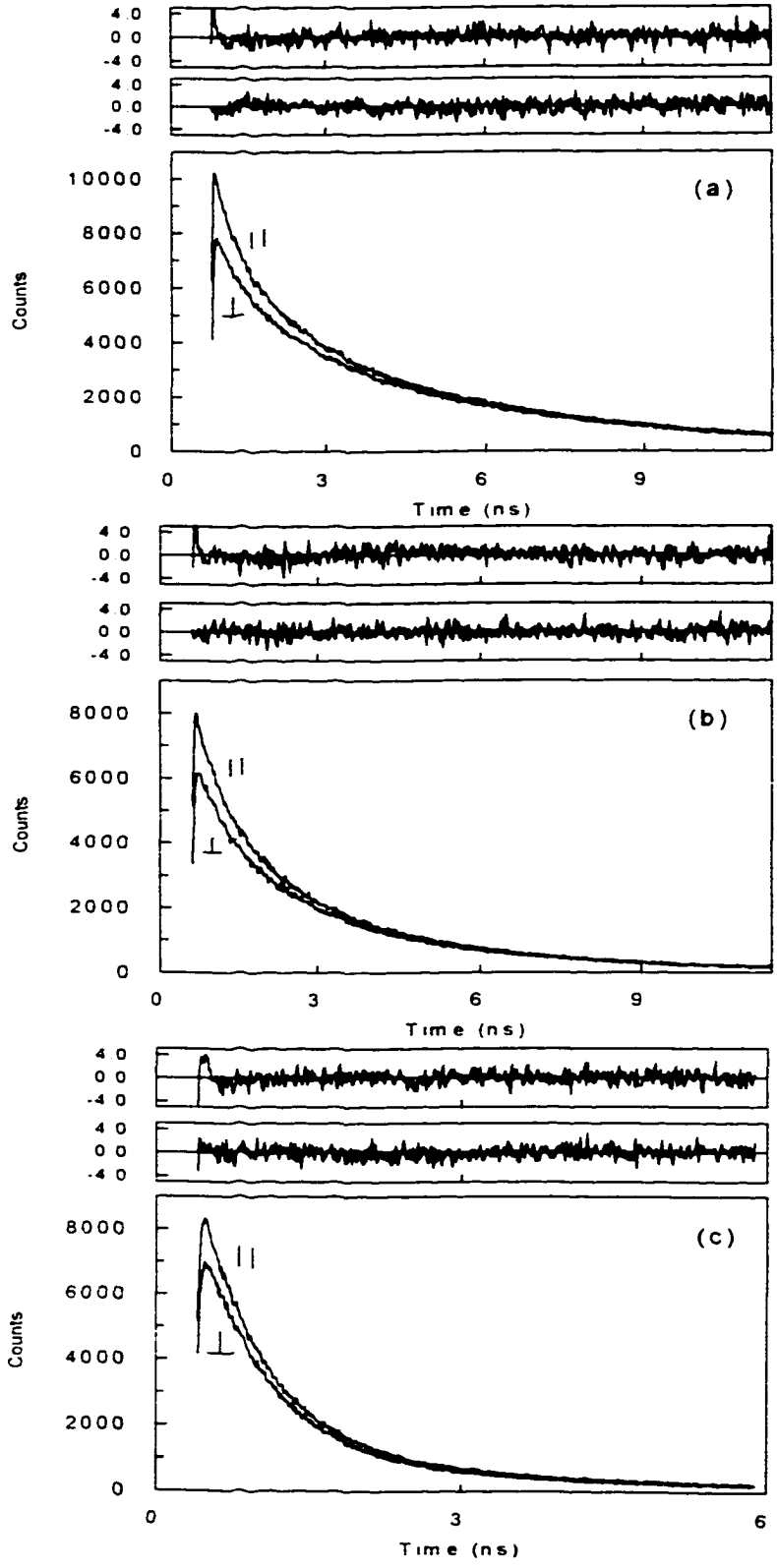
4.0
0.0
-4.0
4.0
0.0
-4.0
10000
8000
6000
4000
2000
0
(a)
||
⊥
Counts
0
3
6
9
Time (ns)
4.0
0.0
-4.0
4.0
0.0
-4.0
8000
6000
4000
2000
0
(b)
||
⊥
Counts
0
3
6
9
Time (ns)
4.0
0.0
-4.0
4.0
0.0
-4.0
8000
6000
4000
2000
0
(c)
||
⊥
Counts
0
3
6
Time (ns)

groups using extrinsic probes attached to a unique cysteine at position 190 of tropomyosin. For example, tropomyosin labeled with N-iodoacetyl-N'-(5-sulfo-1-naphthyl)-ethylenediamine has two measurable anisotropy decay times: one between 3 and 4 ns; and another between 70 and 210 ns [45]. Both time constants are dependent on concentration and ionic strength that affect head-to-tail polymerization of the protein. The longer (70-210 ns) time constant corresponds to the overall tumbling of the tropomyosin coiled-coil [45]. The shorter (3-4 ns) corresponds well with our measurements of 2.1-3.2 ns and probably reflects motions that occur slower than the free rotation of the probe but faster than the overall motion of the protein, for example local segmental fluctuations in secondary or tertiary structure (*i.e.* coiled-coil helix separation, α-helix winding/unwinding). In fact, segments of tropomyosin's tertiary coiled-coil structure seem to be inherently unstable at room temperature [46,47]. The significantly longer rotational diffusion time observed for 5OH122W (3.2 ns) as opposed to that of 122W and 7N122W (2.1-2.5 ns) suggests that the 5-hydroxyl group may be interacting with other functionalities in a manner that dampens these local motions. For example, the 5-hydroxy group may participate in inter- or intrachain H-bonds (see below).

As tropomyosin is a parallel in-register coiled-coil homodimer, one possible contribution to the anisotropy decay is fluorescence energy transfer between the two probes in the dimer. The fluorescent amino acids in these tropomyosin mutants are located at position c of the heptad repeat on opposite sides of the coiled-coil dimer. In a coiled-coil, the C_β atoms of the residues at position c are separated by the polypeptide backbones of the two α-helices by a distance of over 13 Å (the indole moieties by a larger distance, Fig. 2.7). Geometrical considerations of this structure indicate a very low probability of the two tryptophans in the dimer coming within close

contact under the nondenaturing conditions used in this study. It should be mentioned, however, that little is known about the flexibility (breathing) of this particular region of the tropomyosin coiled-coil and that investigations of fragments of tropomyosin suggest a large degree of conformational flexibility in some segments [46]. The spectral overlap integrals between the absorption and emission for tryptophan, 5-hydroxytryptophan and 7-azatryptophan are significantly different and lead to significantly different Förster distances (R_0) and, consequently, different energy transfer times, all of which are long on the time scale of the fluorescence lifetime and anisotropy decays (Fig. 2.4). Therefore, we believe that energy transfer is unlikely to represent a significant mechanism of anisotropy decay in this set of proteins.

Utility and Appropriateness of 5-Hydroxytryptophan and 7-Azatryptophan as Fluorescent Probes.

5-Hydroxytryptophan and 5OH122W. Figure 2.5 presents the absorption and emission spectra for 5-hydroxyindole in the solvents discussed in this article. The spectra shift little as a function of solvent (Fig. 2.5B,D), suggesting that the decay kinetics reported here do not depend strongly on shifts between ^1L_a and ^1L_b states but rather upon the state of protonation of the 5-hydroxy group [42,48]. At high pH (>11) the fluorescence emission of 5-hydroxyindole becomes very weak and significant red shifts are observed for both the absorption spectra and the fluorescence excitation and emission spectra (Fig. 2.5A,C). The shoulder in the absorption and excitation spectra centered at 295 nm in neutral solution shifts to 325 nm in base (Fig. 2.5A; also see the early study by Undenfriend *et al.* [49]).

In base, the decay is best fit to two exponentials, the major contribution coming from a very short component (<30 ps, see Table 2.1). For all other solvents, the fluorescence decay is

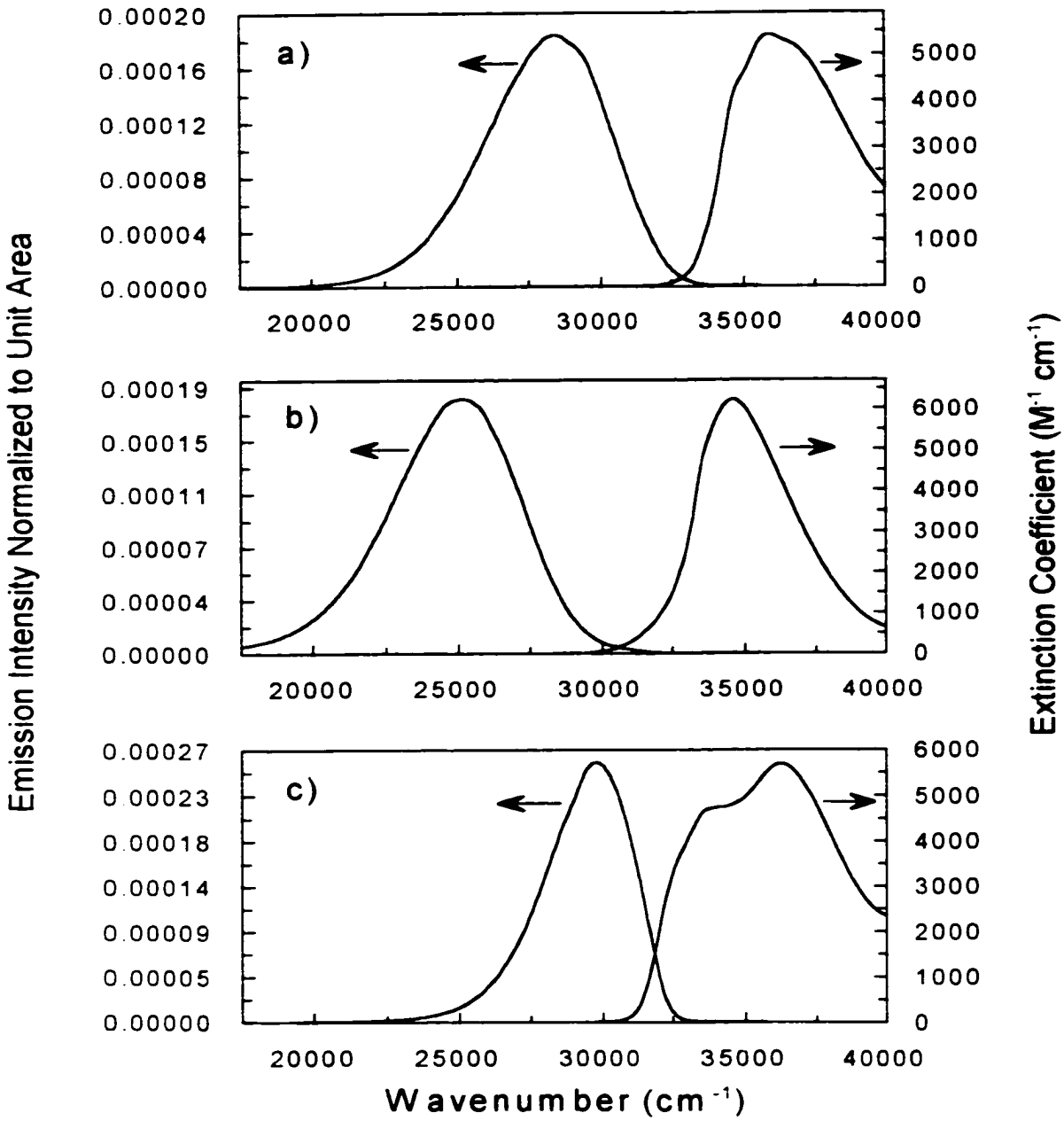

Figure 2.4. Overlap of absorption and emission spectra of (a) tryptophan, (b) 7-azatryptophan, and (c) 5-hydroxytryptophan in aqueous solution at pH ~7 at 20° C. The overlap integrals (58,59) calculated from these spectra are (a) 1.34×10^{-14} cm^6 mol^{-1}, (b) 8.79×10^{-15} cm^6 mol^{-1}, and (c) 1.30×10^{-13} cm^6 mol^{-1}. Arbitrarily taking the distance between the center of the indoles as the separation between donor and acceptor chromophores, molecular modeling based on the coordinates of Chen *et. al.* (40), yields ~15 Å. With the simplifying assumption that the chromophores are free to change relative orientations with respect to each other, energy transfers times of (a) 66.5 ns (b) 179 ns, and (c) 5.57 ns are obtained.

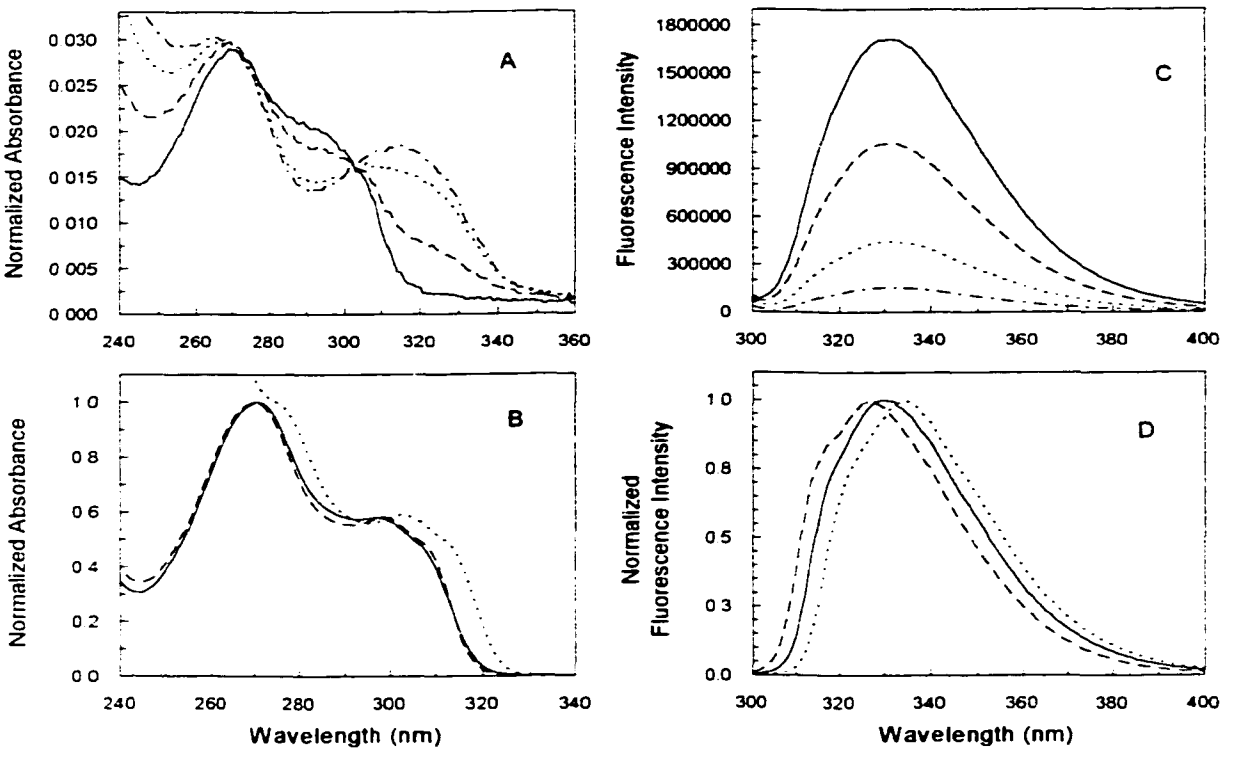

Figure 2.5. A: Absorption spectra of 5-hydroxyindole in water at different pH values: (———) pH 3.98; (– – – –) pH 10.40; (· · · · ·) pH 11.02; (– · – · – · –) pH 11.39.
B: Absorption spectra of 5-hydroxyindole in (———) MeOH, (– – – –) acetonitrile, (· · · · ·) DMSO.
C: Emission spectra of 5-hydroxyindole in water at different pH values: (———) pH 3.98; (– – – –) pH 10.40; (· · · · ·) pH 11.02; (– · – · – · –) pH 11.39.
D: Emission spectra of 5-hydroxyindole in (———) MeOH, (– – – –) acetonitrile, (· · · · ·) DMSO.

single exponential, when emission is collected over the entire band and also when collected at the blue edge and the center of the spectrum (Table 2.1). The decays collected at the red edge are biexponential, most likely due to the red-shift in emission maxima of the deprotonated form. (We did not collect emission at the red edge in water at basic pH because of the reduction in fluorescence quantum yield.) Fluorescence lifetime titrations in water yield a pK_a of 11 for the hydroxyl group of 5-hydroxyindole (Fig. 2.6). The decay kinetics reported here therefore seem to depend on the state of protonation of the 5-hydroxy group. The pH-dependent change in fluorescence of 5-hydroxytryptophan suggests that the short component in the fluorescence decay originates from the interaction of the hydrogen of the 5-hydroxyl group of the six-membered ring with the solvent. Abstraction of this hydrogen or a hydrogen-bonding interaction may open channels of nonradiative decay.

Assuming this hypothesis to be correct, the appearance of a short-lived component (130 ps) in the fluorescence of 5-hydroxytryptophan incorporated at position 122 of tropomyosin may reflect the interaction of the 5-hydroxyl group with a basic or hydrogen-bond accepting group in its microenvironment, leading to its partial deprotonation *via* the formation of a hydrogen bond. This group could be a solvent molecule or could be a protein-derived functional group. In order to investigate the latter hypothesis, we analyzed a molecular model of tropomyosin (50,51) in which position 122 was replaced by 5-hydroxytryptophan (Fig. 2.7). In the tropomyosin primary sequence [52], position 122 is flanked by proton acceptors D121 and E124 and proton donors K117, S123 and R125. Within a single α-helix, the carboxylates of residues 121 and 124 are not easily brought to within hydrogen-bonding distance of the 5-hydroxy group at position 122. However, the carboxylate of E124 from the opposite polypeptide chain is easily

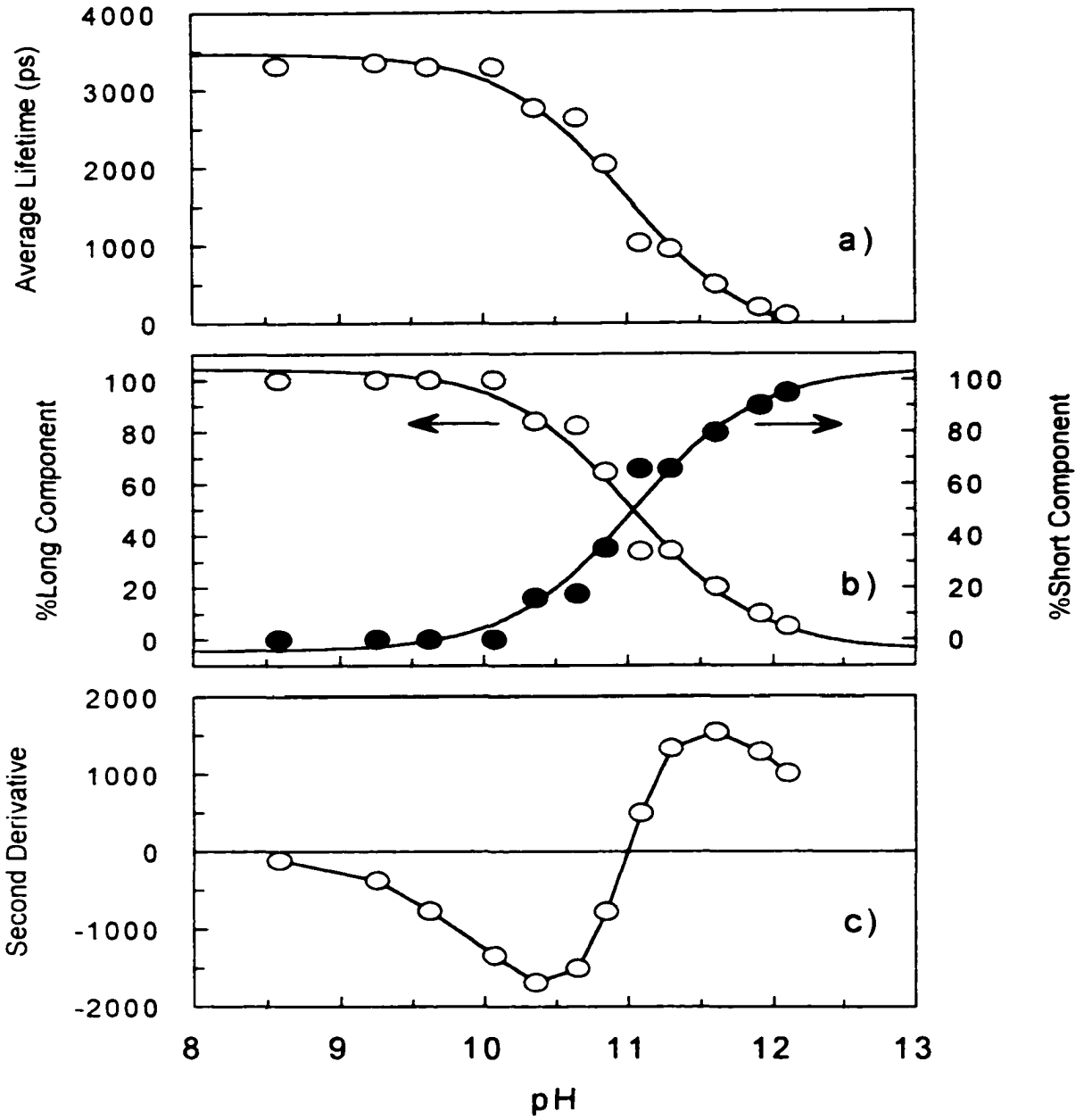

Figure 2.6. (a) Fluorescence lifetime titration curve of 5-hydroxyindole in water. The pH was varied from 8.58 to 12.10. Lifetime decays at various pH units were obtained and fit to no more than two exponentials. The average lifetime values are plotted on the vertical axis. (b) The percentage of each component from the lifetime decays is plotted on separate vertical axes against pH. The short component represents the ionized form of the 5-hydroxyindole and the pH value where 50% ionization occurs (pK_a) is 10.97. Panel (c) presents the second derivative of the titration curve in (a) from which the inflection point was determined to occur at a pH value (pK_a) of 11.04.

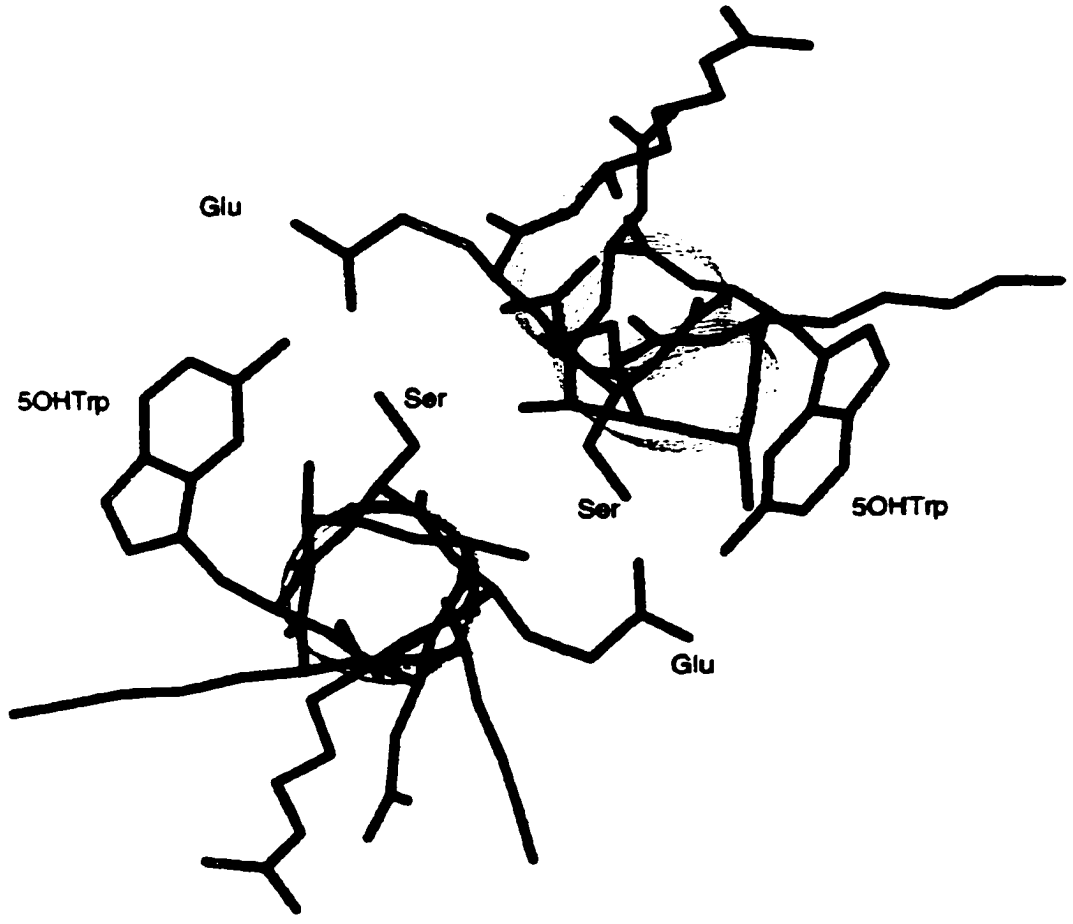

Figure 2.7. Molecular model of a portion of the 5OH122W tropomyosin coiled-coil from residues 117 to 125. The view is parallel to one of the α-helices with the amino-terminal above the page. Only the heavy atoms are shown. Residues 5-hydroxytryptophan-122, serine-123 and glutamate-124 from each strand are labeled. The carboxylate and hydroxyl oxygens of glu-124 (opposite strand) and ser-123 (same strand) side chains can easily be brought to within hydrogen-bonding distance (< 2.6 Å) of the 5-hydroxytryptophan oxygen. This hydrogen-bonding network may result in a partial deprotonation of 5-hydroxtryptophan in this protein and account for the short lifetime component of the fluorescence decay. Note that in the case of 7-azatryptophan, the edge of the indole ring containing the N_1 and N_7 atoms preferentially points away from the coiled-coil surface, diminishing the facility of hydrogen-bond interactions between these atoms and neighboring side-chains. C_α coordinates were obtained from Whitby *et. al.* (50).

oriented such that its carboxylate oxygens are within 2.6 Å of the 5-hydroxy oxygen (Fig. 2.7). In addition, the hydroxyl oxygen of the S123 in the same polypeptide chain as the 5-hydroxytryptophan residue can also be brought to within hydrogen bonding distance of the 5-hydroxyl group (Fig. 2.7). Even though this serine forms part of the hydrophobic interface of the coiled coil (position d), its hydroxyl group may be sufficiently exposed to participate in this interaction. Therefore, residues S123 and E124 could, individually or simultaneously, form interchain or intrachain H bonds with the 5-hydroxyl group. Either interaction could be expected to restrict local breathing of the coiled-coil structure. This could explain the significantly larger probe rotational correlation time observed for 5OH122W compared to 122W and 7N122W.

Based on the arguments in the preceding paragraphs, we may for the moment postulate that there is a protein-protein interaction that coordinates the hydroxyl proton of 5-hydroxytryptophan with, for example, a carboxylate group or hydroxyl group. The result of this interaction is to shorten the lifetime, similar to what we see for 5-hydroxyindole and 5-hydroxytryptophan under basic conditions (Table 2.1). The hypothesis of an intermolecular interaction may be tested in the following manner: (1) conditions capable of denaturing tropomyosin (*i.e.* 8 M urea) should diminish the contribution of the 130 ps component and yield a longer average fluorescence lifetime dominated by a 3-4-ns component, and (2) monitoring the 130 ps component during a pH titration of 5OH122W should reveal a 5-hydroxyl pK_a significantly higher than that of 5-hydroxyindole if hydrogen-bonded to a carboxylate. Figures 2.8 and 2.9 provide the results of such experiments. In Fig. 2.8a the fluorescence lifetime of 5OH122W was measured in 8 M urea. As can be seen, addition of urea only produces a very

Figure 2.8. Fluorescence lifetime decays of 5-OH-tryptophan and 5OH122W tropomyosin, ~10 μM, λ_{ex} = 290 nm and λ_{em} > 335 nm. (a) The effect of urea on the lifetimes of 5-hydroxytryptophan and 5OH122W tropomyosin in pH 7 phosphate buffer.

Decay (1): 5-OH-tryptophan with 4.0 M urea; F(t) = 1.00 exp(-t/3850 ps).
Decay (2): 5-OH-tryptophan with no urea; F(t) = 1.00 exp(-t/3595 ps).
Decay (3): 5OH122W with 8.0 M urea; F(t) = 0.30 exp(-t/204 ps) + 0.47 exp(-t/1534 ps) + 0.24 exp(-t/3981 ps).
Decay (4), 5OH122W with no urea; F(t) = 0.33 exp(-t/226 ps) + 0.42 exp(-t/1586 ps) + 0.26 exp(-t/4206 ps).

(b) Basic pH study of 5OH122W tropomyosin (no urea). Each lifetime was globally fit to a sum of three exponentials with the short component fixed to 130 ps while varying the amplitudes and lifetimes of the other two components.

Decay (1): pH 7.0; F(t) = 0.42 exp(-t/130 ps) + 0.36 exp(-t/1204 ps) + 0.22 exp(-t/3834 ps).
Decay (2): pH 10.1; F(t) = 0.49 exp(-t/130 ps) + 0.35 exp(-t/1259 ps) + 0.16 exp(-t/3581 ps).
Decay (3): pH 11.0; F(t) = 0.68 exp(-t/130 ps) + 0.28 exp(-t/1507 ps) + 0.04 exp(-t/5046 ps).
Decay (4): pH 12.0; F(t) = 0.82 exp(-t/130 ps) + 0.15 exp(-t/1493 ps) + 0.03 exp(-t/4954 ps).
Decay (5): pH 12.8; F(t) = 0.89 exp(-t/130 ps) + 0.10 exp(-t/1413 ps) + 0.01 exp(-t/26882 ps).
There is considerable uncertainty in the value of the longest-lived component of decay (5) given that its amplitude is only 1%.

(c) Acidic pH study of 5-hydroxytryptophan and 5OH122W tropomyosin (no urea).

Decay (1): 5-OH-tryptophan in pH 7.3 buffer; F(t) = 1.00 exp(-t/3500 ps).

Decay (2): 5OH122W tropomyosin in pH 7.0 phosphate buffer; F(t) = 0.33 exp(-t/226 ps) + 0.42 exp(-t/1586 ps) + 0.25 exp(-t/4206 ps).
Decay (3): 5OH122W tropomyosin in buffer, pH 0.93: F(t) = 0.45 exp(-t/566 ps) + 0.49 exp(-t/1586 ps) + 0.06 exp(-t/4206 ps).
Decay (4): 5-OH-tryptophan in buffer, pH 0.96: F(t) = 0.55 exp(-t/395 ps) + 0.45 exp(-t/1712 ps).

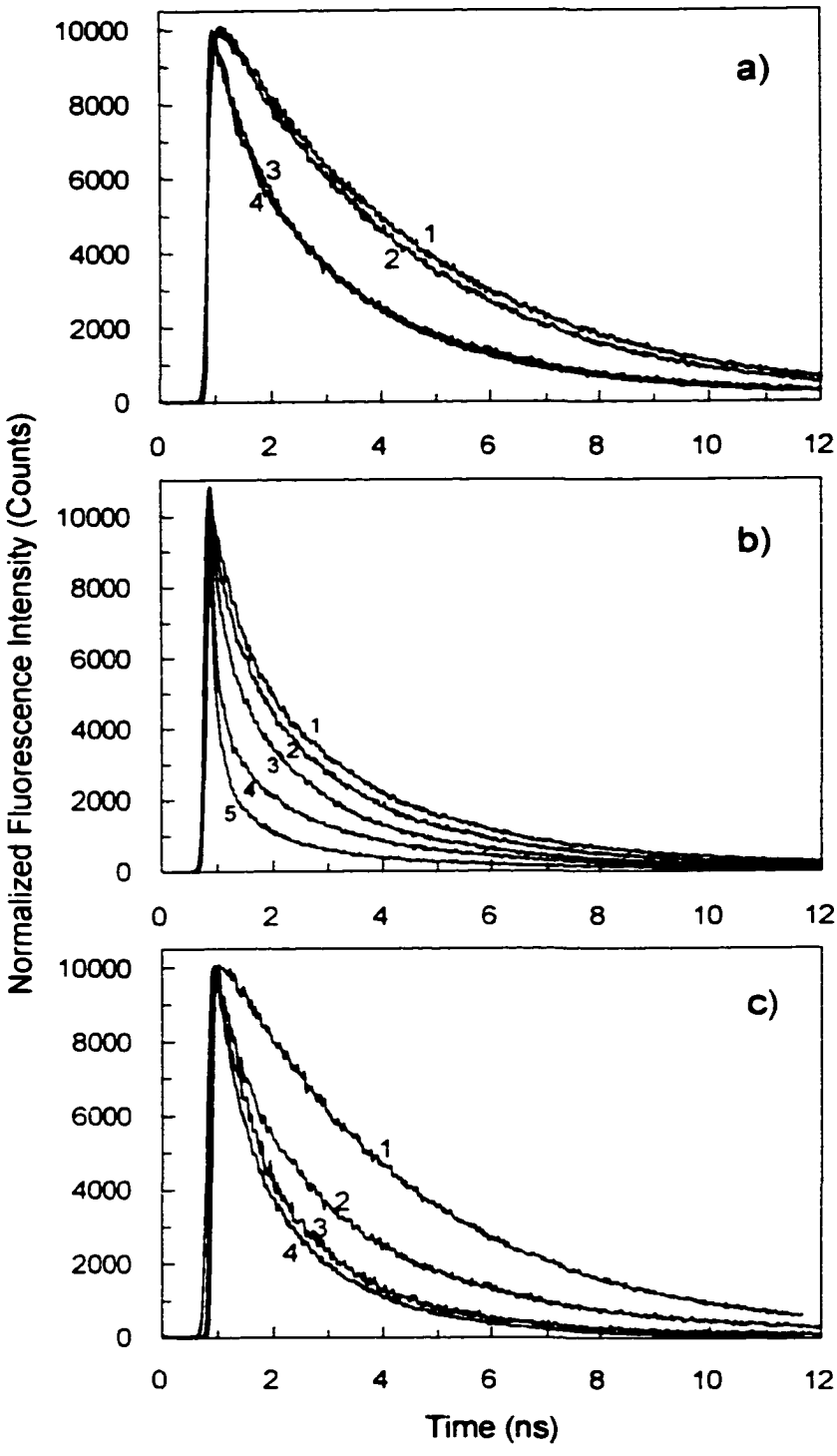
a)
b)
c)
Normalized Fluorescence Intensity (Counts)
Time (ns)
0
2000
4000
6000
8000
10000
0
2
4
6
8
10
12
1
2
3
4
5

minor change in the fluorescence decay (compare traces 3 and 4). This result is inconsistent with the hypothesis that an interchain H bond involving E124 is the source of the short lifetime. In Fig. 2.8b and c we measured the fluorescence lifetime of 5OH122W as a function of pH in the absence of urea in order to find evidence for a titratable group coordinated to the hydroxyl group of 5-hydroxytryptophan. Changing the pH from 7 to 12 greatly shortens the average fluorescence lifetime (Figs. 2.8b and 2.9): up to pH 12.8, the dominant component is 130 ps, as determined by a global fitting procedure in which this component was held fixed at this value. If this component is permitted to vary freely, it decreases from 400 to 90 ps as the pH is increased. The response of the fluorescence lifetime of 5OH122W to pH (pK_a = 10.7, Fig. 2.9) qualitatively follows that of 5-hydroxyindole and 5-hydroxytryptophan (pK_a = 11.04, Fig. 2.6) and the observed pK_a are equal to within the experimental error of the data. This observation also does not support the hypothesis of an intermolecular interaction involving the 5-hydroxy group. Furthermore, lowering the pH to ~1 induces a 600 ps component in 5OH122W (Fig. 2.8c), but the fluorescence lifetime is very similar to that of 5-hydroxytryptophan at this pH (Table 2.1).

The above results indicate that the hydroxyl group of 5-hydroxytryptophan does not participate in an interchain hydrogen bond (lifetimes in urea, Fig. 2.8a) nor does it participate in a hydrogen bond with a titratable hydrogen-bond acceptor (pH titrations, Figs. 2.8b,c and 2.9). One remaining possibility is that of an intrachain hydrogen bond with a nontitratable acceptor sufficiently close in the polypeptide chain that the hydrogen bond be maintained even in the denatured state in 8 M urea. One possible candidate for such an amino acid is Ser123 (Fig. 2.7). A hydrogen bond between the hydroxyl groups of 5-hydroxytryptophan-122 and Ser123 would

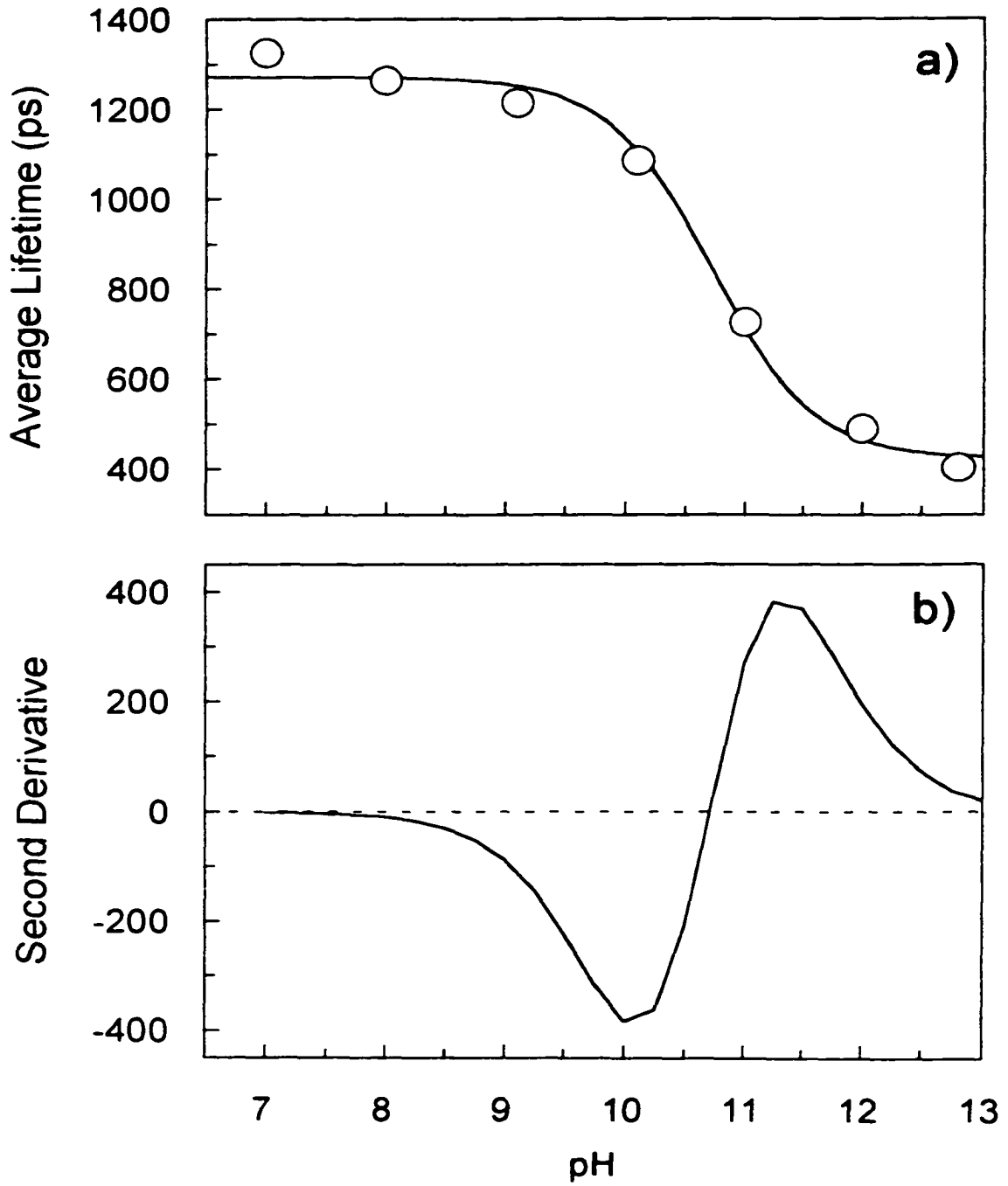

Figure 2.9. (a) Fluorescence lifetime titration curve of 5OH122W tropomyosin (~10 μM). The pH was varied from 7 to 12.8. Lifetime decays cited in the caption to Figure 8 were used to obtain the average lifetime values plotted on the vertical axis. (b) The second derivative of the titration curve from which the inflection point was determined to occur at a pH value (pK_a) of 10.7.

not be expected to result in a large pK_a change as neither serine or 5-hydroxytryptophan protons are significantly labile at neutral pH.

We note that at pH >12 the major component of the lifetime of 5OH122W is 130 ps, instead of ~40 as in the free chromophore. As it is difficult to assign this difference conclusively to an interaction of a neighboring part of the protein, we must consider the possibility that the change in the lifetime is simply a result of the 5-hydroxytryptophan being incorporated into a peptide backbone and consequent modifications in the hydration shell and electric field about the 5-hydroxyindole ring. We are therefore unable to determine the nature of the protein-induced modification that results in the short lifetime component of 5-hydroxyindole in 5OH122W. More detailed investigations into this question will require the study of the photophysics of small peptides of the form X-5-hydroxytryptophan-Y.

7-Azatryptophan and 7N122W. 7-Azatryptophan offers a number of potential advantages over tryptophan as an optical probe of protein structure and dynamics [13-23]. Foremost is the single exponential fluorescence decay of 7-azatryptophan in water over most of the pH range (*e.g.* 780 ps at pH 7 and 20°C when emission is collected over most of the bandwidth). 7-Azatryptophan also has optical spectra that differ significantly from those of tryptophan. The absorption and emission spectra of 7-azatryptophan are red shifted 10 nm and 46 nm, respectively, from those of tryptophan. This makes it remarkably easy to excite 7-azatryptophan selectively in the presence of as many as 40 tryptophans. Consequently, 7-azatryptophan is extremely useful for site-selective studies of protein interactions.

The sensitivity of the 7-azaindole chromophore to its environment depends on both specific and bulk interactions with the solvent [19,22]. Specific interactions with the solvent

are dominated by the N_1 hydrogen that can participate in an excited-state double-proton transfer if properly solvated [13-23]. We have argued that, in water, such a cyclic complex is unfavorable, and that very little (<20% of the population) undergoes excited-state tautomerization [14-16,23] (see also Maliwal *et al.* [53] and Tao and Cho [54] for a discussion of this problem). The bulk interactions of 7-azaindole with the solvent are those typical of most indoles and find their origin in the large dipole change of one of the two closely lying excited states (^1L_a) with respect to its value in the ground state. This dipole change causes the solvent to relax about the new dipole and consequently produces changes in the fluorescence maximum and lifetime of the chromophore [48,55].

It is important to place the photophysics of 7N122W in the context of related studies. We had previously synthesized a 7-azatryptophan-containing tripeptide and octapeptide that mimic the active site of the potato chymotrypsin inhibitor II: NAc-Pro-7-azatrp-Asn-NH_2 and NAc-Lys-Ala-Cys-Pro-7-azatrp-Asn-Cys-Asp-NH_2 [21-23]. The fluorescence lifetime of the 7-azatryptophan tripeptide is single-exponential of 830 ps duration, whereas that of the octapeptide is double exponential (Table 2.1). Thus, not only is the fluorescence decay of 7-azatryptophan in water single exponential, but so is that of the tripeptide containing 7-azatryptophan. In contrast, most derivatives of tryptophan except for the anomalous N-acetyl-tryptophanamide exhibit fluorescence decays that must be fit only to a sum of exponentials [1-3,21]. That the tripeptide exhibits a single-exponential decay likely rules out the possibility that the peptide bond itself is the source of the biexponential decay of the octapeptide, suggesting that the nonexponential behavior arises from the high sensitivity of 7-azaindole to its solvent environment, perhaps as a consequence of excited-state tautomerization of the 7-

azaindole chromophore promoted by solvent organization induced by the peptide backbone or by direct interactions of the 7-azaindole with neighboring amino acid sides chains.

In interpreting the results described above, our organizing assumption is that the double-exponential decay observed for 7N122W, as for the 7-azatryptophan octapeptide [22], is a consequence of excited-state tautomerization that is induced by the protein itself. As we have pointed out elsewhere [22,23] the outstanding question is then to what extent this production of chromophores, that are susceptible to excited-state tautomerization is a result of direct interaction with the peptide, the ability of the peptide to reorganize solvent about the chromophore or a distribution of solvation environments.

Conclusions

The triple-exponential fluorescence decay of 122W is difficult to interpret owing to the intrinsic nonexponential fluorescence decay of tryptophan. Because the α-helices in the tropomyosin coiled-coil used here are identical and have been shown to be parallel and in register [24], the time-averaged microenvironments around the tryptophan residues in each polypeptide chain should be equivalent as has been observed in the slow time-scale in nuclear magnetic resonance studies of coiled-coil peptides [56]. On the other hand, there seem to be several unique environments (protein conformation and solvent interactions) that influence the rate of charge transfer of the indole ring to possible acceptors (solvent or neighboring side chains) and consequently induce the nonexponential fluorescence decay. Some of these environments may also influence the radiative and nonradiative properties of the ^1L_a and ^1L_b levels.

5-Hydroxytryptophan, which has been proposed as an alternative intrinsic optical probe of proteins and which has a single exponential fluorescence decay in water at neutral pH [11,12] (Table 2.1), exhibits a fluorescence decay in 5OH122W that, like tryptophan, requires three components to be described adequately. We indicate here that the fluorescence lifetimes of 5-hydroxyindole and 5-hydroxytryptophan are very sensitive to pH, most likely reflecting the state of protonation or hydrogen-bonding of the 5-hydroxy group [49]. In methanol, acetonitrile, and dimethylsulfoxide (DMSO), nonexponential fluorescence decay can be observed when the red edges of the emission band are collected. This suggests that in these solvents an equilibrium exists between the protonated and anionic forms of the chromophore and that the anionic form has a shorter lifetime than the protonated form. The range of lifetimes observed for 5-hydroxyindole and 5-hydroxytryptophan at high pH and in the nonaqueous solvents is consistent with the lifetimes observed for 5OH122W and is consistent with the idea that the chromophore is in both its protonated and unprotonated or hydrogen-bonded forms in tropomyosin.

For 7N122W, the 240 and 800 ps lifetimes are remarkably similar to those observed in the synthetic octapeptide NAc-Lys-Ala-Cys-Pro-7azatrp-Asn-Cys-Asp-NH_2 [22,23] that we have attributed to the ability of the peptide to solvate a certain subset of chromophores in such a way as to promote excited-state double-proton transfer.

For the three mutants, the fluorescence anisotropy is single exponential, having a rotational time constant of 2-3.2 ns. This value is too small to be a consequence of overall protein motion and too large to correspond to the individual motion of the probe molecules and probably represents local fluctuations in secondary and tertiary structure of the tropomyosin coiled-coil. The absence of any rotational constants corresponding to rapid unrestricted motion

of the individual probe molecules may be because at position 122 the probes are rigidly held by the protein matrix, or because the time resolution of the experiment (~50 ps) is not sufficient to detect those shorter events.

A primary goal of this work has been to provide a photophysical study of the optical probes tryptophan, 5-hydroxytryptophan and 7-azatryptophan in a complex system of biological interest, tropomyosin. In the process, the effect of pH on the excited-state lifetime of 5-hydroxytryptophan has been considered. With the exception of the early and important work of Udenfriend *et al.* [49] and a few other examples [41,57], detailed considerations of the factors influencing the photophysics of 5-hydroxytryptophan have been lacking.

The induced double-exponential fluorescence decay in 7N122W is more easily understood (in terms of excited-state double-proton transfer) than that of the triple-exponential fluorescence decay of 5OH122W, part of which we have attributed to the state of protonation of the 5-hydroxy group. It is concluded that both 7-azatryptophan and 5-hydroxytryptophan are useful and rich optical probes particularly because, unlike the case of tryptophan, the protein induces nonexponential fluorescence decay in these chromophores. That is, the single-exponential fluorescence decays of these two nonnatural amino acids in water provides an important baseline against which protein-induced perturbations can be compared.

Acknowledgments

Part of this work was supported by NSF grants BIR9413969 and CHE-9613962 to J.W.P. and by grants from the Fundação de Amparo à Pesquisa do Estado de São Paulo (FAPESP) to C.S.F. and from FAPESP, the Howard Hughes Medical Institute and the Rockefeller Foundation

to F.C.R.

References

1. Petrich, J. W., M. C. Chang, D. B. McDonald and G. R. Fleming (1983) On the origin of nonexponential fluorescence decay in tryptophan and its derivatives. *J. Am. Chem. Soc.* **105**, 3824-3832.

2. Chang, M. C., J. W. Petrich, D. B. McDonald and G. R. Fleming (1983) Nonexponential fluorescence decay of tryptophan, tryptophylglycine, and glycyltryptophan. *J. Am. Chem. Soc.* **105**, 3819-3824.

3. Chen, L. X.-Q., J. W. Petrich, G. R. Fleming and A. Perico (1987) Picosecond fluorescence studies of polypeptide dynamics: fluorescence anisotropies and lifetimes. *Chem. Phys. Lett.* **139**, 55-61.

4. Hogue, C. W. V., I. Rasquinha, A. G. Szabo and J. P. MacManus (1992) A new intrinsic fluorescent probe for proteins: biosynthetic incorporation of 5-hydroxytryptophan into oncomodulin. *FEBS Lett.* **310**, 269-272.[Abstract]

5. Szabo, A. G. and D. M. Rayner (1980) Fluorescence decay of tryptophan conformers in aqueous solution. *J. Am. Chem. Soc.* **102**, 554-563.

6. Szabo, A. G. and D. M. Rayner (1980) The time-resolved emission spectra of peptide conformers measured by pulsed laser excitation. *Biochem. Biophys. Res. Commun.* **94**, 909-915.

7. Cockle, S. A. and A. G. Szabo (1981) Time-resolved fluorescence spectra of tryptophan in monomeric glucagon. *Photochem. Photobiol.* **34**, 23-27.

8. Werner, T. C. and L. S. Forster (1979) The fluorescence of tryptophyl peptides. *Photochem. Photobiol.* **29**, 905-914.

9. Ross, J. B., K. W. Rousslang and L. Brand (1981) Time-resolved fluorescence and anisotropy decay of tryptophan in adrenocorticotropin-(1-24). *Biochemistry* **20**, 4361-4369.

10. Creed, D. (1984) The photophysics and photochemistry of the near-UV absorbing amino acids-I. Tryptophan and its simple derivatives. *Photochem. Photobiol.* **39**, 537-562.

11. Beechem, J. M. and L. Brand (1985) Time-resolved fluorescence of proteins. *Annu. Rev. Biochem.* **54**, 43-71.

12. Chen, Y., F. Gai and J. W. Petrich (1994) Single-exponential fluorescence decay of the nonnatural amino acid 7-azatryptophan and the nonexponential fluorescence decay of tryptophan in water. *J. Phys. Chem.* **98**, 2203-2209.

13. Négrerie, M., S. M. Bellefeuille, S. Whitham, J. W. Petrich and R. W. Thornburg (1990) Novel noninvasive in situ probe of protein structure and dynamics. *J. Am. Chem. Soc.* **112**, 7419-7421. [Abstract]

14. Chen, Y., F. Gai and J. W. Petrich (1993) Solvation of 7-azaindole in alcohols and water: evidence for concerted, excited-state, double-proton transfer in alcohols. *J. Am. Chem. Soc.* **115**, 10158-10166.

15. Rich, R. L., Y. Chen, D. Neven, M. Négrerie and J. W. Petrich (1993) Steady-state and time-resolved fluorescence anisotropy of 7-azaindole and its derivatives. *J. Phys. Chem.* **97**, 1781-1788.

16. Chen, Y., R. L. Rich, F. Gai and J. W. Petrich (1993) Fluorescent species of 7-azaindole and 7-azatryptophan in water. *J. Phys. Chem.* **97**, 1770-1780.

17. Smirnov, A. V., R. L. Rich, and J. W. Petrich (1994) Synthesis and spectral characterization of 5`-phosphopyridoxyl-D,L-7-azatryptophan, a photophysical probe of protein structure and dynamics. *Biochem. Biophys. Res. Commun.* **198**, 1007-1011.

18. Gai, F., Y. Chen and J. W. Petrich (1992) Nonradiative pathways of 7-azaindole in water. *J. Am. Chem. Soc.* **114**, 8343-8345.

19. Rich, R. L., A. V. Smirnov, A. W. Schwabacher and J. W. Petrich (1995) Synthesis and photophysics of the optical probe N_1-methyl-7-azatryptophan. *J. Am. Chem. Soc.* **117**, 11850-11853.

20. Rich, R. L., M. Négrerie, J. Li, S. Elliot, R. W. Thornburg and J. W. Petrich (1993) The photophysical probe, 7-azatryptophan, in synthetic peptides. *Photochem. Photobiol.* **58**, 28-30.

21. Rich, R. L., F. Gai, J. W. Lane, J. W. Petrich and A. W. Schwabacher (1995) Using 7-azatryptophan to probe small molecule-protein interactions on the picosecond time scale: the complex of avidin and biotinylated 7-azatryptophan. *J. Am. Chem. Soc.* **117**, 733-739.

22. English, D. S., R. L. Rich and J. W. Petrich (1998) Nonexponential fluorescence decay of 7-azatryptophan induced in a peptide environment. *Photochem. Photobiol.* **67**, 76-83.

23. Smirnov, A. V., D. S. English, R. L. Rich, J. Lane, L. Teyton, A. W. Schwabacher, S. Luo, R. W. Thornburg and J. W. Petrich (1997) Photophysics and biological

applications of 7-azaindole and its analogs. *J. Phys. Chem. B* **101**, 2758-2769.

24. Smillie, L. B. (1979) Structure and functions of tropomyosins from muscle and non-muscle sources. *Trends Biochem. Sci.* **4**, 151-155.

25. Lupas, A. (1996) Coiled coils: new structures and new functions. *Trends Biochem. Sci.* **21**, 375-382.

26. Zot, A. S. and J. D. Potter (1987) Structural aspects of troponin-tropomyosin regulation of skeletal muscle contraction. *Ann. Rev. Biophys. Chem.* **16**, 535-559.

27. Chalovich, J. M. (1992) Actin-mediated regulation of muscle contraction. *Pharmacol. Ther.* **55**, 95-148.

28. Farah, C. S. and F. C. Reinach (1995) The troponin complex and regulation of muscle contraction. *FASEB J.* **9**, 755-767.

29. Tobacman, L. S. (1996) Thin filament-mediated regulation of cardiac contraction. *Ann. Rev. Physiol.* **58**, 447-481.

30. Huxley, H. E. (1972) Structural changes in the actin- and myosin-containing filaments during contraction. *Cold Spring Harbour Symp. Quant. Biol.* **37**, 361-376.

31. Lehman, W., R. Craig and P. Vibert (1994) Ca^{2+} -induced tropomyosin movement in *Limulus* thin filaments revealed by three-dimensional reconstruction. *Nature* **368**, 65-67.

32. Holmes, K. C. (1995) The actomyosin interaction and its control by tropomyosin. *Biophys. J.* **68**, 2S-7S.

33. Ross, J. B. A., A. G. Szabo and C. W. V. Hogue (1997) Enhancement of protein spectra with tryptophan analogs: fluorescence spectroscopy of protein-protein and protein-nucleic acid interactions. *Methods Enzymol.* **278**, 151-190.

34. Wong, C.-Y. and M. R. Eftink (1997) Biosynthetic incorporation of tryptophan analogues into staphylococcal nuclease: effect of 5-hydroxytryptophan and 7-azatryptophan on structure and stability. *Protein Sci.* **6**, 689-697.

35. Hogue, C. W. V. and A. G. Szabo (1993) Characterization of aminoacyl-adenylates in *B. subtilis* tryptophanyl-tRNA synthetase, by the fluorescence of tryptophan analogs 5-hydroxytryptophan and 7- azatryptophan. *Biophys. Chem.* **48**, 159-169 (Abstract).

36. Monteiro, P. B., R. C. Lataro, J. A. Ferro and F. De Castro Reinach (1994) Functional α-tropomyosin produced in *Escherichia coli*: a dipeptide extension can substitute the

amino-terminal acetyl group. *J. Biol. Chem.* **269**, 10461-10466.

37. Bevington, P. R. and D. K. Robinson (1992) *Data Reduction and Error Analysis for the Physical Sciences,* 2nd ed. pp. 65-72. McGraw-Hill, Inc., New York.

38. Chang, Y.-C. R. D. Ludescher (1994) Tryptophan photophysics in rabbit skeletal myosin rod. *Biophys. Chem.* **49**, 113-126.

39. Ruggiero, A. J., D. C. Todd and G. R. Fleming (1990) Subpicosecond fluorescence anisotropy studies of tryptophan in water. *J. Am. Chem. Soc.* **112**, 1003-1014.

40. Chen, L. X.-Q., R. A. Engh and G. R. Fleming (1988) Reorientation of tryptophan and simple peptides: onset of internal flexibility and comparison with molecular dynamics simulation. *J. Phys. Chem.* **92**, 4811-4816.

41. Eftink, M. R., L. A. Selvidge, P. R. Callis and A. A. Rehms (1990) Photophysics of indole derivatives: experimental resolution of L_a and L_b transitions and comparison with theory. *J. Phys. Chem.* **94**, 3469-3479.

42. Callis, P. R. (1997) ^1L_a and ^1L_b transitions of tryptophan: applications of theory and experimental observations to fluorescence of proteins. *Methods Enzymol.* **278**, 113-150.

43. Cross, A. J., D. H. Waldeck and G. R. Fleming (1983) Time resolved polarization spectroscopy: level kinetics and rotational diffusion. *J. Chem. Phys.* **78**, 6455-6465.

44. Valeur, B. and G. Weber (1977) Resolution of the fluorescence excitation spectrum of indole into the ^1L_a and ^1L_b excitation bands. *Photochem. Photobiol.* **25**, 441-444.

45. Wahl, P., K. Tawada and J.-C. Auchet (1978) Study of tropomyosin labeled with a fluorescent probe by pulse fluorimetry in polarized light. *Eur. J. Biochem.* **88**, 421-424.

46. Holtzer, M. E., D. L. Crimmins and A. Holtzer (1995) Structural stability of short sequences of the tropomyosin chain. *Biopolymers* **35**, 125-136.

47. Privalov, P. L. (1982) Stability of proteins: proteins which do not present a single cooperative system. *Adv. Protein Chem.* **35**, 1-104.

48. Meech, S. R., D. Phillips and A. G. Lee (1983) On the nature of the fluorescent state of methylated indole derivatives. *Chem. Phys.* **80**, 317-328.

49. Udenfriend, S., H. Weissbach and B. B. Brodie (1958) Assay of serotonin and related metabolites, enzymes, and drugs. *Methods Biochem. Anal.* **6**, 95-130.

50. Whitby, F. G., H. Kent, F. Stewart, M. Stewart, X. Xie, V. Hatch, C. Cohen and G. N. Phillips, Jr. (1992) Structure of tropomyosin at 9 Angstroms resolution. *J. Mol. Biol.* **227**, 441-452.

51. Phillips, G. N., Jr. (1986) Appendix: construction of an atomic model for tropomyosin and implications for interactions with actin. *J. Mol. Biol.* **192**, 128-131.

52. Gooding, C., F. C. Reinach and A. R. MacLeod (1987) Complete nucleotide sequence of the fast-twitch isoform of chicken skeletal muscle α-tropomyosin. *Nucleic Acids Res.* **15**, 8105.

53. Maliwal, B. P., A. D. Cardin, R. L. Jackson and J. R. Lakowicz (1985) Nanosecond motions of the single tryptophan residues in apolipoproteins C-I and C-II: a study by oxygen quenching and fluorescence depolarization. *Arch. Biochem. Biophys.* **236**, 370-378.

54. Tao, T. and J. Cho (1979) Fluorescence lifetime quenching studies on the accessibilities of actin sulfhydryl sites. *Biochemistry* **18**, 2759-2765.

55. Ricchelli, F., M. Beltramini, L. Flamigni and B. Salvato (1987) Emission quenching mechanisms in *Octopus vulgaris* hemocyanin: steady-state and time-resolved fluorescence studies. *Biochemistry* **26**, 6933-6939.

56. Junius, F. K., S. I. O'Donoghue, M. Nilges, A. S. Weiss and G. F. King (1996) High resolution NMR solution structure of the leucine zipper domain of the c-Jun homodimer. *J. Biol. Chem.* **271**, 13663-13667.

57. Kishi, T., M. Tanaka and J. Tanaka (1977) Electronic absorption and fluorescence spectra of 5-hydroxytryptamine (serotonin). Protonation in the excited state. *Bull. Chem. Soc. Jpn.* **50**, 1267-1271.

58. Forster, T. (1965) Delocalized excitation and excitation transfer. In *Modern Quantum Chemistry: Part III: Action of Light and Organic Crystals*. (Edited by O. Sinanoglu), pp. 93-137. Academic Press, New York.

59. Lakowicz, J. R. (1983) Energy transfer. In *Principles of Fluorescence Spectroscopy*. pp. 303-339. Plenum Press, New York.

CHAPTER III. CONFIRMATION OF EXCITED-STATE PROTON TRANSFER AND GROUND-STATE HETEROGENEITY IN HYPERICIN BY FLUORESCENCE UPCONVERSION

A paper published in the *Journal of the American Chemical Society*[1]

D. S. English[2], K. Das[2], K. D. Ashby[2], J. Park[2], J. W. Petrich [2,4], and E. W. Castner, Jr. [3,4]

Abstract

Fluorescence upconversion measurements of hypericin and its methylated analog, *O*-hexamethoxyhypericin, which possesses no labile protons, confirm excited-state proton (or hydrogen atom) transfer as the primary photophysical event in hypericin. The presence of a rising component in the time-resolved fluorescence of hypericin and the absence of such a component for the hexamethoxy analog are consistent with our assignment of excited-state proton or atom transfer as the primary photophysical process in the light-activated antiviral compound, hypericin. The results using the fluorescence upconversion technique, *which detects only emission from the excited state*, are in good agreement with our previous transient absorbance measurements. The results are also consistent with a heterogeneous ground state of hypericin.

---

[2] Department of Chemistry, Iowa State University, Ames, Iowa 50011-3111. K.D. Ashby performed the steady-state measurements. K. Das and D.S. English performed the upconversion experiments.

[3] Department of Chemistry, Brookhaven National Laboratory, Upton, New York 11973.

[4] Authors to whom correspondence should be addressed.

Introduction

Interest in the polycyclic quinone, hypericin (see ref. 1 for reviews, Figure 3.1a), was spawned by the discovery that it possesses extremely high toxicity toward certain viruses, including HIV, and toward tumors [2-4] and that this toxicity absolutely requires light [5]. The interaction of light with hypericin and hypericin-like chromophores is clearly of fundamental biological importance. Previously we have used ultrafast time-resolved transient absorption spectroscopy as a tool to understand the excite-state processes of hypericin (and its analog hypocrellin) [6-13]. We have concluded that the primary nonradiative process [38] in hypericin is excited-state intramolecular proton (or atom) transfer.

In this work, we make use of a complimentary technique, fluorescence upconversion, to measure the excited-state dynamics. In fluorescence upconversion spectroscopy, an ultrashort laser pulse populates the excited state of the sample. The molecular emission is collected efficiently and imaged into a nonlinear optical or gating crystal. The spontaneous emission is gated or "upconverted" with a replica of the excitation pulse: the sum of the emission light frequency and the gating pulse is detected as a function of gate pulse delay time. The excited-state dynamics, as manifested by the spontaneous emission transients, can be observed with <25 fs time resolution in this way. This technique provides the shortest possible time resolution for spontaneous emission dynamics, at least an order of magnitude better than available with direct detection techniques using streak cameras.

Our argument for intramolecular excited-state proton transfer in hypericin is as follows. The hypericin analog lacking labile protons, mesonaphthobianthrone [14] (Figure 3.1d), is significantly fluorescent and has optical spectra that resemble those of hypericin only when its carbonyl groups are protonated [6,7] (Figure 3.2). Previously, we have argued that the

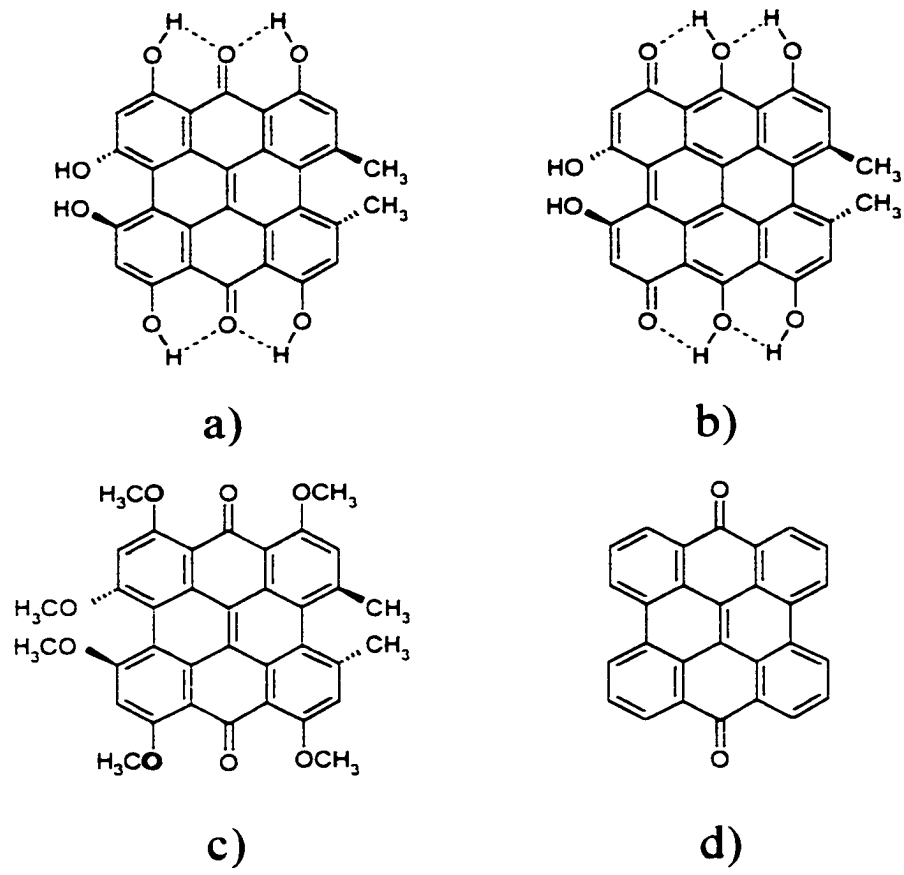

Figure 3.1. Structures of (a) hypericin, (b) one of the three possible hypericin double tautomers (7) (there are two possible monotautomers), (c) *O*-hexamethoxyhypericin, and (d) mesonaphthobianthrone.

Figure 3.2. Steady-state absorbance (———) and emission (- - - -) spectra of (a) hypericin in DMSO and (b) *O*-hexamethoxyhypericin in DMSO. Also presented are emission and absorption spectra for mesonaphthobianthrone (mnb (c)) in DMSO (- - — - - —), methanol (- - - -), and sulfuric acid (———). In panels a and b, the arrows denote the detection wavelengths selected for the transient absorbance and upconversion experiments. Mesonaphthobianthrone (mnb) was prepared (1d) according to the procedure of Koch *et al.* (39). A synthesis of this compound has also been reported by Falk and Vaisburg (14). The absorption spectra of mnb in DMSO and methanol are of higher quality than those presented earlier (1d,7) where the very weak features were hidden by scattering and other artifacts. Note, that the absorption spectra in these solvents are multiplied by a factor of 10 in order to compare them with those in sulfuric acid. In all cases, the emission spectra are normalized to have the same intensity as the corresponding absorption spectra. In order to compare the absorption and emission of hypericin with that of mnb, we cite their extinction coefficients and the fluorescence quantum yields of mnb *relative to that of hypericin in DMSO*. Hypericin/ethanol: ϵ(590 nm) = 40 000 cm^{-1} M^{-1} (40); ϕ_F = 1.00 (the absolute value is conventionally taken as 0.3)(19). Mnb/DMSO: ϵ(428 nm) = 850 cm^{-1} M^{-1}; ϕ_F = 0.056. Mnb/methanol: ϵ(468 nm) = 510 cm^{-1} M^{-1}; ϕ_F = 0.11. Mnb/H_2SO_4: ϵ(510 nm) = 3.0 × 10^4 cm^{-1} M^{-1}; ϕ_f = 1.5. The extinction coefficients we have obtained for mnb in DMSO and methanol are subject to considerable uncertainty. Mnb is very insoluble in these solvents; light scattering from undissolved material, as well as the presence of impurities, contributes to the poor quality of the absorption spectra. Falk and Vaisburg (14) report ϵ(423 nm) = 7000 cm^{-1} M^{-1} in DMSO. The spectra they obtain, especially in methanol, bear qualitative similarity to those presented here. The relative fluorescence quantum yields of mnb in DMSO and methanol must be considered to be upper limits, since even a small amount of highly fluorescent (i.e., long-lived) impurity can contribute to the measured value (10). The value obtained in H_2SO_4 is more certain than those obtained in DMSO or methanol, since in H_2SO_4 mnb is much more fluorescent and has a relatively long-lived fluorescence lifetime of 15 ns (7).

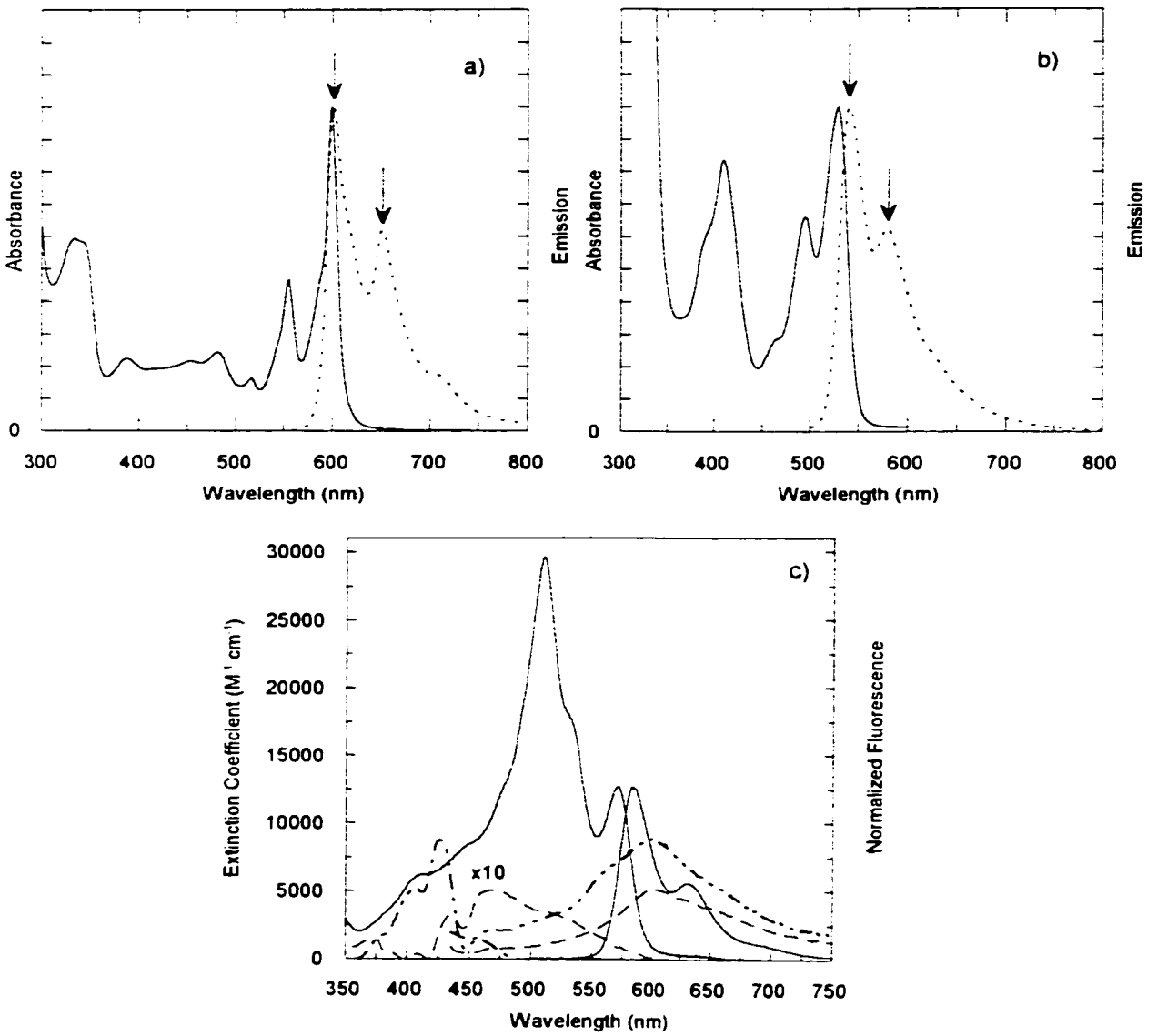
a)
Absorbance
Emission
0
300
400
500
600
700
800
Wavelength (nm)
b)
Absorbance
Emission
0
300
400
500
600
700
800
Wavelength (nm)
c)
Extinction Coefficient (M⁻¹ cm⁻¹)
Normalized Fluorescence
30000
25000
20000
15000
10000
5000
0
x10
350
400
450
500
550
600
650
700
750
Wavelength (nm)

fluorescent state of hypericin grows in on a time scale of several picoseconds, based on transient absorption measurements interpreted in terms of the rise time of stimulated emission of one species and the concomitant decay of the transient absorption of another species. Therefore, the combined observations of the requirement of protonated carbonyls for strong hypericin-like fluorescence and the rise time of fluorescence in hypericin were taken as evidence for intramolecular excited-state proton transfer in hypericin [7,8]. This conclusion was further strengthened by a comparison of the transient absorbance of hypericin and its methylated analog, *O*-hexamethoxyhypericin [9,10]. The assignment of proton transfer also was supported by the observation of a deuterium isotope effect of 1.4 in the excited-state transients of the hypericin analog, hypocrellin [13].

The interpretation of transient absorbance data, however, can be subject to complications because they measure ground-state bleaching, absorption of all excited states present (both singlet and triplet), and stimulated emission [9,10]. Because fluorescence upconversion monitors emission only from the fluorescent singlet state, it is not subject to these complications and hence provides complimentary information not subject to the same ambiguities. The fluorescence upconversion measurements presented here clearly reveals a rising component of ~7 ps in the emission of hypericin and the absence of such a component in the emission of hexamethoxyhypericin, which cannot execute excited-state proton transfer.

Of special relevance to the role of labile proton for light-induced antiviral activity is the observation that hypericin acidifies its surroundings upon light absorption [15-17] and that it retains its toxicity in the absence of oxygen [18]. The retention of toxicity in the absence of oxygen excludes unique assignment of antiviral activity to the trivial generation of singlet

oxygen, even though hypericin does generate triplets in high yield (~70%) [19-21]. Thus, the role of photogenerated protons takes on additional significance, especially in the context of the growing body of literature implicating pH decreases with pharmacologically important functions, such as virucidal activity [22], antitumor activity [23,24], apoptosis (a form of cell death associated with DNA fragmentation and chromatin condensation) [25-27], and the subcellular distribution of hexokinase [28]. We have proposed a chemiluminescent means of activating the pharmacological activity of hypericin and its analogs. [29].

Experimental Section

Hypericin [Carl Roth GmbH (for transient absorption measurements) or Molecular Probes (for upconversion measurements)] was used as received. Anhydrous DMSO from Aldrich was used (freshly opened) without further purification. *O*-Hexamethoxyhypericin was prepared as described elsewhere [9], dissolved in DMSO, and kept under argon for both the upconversion and transient absorbance experiments. (Falk and Mayr have reported the synthesis of an *O*-octamethoxyhypericin.[30]) Storage under argon was necessary to prevent the hexamethoxy sample from degrading, possibly from singlet oxygen formation. Steady-state absorbance spectra were obtained on a Perkin Elmer Lambda 18 double-beam UV-vis spectrophotometer with 1 nm resolution. Steady-state fluorescence spectra were obtained on a Spex Fluoromax with a 4 nm bandpass and corrected for detector response.

The apparatus for transient absorbance measurements is based on an amplified, homemade Ti:sapphire laser system producing pulses of less than 200 fs fwhm at a variable repetition rate as high as 10 kHz. This system is described in detail elsewhere [9].

The fluorescence upconversion apparatus is described in detail elsewhere [31,32] and

is based on a Ti:sapphire oscillator (Spectra physics, Tsunami) producing tunable (750-900 nm) 50-65 fs pulses. Frequency-doubled pulses are used to excite the sample. The residual fundamental wavelength is used as the gate pulse to upconvert the fluorescence, which is collected and focused into a 0.4 mm β barium borate (BBO) crystal with an ellipsoidal reflector. The upconverted signal is separated from the gate beam, from the second and third harmonic beams, and from the fluorescence; it is focused into a monochromator coupled to a Hamamatsu R760 photomultiplier selected for near-zero dark counts. The instrument response function is obtained by collecting a cross-correlation function of the second harmonic and the fundamental: the resulting third harmonic is plotted against delay time. Cross-correlation functions typically have a fwhm of 140-144 fs. All curves were fit and deconvoluted from the instrument function using an iterative convolute-and-compare nonlinear least-squares algorithm.

Results and Discussion

Steady-state absorption and emission spectra for hypericin and O-hexamethoxyhypericin are given in Figure 3.2. Also included in Figure 3.2 are absorption and emission spectra for the simplest hypericin analog that we have investigated, mesonaphthobianthrone. As we noted in the Introduction, this compound has played a pivotal role in our early investigation of the hypericin photophysics and in our identification of intramolecular proton (or atom) transfer as the primary photoprocess. The spectra presented here are of higher quality than those we have previously reported [1d,7].

Figure 3.3 presents a comparison of the fluorescence upconversion and transient absorption traces for hypericin and hexamethoxyhypericin in DMSO. The fluorescence upconversion signal for hypericin clearly shows a rising component (~7 ps), which is not present

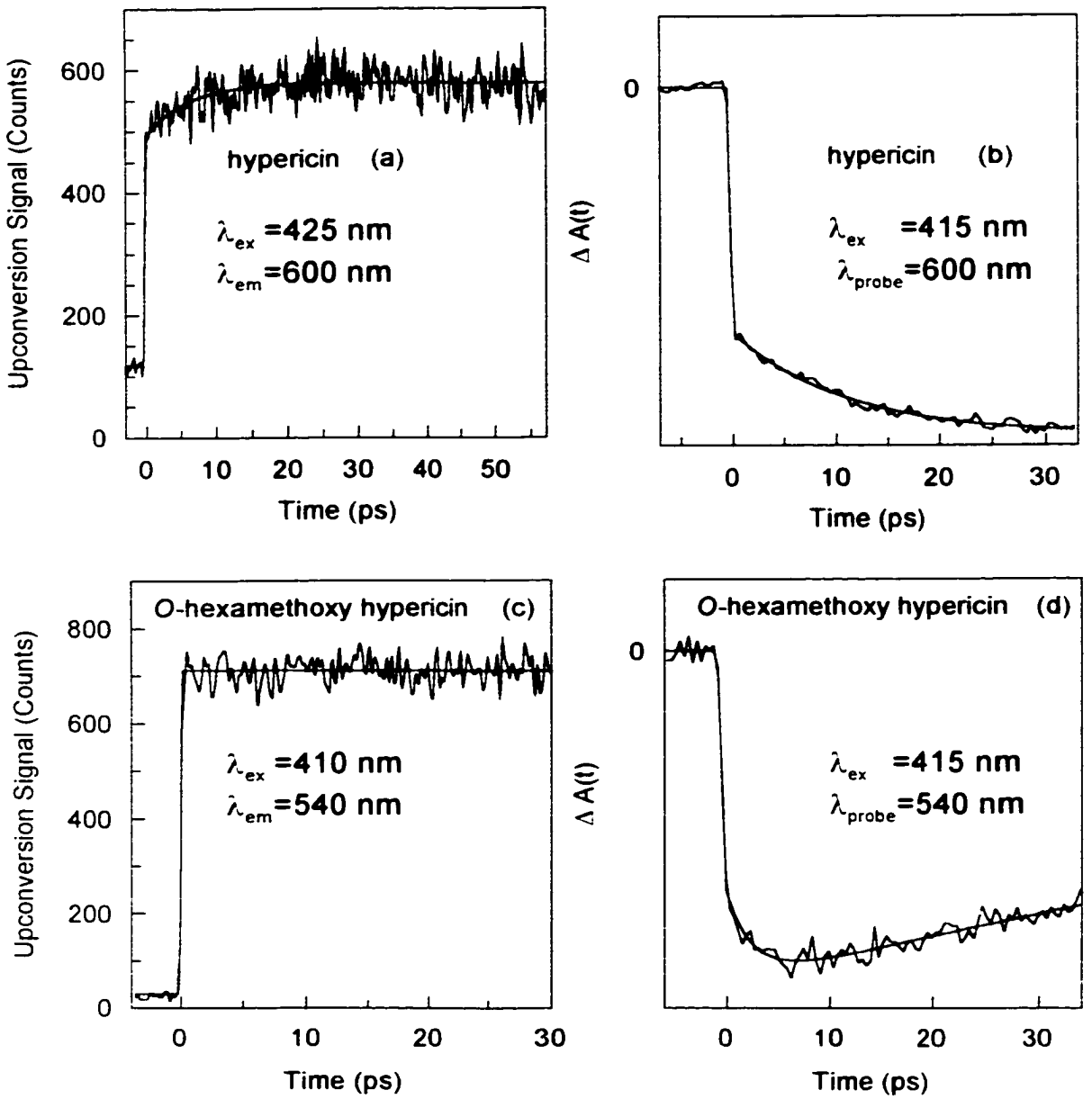

Figure 3.3. Comparison of fluorescence upconversion and transient absorbance traces for hypericin in DMSO at $\lambda_{em} = \lambda_{probe}$ =600 nm and for *O*-hexamethoxyhypericin in DMSO at $\lambda_{em} = \lambda_{probe}$ = 540 nm. These wavelengths correspond to the maxima in the steady-state emission spectra of the respective compounds. In the absorption transients of *O*-hexamethoxyhypericin, there is evidence for a rising component which is not present in the upconversion data. We have assigned this as a rise in the bleach that is attributed to a decay of the excited-state absorbance with a time constant of 2.6 ps. The data are fit to the following functions: (a) F(t) = -0.19 exp(-t/7.3 ps) + 1.0 exp(-t/∞); (b) ΔA(t) = 0.30 exp(-t/11.6 ps) - 1.00 exp(-t/∞); (c) F(t) = 1.00 exp(-t/∞); (d) ΔA(t) = 0.11 exp(-t/2.6 ps) - 1.20 exp (-t/480 ps) + 0.89 exp(-t/∞).

in hexamethoxyhypericin. (Preliminary data indicate an ~2.5 ps rising component in ethanol.) This result is consistent with results obtained using a pump wavelength of 415 nm, in which the rise time is fit to an ~11 ps component.

The fluorescence upconversion signal of hypericin reveals significantly different kinetics in the first 40 ps of the fluorescence decay at the two emission wavelengths investigated, 600 and 650 nm (compare Figures 3.3 and 3.4). At 650 nm, the ~7 ps rising component is completely absent. As we discuss in the Conclusions, these results support our previous suggestions that the ground state of hypericin is heterogeneous.

Figure 3.5 presents data collected on a shorter time scale. For both hypericin and hexamethoxyhypericin at both emission wavelengths, there is evidence of an ~100 fs rise time in the upconversion signal. These ultrafast 100 fs rise times are not instrumental artifacts. The same upconversion spectrometer has been used to observe fluorescence decays for various photoinduced electron transfer systems with lifetimes of <50 fs [32] as well as a series of subpicosecond to several-picosecond decays which have a definite rise time [31a]. In the case of rise times observed for fluorescent coumarin excited singlet states being reductively quenched by aromatic amine solvents, there is good reason to assign these ~100 fs rise times to inertial solvation dynamics, as the polar solvents librate about the very polar coumarin excited state [31b]. Solvation dynamics cannot, however, be invoked to explain the rise times for the hypericins, as the emission displays only a small amount of solvatochromism, indicating a negligible difference between ground- and excited-state dipole moments for the hypericins. A likely assignment for the observed rise times in the hypericins is internal conversion from a higher-lying singlet state, pumped by the ~415 nm laser pulses, to the lowest singlet excited state

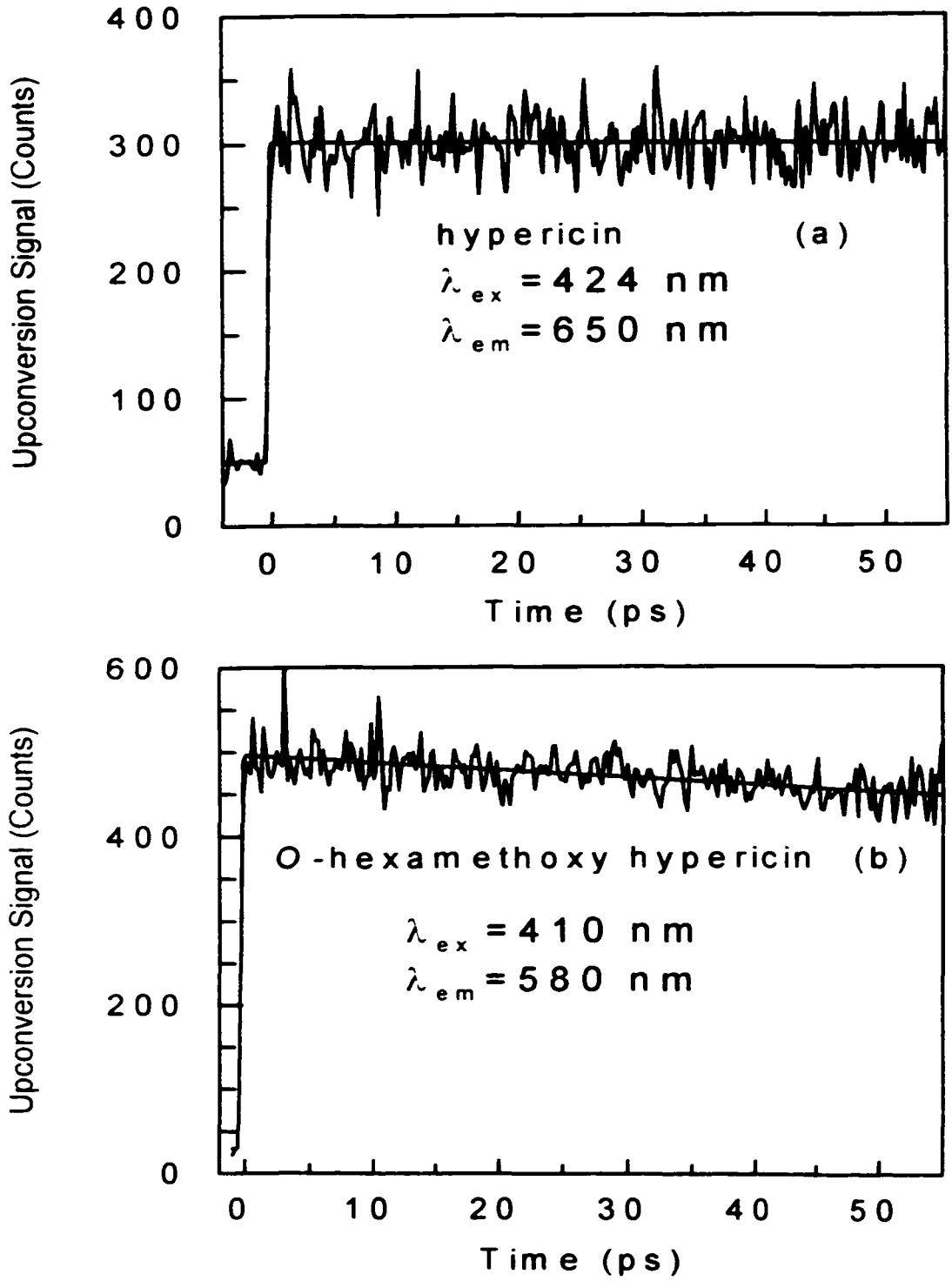

Figure 3.4. Fluorescence upconversion traces of hypericin at 650 nm and *O*-hexamethoxyhypericin at 580 nm. These wavelengths (Figure 2) correspond to the second maxima of the respective fluorescence spectra. The data are fit to the following functions: (a) $F(t) = 1.00 \exp(-t/\infty)$; (b) $F(t) = 1.00 \exp(-t/503\ ps)$.

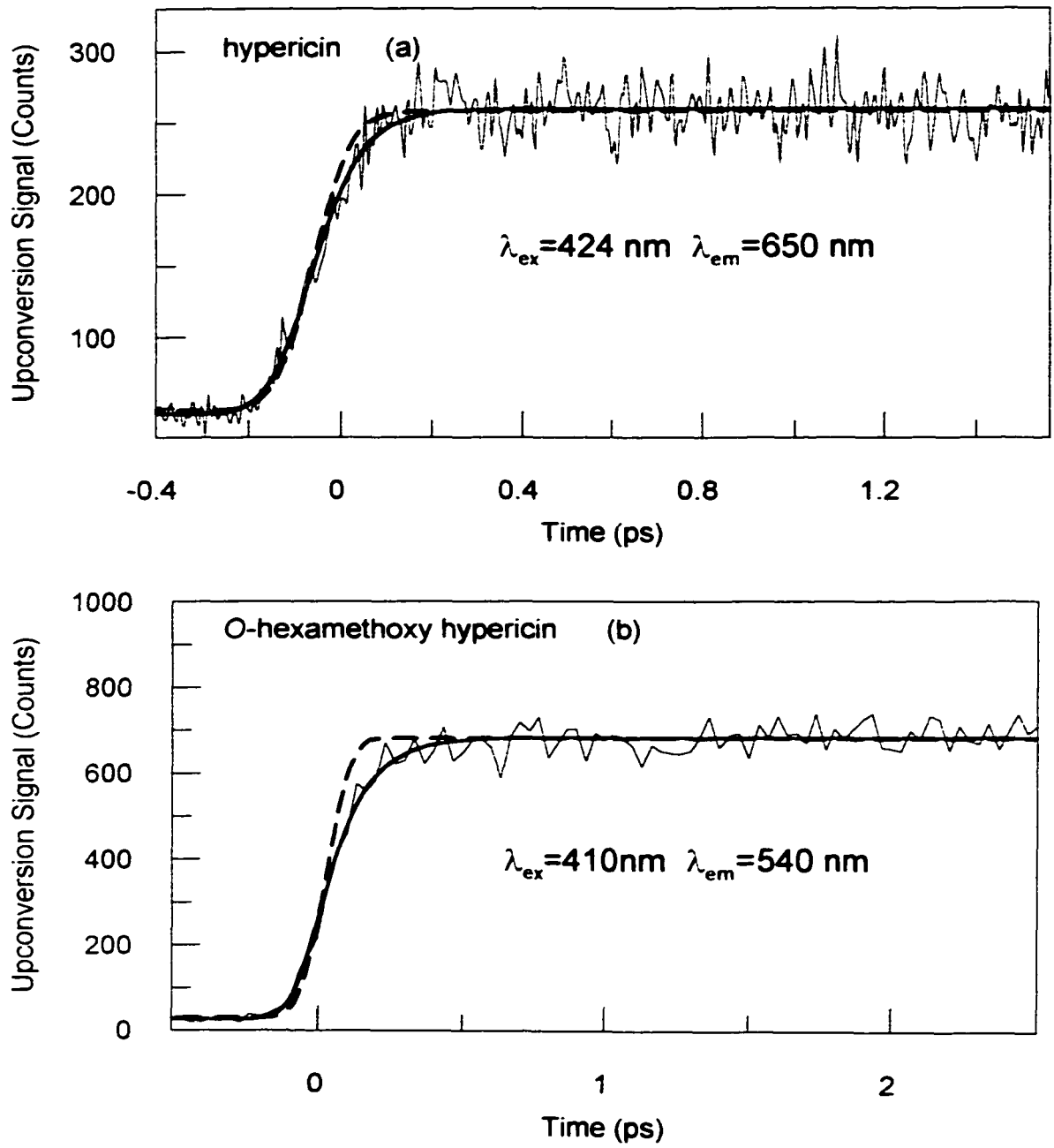

Figure 3.5. Observation of an ~100 fs rise time in the fluorescence upconversion signal. The dashed lines are single exponential fits corresponding to an instantaneous rise time in the fluorescence signal. Fitting the rise of the fluorescence signal to a rise time yields (solid lines) the following: (a) $F(t) = -0.91 \exp(-t/64\text{ fs}) + 1.00\exp(-t/\infty)$; (b) $F(t) = -0.83 \exp(-t/114\text{ fs}) + 1.00 \exp(-t/\infty)$.

near 600 and 540 nm for hypericin and O-hexamethoxyhypericin, respectively. Chudoba et al. have also assigned such 100 fs transients to internal conversion for a different excited-state proton-transfer molecule, 2-(2′-hydroxy-5′ -methylphenyl) benzotriazole [35].

Both in the Introduction and the Conclusions of this paper, we note the potential ambiguities to which transient absorption measurements are subject. In this context, Figure 3.6 presents fits to previous transient absorption data in which the component previously described as a rise in stimulated emission is now attributed to a decay of one species whose excited-state absorption spectrum overlaps the emission spectrum of at least one other species.

Fluorescence anisotropy decays were constructed from upconversion signals polarized parallel and perpendicular to the excitation beam. These are displayed in Figure 3.7 for hypericin and hexamethoxyhypericin. Of significance is that excitation at 410 nm gives rises to a negative anisotropy, i.e., a negative prefactor, $r(0)$. Elsewhere [33] we have presented a detailed investigation of the dependence of the steady-state fluorescence-excitation anisotropy and have observed similar behavior: depending on the excitation wavelength, the prefactor can be positive or negative. This results from the transition dipoles connecting the ground electronic state to the first two excited electronic states being at large angles to each other. If hypericin (which actually has a very twisted aromatic skeleton [13,34]) had C_{2v} symmetry, these transition dipoles would be orthogonal. Also of interest is that the time constant for the anisotropy decay for hexamethoxyhypericin is roughly 3 times greater than that for hypericin and does not decay to zero on the same time scale.

Figure 3.6. Reconsideration of previously obtained transient absorption signals for hypericin in the light of upconversion data presented here. Top: λ_{ex} = 588 nm, λ_{probe} = 645 nm, ethylene glycol (7,8); $\Delta A(t) = -0.56 \exp(-t/2.0\ ps) + 0.43 \exp(-t/6.4\ ps) - 0.19$. Middle: λ_{ex} = 588 nm, λ_{probe} = 658 nm, DMSO (7,8); $\Delta A(t) = -0.19 \exp(-t/2.0\ ps) + 0.27 \exp(-t/6.4\ ps) - 0.30$. Bottom: λ_{ex} = 415 nm, λ_{probe} = 650 nm, DMSO (9); $\Delta A(t) = 0.21 \exp(-t/8.0\ ps) - 0.29$. The spike at "zero time" is not considered in this fit because it is attributed to a cross-phase modulation artifact resulting from the ~150 fs pulses used in the experiment (9,10,41). It is unlikely that this is the case for the top trace, however, since the pulses used for this experiment were no shorter that 1 ps. In each case, the last term in the fit corresponds to a component that does not decay on the time scale of the experiment and that is attributed to the long-lived fluorescent species.

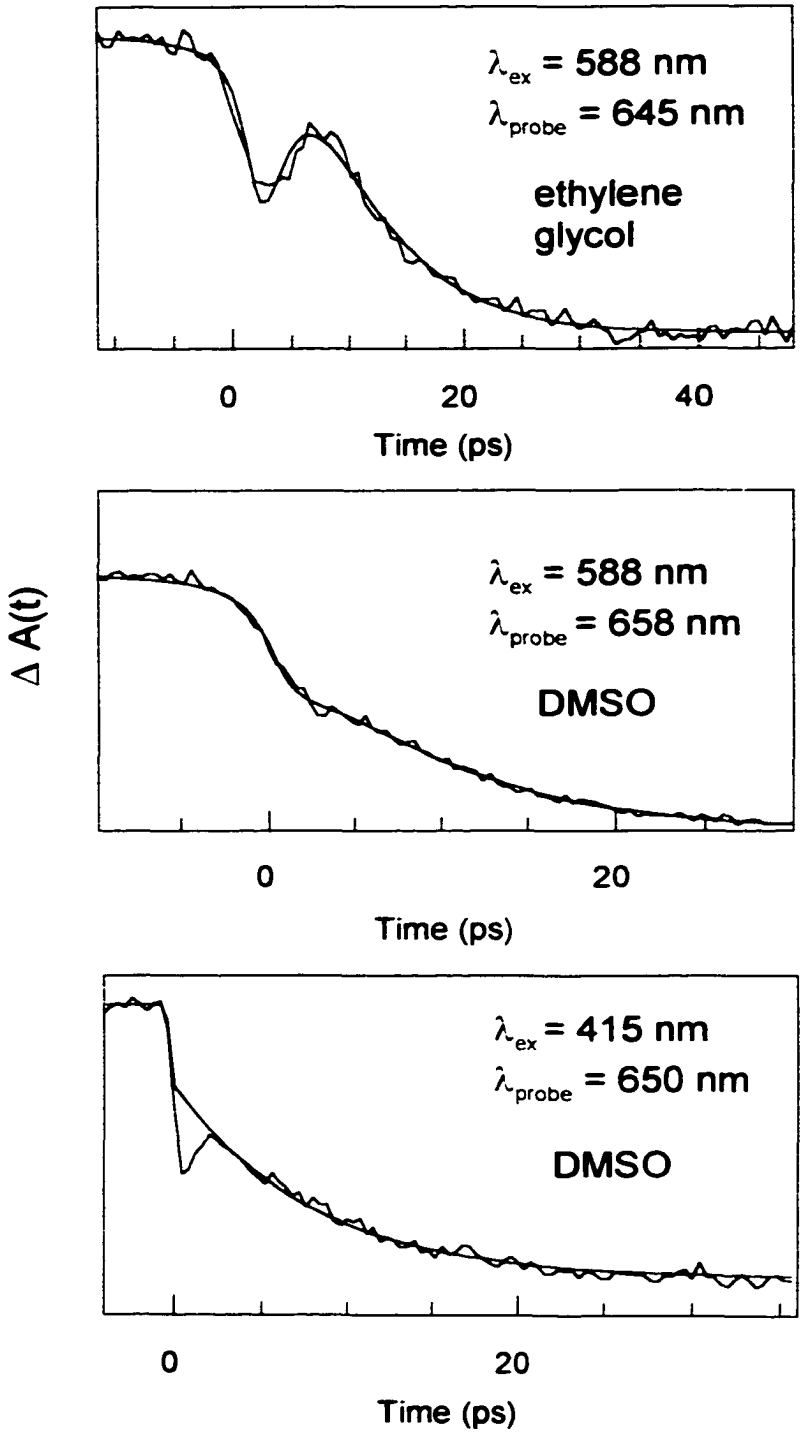
λex = 588 nm
λprobe = 645 nm
ethylene glycol
0
20
40
Time (ps)
Δ A(t)
λex = 588 nm
λprobe = 658 nm
DMSO
0
20
Time (ps)
λex = 415 nm
λprobe = 650 nm
DMSO
0
20
Time (ps)

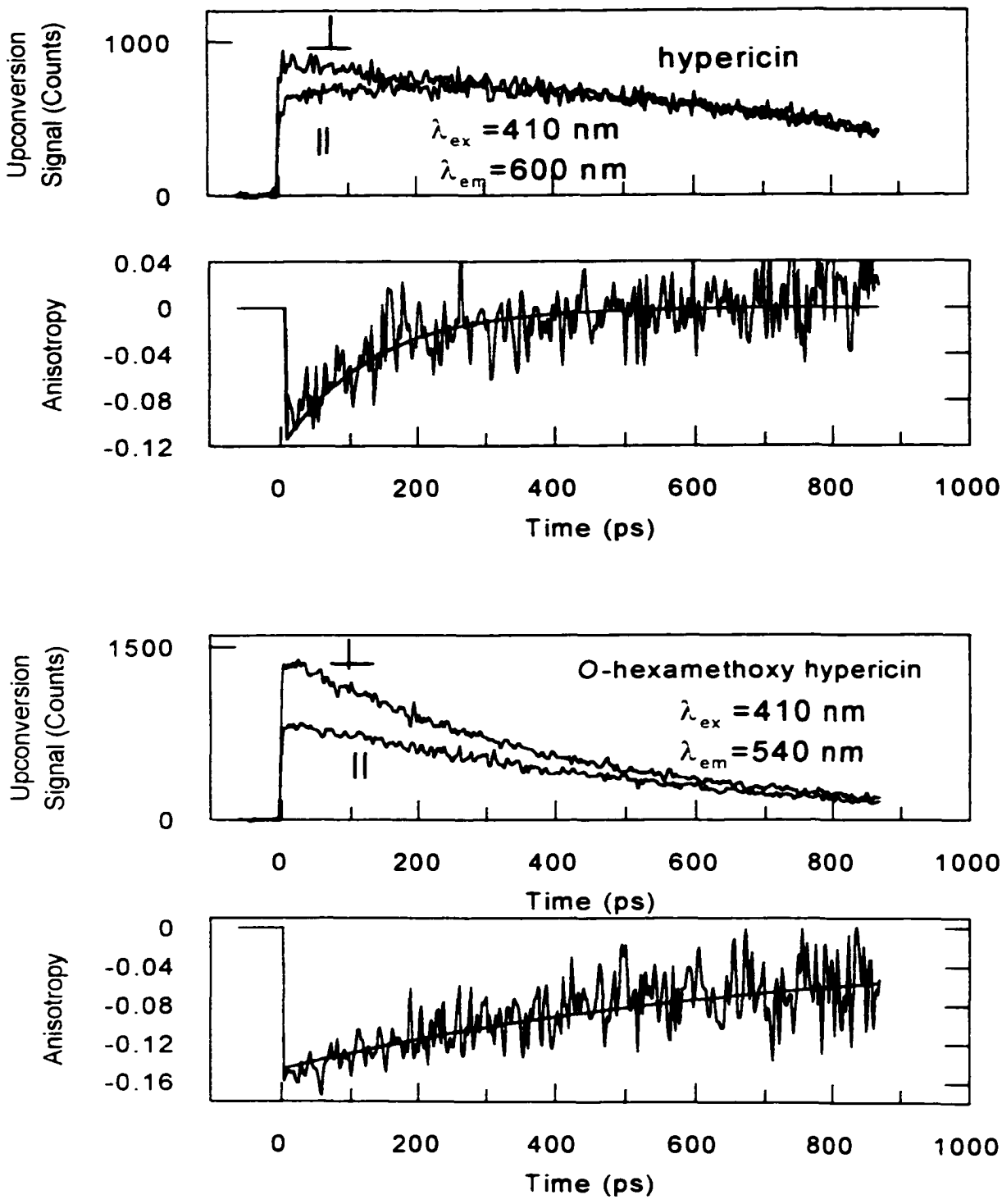

Figure 3.7. Polarized fluorescence traces and anisotropy curves. Hypericin: r(t) = -0.10 exp(-t/192 ps). *O*-Hexamethoxyhypericin: r(t) = -0.10 exp(-t/621 ps - 0.05 exp(-t/2.1 ns).

Conclusions

The fluorescence upconversion technique with 100 fs resolution was applied to hypericin and its synthetic analog, *O*-hexamethoxyhypericin. The results of these studies were compared with previous results obtained by means of transient absorption spectroscopy. Fluorescence upconversion is a powerful technique that is complementary to transient absorption. Transient absorption monitors all absorbing and emitting species (via stimulated emission), given an adequate signal-to-noise ratio. It is difficult, if not impossible, to distinguish ground-state bleaching from stimulated emission in regions where the emission spectrum overlaps the absorption spectrum. Also, emitting species may often be obscured by the presence of absorbing species (singlets and triplets) present in higher concentration or with a larger extinction coefficient. We have discussed and addressed these complications in previous work [7,9,10]. *Because the upconversion technique detects only emission from the exited state, the potential ambiguities in the transient absorption experiment referred to above are obviated.* The fluorescence upconversion results presented here are in complete agreement with the major results and conclusions we have already presented: namely, that excited-state intramolecular proton (or atom) transfer is a primary photophysical event for hypericin and its analogs with labile protons. The upconversion results also validate the transient absorption technique as a means of monitoring proton or atom transfer rates in hypericin, assuming that the transient absorption spectrum is well understood.

In addition, the results presented here support our previous suggestions that the ground state of hypericin is heterogeneous [7,9,10], existing as either various tautomers or conformational isomers, and implies that the same argument can be made for hypocrellin and other hypericin analogs [11-13,33]. We originally suggested that the ground state of hypericin

is heterogeneous in order to rationalize the mirror-image symmetry between its steady-state absorption and emission spectra [7,8]. Such symmetry is atypical of molecules whose excited states undergo nuclear rearrangements, such as proton or atom transfer. The archetypal excited-state proton-transfer system, 3-hydroxyflavone, provides a good example of the absence of such symmetry [36]. The transient absorption data obtained using different excitation wavelengths (415 and 588 nm) presented in Figure 3.6 yield different excited-state kinetics and are also suggestive of such heterogeneity. The upconversion results provide the most direct evidence to date for ground-state heterogeneity in hypericin at ambient temperatures [37]. Not only are the fluorescence profiles for hypericin different at the emission wavelengths of 600 and 650 nm but even at 600 nm there are, in addition to the ~100 fs component, two components to the fluorescence rise time with 7 ps and "instantaneous" time constants. These may be attributed to untautomerized and tautomerized (or at least partially tautomerized) species.

Acknowledgment

This work was supported in part by NSF grant CHE-9613962 to J.W.P. The fluorescence upconversion experiments were carried out at Brookhaven National Laboratory under contract DE-AC02-76CH00016 with the US Department of Energy and supported by its Division of Chemical Sciences, Office of Basic Energy Sciences. We thank Professor H. Falk for comments regarding phenanthrol[1,10,9,8-*opqra*]perylene-7,14-dione.

References

1. (a) Durán, N.; Song, P.-S. *Photochem. Photobiol.* **1995**, *61*, 529-539. (b) Diwu, Z. Photochem. Photobiol. **1995**, *61*, 529-539. (c) Lown, J.W. *Can. J. Chem.* **1997**, *75*, 99-119. (d) Kraus, G.A.; Zhang, W.; Fehr, M.J.; Petrich, J.W.; Wannemuehler, Y.; Carpenter, S. *Chem. Rev.* **1996**, *96*, 523-535.

2. (a) Maruelo, D.; Lavie, G.; Lavie, D. *Proc. Natl. Acad. Sci. U.S.A.* **1988**, *85*, 5230-5234. (b) Degar, S.; Prince, A.M.; Pascual, D.; Lavie, G.; Levin, B.; Mazur, Y.; Lavie, D.; Ehrlich, L.S.; Carter, C.; Maruelo, D. *AIDS Res. Hum. Retroviruses* **1992**, *8*, 1929-1936. (c) Lenard, J.; Rabson, A.; Vaderoef, R. *Proc. Natl. Acad. Sci. U.S.A.* **1993**, *90*, 158-162. (d) Meruelo, D.; Degar, S.; Nuria, A.; Mazur, Y.; Lavie, D.; Levin, B.; Lavie, G. In *Natural Products as Antiviral Agents*; Chu, C.K., Cutler, H.G., Eds.; Plenum Press: New York, 1992; pp 91-119 and references therein.

3. Hudson, J.B.; Zhou, J.; Chen, J.; Harris, L.; Yip, L.; Towers, G.H.N. *Photochem. Photobiol.* **1994**, *60*, 248-254.

4. Thomas, C.; Pardini, R.S. *Photochem. Photobiol.* **1992**, *55*, 831-837.

5. Carpenter, S.; Kraus, G.A. *Photochem. Photobiol.* **1991**, *53*, 169-174.

6. Gai, F.; Fehr, M.J.; Petrich, J.W. *J. Am. Chem. Soc.* **1993**, *115*, 3384-3385.

7. Gai, F.; Fehr, M.J.; Petrich, J.W. *J. Phys. Chem.* **1994**, *98*, 5784-5795.

8. Gai, F.; Fehr, M.J.; Petrich, J.W. *J. Phys.Chem.* **1994**, *98*, 8352-8358.

9. English, D.S.; Zhang, W.; Kraus, G.A.; Petrich, J.W. *J. Am. Chem. Soc.* **1997**, *119*, 2980-2986.

10. English, D.S.; Das, K.; Zenner, J.M.; Zhang, W.; Kraus, G.A.; Larock, R.C.; Petrich, J.W. *J. Phys. Chem.* **1997**, *101A*, 3235-3240.

11. Das, K.; English, D.S.; Fehr, M.J.; Smirnov, A.V.; Petrich, J.W. *J. Phys. Chem.* **1996**, *100*, 18275-18281.

12. Das, K.; English, D.S.; Petrich, J. W. *J. Am. Chem. Soc.* **1997**, *119*, 2763-2764.

13. Das, K.; English, D.S.; Petrich, J.W. *J. Phys. Chem.* **1997**, *101A*, 3241-3245.

14. This compound is more correctly referred to as phenanthro[1,10,9,8-*opqra*]perylene-7,14-dione. Falk, H.; Vaisburg, A.F. *Monatsh. Chem.* **1995**, *126*, 361-364.

15. Fehr, M.J.; McCloskey, M.A.; Petrich, J.W. *J. Am. Chem. Soc.* **1995**, *117*, 1833-1836.

16. Fehr, M.J.; Carpenter, S.L.; Wannemuehler, Y.; Petrich, J.W. *Biochemistry* **1995**, *34*, 15845-15848.

17. (a) Sureau, F.; Miskovsky, P.; Chinsky, L.; Turpin, P.Y. *J. Am. Chem. Soc.* **1996**, *118*, 9484-9487. (b) Chaloupka, R.; Sureau, F.; Kocisova, E.; Petrich, J.W. *J. Am. Chem. Soc.* Submitted for publication.

18. Fehr, M.J.; Carpenter, S.L.; Petrich, J.W. *Bioorg. Med. Chem. Lett.* **1994**, *4*, 1339-1344.

19. Racinet, H.; Jardon, P.; Gautron, R. *J. Chim. Phys.* **1988**, *85*, 971-977.

20. Eloy, D.; Le Pellec, A.; Jardon, P. *J. Chim. Phys. 1996*, *93*, 442-457.

21. Jardon, P.; Gautron, R. *J. Chim. Phys.* **1989**, *86*, 2173-2190.

22. Pinto, L.H.; Holsinger, L.J.; Lamb, R.A. *Cell* **1992**, *69*, 517-528.

23. Newell, K.J.; Tannock, I.F. *Cancer Res.* **1989**, *49*, 4447-4482.

24. Newell, K.J.; Wood, P.; Stratford, I.; Tannock, I. *Br. J. Cancer* **1992**, *66*, 311-317.

25. Barry, M.A.; Reynold, J.E.; Eastman, A. *Cancer Res.* **1993**, *53*, 2349-2357.

26. Li, J.; Eastman, A. *J. Biol. Chem.* **1995**, *270*, 3203-3211.

27. Gottlieb, R.A.; Nordberg, J.; Skowronski, E.; Babior, B.M. *Proc. Natl. Acad. Sci. U.S.A.* **1996**, *93*, 654-658.

28. Miccoli, L.; Oudard, S.; Sureau, F.; Poirson, F.; Dutrillaux, B.; Poupon, M.F. *Biochem. J.* **1995**, *313*, 957-962.

29. Carpenter, S.; Fehr, M.J.; Kraus, G.A.; Petrich, J.W. *Proc. Natl. Acad. Sci. U.S.A.* **1994**, *91*, 12273-12277.

30. Falk, H.; Mayr, E. *Monatsh. Chem.* **1995**, *126*, 699-710.

31. (a) Castner, E.W., Jr. Manuscript in preparation. (b) Horng, M.L.; Gardecki, J.A.; Papazyan, A.; Maroncelli, M. *J. Phys. Chem.* **1995**, *99*, 17311-17337. (c) Rosenthal, S.J.; Jiminez, R.; Fleming, G.R.; Kumar, P.V.; Maroncelli, M. *J. Mol. Liq.* **1994**, *60*, 25-56.

32. Murakoshi, K.; Yanagida, S.; Capel, M.; Castner, E.W., Jr. *Interfacial electron transfer*

dynamics of photosensitized zinc oxide nanoclusters; ACS Symposium Series No. 679 Nanostructured Materials: Clusters, Thin Films, and Composites: Shalaev, V., Moskovits, M., Eds.; American Chemical Society: Washington, DC. In press.

33. Das, K.; Dertz, E.; Paterson, J.; Zhang, W.; Kraus, G.A.; Petrich, J.W. Submitted for publication.

34. (a) Etzlstorfer, C.; Falk, H.; Müller, N.; Schmitzberger, W.; Wagner, U.G. *Monatsh. Chem.* **1993**, *124*, 751-761. (b) Falk, H. Personal communication. (c) Freeman, D.; Frolow, F.; Kapinus, E.; Lavie, D.; Lavie, G.; Meruelo, D.; Mazur, Y. *J. Chem. Soc., Chem. Commun.* **1994**, 891-892.

35. Chudoba, D.; Riedle, E.; Pfeiffer, M.; Elsaesser. T. *Chem. Phys. Lett.* **1996**, *263*, 622-628.

36. (a) Brucker, G.A.' Swinney, T.C.; Kelley, D.F. *J. Phys. Chem.* **1991**, *95*, 3190-3195. (b) Strandjord, A.J.G.; Barbara, P.F. *J. Phys. Chem.* **1985**, *89*, 2355-2361. (c) McMorrow, D.; Kasha, M. *J. Phys. Chem.* **1984**, *88*, 2235-2243. (d) Brucker, G.A.; Kelley, D.F. *J. Phys. Chem.* **1987**, *91*, 2856-2861. (e) Schwartz, B.J.; Peteanu, L.A.; Harris, C.B. *J. Phys. Chem.* **1992**, *96*, 3591-3598.

37. (a) Arabei, S.M.; Galaup, J.P.; Jardon, P. *Chem. Phys. Lett.* **1995**, *232*, 127-134. (b) Pschierer, H.; Friedrich, J.; Falk, H.; Schmitzberger, W. *J. Phys. Chem.* **1993**, *97*, 6902-6906.

38. Intramolecular proton or atom transfer is not, however, the only process of which excited singlets of hypericin are capable. In addition to intersystem crossing [19-21], Song and co-workers have demonstrated the ability of *the long-lived fluorescent state* to transfer and electron to a series of acceptors. Wells, T.A.; Losi, A.; Dai, R.; Scott, P.; Park, S.-M.; Golbeck, J.; Song, P.-S. *J. Phys. Chem.* **1997**, *101A*, 366-372.

39. Koch, W.; Saito, T.; Yoshida, Z. *Tetrahedron* **1972**, *28*, 3191.

40. Jardon, P.; Lazortchak, N.; Gautron, R. *J. Chim. Phys.* **1986**, *83*, 311-315.

41. Diels, J.-C.; Rudolph, W. *Ultrafast Laser Pulse Phonomena*; Academic Press: San Diego, CA, 1996; p 142.

CHAPTER IV. TEMPERATURE DEPENDENCE OF THE EXCITED-STATE INTRAMOLECULAR PROTON TRANSFER REACTION IN HYPERICIN AND HYPOCRELLIN A

A paper published in the *Journal of Physical Chemistry B*[1]

K. Das, K. D. Ashby, J. Wen, and J. W. Petrich[2]

Abstract

The excited-state intramolecular proton-transfer reactions of hypericin and hypocrellin A are measured as a function of temperature in an ethanol/methanol mixture. The data yield activation energies of 0.044 ± 0.008 and 2.12 ± 0.070 kcal/mol for hypericin and hypocrellin A, respectively. The negligible activation energy of hypericin is consistent with previous suggestions that the proton-transfer reaction is adiabatic (K. Das, et al., *J. Phys. Chem.* **1997**, *101A*, 3241.) and that a very low-amplitude displacement in at least one other coordinate be taken into account in order to describe the reaction dynamics. The proton transfer for hypocrellin is also considered to occur in the adiabatic regime, but the significant activation energy suggests that a larger amplitude motion than that for the case of hypericin comprises part of the reaction coordinate. Much of the barrier cited above for hypocrellin A results from the temperature dependence of the viscosity of the solvent mixture. The viscosity independent part of the activation barrier is 0.41 ± 0.088 kcal/mol.

---

[1] Reprinted with permission from the *Journal of Physical Chemistry B*, **1999**, *103*, 1581-1585.

[2] Author to whom correspondence should be addressed. K.D. Ashby performed the Hypericin temperature dependence experiments.

Introduction

The naturally occurring polycyclic quinones hypericin and hypocrellin (Figure 4.1) are of interest because of their light-induced antiviral (especially anti HIV) and antitumor activity (see refs 1-6 and citations therein). By applying the techniques of time-resolved absorption spectroscopy [7-13] and fluorescence upconversion [14] to hypericin, hypocrellin, and their methoxy analogs, we have demonstrated unequivocally that intramolecular excited-state proton (or hydrogen atom) transfer is a dominant nonradiative process in hypericin and hypocrellin. This transfer occurs between one (or possibly more) of the hydroxyls peri to the carbonyls (Figure 4.1). Of special relevance to the role of labile protons for this light-induced biological activity is the observation that hypericin and hypocrellin acidify their surroundings upon light absorption.[5,15-17] The role of photogenerated protons takes on significance in the context of the growing body of literature implicating pH decreases with pharmacologically important functions (see refs 5,6,13,17-20 and citations therein).

At first glance, the similarity of the structures (Figure 4.1) and the spectra (Figure 4.2) of hypericin and hypocrellin would lead one to believe that they exhibit, at least superficially, similar excited-state photophysics. This is not the case. The time constant for excited-state proton transfer in hypericin is ~10 ps and essentially independent of solvent [7,8], whereas for hypocrellin it ranges from 50 to 250 ps in the solvents we have investigated [12]. Also, the proton-transfer reaction in hypericin exhibits no isotope effect [7], whereas in hypocrellin a small isotope effect of 1.4 is observed [11].

To gain additional information on these fascinating excited-state proton-transfer reactions, we have studied them as a function of temperature in 1:1 ethanol/methanol mixtures.

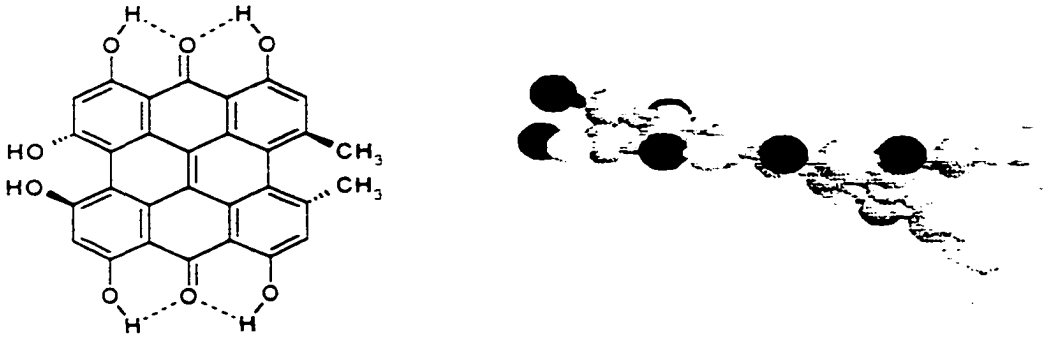

Hypericin

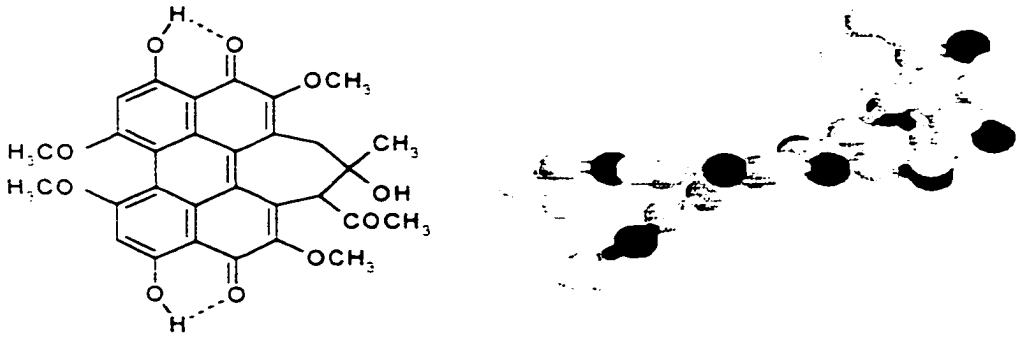

Hypocrellin

Figure 4.1. Structures of hypericin and hypocrellin A. Also indicated are side-on views indicating the magnitude of the out-of-plane deformations induced by the substituents in the bay regions.

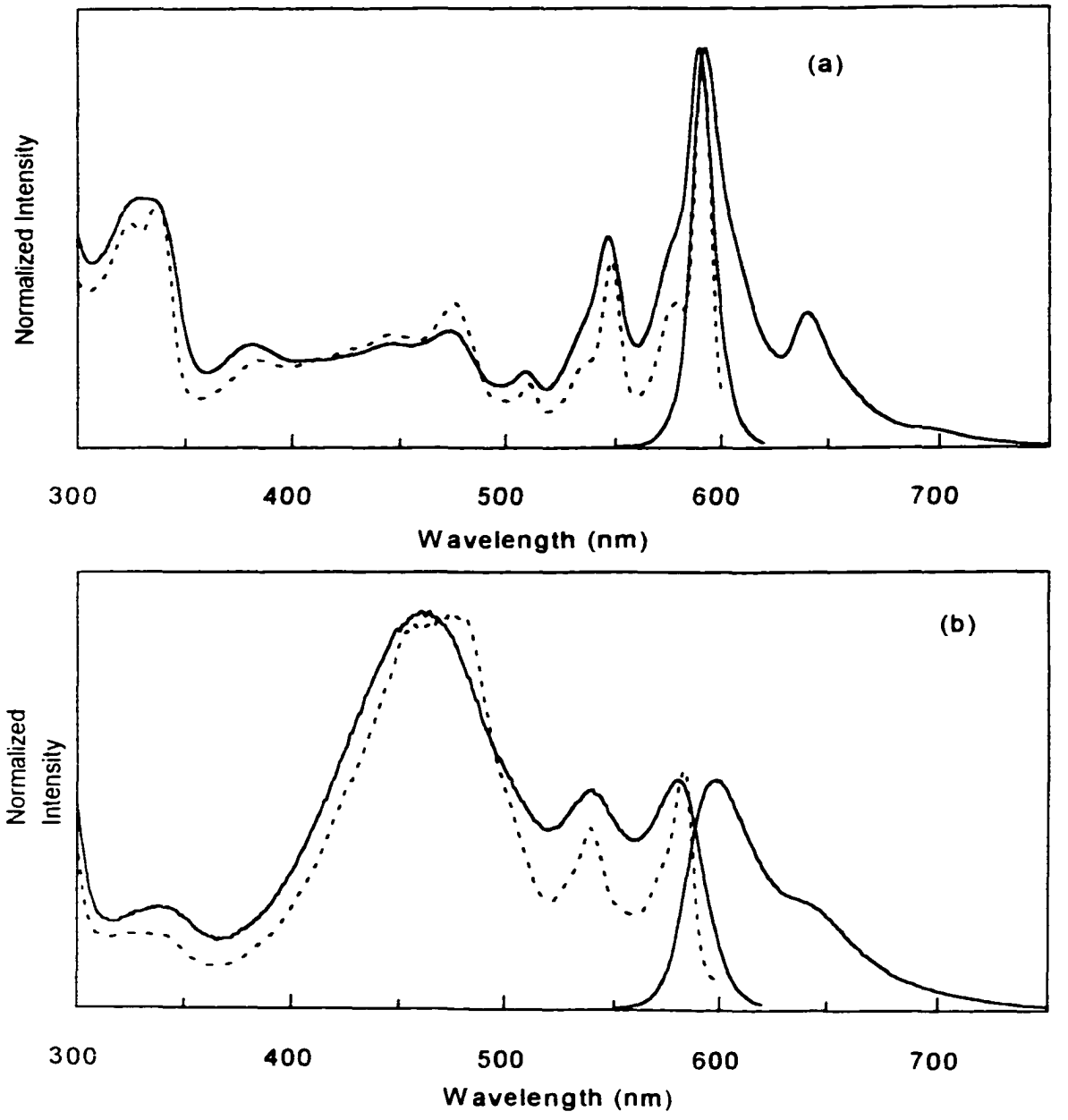

Figure 4.2. Comparison of the fluorescence excitation and emission spectra of hypericin and hypocrellin in a 1:1 ethanol/methanol mixture at 295 K (solid line) and at 77 K (dashed line). The excitation spectra were monitored at 650 nm at 295 K and at 620 nm at 77 K.

Experimental Section

Hypericin and hypocrellin A were obtained from Molecular Probes and were used as received. All the solvents, (Aldrich, spectroscopic grade) were also used as received. Pump-probe experiments were performed with amplified dye laser pulses of 1~3 ps duration [7]. The temperature was controlled to within ± 0.2 K using a Joule-Thomson refrigerator along with a programmable temperature controller (K20) from MMR Technologies. For the low-temperature experiments, samples were prepared in neat ethanol, neat acetonitrile, or in a 1:1 ethanol/methanol mixture; then several freeze-pump-thaw cycles were performed to eliminate the presence of any dissolved gases. The samples were sealed in a quartz cuvette whose optical path length is 1mm. The concentration of the sample was approximately millimolar. A freshly prepared sample was used after every three or four experiments. The pump wavelength for all the experiments was 588 nm. The probe wavelength for hypericin was 600 nm; that for hypocrellin was 595 nm. The probe wavelength are those that have been previously determined [7,8,11,21] to be the clearest signatures of excited-state intramolecular proton transfer in these molecules. All the kinetic traces were obtained with the probe beam polarized at the magic angle (54.7°) to the pump beam. For hypericin the transients were collected on a 40 ps time scale; for hypocrellin, a 200 ps time scale. For hypocrellin at the lowest temperatures, to obtain a more accurate estimate of the time constant, a full scale of 500 ps was used. The time constants are extracted from the kinetic traces using Spectra Solve™ software. The rate constants for Arrhenius plots were constructed from the inverse of the proton-transfer times obtained from the fits to the data.

Finally, to determine the intrinsic activation energy of the proton-transfer process in hypocrellin A, it was necessary to measure the kinetics as a function of temperature in such a

fashion that the temperature dependence of the viscosity did not intervene. Five two-point isoviscosity plots were thus constructed (Figure 4.8). The rate constants for hypocrellin were measured in five different solvents (cyclohexanone, butanol, pentanol, nonanol, and decyl alcohol) at room temperature. The rates were then measured in neat ethanol at the five different temperatures where the viscosity of ethanol is equal to that of the five solvents noted above. These measurements permitted the construction of five sets of isoviscous Arrhenius plots for hypocrellin. At least five measurements were made at each temperature. The error bars represent one standard deviation from the mean.

Results and Discussion

The transient absorption traces at various temperatures for hypericin and hypocrellin are displayed in Figures 4.3 and 4.4, respectively; and the proton-transfer times are compiled in Table 4.1. The Arrhenius plots constructed from these data are displayed in Figure 4.5. The activation energy for the hypericin reaction is 0.044 ± 0.008 kcal/mol; for the hypocrellin reaction, 2.12 ± 0.070 kcal/mol. (In a previous study we estimated an activation energy for the hypericin reaction, but this was over a very limited temperature range [8].) The most striking features of the Arrhenius plots are (i) the difference in activation energies, (ii) the essentially zero activation energy of hypericin, and (iii) that the liquid-glass transition of the solvent does not have an effect on the hypericin plot; but, as this transition is approached, there is a dramatic effect on the hypocrellin kinetics (Figure 4.6).

The first two of these features are consistent with the lack of an isotope effect in hypericin and the small isotope effect in hypocrellin. In particular, the zero activation energy

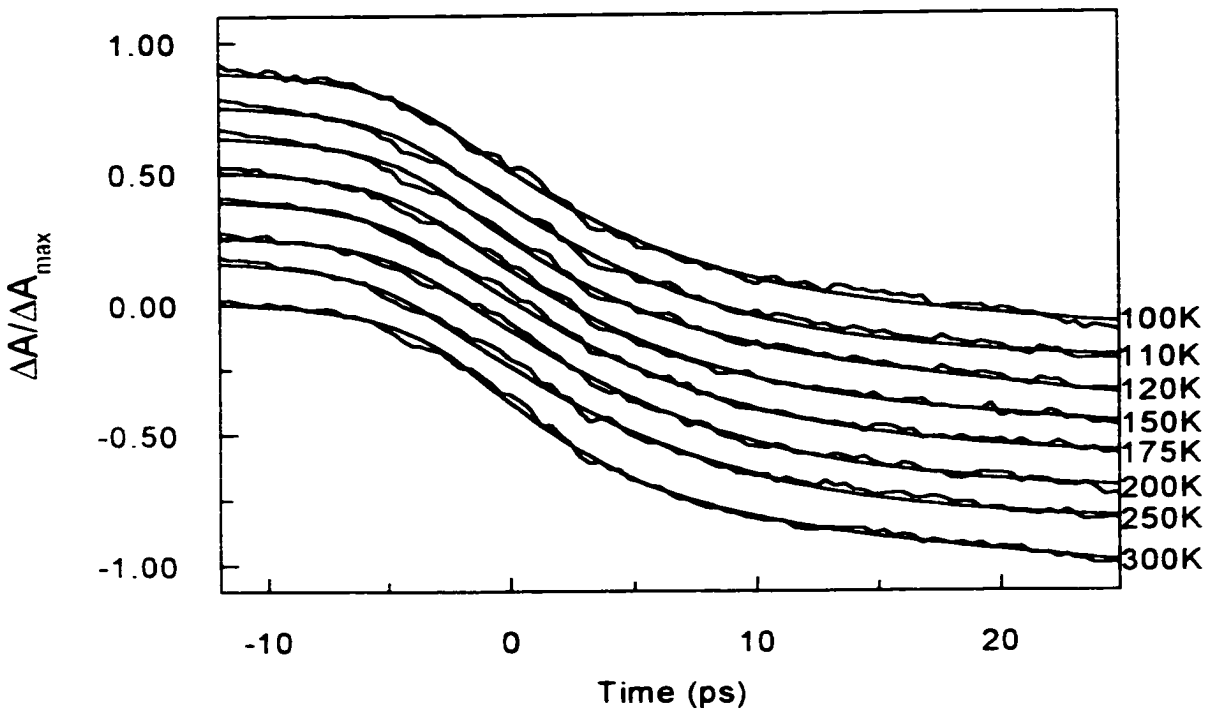

Figure 4.3. Transient absorbance traces of hypericin at various temperatures: $\lambda_{pump} = 588$ nm; $\lambda_{probe} = 600$ nm. Because the traces are virtually identical, they are displaced vertically with respect to each other.

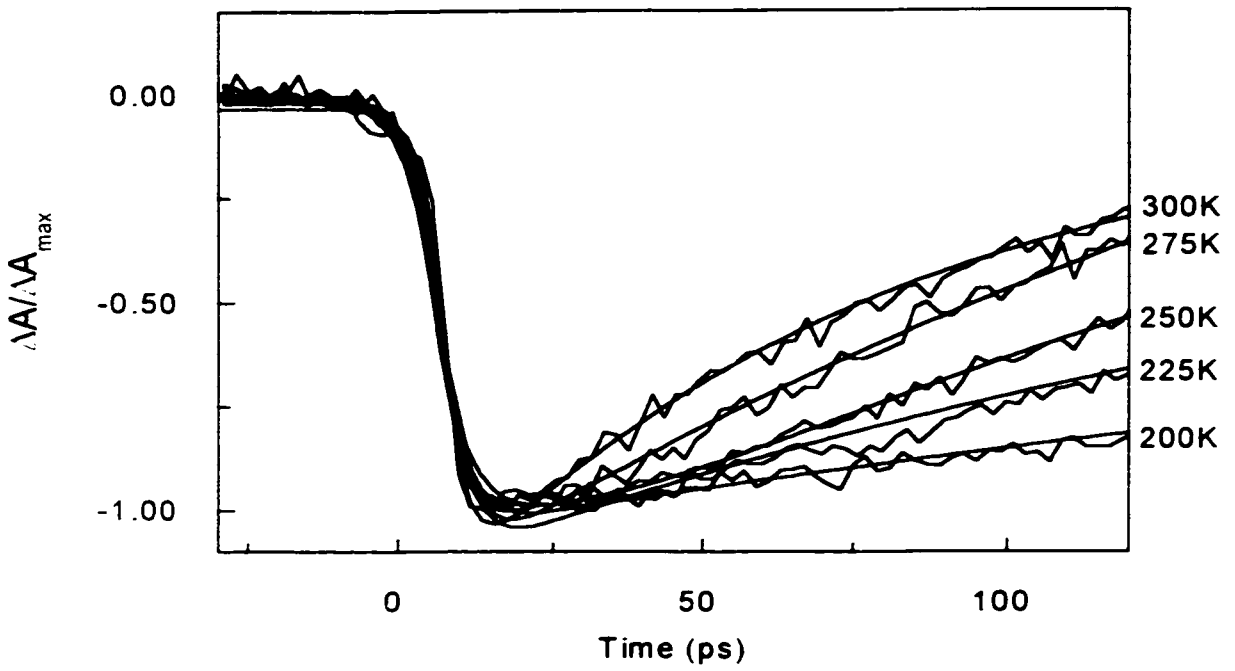

Figure 4.4. Transient absorbance traces of hypocrellin at various temperatures: λ_{pump} = 588 nm; λ_{probe} = 595 nm.

Table 4.1: Proton transfer times for Hypericin and Hypocrellin A.

Sample	Temp (K)	a_1	τ_1 (ps)	a_2	τ_2[c]
Hypericin[a]	300	0.15 ± 0.03	5.6 ± 2.5	0.9 ± 0.1	∞
in 1:1 EtOH/MeOH	250	0.13 ± 0.04	5.5 ± 3.0	0.9 ± 0.3	∞
	200	0.11 ± 0.01	6.0 ± 1.5	0.9 ± 0.1	∞
	175	0.11 ± 0.03	5.7 ± 3.0	0.8 ± 0.3	∞
	150	0.15 ± 0.03	6.5 ± 3.0	0.9 ± 0.3	∞
	120	0.13 ± 0.02	6.4 ± 2.0	0.9 ± 0.1	∞
	110	0.14 ± 0.02	6.4 ± 2.0	0.9 ± 0.1	∞
	100	0.11 ± 0.01	6.6 ± 1.5	0.9 ± 0.1	∞
Hypocrellin A[b]	300	0.8 ± 0.3	76 ± 7	0.01 ± 0.005	∞
in 1:1 EtOH/MeOH	275	0.9 ± 0.1	95 ± 13	0.01 ± 0.003	∞
	250	0.9 ± 0.2	149 ± 12	0.05 ± 0.02	∞
	225	0.7 ± 0.2	244 ± 28	0.02 ± 0.006	∞
	200	0.9 ± 0.1	438 ± 78	0.01 ± 0.003	∞
Hypocrellin A[b]	300	0.7 ± 0.1	43 ± 6	0.02 ± 0.002	∞
in acetonitrile	275	0.7 ± 0.2	53 ± 7	0.03 ± 0.003	∞
	265	0.8 ± 0.3	58 ± 3	0.01 ± 0.002	∞
	255	0.9 ± 0.1	68 ± 6	0.02 ± 0.001	∞
	245	0.9 ± 0.3	79 ± 5	0.02 ± 0.001	∞

[a]The data for hypericin were fit to the following form: $\Delta A(t) = - a_1 [\exp(-t/\tau_1) - 1] - a_2 \exp(-t/\tau_2)$.

[b]The data for hypocrellin were fit to the following form: $\Delta A(t) = - a_1 \exp(-t/\tau_1) - a_2 \exp(-t/\tau_2)$

[c]On the time scale on which the data were collected, the longer-lived component cannot be accurately determined and is given by infinity.

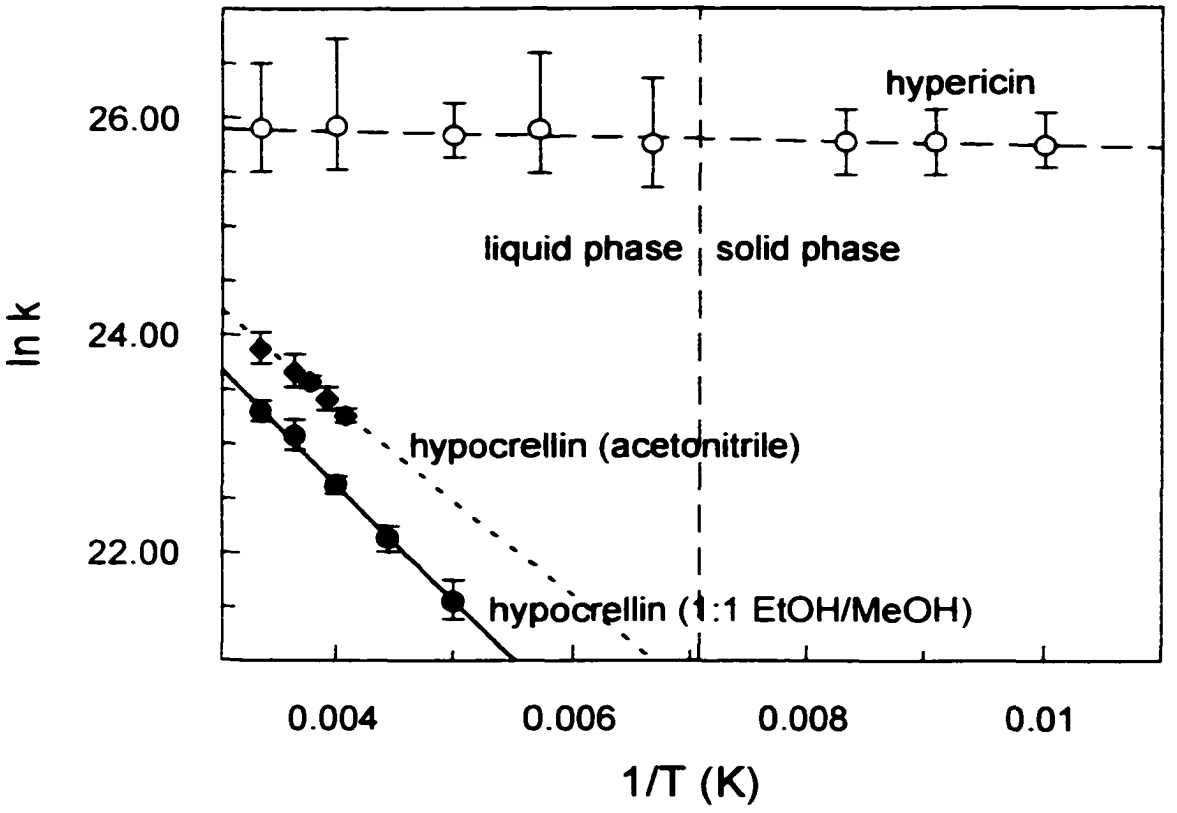

Figure 4.5. Arrhenius plots for hypericin and hypocrellin based on the data obtained from Figures 3 and 4. Each point represents the average of at least five experiments. The error bars are ± one standard deviation from the mean. The Arrhenius prefactors and activation energies obtained from these plots are: hypericin, $A = (1.89 \pm 0.06) \cdot 10^{11}\ s^{-1}$ and $E_a = 0.044 \pm 0.008$ kcal/mol; hypocrellin, $A = (4.65 \pm 0.62) \cdot 10^{11}\ s^{-1}$ and $E_a = 2.12 \pm 0.070$ kcal/mol. (This activation energy is close to the viscisity activation energies of methanol and ethanol, 2.61 and 3.54 kcal/mol, respectively.) Also included is a plot for hypcrellin in acetonitrile, for which we obtain $A = (4.54 \pm 1.11) \cdot 10^{11}\ s^{-1}$ and $E_a = 1.75 \pm 0.14$ kcal/mol. The dependence of the activation energy of hypocrellin in these two solvent systems clearly reflects the temperature dependence of the viscosity. (From 300 to 245 K, the viscosity of acetonitrile goes from 0.35 to 1.08 cP. Viscosity data are obtained from ref 33.)

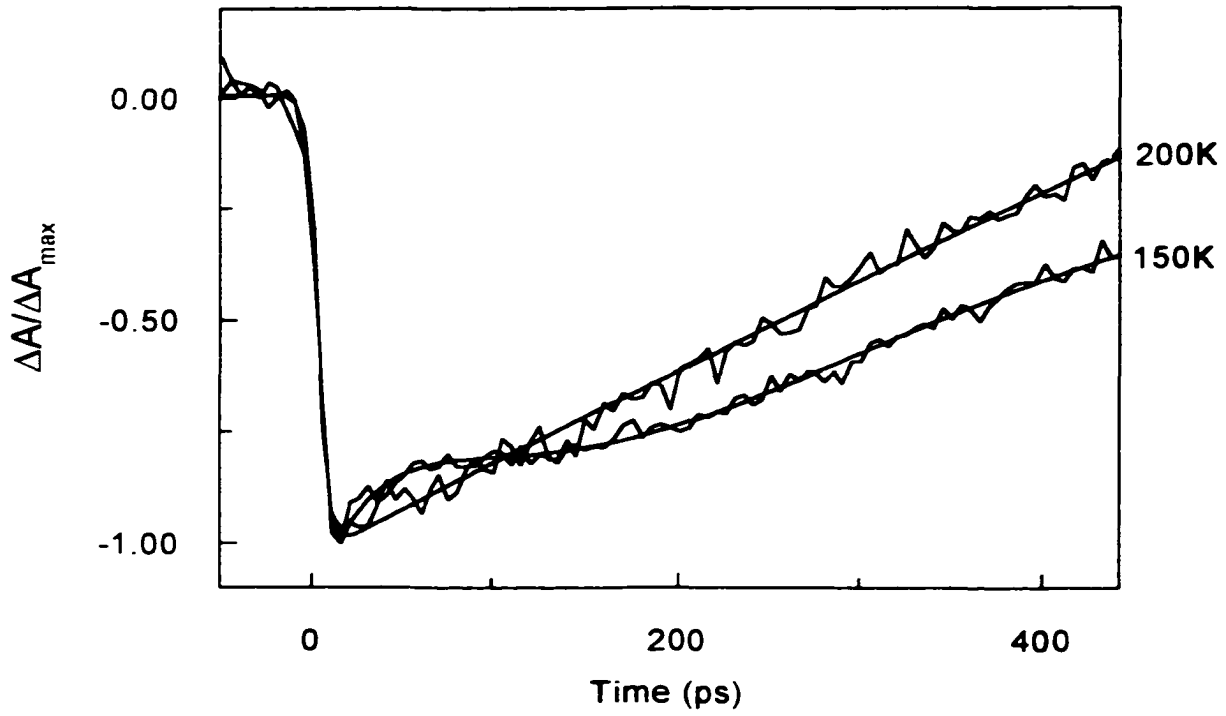

Figure 4.6. Comparison of kinetic traces for hypocrellin at 200 K and at 150 K: $\lambda_{pump} = 588$ nm; $\lambda_{probe} = 595$ nm. As discussed in detail elsewhere [13], at probe wavelengths of 595 nm, two species whose transition dipole moments are at large angles to each other are simultaneously probed. From 300 to ~200 K, the form of the parallel absorption traces, $\Delta A_{\parallel}(t)$, are nearly identical to those of the magic angle traces, $\Delta A(t) = \Delta A_{\parallel}(t) + 2\,\Delta A_{\perp}(t)$. (At $\lambda_{probe} = 595$ nm, $\Delta A_{\parallel}(t)$ and $\Delta A_{\perp}(t)$ have *opposite* signs). This indicates that $\Delta A_{\perp}(t)$ fortuitously complements $\Delta A_{\parallel}(t)$ up to ~200 K. Below ~200 K, however, the form of the kinetic traces abruptly changes. This suggests a change in the relative population of ground-state species whose transition dipole moments are at large angles to each other. These phenomena are consistent with the glass transition inducing a perturbation in the population of ground-state isomers or tautomers. The differences in the hypericin and, especially, the hypocrellin excitation spectra between 295 K and 77 K may reflect such changes in ground-state population (Figure 2).

in hypericin is consistent with our previous proposal that the proton-transfer reaction is adiabatic in the proton coordinate and that the zero-point vibrational energy lies above the barrier in this coordinate (Figure 4.7). As discussed in the work of Hynes, Borgis, and coworkers [22-25], a major factor in reducing the barrier is the proximity between the heavy atoms between which the proton is transferred. It is considered that if the heavy-atom distance is 2.5 Å or less, the proton-transfer reaction will lie in the adiabatic limit. X-ray data [26] and ab initio calculations [27] indicate that this is the case for hypericin. There are also X-ray data [28] indicating that hypocrellin lies in this limit as well.

If the zero-point energy lies above the barrier in the proton coordinate (Figure 4.7a), the proton (or hydrogen atom) is effectively delocalized between the two oxygen atoms until a change in another coordinate can trap the system in the tautomerized form (Figure 4.7b). We propose that it is the time-scale for this latter conformational change that determines the observed proton-transfer time.

In the model system for excited-state proton transfer, 3-hydroxyflavone, the reaction occurs in ~100 fs in dry nonhydrogen bonding solvents [29]. In hydrogen bonding solvents such as alcohols, the observed proton-transfer time in 3-hydroxyflavone reflects the time required for the displacement of the solvent hydrogen-bonded to the enol proton of the solute, thus permitting the proton to effect its transfer [30]. Specific hydrogen bonding interactions between hypericin and hypocrellin with solvent cannot explain the relatively slow proton-transfer times ($>$ 10 ps) because the hypericin reaction is insensitive to solvent [7,8] and because the hypocrellin reaction, while sensitive to solvent, is only well correlated to the bulk viscosity of different solvents and not to solvents of a given "type" [12]. The insensitivity of the hypericin

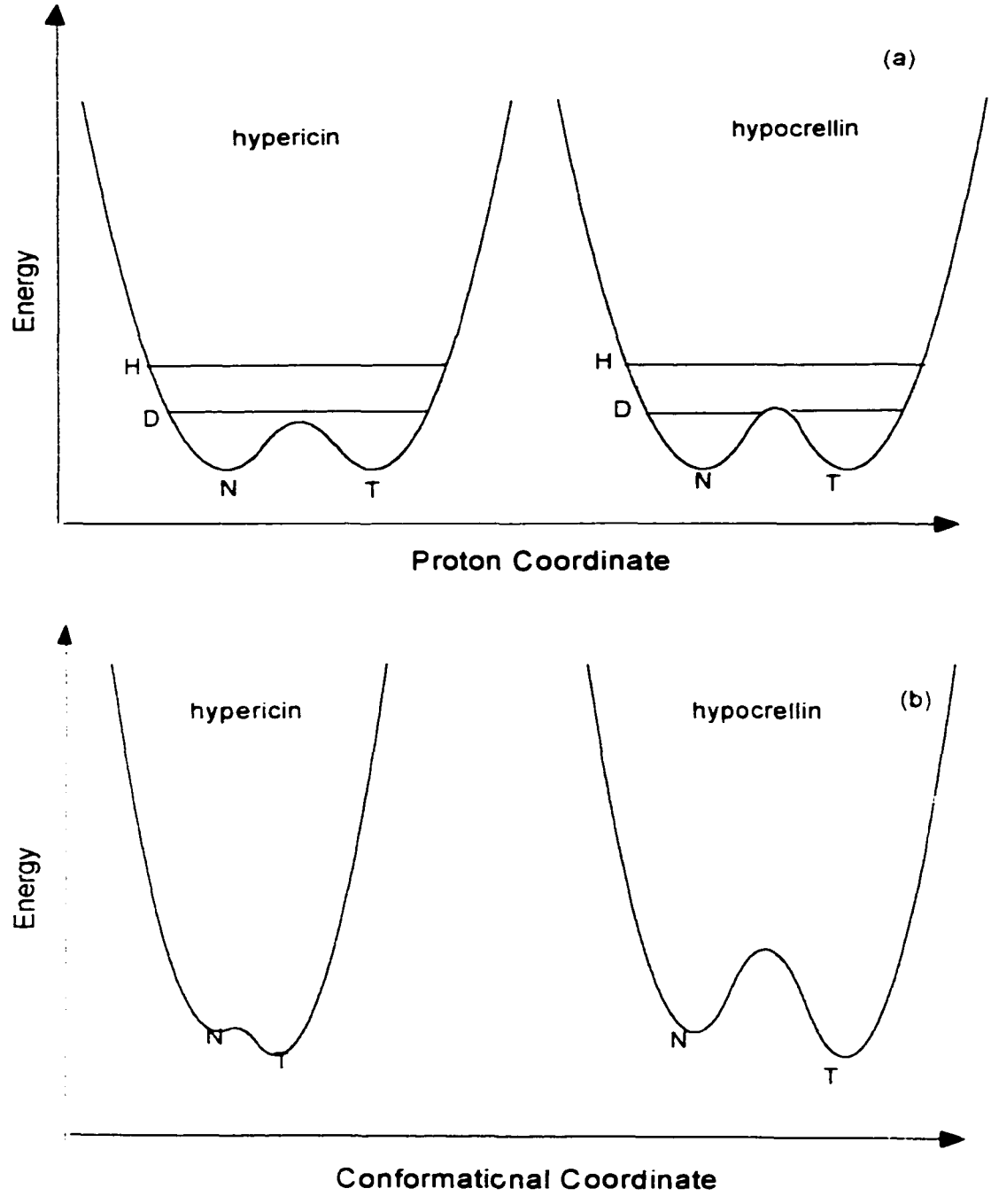

Figure 4.7. Schematic illustrations of the potential energy surfaces of hypericin and hypocrellin in the proton and "conformational" coordinates. Our justification for the placement of the zero-point level slightly below the barrier for deuterated hypocrellin is explained in detail elsewhere. Briefly, it provides an elegant means, suggested by Staib et al. [25], to introduce an isotope effect in a situation where there is an adiabatic proton transfer and where the zero-point vibrational level for the protiated species lies above the barrier.

reaction to solvent is most likely a result of the strong association of the proton with the oxygens of both the peri hydroxyl and the carbonyl groups.

Since this oxygen-oxygen distance is essentially the same in both hypericin and hypocrellin (2.5 Å [11,26,28]), a different origin for the solvent dependence of the hypocrellin reaction must be found. The 2.12 ± 0.070 kcal/mol activation energy for hypocrellin, in addition to the strong dependence of its proton-transfer reaction on viscosity [12], indicates that, unlike hypericin, its conformational change must be rather large in amplitude and may involve torsions of the aromatic skeleton or displacements of its seven-membered ring [31]. Consistent with the idea of a large-amplitude transition occurring in hypocrellin is that the form of the kinetic traces changes drastically as the liquid-glass transition is approached (Figure 4.6).

That the proton transfer reaction in hypocrellin A strongly depends on viscosity [12] strongly suggests that part of the activation barrier measured in the methanol/ethanol mixture arises from the temperature dependence of the viscosity of this solvent system. That the activation barrier in hypocrellin A depends on viscosity is indicated by constructing another Arrhenius plot in acetonitrile (Figure 4.5). To determine that part of the barrier that does not depend on viscosity (the "intrinsic barrier" to the reaction), we constructed isoviscosity plots [32] as described in the Experimental section and in the caption for Figure 4.8. The plots indicate that the viscosity-independent barrier to the reaction is 0.41 ± 0.088 kcal/mol. Thus, the viscosity-independent barrier in hypocrellin A is small on an absolute scale, but still 10 times larger than that for hypericin.

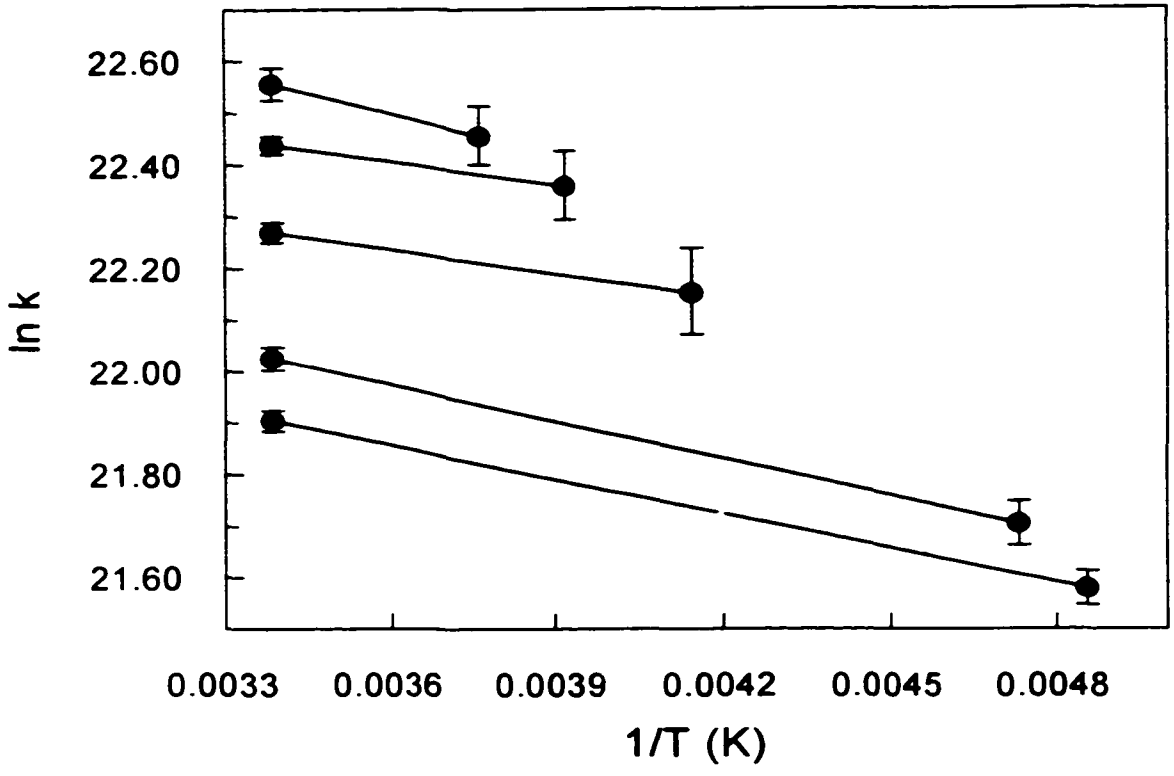

Figure 4.8. Five sets of isoviscosity plots for hypocrellin A. The points on the left-hand side of the figure correspond to five different solvents: from top to bottom, cyclohexanone (2.12 cP), butanol (2.73 cP), pentanol (3.93 cP), nonanol (10.03 cP), and decyl alcohol (12.13 cP) at room temperature. The points on the right-hand side of the figure correspond to pure ethanol at a temperature adjusted so that its viscosity is the same as that of its solvent partner. The viscosity-independent Arrhenius activation energy obtained from these plots is $E_a = 0.41 \pm 0.088$ kcal/mol.

Conclusions

The negligible activation energy for hypericin is consistent with previous suggestions that the proton-transfer reaction is adiabatic [7,8,11,13] and requires that displacement in at least one other coordinate be taken into account in order to describe the reaction dynamics. The negligible activation energy for hypericin also indicates that the displacement in the "conformational" coordinate is very low-amplitude. The proton transfer for hypocrellin is also considered to occur in the adiabatic regime, but the activation energy for the process is significant (2.12 ± 0.070 kcal/mol), consistent with the strong correlation for the proton-transfer reaction on bulk viscosity [12], and suggesting that a larger amplitude motion than for the case of hypericin comprises part of the reaction coordinate. The intrinsic barrier for the hypocrellin A reaction, 0.41 ± 0.088 kcal/mol, is larger than that for hypericin but still quite small. The conformational changes that are coupled to the proton transfer reaction in hypericin and hypocrellin have yet to be identified and are currently under investigation.

Acknowledgment

This work was supported by NSF grant CHE-9613962 to J. W. P.

References and Notes

1. Duran, N.; Song, P.-S. *Photochem. Photobiol.* **1995**, *61*, 529.

2. Lown, J. W. *Can. J. Chem.* **1997**, *75*, 99.

3. Kraus, G. A.; Zhang, W.; Fehr, M. J.; Petrich, J. W.; Wannemuehler, Y.; Carpenter, S. *Chem. Rev.* **1996**, *96*, 523.

4. Carpenter, S.; Fehr, M. J.; Kraus, G. A.; Petrich, J. W. *Proc. Natl. Acad. Sci. U.S.A.*

1994, *91*, 12273.

5. Mirossay, L.; Mirossay, A.; Kocisova, E.; Radvakova, I.; Miskovsky, P.; Mojzis, J. Hypericin-induced apoptosis of human leukemic cell line HL-60 is potentiated by omeprazole, an inhibitor of H^+K^+-ATPase and 5'-(N,N-dimethyl)-amiloride, an inhibitor of Na^+/H^+ exchanger. *Physiological Research*, submitted.

6. Das, K; Smirnov, A. V.; Wen, J.; Miskovsky, P.; Petrich, J. W. Photophysics of hypericin and hypocrellin A in complex with subcellular components: Interactions with human serum albumin. *Photochem. Photobiol.*, submitted.

7. Gai, F.; Fehr, M. J.; Petrich, J. W.; *J. Phys. Chem.* **1994**, *98*, 5784.

8. Gai, F.; Fehr, M. J.; Petrich, J. W.; *J. Phys. Chem.* **1994**, *98*, 8352.

9. English, D. S.; Zhang, W.; Kraus, G. A.; Petrich, J. W. *J. Am. Chem. Soc.* **1997**, *119*, 2980.

10. English, D. S.; Das, K.; Zenner, Z. M.; Zhang, W.; Kraus, G. A.; Larock, R. C.; Petrich, J. W.; *J. Phys. Chem.* **1997**, *101A*, 3235.

11. Das, K.; English, D. S.; Petrich, J. W. *J. Phys. Chem.* **1997**, *101A*, 3241.

12. Das, K.; English, D. S.; Petrich, J. W. *J. Am. Chem. Soc.* **1997**, *119*, 2763.

13. Das, K.; Smirnov, A. V.; Snyder, M. D.; Petrich, J. W. *J. Phys. Chem. B* **1998**, *102*, 6098.

14. English, D. S.; Das, K.; Ashby, K. D.; Park, J.; Petrich, J.W.; Castner, E. W., Jr. *J. Am. Chem. Soc.* **1997**, *119*, 11585.

15. Fehr, M. J.; McCloskey, M. A.; Petrich, J. W. *J. Am. Chem. Soc.* **1995**, *117*, 1833.

16. Sureau, F.; Miskovsky, P.; Chinsky, L.; Turpin, P. Y. *J. Am. Chem. Soc.* **1996**, *118*, 9484.

17. Chaloupka, R.; Sureau, F.; Kocisova, E.; Petrich, J.W. *Photochem. Photobiol.* **1998**, *68*, 44.

18. Fehr, M. J.; Carpenter, S. L.; Wannemuehler, Y.; Petrich, J. W. *Biochemistry* **1995**, *34*, 15845.

19. Fehr, M. J.; Carpenter, S. L.; Petrich, J. W. *Biorg. Med. Chem. Lett.* **1994**, *4*, 1339.

20. We had previously reported that hypericin does not require oxygen for its antiviral

activity [3,14,18-20]. This conclusion was based on a previous inability to estimate accurately low oxygen levels in our virus samples. We consequently now believe that while antiviral pathways independent of oxygen may exist, the role of oxygen in this activity is significant. The ability of photogenerated protons to enhance the activity of activated oxygen species [17] is still considered to be of importance (Park, J.; English, D. S.; Wannemuehler, Y.; Carpenter, S.; Petrich, J. W. The role of oxygen in the antiviral activity of hypericin and hypocrellin. *Photochem. Photobiol.* 1998, *68*, 593-597.

21. Das, K.; English, D. S.; Fehr, M. J.; Smirnov, A. V.; Petrich, J. W. *J. Phys. Chem.* **1996**, *100*, 18275-18281.

22. Borgis, D.; Hynes, J. T. In *The Enzyme Catalysis Process*; Cooper, A., Houben, J. L., Chien, L. C., Eds.; NATO ASI Series, Plenum Press: NY, 1989; Vol. 178, p 293.

23. Borgis, D.; Hynes, J. T. *J. Chem. Phys.* **1991**, *94*, 3619-3628.

24. Azzouz, H.; Borgis, D. *J. Chem. Phys.* **1993**, *98*, 7361-7374.

25. Staib, A.; Borgis, D.; Hynes, J. T. *J. Chem. Phys.* **1995**, *99*, 2487-2505.

26. Freeman, D.; Frolow, F.; Kapinus, E.; Lavie, D.; Lavie, G.; Meruelo, D.; Mazur, Y. *J. Chem. Soc. Commun.* **1994**, 891; Etzlstorfer, C.; Falk, H.; Müller, N.; Schmitzberger, W.; Wagner, U. G. *Monatsh. Chem.* **1993**, *124*, 751-761.

27. Petrich, J. W.; Gordon, M. S.; Cagle, M. *J. Phys. Chem. A* **1998**, *102*, 1647-1651.

28. Wei-shin, C.; Yuan-teng, C.; Xiang-yi, W.; Friedrichs, E.; Puff, H.; Breitmaier, E. *Liebigs Ann. Chem.* **1981**, 1880-1885.

29. Schwartz, B. J.; Peteanu, L. A.; Harris, C. B. *J. Phys. Chem.* **1992**, *96*, 3591-3598.

30. (a) Brucker, G. A.; Swinney, T. C.; Kelley, D. F. *J. Phys. Chem.* **1991**, *95*, 3190-3195. (b) Strandjord, A. J. G.; Barbara, P. F. *J. Phys. Chem.* **1985**, *89*, 2355-2361. (c) McMorrow, D.; Kasha, M. *J. Phys. Chem.* **1984**, *88*, 2235-2243.

31. Smirnov, A. V.; Fulton, B.; Andreotti, A. H.; Petrich, J. W. Investigations of the ground-state conformations of hypericin and hypocrellin by NMR. In preparation.

32. Courtney, S. H.; Fleming, G. R. *J. Chem. Phys.* **1985**, *83*, 215-222

33. Viswanath, D.S.; Natarajan, G. *Data Book on the Viscosity of Liquids*; Hemisphere Publishing Corporation: New York, 1989.

CHAPTER V. STEADY-STATE AND TIME-RESOLVED SPECTROSCOPY OF F_{420} EXTRACTED FROM METHANOGEN CELLS AND ITS UTILITY AS A MARKER FOR FECAL CONTAMINATION ON MEAT SURFACES

A paper submitted to the *Journal of Agricultural and Food Chemistry*[1]

Kyle D. Ashby[2], Thomas A. Casey[3,4], Mark A. Rasmussen[3,4], and Jacob W. Petrich[2,4]

Abstract

Methanogenic bacteria contain the compound F420 (Factor 420), a 7-8-didemethyl-8-hydroxy-5-deazariboflavin chromophore, which may be useful as a fluorescent marker for the detection of fecal and ingesta contamination on carcasses of animals from which these bacteria are common inhabitants. Using a single anion exchange chromatographic process, F420 was separated from other cell components of a *Methanobrevibacter ruminantium* cell culture. The extent of separation was determined spectroscopically. To aid in the development of possible techniques for the detection of fecal contamination using F420 as a marker, further spectroscopic investigation of F420 was conducted using steady-state and time-resolved fluorescence methods. The fluorescence lifetime of F420 in the elution buffer of pH 7.5 is 4.2 ns. At higher pH the fluorescence decay, F(t), is best described by a sum of two exponentials:

---

[1] The *Journal of Agricultural and Food Chemistry* is a publication of the American Chemical Society.

[2] Department of Chemistry, Iowa State University, Ames, IA 50011-3111.

[3] U. S. Department of Agriculture, Agriculture Research Service National Animal Disease Center, Ames, IA 50010.

[4] To whom correspondence should be addressed.

at pH 13, F(t) = 0.31 exp (-t / 4.20 ns) + 0.69 exp (-t / 1.79 ns). Further investigation using front-faced fluorescence techniques has shown that emission from F420 can be collected efficiently from the surface of methanogen and fecal samples.

Introduction

A study was initiated to identify fluorescent markers useful for the detection of fecal and ingesta contamination. Such contamination can carry harmful bacteria onto animal carcasses and meat products during processing. A survey of fluorescent compounds known to occur in anaerobic bacteria was conducted and included the methanogenic bacteria, common inhabitants of the anaerobic environment of the gut. One of the interesting features of methanogen cells is their blue-green fluorescence. This characteristic is caused by the fluorescent coenzyme F420 (Fig. 5.1). This coenzyme is ubiquitous among methanogens and serves metabolically as an electron donor for the reduction of carbon dioxide to methane. (1,2,3,4). Its trivial name is derived from the 420-nm absorbance maximum observed for the oxidized form of the coenzyme (5). This form of the molecule (Fig. 5.1A) exhibits a blue-green fluorescence at 470 nm with a quantum yield of fluorescence, ϕ_f, of 0.17, which we have measured using tryptophan as a reference ($\phi_f = 0.18$ (6)). This fluorescent property has been used by microbiologists to identify methanogenic bacteria by fluorescence microscopy (7,8).

The spectral features of oxidized F420 are pH dependent (1,2,9), and in acidic media, the absorbance maximum at 420 nm shifts to 380 nm (7,10,11). There is an isobestic point at 401 nm with an extinction coefficient of 2.59×10^4 $M^{-1}cm^{-1}$ (5,7). The extinction coefficient at 420 nm is $4.14 \cdot 10^4$ $M^{-1}cm^{-1}$ (pH = 7.5, 25° C) (10,12). This coefficient changes as a function of temperature due to effects upon the pK_a of the 8-OH group (pK_a 5.3)(1,2,12). The pK_a for the

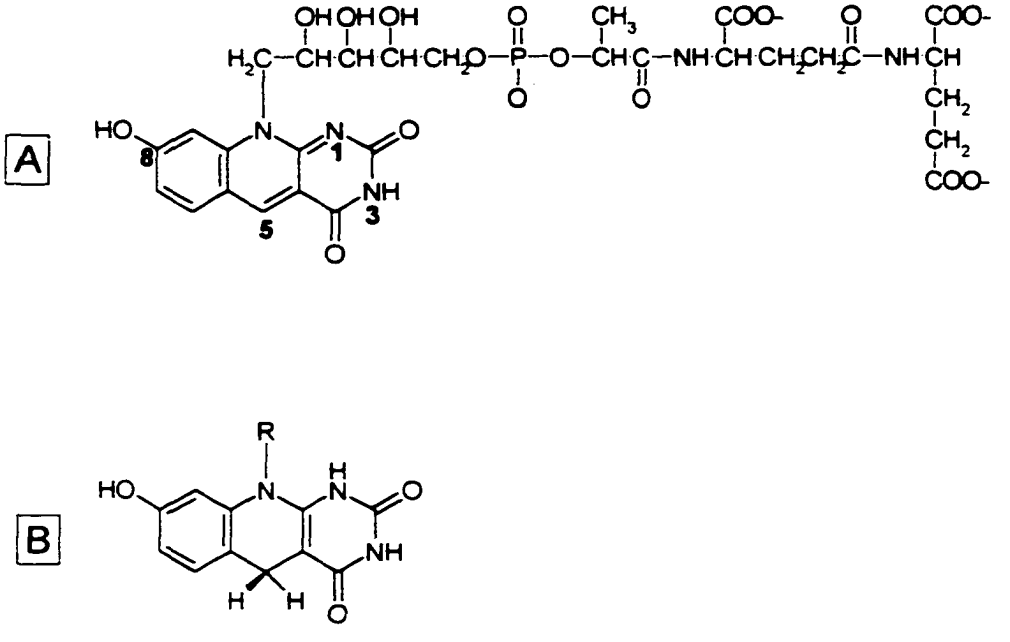

Figure 5.1. Structure of the methanogen electron carrier, F420. (A) is the oxidized, fluorescent form of F420 and (B) is the reduced, nonfluorescent form.

nitrogen at the 3 position is 12.3 (1). The reduced form of F420 (Fig. 5.1B) loses its absorbance at 420 nm and becomes nonfluorescent (2,7,11). In vivo, the coenzyme is reduced by F420-reducing hydrogenases or by NADP reductases. The coenzyme is subject to oxidative and photo-decomposition (10,11).

In this study, we isolated F420 from methanogen cells and examined its steady-state and time-resolved fluorescent properties and concluded that it may be quite useful as a fluorescent marker for the detection of fecal or ingesta contamination on the carcasses of food animals.

Experimental Section

Isolation of Methanogen Cells.

A methanogen was isolated from the ruminal contents of a cow using basal salts, rumen fluid, and bicarbonate-buffered, anaerobic culture broth (13). A headspace atmosphere of H_2/CO_2; 80%/20%, v/v was used with hydrogen serving as the primary substrate for growth. Pressurized (200 kPa) culture tubes were incubated at 39°C with agitation to facilitate gas transfer. For single colony isolation, the culture medium was supplemented with 1.5% w/v agar. Ten-fold dilutions from the primary culture were inoculated into molten agar medium (55°C), and solidified agar roll tubes were prepared (13). Agar roll tubes were incubated at 39 °C under an atmosphere of hydrogen and carbon dioxide. Roll tubes were flushed with fresh gas mixture daily. Well isolated colonies were picked from the roll tubes under anaerobic conditions and transferred to the liquid culture medium. The isolated bacteria was determined to be *Methanobrevibacter ruminantium*. Identification was based upon cell fluorescence, cell morphology, growth on and production of methane from hydrogen, lack of growth on carbohydrates and several other physiological features. Cell pastes of the methanogen were

prepared from liquid cultures by centrifugation under anaerobic conditions. Exposure to light and oxygen was minimized and the cell pastes were kept frozen until use.

Extraction of F420 From Methanogen Cells.

The method for extraction and isolation of the F420 was similar to that reported by Schonheit et al. (10). Briefly, acetone was precooled to −15 °C. Two mL of the precooled acetone was added to a vial containing the cell paste. This was stirred using a magnetic stirring plate for 30 minutes. The suspension was centrifuged and the supernate fluid was collected. A second 2-mL volume of 50% acetone(chilled)/water was added to the pellet, stirred for 30 minutes and clarified by centrifugation. The supernates from both extractions were combined and diluted 1:2 with a 0.3 M NaCl, 50 mM Tris-HCl buffer (pH = 7.5). The resulting solution was loaded onto a Sephadex QAE A-25 ion exchange column that had a diameter of 1 cm and length of 4.5 cm. The ion exchange resin was pre-equilibrated in the dilution buffer and the column was initially washed with 15 mL of this buffer. After sample loading, the column was eluted with 45 mL of 0.3 M NaCl, 50 mM Tris-HCl buffer. Under these conditions, the F420 was retained on the column, as indicated by the yellow band observed, while all other components were eluted and discarded. To elute the F420, 15 mL of a 1.0 M NaCl, 50 mM Tris-HCl buffer (pH = 7.5) was applied to the column and 3-mL fractions were collected. Fractions containing the F420 were combined and used for the steady-state and time-resolved measurements.

Steady-State Fluorescence Measurements.

The absorbance spectrum of the F420 in the eluting buffer was obtained using a Perkin-Elmer Lambda 18 UV-Visible spectrophotometer. Excitation and emission spectra were

obtained using a SPEX FluoroMax using an emission wavelength of 470 nm and excitation wavelengths of 295 nm and 420 nm, respectively.

For solid or opaque samples the front-faced fluorescence technique was utilized in both steady-state and time-resolved measurements, collecting emission from the surface of a 45°-cuvette at right angles to the excitation. Samples were also prepared by adding acetone to methanogen cell paste and stirring for about 30 minutes. Acetone lyses the bacterial cells and releases cellular components, including F420. The resulting lysate was very opaque; therefore the emission spectrum was collected using the front-faced technique with an excitation wavelength of 420 nm.

Emission spectra were obtained from rumen, cecum, and fecal samples of two different cows and one pig fecal sample. Small volumes (10 μL) of each sample were placed in a separate 1 cm · 1 cm cuvette containing 3 mL of the 50 mM Tris buffer (pH 7.5). These small volumes were used to reduce the opacity of the samples as these spectra were obtained before the front-faced technique was utilized. The excitation wavelength was 430 nm. A Tris buffer blank spectrum was obtained so that contributions to each sample spectrum from water Raman scattering could be subtracted.

Time-Resolved Fluorescence Measurements.

Time-correlated single photon counting measurements were performed to determine the fluorescence lifetime of F420 in the elution buffer at pH 7.5 and pH 13. A Coherent 701 Rhodamine 6G dye laser was pumped with 1-2 W of 532 nm output from an Antares 76s CW mode locked Nd:YAG laser. The 701 dye laser was cavity-dumped at 3.8 MHz. The dye laser pulses had an autocorrelation of about 7 ps full width at half maximum (fwhm). Excitation of

F420 at 295 nm was effected by focusing the dye laser pulses with a 5-cm lens into a crystal of $LiIO_3$ or KDP. Fluorescence was collected at right angles through a polarizer mounted at 54.7° to the excitation polarization and then passed through cutoff filters. A Hamamatsu 2809u microchannel plate, amplified by a B&H Electronics Type AC3020 3.15 GHz preamplifier, provided the start signal while the sync out from the cavity dumper driver provided the stop signal. Constant-fraction discrimination of these signals was performed by a Tennelec TC 455, and time-to-amplitude conversion, by an ORTEC 457. Data were stored in a Norland 5500 multichannel analyzer before transfer to and analysis with a personal computer. The time scale for the time-resolved experiments was 12.5 ns. The instrument response function of this system has a fwhm of 70-100 ps. Time-resolved fluorescence data were fit to a single exponential or a sum of exponentials,

$$F(t) = \sum_{n=1}^{n} a_n \exp(-t/\tau_n)$$

by iteratively convoluting trial decay curves with the instrument response function and employing a least-squares fitting procedure to determine the lifetimes, τ_n, and preexponential factors, a_n. A good fit is determined largely by the χ^2 criterion (15): $0.8 \leq \chi^2 \leq 1.2$.

The time-resolved fluorescence decay of fecal matter was obtained using the front-faced technique with a 45° cuvette. The solid fecal matter was diluted with nanopure water, which allowed for easier placement of the sample into the cuvette. The experiment was then performed in an identical manner as previously described for the F420 lifetime measurements with greater care in filtering out the scattered excitation laser light. A large amount of excitation light was, nevertheless, reflected and scattered toward the detector from the front surface of the 45 ° cuvette. Despite our precautions, a considerable amount of this scattered light was detected

in our measurements. We have ignored its contribution in analyzing the data.

Results and Discussion

Our success in purifying F420 from other components in the methanogen extract is demonstrated by the absorbance spectrum shown in figure 5.2. This spectrum is very similar to spectra previously published for F420 (2,10). The particular absorbance spectrum in figure 5.2 was included to illustrate the effect of impurities in the eluted F420 sample. This preparation did show an anomalous absorption band near 350 nm, but this band was not observed in the excitation spectrum and thus did not effect our fluorescence measurements. Additional preparations did not show any anomalous absorption bands. Thus, the separation technique was very satisfactory in providing us with the F420 compound separated out from any other possible fluorescent impurities. There were no observed differences, other than magnitude of intensity, in the emission spectrum (Fig. 5.2) when the F420 sample was excited at 420 nm as compared to 295 nm, which was the excitation wavelength used for time-resolved measurements.

F420, once separated and diluted in the elution buffer, was used in time-correlated single photon counting to determine its lifetime. Figure 5.3 presents the fluorescence decays of F420 obtained at pH 7.5 and at pH 13. As the pH was increased through the pK_a of the nitrogen at the three position, a second component of fluorescence decay was observed. This was due to the ionization of this nitrogen group. In each case, these measurements yielded the same 4.2-ns lifetime component. Lifetimes were not measured at pH values below 7 due to the pH induced changes in the absorption spectrum. At low pH, the sample could not be sufficiently excited for the fluorescence decay to be determined.

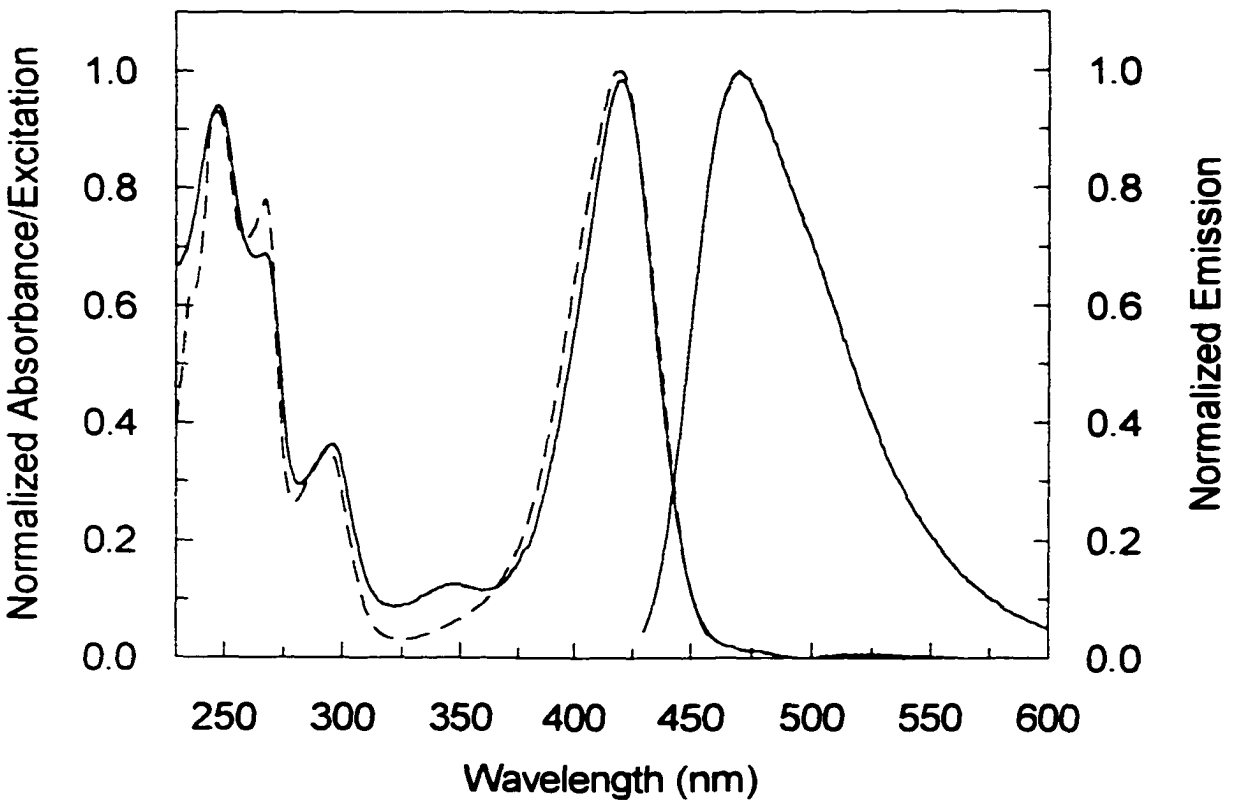

Figure 5.2. Absorbance (——), excitation (- - - - -), and emission (——) spectra of F420 in the elution buffer. The excitation wavelength for the emission spectrum was 295 nm. The emission wavelength for the excitation spectrum was 470 nm.

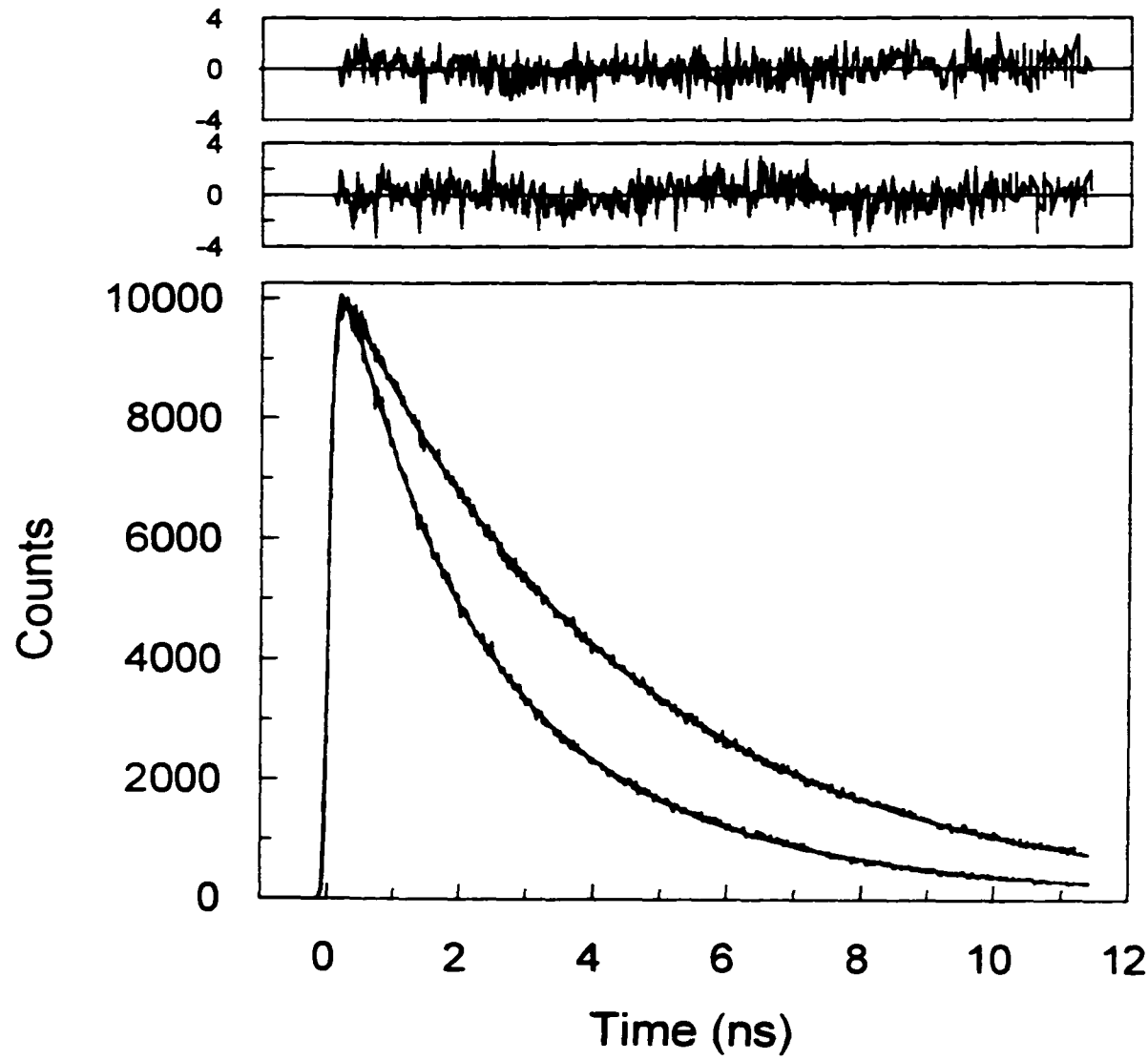

Figure 5.3. Lifetimes of F420 at pH 7.5 and 13. At pH 7.5 (upper decay and residuals) F(t) = 1.0 exp (-t/4.25 ns ± 0.02) with a χ^2 = 1.15 ± 0.1. At pH 13 (lower decay and residuals) F(t) = 0.31 exp (-t/4.20 ns) + 0.69 exp (-t/1.79 ns) with a χ^2 = 1.39.

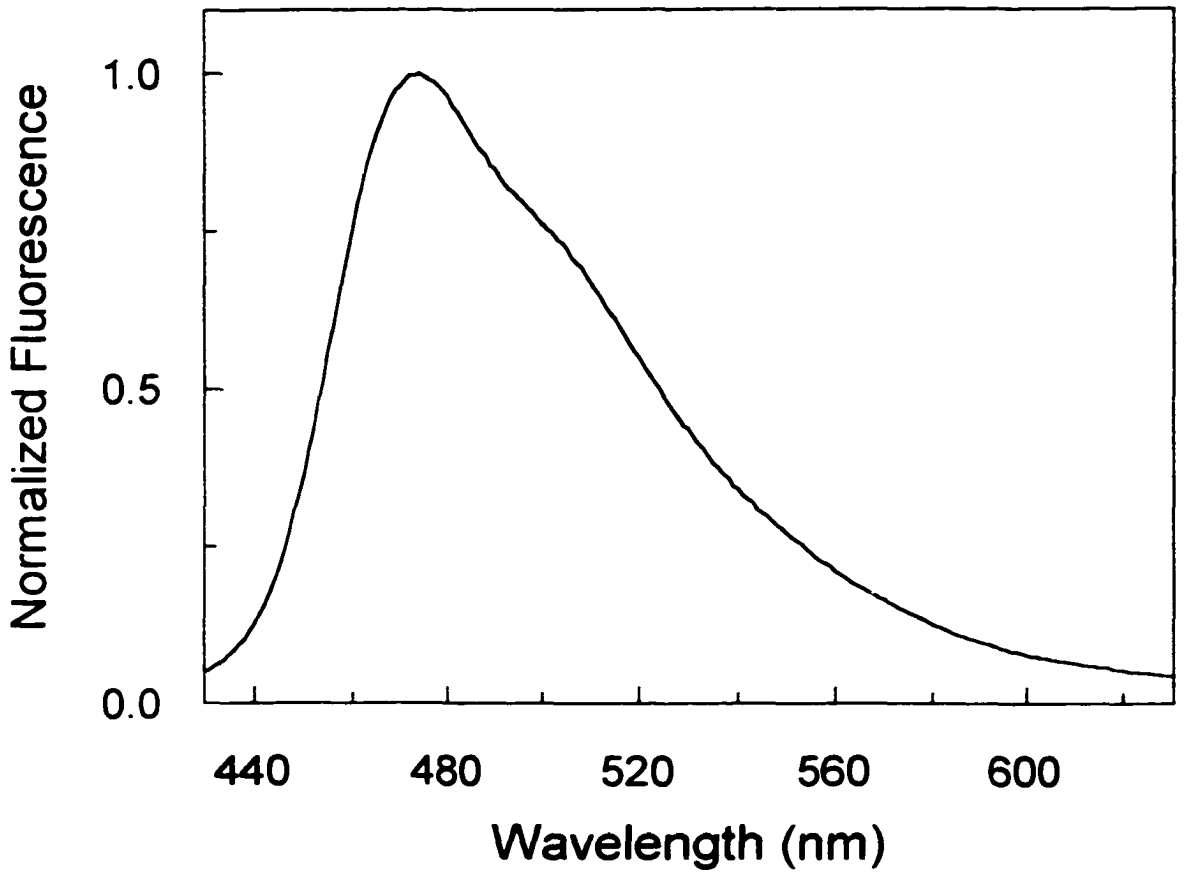

Figure 5.4. Emission spectrum of acetone extract of methanogen cells. Excitation wavelength was 420 nm. Front-faced technique was utilized.

The utility of F420 as a marker for contamination on meat surfaces was realized when methanogen cells, feces, and other ingesta, were examined. As shown in figure 5.4, the emission of F420 is observed from methanogen cells. In fact, the emission spectrum was nearly identical to that of the purified F420 chromophore in figure 5.2. The front-faced method was used to obtain this spectrum, demonstrating the ability to collect the emission from surfaces of opaque samples. Similarly, and perhaps most importantly, was that the "F420-like" emission was also observed from feces, cecum, and rumen samples, the actual samples likely to contaminate meat surfaces (Figure 5.5). This illustrates the ability to detect F420 in these ingesta samples at wavelengths around 470 nm and thus to detect the contaminants using F420 as a fluorescent marker.

F420 has a fluorescence lifetime of 4.2 ns. To use time-resolved methods of detecting F420 from fecal samples, its lifetime must be resolved from scattered light and fluorescence from other emitting species. Figure 5.6 shows the lifetime decay of a fecal sample with a small amount of water added. A 45° cuvette was used because the opaque sample did not transmit the excitation light. Even though care was taken to filter out the scattered and reflected excitation light, it can be seen that the decay does contain significant extraneous contributions at short times. In order to avoid these contributions in our analysis, the data were fit by ignoring the early-time part of the decay curve and by beginning the fit of data at longer times. If this is not done then the artifactual short-time components dominate the fit and make it more difficult to resolve the contributions of actual fluorescent components. The fit revealed a 4.2 ns component with an amplitude of 0.24, illustrating the ability to observe emission from F420 even in a time-resolved measurement of a fecal sample. The amount of the emission arising

Figure 5.5. Fluorescence spectra of (A) rumen, (B) cecum, and (C) feces samples from two different cows, labeled 1 and 2, and a fecal sample of a pig. The excitation wavelength was 430 nm. The baseline in each panel at zero intensity is the emission from the 50 mM Tris dilution buffer after correction for Raman scattering from water. Each emission spectrum was corrected for Raman scattering by subtracting the contribution of Raman scattering from the Tris buffer. In panel (A) spectra **a** and **b** are rumen samples from cow 1 and spectrum **c** is from cow 2. (B) is a cecum sample from cow 2. In (C), spectrum **a** is a feces sample from cow 2, spectrum **b** and **d** are from cow 1, and spectrum **c** is a pig feces sample. The spectrum with each set of samples with highest intensity was normalized to one with the other spectra normalized relative to it to preserve the relative fluorescence intensities.

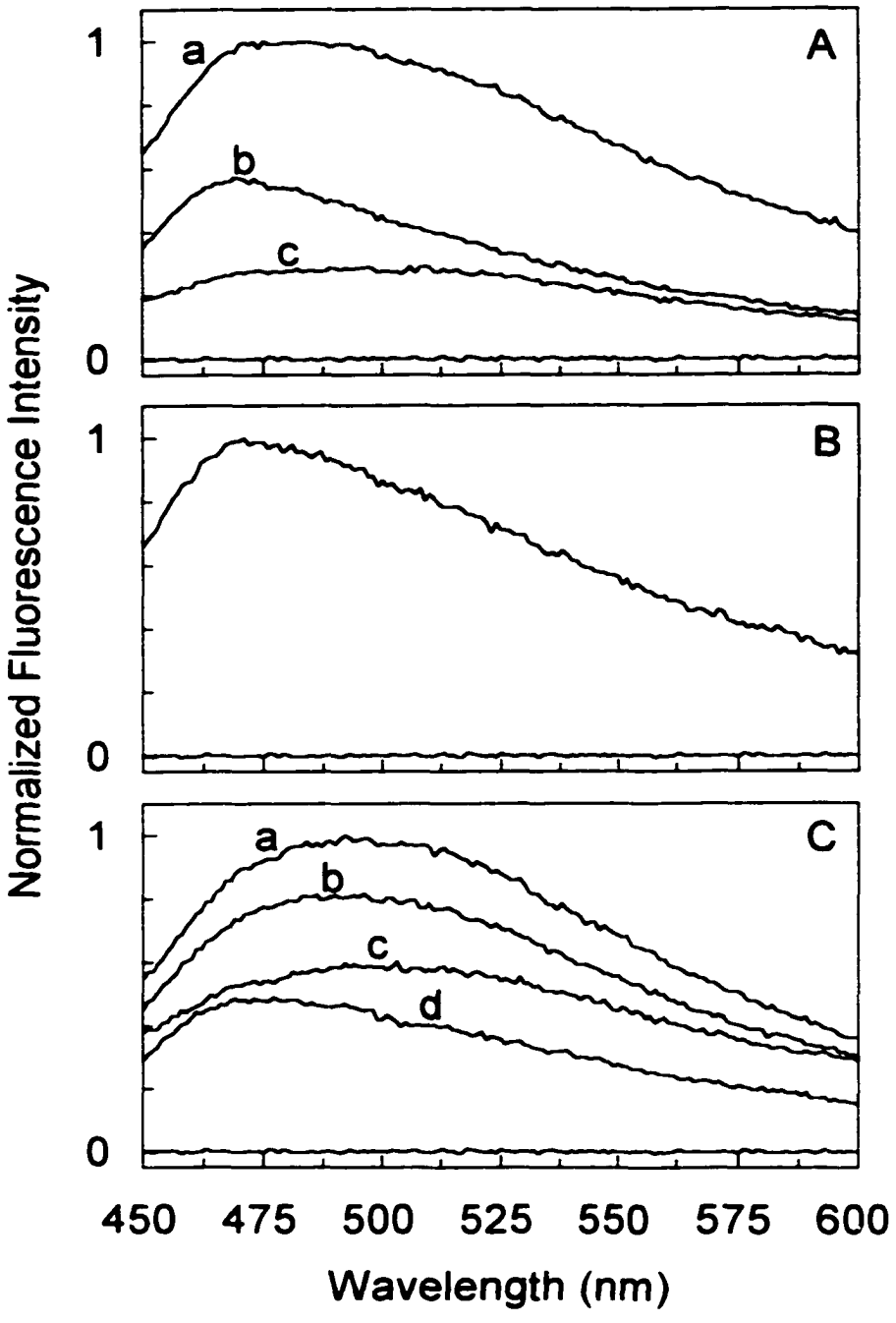
A
B
C
a
b
c
d
1
0
Normalized Fluorescence Intensity
450
475
500
525
550
575
600
Wavelength (nm)

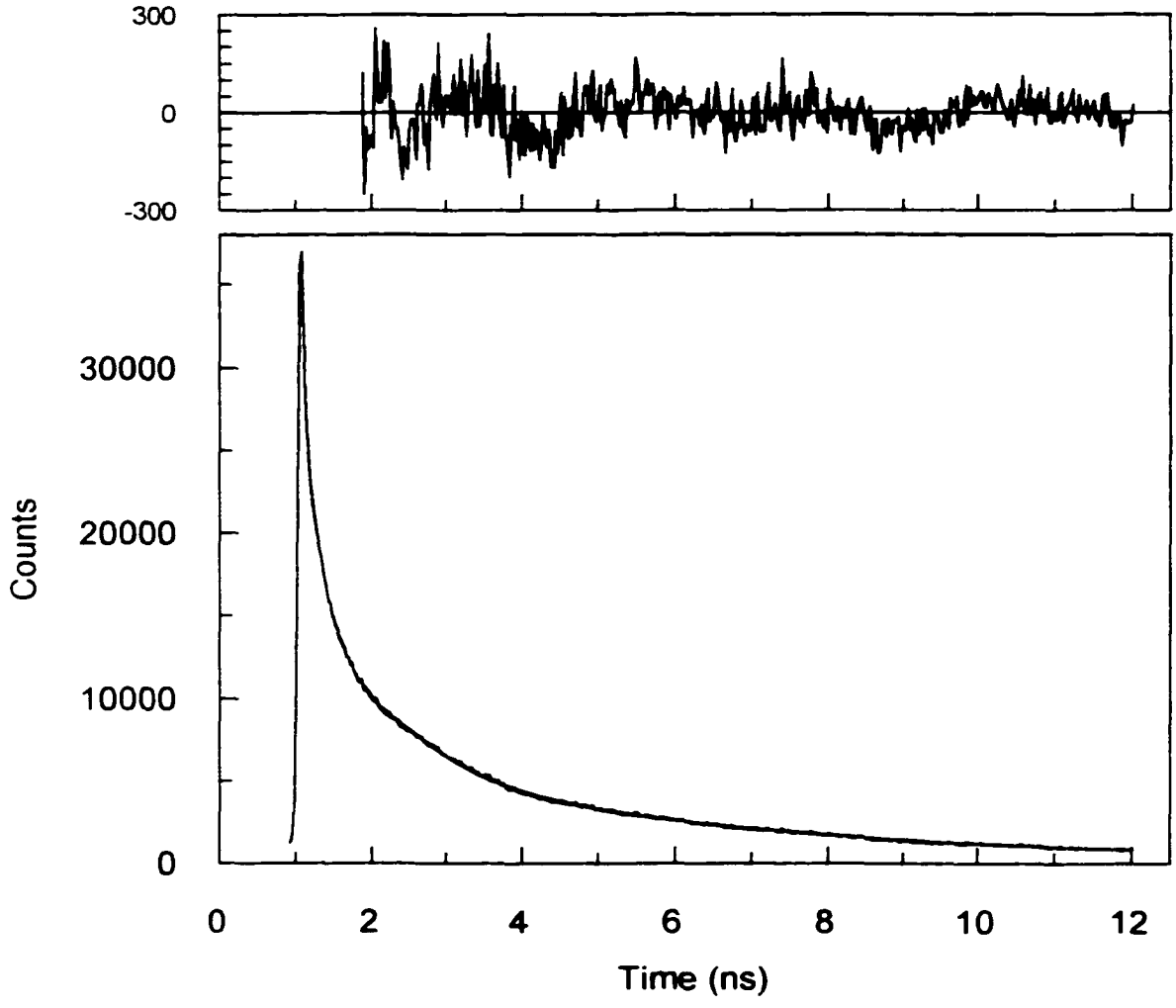

Figure 5.6. Fluorescence decay of fecal material using the front-faced technique. F(t) = 0.38 exp(-t/0.140 ns) + 0.38 exp(-t/0.682 ns) + 0.24 exp (-t/4.20 ns); χ^2 = 1.55. The fit was started at about 30% of the decay so as not to fit contributions to the decay from scattered or reflected excitation light. The residuals show some RF oscillations for which where was no correction.

from F420 was most likely larger given that where we chose to begin the fitting procedure is somewhat arbitrary and that we have totally ignored all the scattered light contributions.

Conclusions

Methanogenic bacteria are present in the rumen and cecum of animals. These bacteria contain the F420 chromophore. We have isolated F420 from the bacterium, *Methanobrevibacter ruminantium*, obtained from the rumen content of a cow, and we have obtained its absorption and fluorescence excitation and emission spectra, which are in the visible region of the spectrum. F420 has a relatively high fluorescence quantum yield (0.17) and a long fluorescence lifetime (4.2 ns). Consequently, these bacteria may be good optical probes of fecal and ingesta contamination of animal carcasses that may occur during processing. We have demonstrated that F420 fluorescence can be collected from this methanogen. Finally, and most importantly for applications to problems of food safety, we have demonstrated that solid samples of fecal material contain optical signatures of F420. Consequently, there are intrinsic optical tags in the gut of animals that can be used to monitor fecal and ingesta contamination of meat products.

Acknowledgment

This work was funded by a grant from the Food Safety Consortium and by a Specific Cooperative Agreement 58-3625-7-113 with the USDA.

References

1. Kates, M.; Kushner, D.J.; Matheson, A.T. *The Biochemistry of Archaea (Archaebacteria)*; Elsevier: Amsterdam, 1993; pp 41-61.

2. Eirich, L.D.; Vogels, G.D.; Wolfe, R.S. *Biochem.* **1978**, 17,4583-4593.

3. Ashton, W.T.; Brown, R.D.; Jacobson, F.; Walsh, C.J. *Amer. Chem. Soc.* **1979**, 101, 4419-4420.

4. Gorris, L.G.M.; van der Drift, C. *Biofactors* **1994**, 4, 139-145.

5. Danson, M.J.; Hough, D.W.; Lunt, G.G. *The Archaebacteria:Biochemistry and Biotechnology*; Portland Press: London, 1992; pp143-179.

6. Avouris, P.; Yang, L.L.; El-Bayoumi, M. A. *Photochem. Photobiol.* **1976**, 211-216.

7. DiMarco, A.A.; Bobik, T.A.; Wolfe, R.S. *Annu. Rev. Biochem.* **1990**, 59, 355-394.

8. Doddema, H.J.; Vogels, G.D. *Appl. Environ. Microbiol.* **1978**, 36, 752-754.

9. Eirich L.D.; Vogels, G.D.; Wolfe, R.S. *J. Bacteriol.* **1979**, 140, 20-27.

10. Schonheit, P.; Heribert, K.; Thauer, R.K. *FEMS Microbiol. Lett.* **1981**, 12, 347-349.

11. Cheeseman, P.; Toms-Wood, A.; Wolfe, R.S. *J. Bacteriol.* **1972**, 112, 527-531.

12. Purwantini, E.; Mukhopadhyay, B.; Spencer, R.W.; Daniels, L. *Anal. Biochem.* **1992**, 205, 342-350.

13. Ogimoto, K.; Imai, S. *Atlas of Rumen Microbiology*; Japan Scientific Societies Press; Tokyo, 1981; pp. 171-173 and 185.

14. Chen, Y.; Rich, R.L.; Gai, F.; Petrich, J.W. *J. Phys. Chem.* **1993**, 97, 1770-1780.

15. Chang, M. C.; Courtney, S. J.; Cross, A. J.; Gulotty, R. J.; Petrich, J. W.; Fleming, G. R. *Anal. Instrum* **1985**, *14*, 33. Cross, A. J.; Fleming, G. R. *Biophys. J.* **1984**, *46*, 45.

CHAPTER VI. REAL-TIME DETECTION OF FECAL AND INGESTA CONTAMINATION ON MEAT SURFACES UTILIZING INTRINSIC FLUORESCENT MARKERS: THE "F-DETECTOR"

Abstract

Outbreaks of serious illness due to *E. coli.* O157:H7 are most often traced to undercooked ground meats. The source of this contamination stems from fecal and ingesta material being transferred to the animal carcass during evisceration. *E. coli.* bacteria commonly inhabit the guts of animals used for meat. Visual inspection of random carcasses remains the only means of detecting fecal and ingesta contamination. As a means of detecting possible *E. coli.* contamination we describe a method and system for detecting the vector of the *E. coli.* bacteria, namely the fecal material itself, on the meat surface. The chlorophyll metabolite, pheophorbide *a*, within the fecal and ingesta material is used as a fluorescent maker to signal the presence of contamination. A laser based detector, the "F-Detector", has been built and successfully demonstrated to show its ability to quickly detect low levels of fecal material on meat surfaces. The detector uses phase-sensitive detection with a 100 ms time constant to provide as essentially "instantaneous" signal of contamination with sufficient selectivity to detect only the fluorescent marker, pheophorbide *a*. The F-Detector successfully detected pheophorbide *a* in solution down to approximately 10^{-10} M (~3:1 signal to noise ratio) with a sensitivity on the order of 10^7 to 10^8 mV/M. A 25 mV signal from the F-Detector correlates to a pheophorbide concentration of 1.0×10^{-6} M and an equivalent fecal concentration of 1.8 mg/mL of diluted fecal solution. Our results illustrate the usefulness of the F-Detector as an

optical detection system with much greater detection limits, selectivity, and sensitivity over the current visual methods of inspection.

Introduction

There continues to be growing concern with regard to the cleanliness of the food that is consumed by the public. Harmful and even deadly bacterial contamination may occur during the initial processing of meat products [1-3]. During the last few years the meat industry has been in the spotlight with extensive recalls of *E. coli.* contaminated meat, in particular, ground beef. The particular bacterial strain, *E. coli.* O157:H7, is the culprit in such recalls [4-6]. This strain is a common inhabitant of the digestive system of animals, such as cows, used for meat [1,6]. It produces Vero cytotoxins which can cause severe damage to the lining of the large intestine [4,6] and can lead to other severe and life-threatening complications such as hemolytic uremic syndrome [7,8]. Thus, if any of the contents from the viscera (if it is punctured), fecal material, or contaminants from the hide of the animal, is transferred to the carcass during processing, the probability of *E. coli.* O157:H7 contamination of the meat is extremely high [1-3,9,10]. While this remains a source for contamination of the exterior of the meat, the grinding process spreads it throughout the product [2,8]. The detection of fecal material and ingesta on the carcasses of meat is of great importance and therefore, the focus of this and previous work [11, Chapter 5 of this dissertation].

Our previous efforts led us to investigate the intrinsic fluorescent probe, F420, an electron carrier in methanogenic bacteria [12-16], also common inhabitants of cows. A spectroscopic investigation of F420 was initiated with the prospect of using this fluorescent marker as a means to detect fecal and ingesta contamination on meat surfaces, thus detecting

the possible presence of *E. coli*. Although this probe was found to be quite useful, further investigation revealed an additional fluorescent marker that proved to be more attractive than F420, one that is a chlorophyll metabolite within fecal material and ingesta of herbivorous animals [17-19].

To ensure that proper processing procedures are followed within the production facility, especially during those steps which have been identified as the major sources of contamination, namely skinning and evisceration, inspectors observe the process and visually inspect the carcasses for visible soiling of hair, dirt, feces, and ingesta [2,10]. As one might conclude, this method of "naked-eye" inspection has some limitations. The human eye can see only finite sized spots and may not be able to distinguish between fecal spots and other, non-contaminating spots, such as blood spots. Visual inspections can be slow and cumbersome, and only a random sampling of a much larger production volume is actually inspected and sampled [1]. Once a carcass has been chosen for inspection only a few locations on the carcass are actually swabbed (those that represent the most probable locations for visceral or fecal contamination) for the purpose of "counting" or detecting bacteria; *E. coli*. being the indicator of fecal contamination [1,3]. Bacterial contamination may not be widespread over the whole carcass and so a few random samples of a carcass may not truly represent the extent of contamination. The current guideline is "zero-tolerance", as to the amount of fecal material, ingesta, etc. allowed to be present on a single carcass following evisceration. This zero tolerance guideline creates a daunting task for meat producers and inspectors to provide the public with safe meat products [2]

We describe here a real-time, low detection limit system for detecting fecal matter and

ingesta on meat carcasses. A prototype instrument, the "F-detector", has been designed, built, and effectively demonstrated to exploit the optical properties of intrinsic fluorescent markers within the contaminants, namely the chlorophyll metabolite, pheophorbide *a* (Figures 6.1 and 6.2) [17], and provide a real-time signal (100 ms time constant) as to its presence on the meat carcass. While our system is still in the prototype stage, the concept and design is currently being engineered into commercial instrumentation to insure a safer meat product for the public while providing a more efficient and accurate way for meat producers to do so.

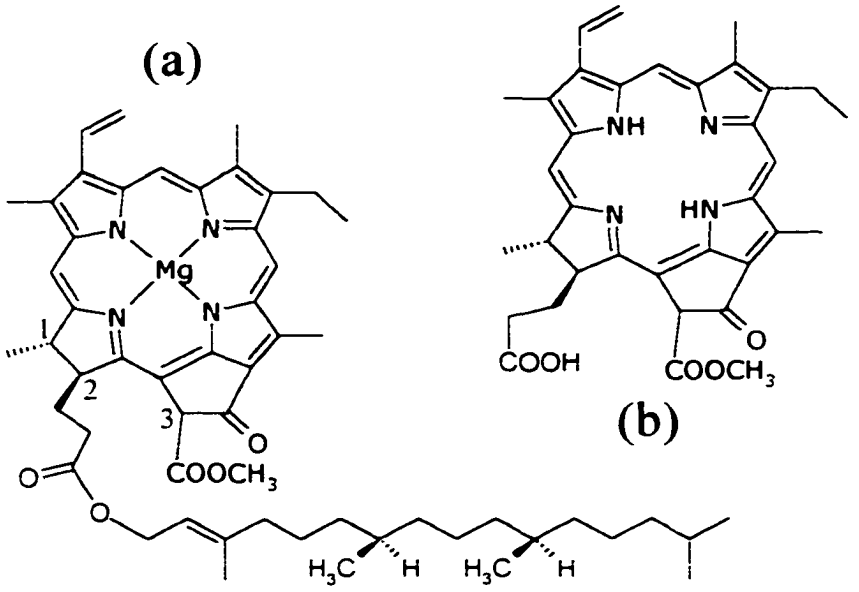

Figure 6.1. The structures of (a) chlorophyll *a* and (b) pheophorbide *a*. The numbers in (a) do not represent standard numbering among chlorophylls but only the locations where certain metabolic changes occur in chlorophyll as outlined in figure 6.2.

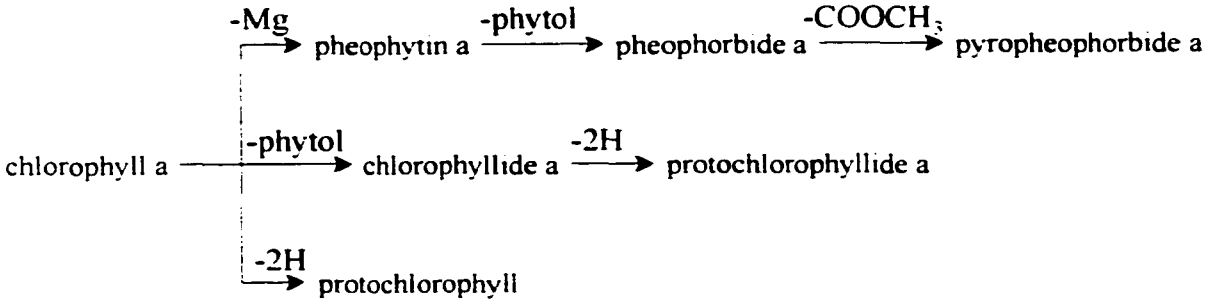

Figure 6.2. Several metabolic pathways of chlorophyll *a* [1]. With reference to the numbered positions on the chlorophyll ***a*** structure in figure 6.1a, the groups above the arrows are those groups which are lost during metabolic reactions: the -2H is the loss of hydrogen atoms form the carbon atoms at positions 1 and 2 in figure and the $-COOCH_3$ is that group which is lost at position 3 in the figure. The fluorescent marker we focus on in this work is pheophorbide *a* which has lost the Mg ion and the phytol group, the long hydrocarbon chain on chlorophyll *a*.

Experimental Section

Steady-state Absorption and Emission Investigation

Feces, rumen and cecum samples were obtained from cows housed at the National Animal Disease Center (ARS, USDA, Ames, IA). Additional samples of fecal material were obtained from other sources. Chlorophyll *a* and pheophorbide *a* (Figure 6.1) were obtained from Porphyrin Products, Inc., Logan, Utah, and were used as received (pheophorbide *a* ~95 % pure with major impurity being pyropheophorbide *a* (Figure 6.2)[20]). The solvents used were freshly purchased and used as received, and water was of nanopure quality. The extinction coefficient, ϵ, of the commercial pheophorbide *a* in acetone at 665 nm was determined to be $2.03 \times 10^4\ M^{-1}\ cm^{-1}$.

Absorbance spectra were obtained using a Perkin-Elmer Lambda 18 UV-Visible spectrophotometer. Excitation and emission spectra were obtained using a SPEX FluoroMax with a 4-nm bandpass resolution. For solid or opaque samples the front-faced fluorescence technique, with a 45° triangular cuvette, was utilized.

For the fecal and ingesta samples obtained from animals (two different cows and one pig) housed at the NADC, emission spectra were obtained by adding small volumes of the sample (~10 μL) to a 1 cm × 1 cm cuvette and diluting with 3 mL of a 50 mM Tris buffer (pH 7.5). The small sample volumes were necessary to reduce the opacity of the samples as these spectra were obtained before the front-faced technique was utilized. The excitation wavelength was 430 nm. A Tris buffer blank spectrum was also obtained so that contributions to each sample spectrum from Raman scattering could be subtracted.

Emission spectra from the additional fecal samples of other sources were obtained by placing the solid sample directly into the 45° cuvette and exciting at 400 nm.

Additional front-faced emission spectra were obtained of clean meat samples and then of these same meat samples spotted with a very small amount of fecal material on the front surface. The excitation wavelength used to obtain these spectra was 420 nm. The meat samples were placed directly into the 45° cuvette and the fecal material was spotted onto the meat surface via a spatula that had been dipped into the fecal material, and sliding the spatula down between the meat surface and the cuvette face. The amount of fecal material spotted on the meat surface was not quantified. Only qualitative measurements were desired.

The F-detector.

Among the many names given to the prototype detector instrument, the name, "F-detector", has remained the most common, although least colorful, designation. Two prototype

instruments were designed and built to detect the pheophorbide signal at around 670 nm. In this Experimental section each prototype will be described along with the specific equipment used for their production.

The First-Generation Prototype. The first-generation F-Detector prototype (Figure 6.3) is based upon the design in figure 6.4. A Coherent Antares 76s CW mode locked Nd:YAG laser was used as the excitation source. The 1064 nm fundamental is frequency doubled to provide an output wavelength of 532 nm.. The green, 532 nm output from the laser was coupled into a 3M single mode optical fiber (Thorlabs, Inc.) and subsequently delivered to the detector. Within the detector the light was reflected off a CVI 532 nm reflecting (610 - 1037 nm transmitting) dichroic mirror (D1 in Figure 6.4) and coupled into a second optical fiber (3M multimode fiber; Thorlabs, Inc.). Both fibers utilized SMA type collimating/coupling lenses (Thorlabs) which will focus a collimated laser beam onto the end of the fiber and thus helps to couple the light more efficiently into the fiber and also help to collimate light exiting the end to the fiber. The meat/sample was excited with the green light exiting the second fiber and the subsequent emission was collected via coupling through the same optical fiber. The "red" emission is transmitted through the first, 532 nm reflecting dichroic, D1 (see Figure 6.4), and impinges upon D2, a CVI 610 nm reflecting/670 - 1037 nm transmitting, dichroic mirror. At D2 the emission is split and each component is sent to one of two Hamamatsu R928 (185 - 900 nm) photomultiplier tubes (PMT) each power by its own Condor HBB15-1.5A+ ±15 V(1.5 A)/±12 V(1.7 A) power supply purchased from Allied Electronics. The signal PMT is set to detect the emission maximum at around 670 nm with the use of a CVI 670 nm interference filter (10 nm bandpass), F2 (Figure 6.4), placed in front of the PMT. The second PMT is set to detect

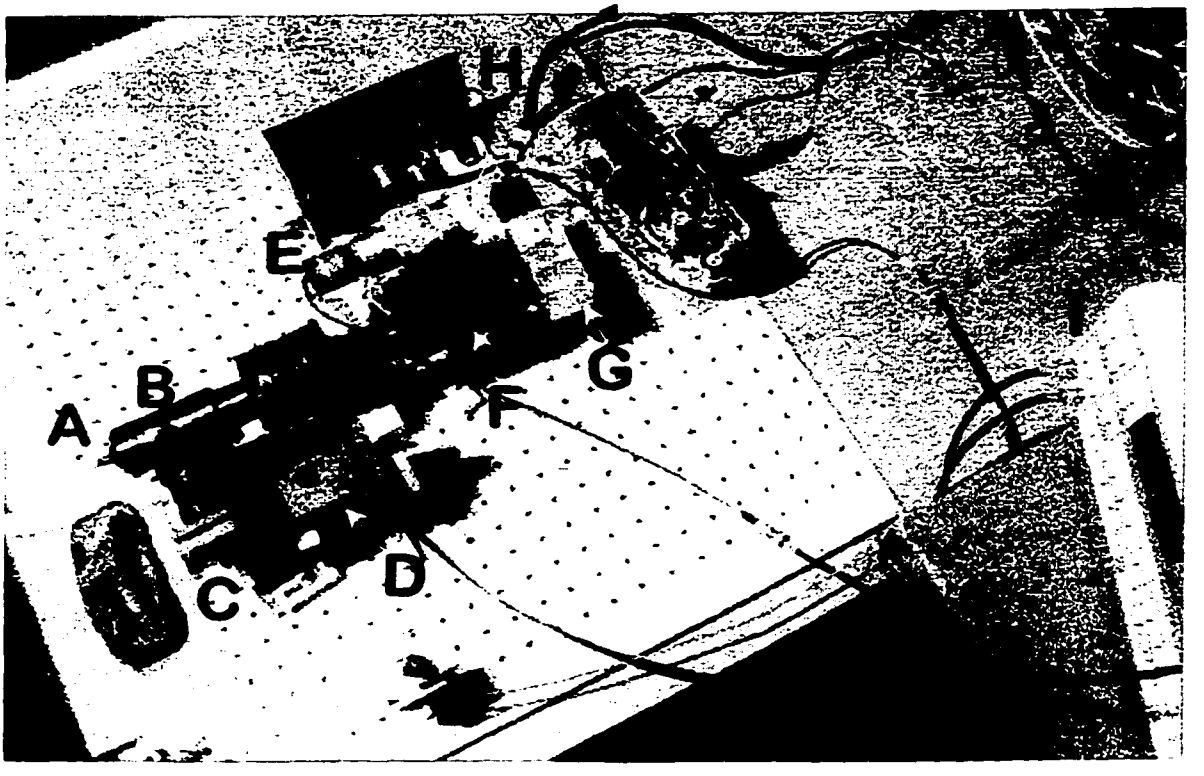

Figure 6.3. The first-generation F-Detector prototype. From left to right; **A** is the optical fiber which delivers the 532-nm excitation light to the sample and subsequently collects the emission. **B** is the where the 532 nm reflecting/610 - 1037 nm transmitting dichroic mirror is located. **C** is the optical fiber that delivers the 532-nm excitation light directly from the Nd:YAG laser. **D** is the chopper that modulates the excitation light at a frequency of 220 Hz. **E** is a PMT with a 610-nm interference filter. **F** is the location of the 610 nm reflecting/670 - 1037 nm transmitting dichroic mirror. **G** is the second PMT with a 670 nm interference filter. **H** are the PMT power supplies. **I** is the lock-in amplifier where the two outputs of the PMTs are connected. The 610-nm signal is subtracted from the 670-nm signal, amplified, and detected using phase-sensitive detection.

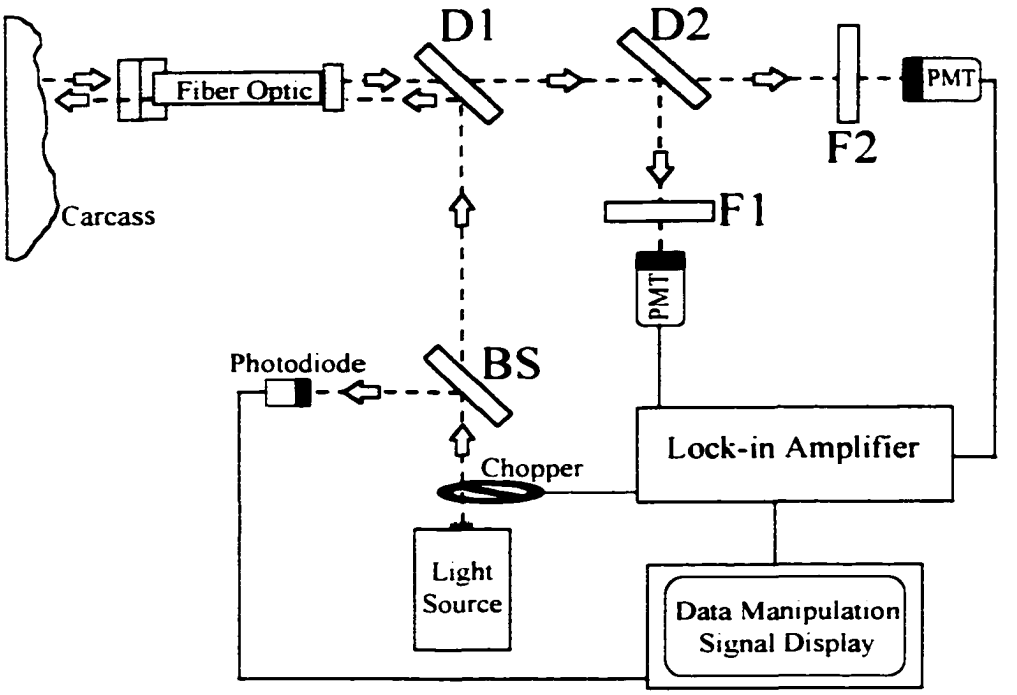

Figure 6.4. The basic design layout of the F-Detector. The details of the components are given in the text. BS is a beam splitter which may be used to pick off a small portion of the excitation light for normalization purposes. D1 is the 532-nm reflecting/610 - 1037-nm transmitting dichroic mirror. D2 is the 610-nm reflecting/670 - 1030-nm transmitting dichroic mirror. F1 is a 610 nm interference filter and F2 is a 670 nm interference filter.

light at a minimum in the overall emission signal with the use of a CVI 610 nm interference filter (10 nm bandpass), F1 (Figure 6.4), placed in front of the PMT. Each PMT was housed within and aluminum casing that included a shutter and fitted with filter mounts to eliminated any undesired scattered light. The overall signal from the sample was determined to be the difference between the two PMT signals: signal(670 nm) - signal(610 nm).

The emission collected from the sample is very low intensity light and thus to improve signal to noise an SRS (Stanford Research Systems, Inc.) model SR830 DSP lock-in amplifier was utilized (phase-sensitive detection). The green output from the YAG was modulated using a New Focus, Inc. 3501 Optical Chopper at a frequency of 220 Hz. The reference output from the chopper was connected to the reference input of the lock-in via BNC connectors. Both outputs from the photomultiplier tubes were also connected to the lock-in through BNC cables into two separate channels, A and B, on the lock-in and the instrument was set to take the difference in the signals, A - B (670 nm - 610 nm). The lock-in amplifier accepts current input signals and thus no further external treatment of the PMT output signal was needed.

The particular lock-in amplifier used essentially has two phase-sensitive detectors which have a reference signals that are 90° out of phase with each other. The combination of the two phase-sensitive detectors in essence provides a signal maximum which has no phase dependency between the reference signal and the detected signal (See Appendix A) and therefore no external adjustment of the lock-in is necessary. A 100 ms lock-in amplifier time constant was used.

The first-generation F-Detector was tested using samples/trimmings from actual production line beef carcasses supplied by IBP.

The Second-Generation Prototype. The second-generation prototype (Figure 6.5) is

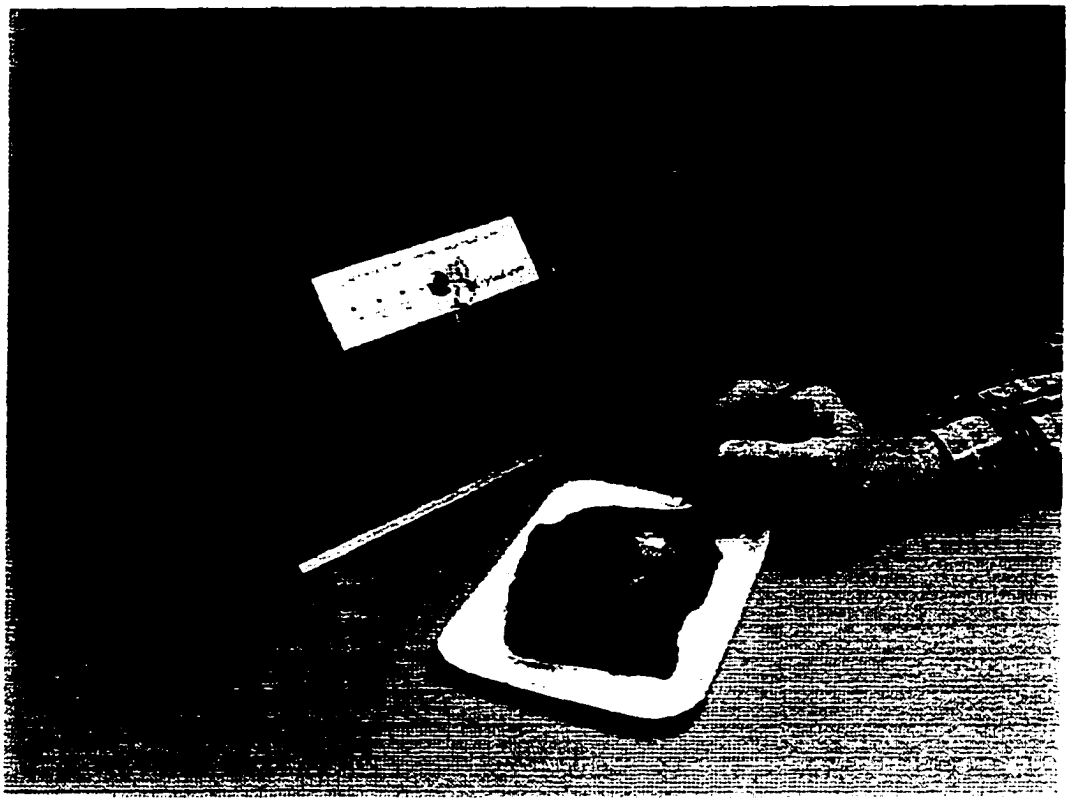

Figure 6.5. The second generation F-Detector prototype.

based upon the same design illustrated in Figure 6.4 with some modifications in the equipment so as to make it small, portable and easily handled. The light source for this prototype is a CL-1001-Diode Pumped Green *CrystaLaser*, Nd: YVO_4, TEM_{00}, CW laser (model # GCL-050-M, *CrystaLaser*, Reno, NV, USA) with an output of 50 mW maximum at 532 nm (our measurements indicate ~42 mW output). The 1064 nm fundamental is frequency doubled using an intracavity KTP crystal. The laser is easy to operate and is very compact, the laser head dimensions being, 3 × 3 × 12 cm, and weighs less than one pound, and has a metal baseplate for easy mounting. Supplied with the laser is a 110 VAC power supply/controller with dimensions of 5 × 13 × 15 cm and weighs about 2.5 pounds.

The fiber optic used is a Visionex - Enviva Biomedical Probe: Raman V1.0. This probe consists of two fiber optic leads: a laser lead and a collection lead. The laser lead is for the coupling of the laser excitation light into the fiber. It consists of a single 300 μm, silica fiber with a numerical aperture of 0.22 and an SMA termination to which a beam collimating lens is attached to aid coupling the green laser light into the fiber. The collection lead consists of seven silica fibers each with a 300 μm core. The numerical aperture at instrument end (opposite probe tip) is 0.22 with an SMA termination and collimating lens to collimate the emission light for greater efficiency in transmitting the emission light to the PMTs. About 14 cm from probe tip is the bifurcation start where the two leads come together in an optical configuration that consists of one delivery fiber (laser lead) encircled about by the seven collection fibers. The probe tip is a stainless steel needle with a diameter of about 1.5 mm. This particular probe was chosen because of its "In-The-Tip" filters to filter out Raman scattering both in the laser and collection leads. The overall probe length is 1.5 m which was extended with the addition of a 3 m length of optical fiber coupled to each lead of the probe with SMA type bushings.

The green laser light was modulated at a frequency of 220 Hz using a CH-10 Tuning Fork Resonant Chopper purchased from Electro-Optical Products Corp. The tuning fork chopper is electromechanically driven by their Drive Electronics Type ED Driver which also provides a square wave reference output signal. The tuning fork chopper is small (~1.6 cm · 2.5 cm · 6.4 cm, which includes the tuning fork and vanes; the ED Driver is of comparable size, though not as long), lightweight and rugged with no wearing parts. The modulation provided by the chopper is sinusoidal with a 50% duty cycle.

The modulated emission from off the surface of the sample is collected through the

collection fibers and into the collection lead of the probe. The collection lead utilizes a Thorlabs, Inc. SMA collimating lens to transmit the light more efficiently to a CVI 610 nm reflecting/670 - 1037 nm transmitting dichroic mirror. Two Hamamatsu H6780-01 Series Photosensor Modules (300 - 820 nm) detect the light signals. Each module contains a compact photomultiplier tube and high voltage power supply and are very compact with dimensions of 22 mm · 22 mm · 50 mm. The supply voltage to each module is +12 V to +15 Vdc. The sensitivity of each module is controlled with a 10 kΩ potentiometer. A 610 nm (10 nm bandpass) interference filter was placed in front of the PMT that detects the reflected light from off the dichroic and a CVI 670 nm (10 nm bandpass) interference filter was placed in front of the PMT detecting the transmitted light from the dichroic mirror.

The output from each PMT is a current signal. The Pocket Lock-In™ Amplifiers Model VK-90 from ElectroSolutions, Inc. used for this detector only accept voltage signals so the PMT output is first converted to voltage through a simple current to voltage amplifier circuit (see Appendix B) [21-23]. As the name of the lock-in amplifiers suggests, they are small (~7.6 cm · 2.5 cm · 18 cm) and light weight. The voltage output of these lock-in amplifiers has no phase dependency due to the use of two phase sensitive detectors or mixers whose phase angle difference is 90° relative to each other. This is similar to what was described for the SR830 lock-in described above and in Appendix A. The two mixers work to keep the phase angle difference between the reference and the signal at a zero value thus the output is always kept at the signal maximum without any external control of the reference phase angle. The second-generation F-Detector contains two such Pocket Lock-Ins, one for each of the signals detected; 610 nm and 670 nm. These two signals are subsequently subtracted to provide the overall

desired signal from the sample.

A basic difference amplifier circuit was made to accept the two outputs from the lock-in amplifiers and subtract them (See Appendix B for further details)[21,22]. The subtracted output is then displayed by a digital panel meter providing the voltage readout of the overall emission signal.

One Condor HBB15-1.5A+ ±15 Vdc(1.5 A)/±12 Vdc(1.7 A) power supply (Allied Electronics) was used to power all of the above components of the second-generation F-Detector prototype (except for the CrystaLaser). A PacTec CLH-45 CL Series enclosure/instrument box (14.6 · 31.8 · 29.5 cm) was purchased (Allied Electronics) and all of the detector components were mounted inside of the box. The dc power supply and the CrystaLaser was wired to the same 110 VAC power plug and a single on/off switch.

A calibration curve illustrating the response and detection limits of this second-generation F-Detector to solutions of commercial pheophorbide in ethanol was obtained. The concentrations used are shown in Table 6.1. A 1 mm-pathlength quartz cuvette which contained the various concentrations of solution was placed in front of the probe tip. The probe tip was fixed in a horizontal position a distance of 2 -3 mm from the cuvette surface. The probe tip and cuvette were kept in fixed positions for each voltage reading on the detector. The reasons for this will be explained in the Results and Discussion section.

Since the second-generation F-Detector was built to detect fecal contamination on the surface of meat carcasses as well a used as a model for future designs an "equivalent fecal unit" was roughly determined. Essentially this "equivalent fecal unit" is a measure of the amount of fecal material that is equivalent to a given amount of pheophorbide giving rise to the same

Table 6.1. Data for the calibration curve of pheophorbide *a* in ethanol using the second-generation F-Detector.

Pheophorbide Conc. (M)	F-Detector Signal (mV)
6.87×10^{-7}	143.3 ± 0.2
1.72×10^{-7}	32.1 ± 0.2
1.29×10^{-7}	29.5 ± 0.5
4.29×10^{-8}	16.3 ± 0.2
3.22×10^{-8}	12.0 ± 0.1
1.07×10^{-8}	7.5 ± 0.1
8.05×10^{-9}	7.8 ± 0.2
2.68×10^{-9}	4.7 ± 0.1
2.01×10^{-9}	4.3 ± 0.2

detected signal.

To make this type of determination the *CrystaLaser* power had to be measured to determine the number of photons exciting the sample. About 42 mW of 532 nm output was measured from the *CrystaLaser*. After passing through the chopper and coupling the beam into the laser lead of the fiber optic probe the output from the probe tip was about 15 mW. As a model to simulate an opaque fecal sample or a fecal spot, in which emission would be collected from the surface of the sample, a 0.1 mm thick TLC plate was utilized to which 1 µL volumes of pheophorbide *a*/ethanol and feces/H_2O solutions were spotted (2.5 mm diameter spots). The solutions were made by weighing the pheophorbide and fecal material and diluting in the respective solvent. The spot size of the 532 nm output from the probe tip was 1 mm. Two curves, F-Detector signal versus concentration of pheophorbide (M) and feces (g/mL), were

obtained. The purpose of this was to obtain the amounts of pheophorbide and fecal material that give rise to a certain F-Detector signal. The quantum yield of pheophorbide a is 0.12 and the extinction coefficient, ϵ, at 532 nm is $3.60 \cdot 10^3$ M^{-1} cm^{-1}. The percentage of photons located in the emission band centered around 675 nm, of pheophorbide, is 69% (or the quantum yield of the 675 nm band is 0.69, calculated by the ratio of the integrated 675 nm band wavenumber spectrum to the integrated total emission wavenumber spectrum).

Results and Discussion

The Fluorescent Marker, Pheophorbide a

Chlorophyll is the green pigment in plants responsible for photosynthesis [17-19]. Once ingested by herbivorous animals, chlorophyll undergoes metabolic changes and those products can be used as a marker in the detection of fecal and ingesta contamination. Ma and Dolphin estimate that chlorophyll *a* makes up 75 % (or higher) of the green pigments in plants, obviously the most abundant [17]. Herbivorous animals that consume large amounts of green plants have large amounts of chlorophyll *a* that enters their digestive systems. Metabolic changes in chlorophyll *a* subsequently take place and little intact chlorophyll *a* emerges from the animals [17,19]. In figure 6.2 a few of the different reaction pathways that chlorophyll may be subject to are shown [18].

In order to design a detection system to detect chlorophyll metabolites in fecal material and ingesta it is necessary to obtain a qualitative idea as to which molecule or group of molecules that would be most feasible to use as a marker for contamination. In biological systems such as the stomach and digestive tract where acidic conditions exist, chlorophyll *a* readily becomes demetallated [18,19]. Indeed, Ma and Dolphin [17] indicate that the most

common species from extracts of herbivores are the demetallated chlorophyll *a*, as well as pheophorbide *a*, and under "harsher" conditions, pyropheophorbide *a*. This led us to investigate the group of compounds along the top reaction pathway in figure 6.2.

Several samples of fecal material and ingesta were obtained and front-faced emission spectra were collected. Figures 6.6 and 6.7 show the rumen, cecum and feces spectra. The main spectral feature of interest is the emission band around 675 nm. Chlorophyll *a* as well as many of its metabolites have emission bands in this region [18,19].

Several measures where undertaken to obtain a qualitative idea as to the origin of the particular ~675 nm emission band. While the emission may very well be from more than one metabolite it remains necessary to determine which metabolite is contributing most to the ~675 nm emission band.

Chlorophyll *a*, and its metabolites, have been investigated for many years and the literature is replete with absorbance and emission spectra. In order to compare with the literature, clearer emission and excitation spectra were obtained of acetone/water extracts of fecal material (Fig. 6.8c). The spectra obtained of the extracted fecal material was in good agreement to spectra of pheophorbide *a* from the literature. We also obtained our own absorption/excitation and emission spectra of commercial chlorophyll *a* and pheophorbide *a* (Fig. 6.8a,b) and when compared, the pheophorbide *a* spectra in figure 6.8b agrees quite well to the extracted fecal material. Thus, by spectroscopic means it is determined that the fecal material does contain pheophorbide *a* and is most likely the origin of the ~675 nm emission band.

Thin-layer chromatography (TLC) also qualified this conclusion. Commercial

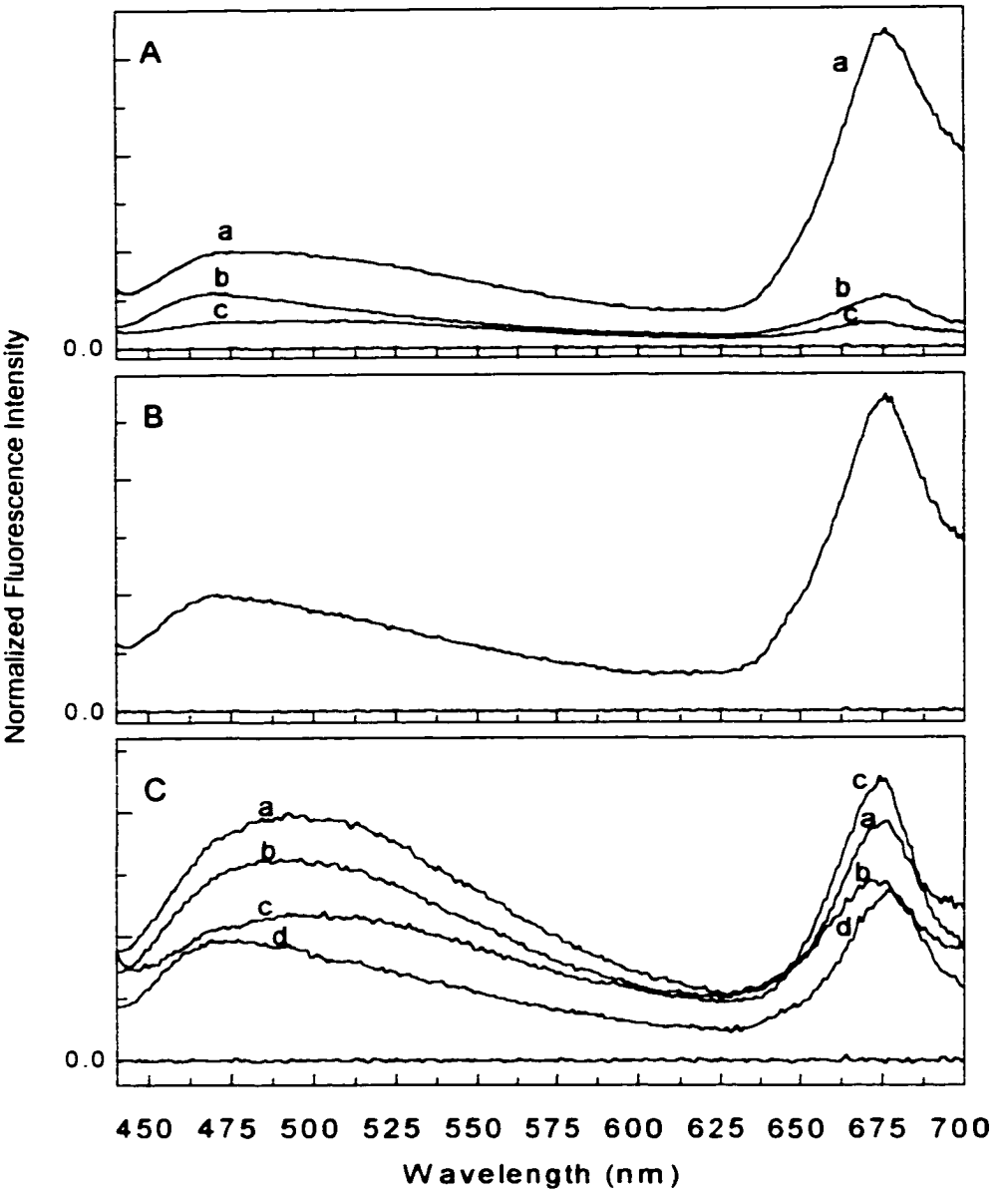

Figure 6.6. Fluorescence spectra of (A) rumen, (B) cecum,and (C) feces samples from two different cows, labeled 1 and 2, and fecal sample of a pig. The excitation wavelength was 430 nm. The baseline in each panel at zero intensity is the emission from the 50 mM Tris dilution buffer after correction for Ramen scattering from water. Each emission spectrum was corrected for Raman scattering by subtracting the contribution of Raman scattering from the Tris buffer. In panel (A) spectra **a** and **b** are rumen samples from cow 1 and spectrum **c** is from cow 2. (B) is a cecum sample from cow 2. In (C), spectrum **a** is a feces sample from cow 2, spectra **b** and **d** are from cow 1, and spectrum **c** is a pig feces sample. The prominent emission band around 675 nm is from the chlorophyll metabolite pheophorbide *a*.

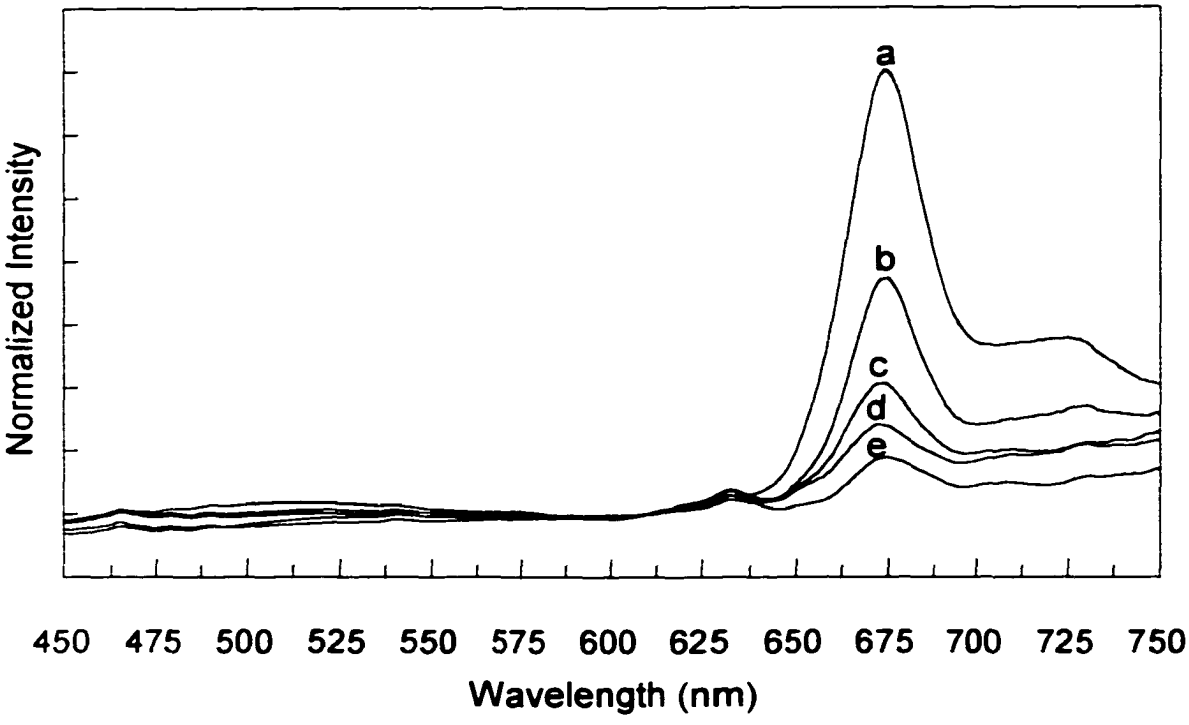

Figure 6.7. Front-faced emission spectra of fecal samples from various sources. (a) and (b) are Colorado samples. (c) and (d) are Iowa samples. (e) is a Georgia chicken sample. The prominent emission band around 675 nm is due to the chlorophyll metabolite pheophorbide *a*. Differences in the intensity of the 675-nm emission band is due to differences in diet among the various animals as well as the particular time the sample was taken.

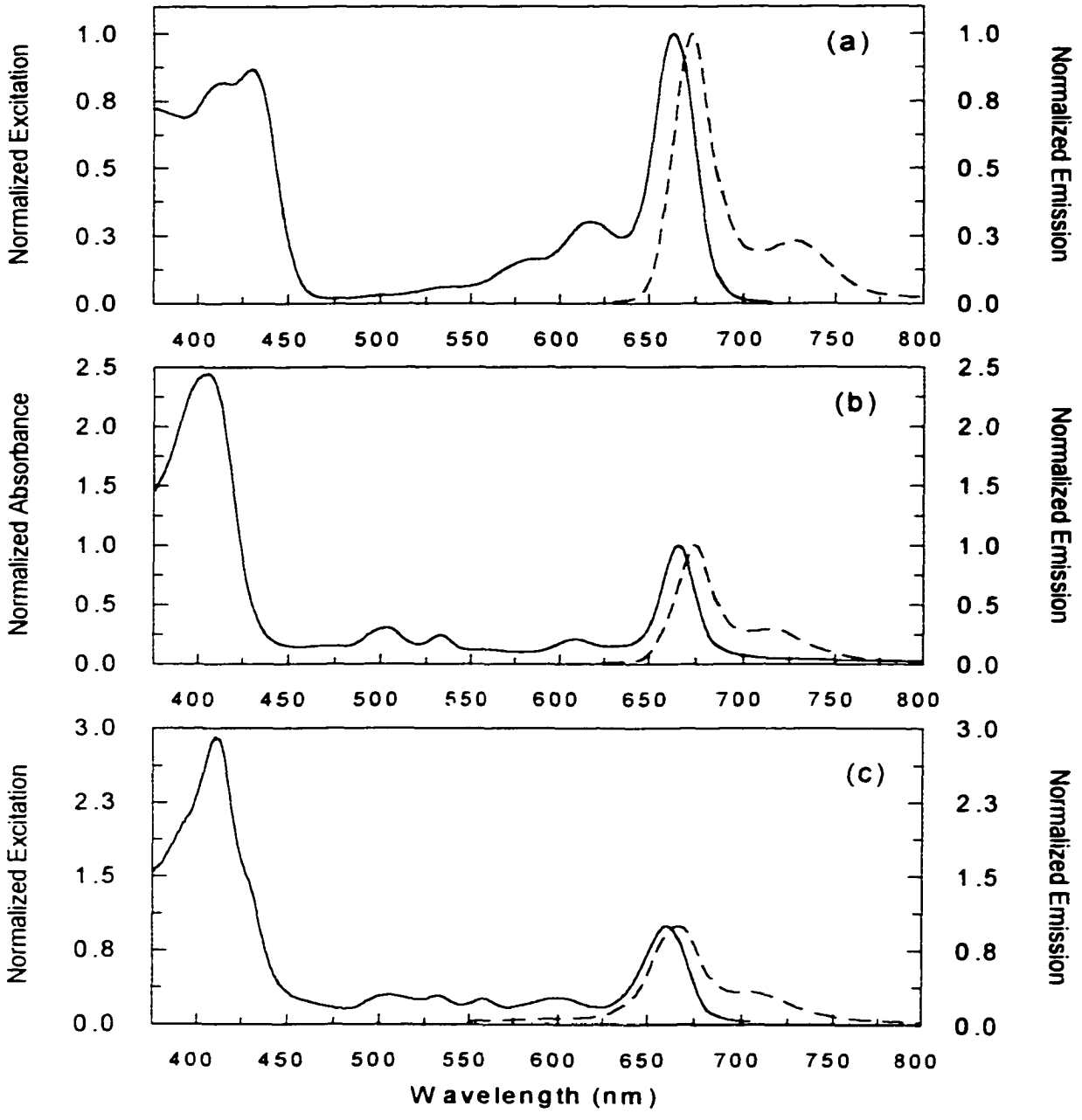

Figure 6.8. (a) The normalized excitation and emission spectra of chlorophyll *a* in ethanol. The emission maximum is 673 nm. (b) The normalized absorption and emission spectra of pheophorbide *a* in acetone. The emission maximum is 675 nm. (c) The normalized excitation and emission spectra of an acetone/water extract of cow fecal material. The similarities between the fecal extract spectra and the pheophorbide *a* spectra can be identified. The fecal extract does show some absorbance from other fluorescent species around 550 nm, but even with these anomalous features the pheophorbide spectral features can be seen. Through this spectroscopic comparison it is clear that fecal material contains pheophorbide *a* and is probably the main metabolite in the feces of herbivorous animals.

pheophorbide *a* in acetone was run against the acetone extracted fecal material on silica gel TLC plates. Using a UV lamp to detect the spots, it was determined that the fecal spot did indeed have the same R_f value as the pheophorbide *a* spot.

For a detector to successfully detect fecal and ingesta contamination on a meat carcass using pheophorbide *a* as a marker, the pheophorbide emission must be detected above any background emission or scattered light. Using the front-faced fluorescence technique emission spectra were obtained of clean meat (hamburger) and "dirty" meat, spotted with feces. Figure 6.9 illustrates the difference in the spectra, before and after the meat was spotted. Also, shown is the pheophorbide-like spectrum around 675 nm after the spectra were normalized at 610 nm and subtracted. Thus, amidst the background and scattered light, fecal material can be detected on a meat surface using pheophorbide as the marker. While this observation is purely qualitative, it represents probably the most unfavorable situation, and yet still successfully detects the fecal material. The design of a detection system using phase sensitive detection would be able to discriminate from scattered light or spurious signals of a dc nature or others which are not at the modulation frequency of the excitation source. Filtering also will add some selectivity, allowing only those wavelengths of interest to be detected and amplified, namely the ~675 nm emission band from pheophorbide in fecal material. Thus, a greater sensitivity and selectivity can be achieved.

The First Generation F-Detector Prototype

Figure 6.3 is a photograph of the first F-Detector prototype based upon the design illustrated in figure 6.4. Although this prototype may not appear attractive or sophisticated the purpose of its construction was to prove that this type of real-time detection could be achieved. Examples of the prototype's success are illustrated in figures 6.10 and 6.11. Actual trimmings

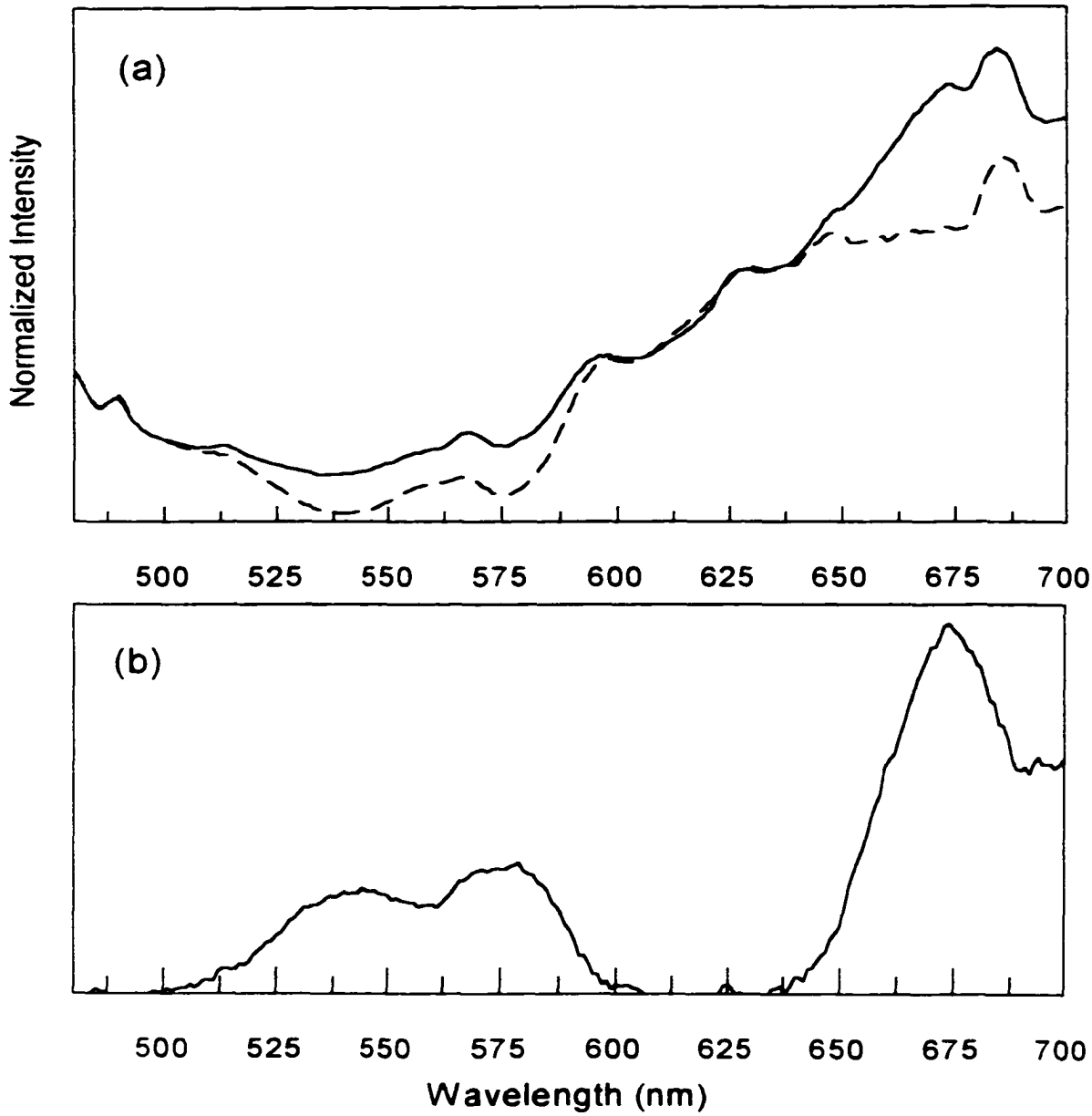

Figure 6.9. (a) Front-faced emission spectra of clean hamburger meat (dashed line) and the same meat spotted with fecal material (solid line). The two spectra were normalized to unity at 610 nm, the same wavelength whose intensity is subtracted from the pheophorbide *a* emission (670 nm) in obtaining the net F-Detector signal. (b) is the resultant spectrum after the clean meat spectrum was subtracted from the spotted meat spectrum. This plainly shows the pheophorbide-like emission around 675 nm. A minimum occurs in the subtracted spectrum between 600 and 630 nm. By taking the difference between the 670 nm and 610 nm intensities, a net signal corresponding to pheophorbide *a* is obtained as is done in the F-Detector. This way the pheophorbide signal may be extracted selectively among scattered light or other background emission.

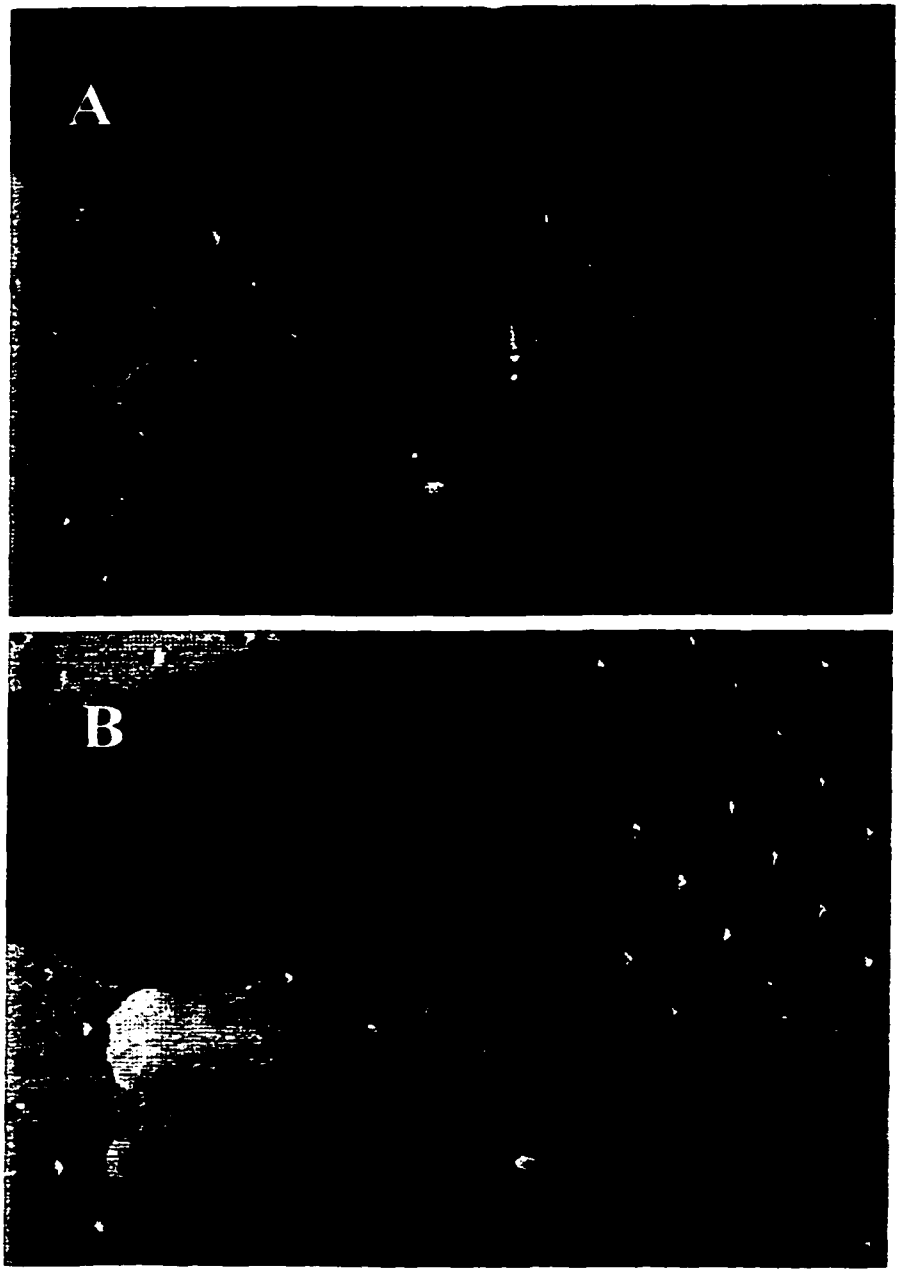

Figure 6.10. Carcass trimmings consisting of subcutaneous fat and some exposed meat surfaces were analyzed to demonstrate the utility of the F-Detector. Some sample trimmings were clean while others contained visible defects of animal hair, feces, and ingesta material. In panel A, a clean sample shows essentially no signal from the surface when the optical fiber probe is scanned across the surface. To demonstrate that pheophorbide could be detected on the surface of this sample, a dilute pheophorbide solution was spotted on the surface. The subsequent scan across the spot resulted in a +1.137 V signal (panel B).

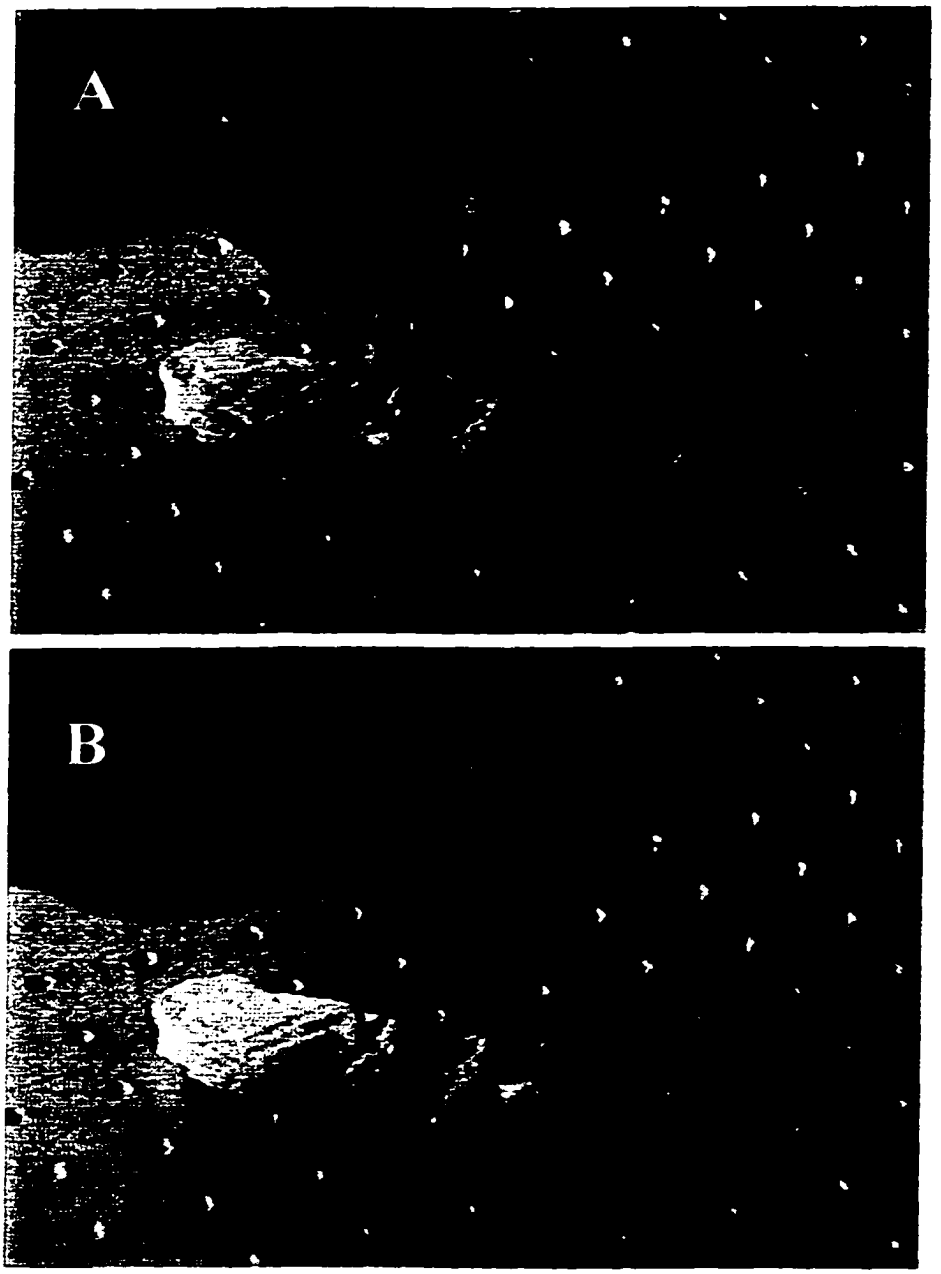

Figure 6.11. In this figure a piece of subcutaneous fat contains two visible defects. In panel A, it is again shown that the clean portion of the sample does not give any resultant signal. Panel B shows the +0.239 V signal that results when the probe tip is scanned across one of the defects establishing it is of fecal origin. The second visible spot did not give any signal showing it is not of fecal origin.

(mainly subcutaneous fat with some exposed meat) from a production line beef carcass (provided by IBP) were brought to the lab and used for analysis and demonstration purposes. These trimmings had a variety of visible hair and fecal defects ranging from <1 mm up to 5 mm in size. First, in figure 6.10, a small droplet of a dilute pheophorbide solution from a capillary tube was placed upon a clean trimming. The subcutaneous fat did not show any signal as indicated in panel A of figure 6.10. The spot was detected easily as shown in panel B of figure 6.10 with a maximum voltage of +1.137 V. The fecal spots were detected quickly as the probe tip of the optical fiber was moved across the surface over the defect as illustrated in figure 6.11. The particular sample in figure 6.11 had two distinct defects but only one spot, as indicated in panel B of figure 6.11 gave a positive reading indicating fecal contamination and a maximum signal of 0.239 V. These demonstrations also showed that blood clots do not give a signal which provides some selectivity over non-fecal defects.

The green excitation light exiting the optical fiber tip excited the fluorescent markers (pheophorbide) within the fecal spot and the emission was collected through the same optical fiber. The emission is transmitted to the 610 nm reflecting/670 nm transmitting dichroic mirror essentially splitting the emission signal, each one being sent to the lock-in amplifier. The two signals are then subtracted and amplified and enhanced using phase-sensitive detection. A 100 ms time constant was set on the lock-in, so in essence an "instantaneous" voltage was displayed corresponding to the emission from the fecal spot.

Fluorescence from a fecal spot is emitted isotropically from the surface with a certain radiant intensity (W/sr). Therefore, the distance the probe tip is from the surface will therefore affect the magnitude of the voltage signal displayed by the lock-in, in a couple of ways. First,

although a coupling/collimating lens was used on the probe tip the excitation light did diverge as it exited the fiber tip. Therefore the radiant power of the excitation light per unit area will change, and hence the number of photons exciting the fecal spot will change, depending on the probes distance from the surface. In general, the fewer the photons exciting the feces the fewer the photons emitted. Second, the number of photons emitted per solid angle will remain constant for a given emittance (W/cm) of excitation light, but at distances further from the surface, fewer emission photons will be collected through the fiber tip. Since the aperture of the lens on the fiber tip is only ~6 mm it was necessary to keep the probe tip close to the surface, between 1 and 2 cm. Although the excitation spot size was kept small at these distances, the emittance was high and more emission photons were collected and detected.

A couple of additional aspects that will affect the number of photons exciting the fecal spot and the number of photons collected by the probe tip are the contours of the surface (it is not flat) and the angle of the probe tip to the surface. While all of these aspects will effect the overall magnitude of the signal displayed on the lock-in as the probe tip is scanned (by hand) across the surface of the carcass (or meat sample) they do not undermine the overall success of the initial prototype design, and will be addressed in the engineering phase of the work.

The Second Generation F-Detector Prototype

The impetus for the building of the second prototype (Fig. 6.5) was to have a small and easily handled device that could be transported readily and demonstrated on an actual meat production line. The same design was used as the first-generation F-Detector prototype but smaller components were purchased that would all fit within the same enclosure. The Experimental Section describes the components in detail.

In order to obtain an estimate as to the response of the detector as well as the detection

limit of pheophorbide *a* a calibration curve, pheophorbide concentration (M) versus F-Detector signal (mV), was made. The calibration curve (Figure 6.12) has a linear correlation coefficient of 0.987 with a slope of $2.00 \cdot 10^8$ mV/M (200 mV/μM). The linear dynamic range of the instrument, according to the calibration curve, spans almost three orders of magnitude. In Table 6.1 the magnitude of the average F-Detector signal is given for each pheophorbide *a* solution. A time constant of 100 ms is used in the measurement of the fluorescent signal from pheophorbide *a*. This provides a real-time signal output from the fluorescent marker. The uncertainties given in Table 6.1 are the magnitudes of the fluctuations around the average F-Detector signal. In obtaining this calibration curve, both the sample and the probe tip remained

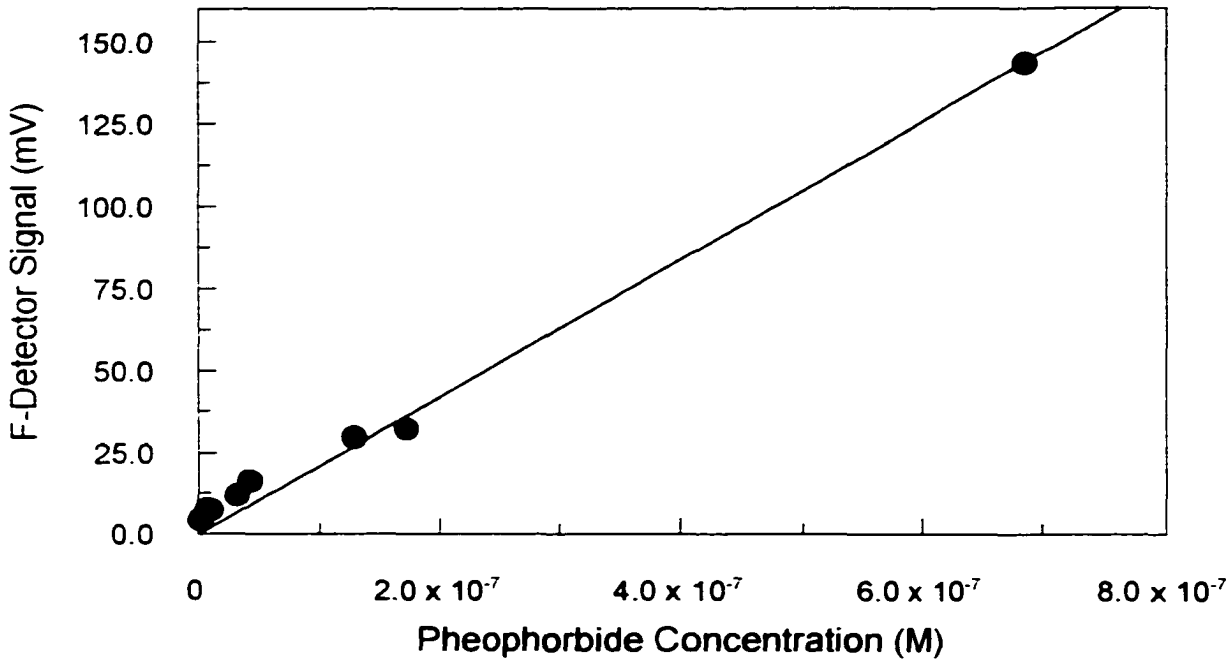

Figure 6.12. Calibration plot of F-Detector signal versus molar concentration of pheophorbide *a* in solution. The correlation coefficient of the linear fit through zero is 0.987. The slope of the line representing the sensitivity of the F-Detector to pheophorbide is $2.00 \cdot 10^8$ mV/M (200 mV/μM). The detection limit (~3:1 signal to noise ratio) is on the order of 10^{-10} M under the respective experimental conditions as outlined within the text.

in a fixed position in order to maintain a constant distance and angle between them. This resulted in rather small fluctuations and a detection limit of pheophorbide *a* in solution on the order of 10^{-10} M (signal to noise ratio of ~3:1). Although solutions of the pure pheophorbide *a* were used to obtain this curve, this clearly illustrates the sensitivity of the detector to the fluorescent marker.

Using the 1 mm pathlength cuvette to measure the calibration curve *approached* a surface fluorescence measurement but the samples were far from opaque and photons emitted from molecules even at the 1 mm depth added to the overall signal. To better simulate surface fluorescence, such as emission from fecal spots on meat surfaces, and obtain an "equivalent fecal unit", as to the amounts (concentration) of pheophorbide and feces detected for a given F-Detector signal, silica gel TLC plates with a 0.1 mm thick stationary phase were used.

Analyzing the two calibration plots obtained utilizing the TLC plates, one for pheophorbide and another for diluted fecal material, a $1.0 \cdot 10^{-6}$ M pheophorbide sample gave rise to a 25 mW signal which is equivalent to 1.8 mg of fecal material per mL of solution. The fecal spots on the TLC plates at low concentrations, 10^{-3} to 10^{-5} g fecal material/mL, after the solvent evaporated could not be seen visually, but detectable only with the aid of the F-Detector. The sensitivity of the F-Detector to the diluted fecal material was $\sim 1.4 \cdot 10^{4}$ mV/(g/mL). This illustrates how beneficial this instrument could be to detect fecal material from meat surfaces even when the defects are not visible to the "naked-eye". This correlation of the F-Detector signal to a given amount of pheophorbide and the equivalent amount of fecal material provides, of course, just estimates of the amounts of fecal material that can be detected. The amount of fluorescent marker within the fecal material of different animals will fluctuate depending upon

the diet of the specific animal, among other things. Based upon the representative fecal material used, our results indicate that a range of ±2 orders of magnitude around the 1.8 mg/mL fecal material giving rise to the 25 mW signal, could be detectable. This provides about four orders of magnitude of dynamic range to account for differences in the animal's diet and the size of the defect on the carcass.

Conclusions

We have successfully demonstrated the utility of the F-Detector prototype to detect the fluorescent marker, pheophorbide *a*, in fecal and ingesta material. Pheophorbide *a* is a major chlorophyll metabolite of herbivorous animals and makes it a very useful marker for fecal and ingesta contamination on meat carcasses, thus detecting the possible presence of *E. coli*. The F-Detector allows for an "instantaneous" detection of contamination by employing a 100 ms time constant. This fast detection, along with the low detection limit, high sensitivity, and selectivity for only the chosen fluorescent marker, establishes this technology as an extremely attractive asset in helping the meat industry, in addition to the inspectors and regulators of the industry, in providing the public with a safer product.

Currently the technology is being engineered into commercial instruments that will better suit the meat industries needs. We fulfilled many of those needs with our current prototype. Future instruments will effectively address the need to scan the whole carcass quickly and efficiently and thus allow inspection of *all* carcasses that are processed. This technology would go along way toward approaching the "zero-tolerance" guideline established by regulators that current visual inspections do not.

Acknowledgment

Grants and other support for this research were provided by the U.S. Department of Agriculture and eMERGE Interactive, Inc.

References

1. Davies, A.; Board, R.; Eds. *The Microbiology of Meat and Poultry*; Blackie Academic & Professional: New York, 1998; Chapter 4.

2. National Advisory Committee on Microbiological Criteria for Foods *Food Microbiol.* **1993**, *10*, 449-488.

3. U.S. Department of Agriculture *Fed. Regist.* **1996**, *61*, 38805-38989.

4. Matthews, D.D., Ed. *Food Safety Sourcebook*; Onmigraphics, Inc.: Detroit, MI, 1999; Chapter 21.

5. Tansey, G; D'Silva, J., Eds. *The Meat Business: Devouring a Hungry Planet*; St. Martin's Press: New York, 1999; p. 26.

6. Doyle, M.P; Ed. *Foodborne Bacterial Pathogens*; Marcel Dekker, Inc.: New York, 1989; Chapter 6.

7. Feng, P. *Emerging Infectious Diseases* **1995**, *1*(2).

8. Crutchfield, S.R.; Buzby, J.C.; Roberts, T.; Ollinger, M.; Jordan Lin, C.-T. *Economic Research Service USDA* **1997**, Agricultural Economic Report No. 755, 1-21.

9. Forrest, J.C.; Aberle, E.D.; Hedrick, H.B.; Judge, M.D.; Merkel, R.A. *Principles of Meat Science*; W.H. Freeman and Company: San Fransisco, CA, 1975; pp. 228-229.

10. Gill, C.O. *Can. J. Anim. Sci.* **1995**, *75*, 1-13.

11. Ashby, K.D.; Casey, T.A; Rasmussen, M.A.; Petrich, J.W. Submitted.

12. Kates, M.; Kushner, D.J.; Matheson, A.T. *The Biochemistry of Archaea (Archaebacteria)*; Elsevier: Amsterdam, 1993; pp. 41-61.

13. Eirich, L.D.; Vogels, G.D.; Wolfe, R.S. *Biochem.* **1978**, *17*, 4583-4593.

14. Ashton, W.T.; Brown, R.D.; Jacobson, F; Walsh, C.J. *Amer. Chem. Soc.* **1979**, *101*, 4419-4420.

15. Gorris, L.G.M.; van der Drift, C. *Biofactors* **1994**, *4*, 139-145.

16. Danson, M.J.; Hough, D.W.; Lunt, G.G. *The Archaebacteric: Biochemistry and Biotechnology*; Portland Press: London, 1992; pp. 143-179.

17. Ma, L.; Dolphin, D.; *Phytochemistry* **1999**,*50*, 195-202.

18. Vernon, L.P.; Seely, G.R., Eds. *The Chlorophylls*; Academic Press: New York, 1966; pp 6-18.

19. Scheer, H., Ed. *Chlorophylls*; CRC Press, Inc.: Boca Raton, FL, 1991.

20. Personal communication with Prophyrin Products, Inc. personnel.

21. Malmstadt, H.V.; Enke, C.G.; Crouch, S.R. *Making the Right Connections*; American Chemical Society: Washington DC, 1994; pp. 136-138, 208-210.

22. Uffenbeck, J.E. Introduction to Electronics: Devices and Circuits; Prentice-Hall, Inc.: Englewood Cliffs, NJ, 1982; Chapters 11 and 12.

23. Hamamatsu Photonics K.K. *Photomultiplier Tubes*; Hamamatsu: Japan, 1997; pp. 4 - 23.

GENERAL SUMMARY AND CONCLUSIONS

This dissertation illustrates the diverse information that lasers and their experimental techniques can provide in biophysical and analytical chemistry. The ability to produce spectrally and temporally narrow laser pulses allows the investigation of fast excited-state processes and the ability to take advantage of phenomena within nonlinear crystals such as second harmonic generation and sum frequency generation. The generation of white light within water also results from nonlinear effects due to the pulsed high electric fields of the laser.

We have exploited the fluorescence properties of the indole chromophore to quantify the trapping of 3-methylindole within micelles. The sensitivity of the indole chromophore to the polarity of its environment allows investigation of proteins to elucidate protein dynamics and structure. We have described the fluorescence properties of 7-azatryptophan and 5-hydroxytryptophan alone and incorporated into the protein, tropomyosin. These non-natural amino acids offer greater utility than tryptophan in both steady-state and time-resolved experiments.

The intramolecular hydrogen atom transfer reaction was confirmed to be the primary photophysical event in hypericin using fluorescence upconversion. This reaction has an extremely small energy barrier as determined by temperature dependent pump-probe experiments.

New technology in semiconductor lasers will allow for new excitation sources in the blue region (400 - 470 nm) of the electromagnetic spectrum. As these blue diode lasers become more stable and their usable lifetime becomes extended they will be a great asset for use in the F-

Detector. The extinction coefficient of pheophorbide, the fluorescent marker used to detect fecal contamination on meat surfaces, increases in this region of the spectrum. Exciting in this region may increase the sensitivity and detection limit of pheophorbide. Caution is warranted in going too far into the blue region away from our normal 532-nm F-Detector excitation wavelength, as more chromophores within the fecal material may possibly fluoresce and artificially contribute to the signal (if they have emission around 670 nm). We have attempted to use blue LEDs (light emitting diodes) from various sources but have found their spectral bandwidth is much too large for our purposes creating large background problems. The narrow spectral bandwidth of a diode laser will obviate this problem. Even with the 532-nm excitation light currently utilized, the F-Detector is extremely successful in selectively detecting low levels of fecal and ingesta material on meat carcasses. Commercialization of this technology is important in providing safer meat products for the public and a more sensitive and accurate means of inspecting meat carcasses as they are processed.

The applications of lasers is seemingly endless as a result of their unique properties in comparison to conventional light sources. The introductory remarks of Plinius concerning the "Laser" are assuredly applicable to the laser of today!

APPENDIX A. THE LOCK-IN AMPLIFIER

The purpose of a lock-in amplifier is to detect low-level AC signals and, through phase sensitive detection, single out only those components of the signal at a specific frequency and phase. All other signals (noise), at other frequencies, are therefore rejected (depending upon the low pass AC filter bandwidth).

The lock-in amplifier requires a frequency reference, usually a square wave at frequency ω_r, which is provided by the chopper driver (same modulation frequency of the excitation light). The lock-in generates its own sine wave at the same frequency but designated as ω_L (figure A.1). The lock-in then detects only signals from the experiment at the same frequency, achieving maximum signal when the phase angle between the lock-in reference and the experiment signal is made zero by adjusting the lock-in reference phase angle. The details of this are given below.

The lock-in amplifies the input signal (from experiment) and then multiplies it by the lock-in reference signal. The output signal, V_{OUT}, is simply the product of two sine waves; the signal = $V_{sig}\sin(\omega_r t + \theta_{sig})$, where V_{sig} is the amplitude of the signal and θ_{sig} is the phase angle with respect to the reference and the lock-in reference = $V_L\sin(\omega_L t + \theta_{ref})$, where V_L is the amplitude of the lock-in reference signal and θ_{ref} is the phase angle also with respect to the reference.

$$V_{OUT} = V_{sig}V_L \sin\left(\omega_r t + \theta_{sig}\right)\left(\omega_L t + \theta_{ref}\right)$$

$$V_{OUT} = \frac{1}{2}V_{sig}V_L \cos\left(\left[\omega_r - \omega_L\right]t + \theta_{sig} - \theta_{ref}\right) - \frac{1}{2}V_{sig}V_L \cos\left(\left[\omega_r + \omega_L\right]t + \theta_{sig} + \theta_{ref}\right)$$

Thus, the phase sensitive detector output is two AC signals, one at the difference

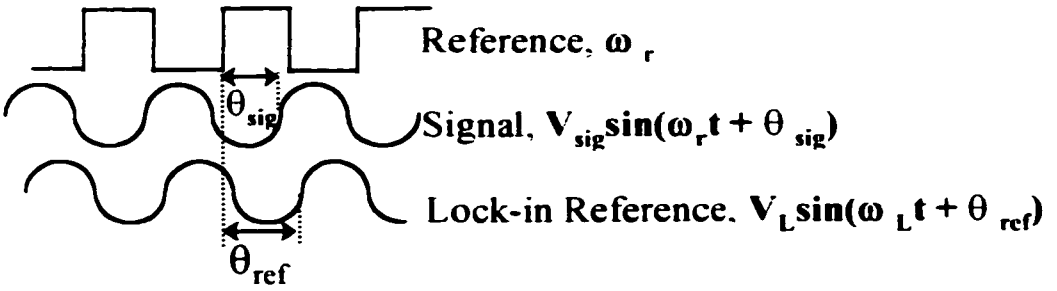

Figure A.1. The square-wave, reference signal at frequency, ω_r is obtained from the output of a modulation device or function generator. The signal sine wave is the detected emission signal that results from excitation of the modulated light source. V_{sig} is the signal amplitude (i.e. voltage),ω_r is the frequency of the emission signal (should be the same as the reference frequency or the frequency of the light source modulation), and θ_{sig} is the phase difference between the reference signal and the emission signal. The lock-in reference is the sine wave signal generated by the lock-in amplifier at a frequency, ω_L, V_L is the lock-in reference amplitude, and θ_{ref} is the phase difference between the reference signal and the lock-in reference.

frequency (ω_r - ω_L) and the other at the sum frequency (ω_r + ω_L). The output is then passed through a low pass filter which removes or attenuates the AC signals. However, if $\omega_r = \omega_L$, the difference frequency component will be a DC signal and the filtered output will be:

$$V_{OUT} = \frac{1}{2} V_{sig} V_L \cos\left(\theta_{sig} - \theta_{ref}\right)$$

The output is therefore dependent upon the phase difference between the signal and the lock-in reference. By adjusting θ_{ref} the phase difference, θ_{sig} - θ_{ref} can be made zero and the output, V_{OUT}, will be a DC signal proportional to the experimental signal.

The phase dependency can be eliminated by adding a second lock-in or phase sensitive detector whose phase is shifted by 90° relative to the first phase sensitive detector (lock-in$_2$ reference = V_{L2} sin(ω_Lt + θ_{ref} +90°)) The resulting output from the second lock-in after multiplication with the signal will be:

$$V_{OUT\,2} = \frac{1}{2} V_{sig} V_L \sin\left(\theta_{sig} - \theta_{ref}\right)$$
$$V_{OUT\,2} \approx V_{sig} \sin\theta$$

Now there are two ouputs: $V_{OUT\,1} \approx V_{sig}\cos\theta$ and $V_{OUT\,2} \approx V_{sig}\sin\theta$. To make things a little simpler to look at, let $X = V_{sig}\cos\theta$ and $Y = V_{sig}\sin\theta$, where $\theta = \theta_{sig} - \theta_{ref}$. Because the two lock-ins are 90° out of phase the relationship between X and Y is such that when $\theta = 0$, X measures the signal and Y is zero. The output signal, V_{sig}, is thus calculated by:

$$V_{sig} = \left(X^2 + Y^2\right)^{1/2}$$

Therefore the signal amplitude is measured and does not depend upon the phase between the signal and the lock-in references.

Reference

1. Stanford Research Systems, Inc., *Model SR830 DSP Lock-in Amplifier Operation Manual*, Revision1.3; Sunnyvale, CA, 1993; Section 3.

APPENDIX B. ELECTRONIC CIRCUITS

Current to Voltage Amplifier

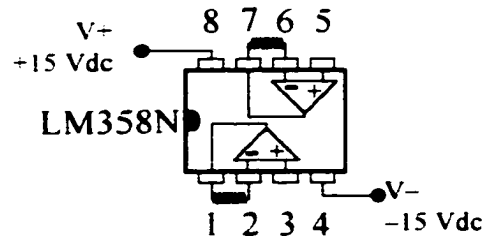

(a)

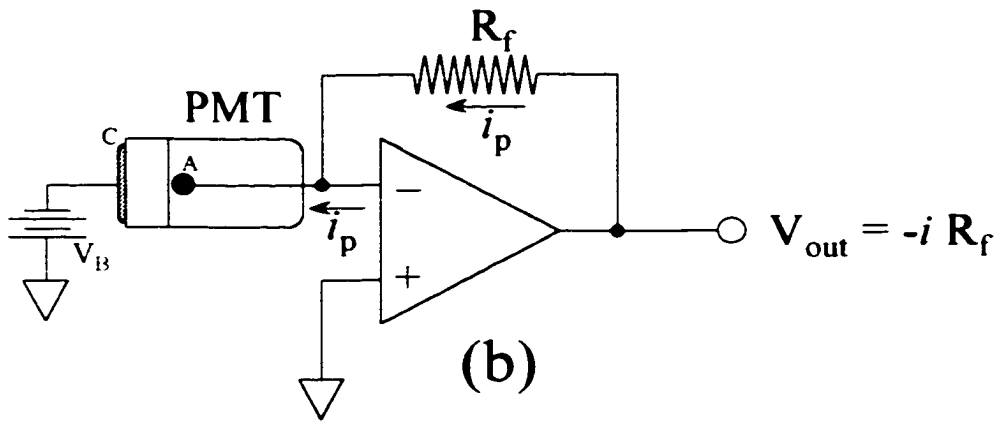

(b)

Difference Amplifier

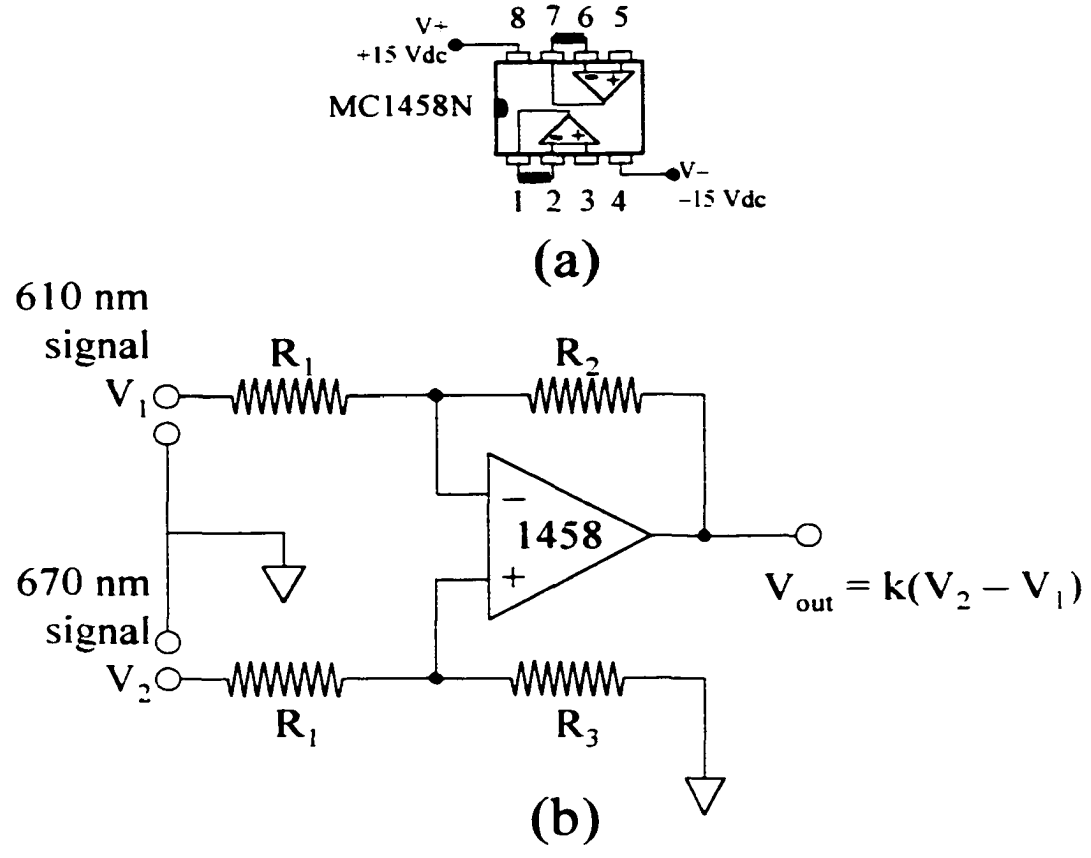

R_3 is a multiturn trimmer with a resistance a little larger than R_2. The resistance of R_3 is adjusted in order to balance circuit such that when voltage signals of the same magnitude are applied to the imputs the output will be exactly zero. This can be observed on an oscilloscope.